UNIVERSITY OF ALBERTA

GEOMECHANICAL PERFORMANCE ASSESSMENT OF CO_2 – EOR GEOLOGICAL STORAGE PROJECTS

by

©

JAIME ALBERTO JIMENEZ GOMEZ

A THESIS

SUBMITTED TO THE FACULTY OF GRADUATE STUDIES AND RESEARCH IN PARTIAL FULFILLMENT OF THE REQUIREMENTS FOR THE DEGREE OF

DOCTOR OF PHILOSOPHY

IN GEOTECHNICAL ENGINEERING

Department of Civil and Environmental Engineering

Edmonton, Alberta

Fall 2006

Library and
Archives Canada

Published Heritage
Branch

395 Wellington Street
Ottawa ON K1A 0N4
Canada

Bibliothèque et
Archives Canada

Direction du
Patrimoine de l'édition

395, rue Wellington
Ottawa ON K1A 0N4
Canada

Your file Votre référence
ISBN: 978-0-494-23049-7
Our file Notre référence
ISBN: 978-0-494-23049-7

NOTICE:
The author has granted a non-exclusive license allowing Library and Archives Canada to reproduce, publish, archive, preserve, conserve, communicate to the public by telecommunication or on the Internet, loan, distribute and sell theses worldwide, for commercial or non-commercial purposes, in microform, paper, electronic and/or any other formats.

The author retains copyright ownership and moral rights in this thesis. Neither the thesis nor substantial extracts from it may be printed or otherwise reproduced without the author's permission.

AVIS:
L'auteur a accordé une licence non exclusive permettant à la Bibliothèque et Archives Canada de reproduire, publier, archiver, sauvegarder, conserver, transmettre au public par télécommunication ou par l'Internet, prêter, distribuer et vendre des thèses partout dans le monde, à des fins commerciales ou autres, sur support microforme, papier, électronique et/ou autres formats.

L'auteur conserve la propriété du droit d'auteur et des droits moraux qui protège cette thèse. Ni la thèse ni des extraits substantiels de celle-ci ne doivent être imprimés ou autrement reproduits sans son autorisation.

In compliance with the Canadian Privacy Act some supporting forms may have been removed from this thesis.

While these forms may be included in the document page count, their removal does not represent any loss of content from the thesis.

Conformément à la loi canadienne sur la protection de la vie privée, quelques formulaires secondaires ont été enlevés de cette thèse.

Bien que ces formulaires aient inclus dans la pagination, il n'y aura aucun contenu manquant.

Canada

Abstract

Geological storage of CO_2 in disused oil and gas reservoirs is perhaps the most promising technique to reduce CO_2 emissions into the atmosphere because of the economic benefits that incremental oil recovery can bring in a tight energy market. However, the acceptance of this new paradigm will require a perception of geological storage as a safe and environmentally sound practice. Therefore, it is necessary to make CO_2 storage predictable to avoid any negative impacts to the environment or society and implement a carbon emissions market. In the short-term, or injection stages, the main trapping element is a competent caprock, and its performance is a vital component of the risk assessment of any CO_2 storage project. Geomechanics plays a key role in the performance assessment of the caprock and the reservoir as the hydraulic integrity of this system must be ensured both during the exploitation and production stages (pre-CO_2 injection), and during CO_2 injection in any CO_2-EOR storage project. The IEA Weyburn CO_2 Monitoring and Storage Project has offered a unique opportunity to conduct a geomechanical performance assessment of a caprock system overlying a large scale CO_2-EOR storage project. New experimental facilities to evaluate the hydro-mechanical properties of caprocks at high pressures and high temperatures were built. In-situ stresses evolution and thermomechanical considerations were identified as the most relevant issues for any CO_2-EOR storage project from a geomechanical perspective. In-situ stress measurements and downhole monitoring of pressure and temperature should become mandatory as part of the regulatory and/or operational process for these projects. These conclusions were achieved through the systematic use of performance assessment techniques that include scenario analysis, model development, and development of working criteria. Moreover, it was found that the Weyburn field is a safe and sound sink for CO_2 storage as long as the CO_2 injection does not cause the development of tensional thermal stresses in the caprock, and the injection pressure remains below the minimum horizontal stress. Finally a methodology to carry out geomechanical performance assessments in CO_2-EOR storage projects and manage uncertainty was developed, which can be applied elsewhere.

Acknowledgments

I would like to express my gratitude to my supervisor, Dr. Rick Chalaturnyk, whose expertise, understanding, thought-provoking discussions and patience added considerably to my graduate experience. He provided me with direction, technical support and became more of a mentor and friend than a professor. I greatly appreciate his effort to look after my future, and taking the time to teach me other non-technical skills that come with the 'business'.

I gratefully acknowledge the financial suppot provided by ASRA, PTRC and EnCana and I want to express my gratitude to these organizations.

A big thanks goes out to Dr. Irene Meglis for the endless effort she put into the seismic component of the experimental work, it was a great learning experience for me. I would also like to express my gratitude to Dr. Derek Martin for providing very interesting discussions and insight about rock mechanics throughout this thesis, and Dr. Stephen Talman for his willingness to answer all my questions about geochemistry and fluid flow. I also thank the other staff members in the Geotechnical Group for their continuing encouragement and especially Dr. Dave Sego for his kind and wise words.

I thank Steve Gamble for all his help in the laboratory, for the never-ending encouragement, good sense of humor and willingness to collaborate. I also wish to thank Gerry Cyre for his help and ingenuity in the laboratory, and Christine Hereygers for her laboratory help and sense of humour.

I need to thank some people who I met during the research leg of my thesis journey. Steve Whittaker, Kim Kreis and Erick Nickel from Saskatchewan Industry and Resources for their collaboration with the geology of Weyburn; Randy Burke from the North Dakota Geological Survey for his interesting discussions in salt dissolution, and the people at EnCana (Ryan Adair and Geoff Burrowes) for answering all our questions and providing us with all the information we requested.

I also appreciate the constructive criticism and effort put by the committee to make this work more accurate, comprehensive and elegant, especially Dr. Ben Rostron and Dr. Chris Hawkes.

I would like to thank my friends and colleagues for their assorted efforts during my journey. Santiago Paz for his enormous help developing automatic routines for multiple tasks in this thesis, Nathan Deisman for his help with the geological models of Weyburn and correcting the grammar of this thesis, Andrew Corkum for his critical reading of this work, and Anna Ho, Francisco Moreno, Stephanie Banks, Salina Young and Scott Martens for their collaboration at different points in this research.

Needless to say, this entire exercise would be at most a dream were it not for my loving family. I would like to express my deepest gratitude to my parents for their love, support, encouragement and their eternal optimism throughout this journey. They provided me with the tools, inspiration and emotional support needed to accomplish this work. Finally, a special thanks to Mathilde Ponsart for being a constant source of love and happiness during these years.

Dedication

A mis padres

Table of Contents

1 Introduction 1

1.1 Statement of the Problem 1

1.2 Objectives and Scope 2

1.3 Organization of Thesis 3

2 Geological Storage 4

2.1 Introduction 4

2.2 The Concept of Geological Storage of GHG 5

2.3 Geological Sink: What it is 6

2.3.1 The Porous Medium 6

2.3.2 Bounding Seals 7

2.3.3 The Concept of Hydraulic Integrity 7

2.4 Possible Geological Sinks 8

2.4.1 Geological Storage in Deep Saline Aquifers 8

2.4.2 Disused Oil and Gas Reservoirs 9

2.4.3 Salt Caverns 10

2.4.4 Unmineable Coal Beds 10

2.5 The IEA Weyburn CO_2 Monitoring and Storage Project 11

2.5.1 History of the Weyburn Field 11

2.6 Figures 13

3 Performance Assessment for CO_2-EOR Projects 15

3.1 Introduction 15

3.2 Performance and Safety Assessment 16

3.2.1 Performance Assessment and Risk Management 19

3.3 Performance and Risk Assessment Methodology for Geological Storage of CO_2 19

3.3.1 Scenario Analysis 19

3.3.2 Model Development and Application 20

3.3.3 Consequence Analysis 20

3.3.4 Confidence Building and Performance Criteria 21

3.4 The Observational Method 21

3.5 Approach to Geomechanical Performance Assessment of CO_2-EOR Storage Projects 23

3.5.1 The Caprock System 26

3.6 Performance Criteria 26

3.6.1 Natural Analogues 26

3.6.1.1 The UK Central Graben 26

3.6.1.2 The Uinta Basin 27

3.6.1.3 The Snorre Field, Norway 27

3.6.1.4 Microfractures at the Frio Formation 28

3.6.1.5 The Gullfaks Area, North Sea 28

3.6.1.6 Fault Reactivation in a Tertiary Basin in south-East Asia 29

3.6.1.7 South Eugene Island 330 Field, Gulf of Mexico 29

3.6.2 Deep Storage and Disposal 29

3.6.2.1 Leroy Storage Facility 30

3.6.2.2 Suffield Upper Mannville I (Gas Storage Project) 31

3.6.2.3 Well Problems in Natural Gas Storage 32

3.6.3 Criteria 32

3.7 Uncertainty and its Management 33

3.8 Summary 34

3.9 Figures 35

4 Disused Oil and Gas Reservoirs as Sinks for Geological Storage of CO_2 40

4.1 Introduction 40

4.2 Caprock (Seals): Petroleum Approach vs. Storage Approach 41

4.2.1 Capillary Leakage 41

4.2.2 Hydraulic Fracturing 42

4.2.3 Pre-Existing Fissures and Fractures 42

4.2.4 Shear Deformation/Fracturing 43

4.2.5 Fault-Related Flow 44

4.2.6 Molecular Transport (Diffusion) 44

4.2.7 Tectonic Failure 44

4.3 Wellbores and Their Hydraulic Integrity 44

4.3.1 Casing Shear 45

4.3.2 Compression and Buckling Damage 46

4.4 Summary 46

4.5 Figures 47

5 Experimental Facilities and Permeability Measurements 49

5.1 Introduction 49

5.2 Experimental Facilities 49

5.2.1 High-Pressure Cell 49

5.2.2 Loading System 50

5.2.3 Local Strain Measurements 50

5.2.4 Acoustic Measurements 50

5.2.5 Hydraulic System 51

5.2.6 Logging System 51

5.2.7 Procedure and Preliminary Results 52

5.2.7.1 Sample Preparation 52

5.2.7.2 Test preparation 52

5.2.7.3 Test Procedure 53

5.3 Permeability Measurements 53

5.3.1 Flow Pump ... 53

5.3.2 Transient Pulse Technique ... 55

5.3.2.1 Brace's Solution ... 55

5.3.2.2 Finite Differences Solution ... 57

5.3.2.3 Analytical-Graphical Solution ... 58

5.3.2.4 Oscillation method ... 59

5.3.2.5 Parameter Identification Solution ... 61

5.3.3 Which Technique to Use ... 63

5.3.3.1 Application Considerations ... 64

5.3.4 Procedure and Preliminary Results ... 65

5.4 Summary ... 67

5.5 Figures ... 68

6 Behavior of Shales and Anhydrites as Caprocks ... 80

6.1 Overview ... 80

6.2 Shales: Hard Clays and Mudrocks ... 80

6.2.1 Classification of Argillaceous Stiff Soils and Soft Rocks ... 80

6.2.2 Mechanical Behaviour of Stiff Clays and Shales ... 81

6.2.2.1 Mechanics of Shear Resistance in Mudstones and Stiff Clayes ... 81

6.2.2.2 Sedimentation, Diagenesis and Bonding ... 82

6.2.2.3 Peak Strength ... 83

6.2.2.4 Post-Peak Strength ... 84

6.2.2.5 Brittle-Ductile Behavior ... 85

6.2.2.6 Residual Strength ... 86

6.2.2.6.1 Shear Zones and its Structure ... 87

6.2.2.7 Softening ... 88

6.2.2.8 Fissures and Joints ... 88

6.2.2.8.1 Fissility 89

6.2.2.8.2 Syneresis 90

6.2.2.8.3 Desiccation 90

6.2.2.8.4 Tectonism 90

6.2.2.8.5 Glaciotectonics 91

6.2.2.8.6 Erosion and Stress Relief 91

6.2.2.8.7 Relict Landslides 92

6.2.3 Groundwater Flow and Permeability in Stiff Clays and Shales 92

6.2.3.1 Groundwater Flow 92

6.2.3.1.1 Regional Flow in the Cretaceous Shales of Mid North America 92

6.2.3.1.2 Tournemire Tunnel, Southern France 94

6.2.3.1.3 Opalinus Clay, Fractured Jurassic Shale 94

6.2.3.2 Hydro-Mechanical Response of Clays and Shales 95

6.3 Anhydrites 100

6.3.1 Origin and Formation 100

6.3.2 Mechanical Behaviour of Anhydrites 100

6.3.3 Hydraulic Properties 104

6.3.4 Experimental Results 105

6.3.4.1 Mechanical and Hydraulic Testing 106

6.3.4.2 Geochemical Testing 108

6.4 Transport Properties and CO_2 109

6.5 Implications for Geological Storage 110

6.6 Summary 111

6.7 Figures 112

7 The Weyburn CO_2-EOR Storage Project: Mechanical Earth Model 138

7.1 Overview 138

7.2 Mechanical Earth Model (MEM) 138

7.2.1 Geological Model 138

7.2.1.1 Geological Setting 138

7.2.1.2 Salt Dissolution 139

7.2.1.3 Reservoir Characterization 140

7.2.1.4 Depositional Environment 142

7.2.2 Hydrogeological Model 143

7.2.3 Role of Fractures 143

7.2.3.1 Midale Field 143

7.2.3.2 Weyburn Field 144

7.2.3.3 Fractures and Reservoir Performance 145

7.2.3.4 Fractures in the Caprock 145

7.2.3.5 Fractures in the Williston Basin 146

7.2.3.6 Structural Features in the Williston Basin 147

7.2.3.7 Origin of the Fractures 147

7.3 Mechanical Earth Model for Weyburn 150

7.3.1 Mechanical Properties 150

7.3.2 In-situ Stresses 155

7.3.3 Base Case Scenario and Alternative Scenarios 157

7.4 Summary 158

7.5 Figures 159

8 Geomechanical Performance of the Weyburn Field 172

8.1 Introduction 172

8.2 Geomechanical Model 172

8.2.1 Hydromechanical Coupling 172

8.2.2 Boundary Conditions 174

8.2.3 Grid and Pressures 175

8.3 Reservoir History 175

8.4 Geomechanical Modeling and Performance 176

8.4.1 Capillary Leakage 176

8.4.2 Hydraulic Fracturing 177

8.4.3 Shear Failure 179

8.4.4 Fault-Related Flow 181

8.4.5 Pre-Existing Fissures 184

8.5 Summary 184

8.6 Figures 185

9 Impact of Salt Dissolution on Weyburn's Performance 203

9.1 Introduction 203

9.2 Mechanisms of Salt Dissolution 203

9.2.1 Classification of Salt Dissolution Mechanisms 203

9.2.2 Salt Dissolution Consequences 204

9.3 Dissolution of the Prairie Evaporite 205

9.3.1 Prairie Evaporite 205

9.3.2 Dissolution and Timing 205

9.3.3 Dissolution near the Weyburn Field 206

9.4 Geomechanical Modeling 206

9.4.1 Model 206

9.4.2 Results and Discussion 208

9.4.2.1 Elastic Analysis 208

9.4.2.2 Plastic Analysis 210

9.5 Summary 211

9.6 Figures 212

10 Thermal Effects Associated with CO_2 Injection in the Integrity of Bounding Seals 217

10.1 Introduction 217

10.2 Theoretical Background 217

10.3 Conceptual Models 218

10.4 Results 221

10.4.1 Carbonate Reservoir 221

10.4.2 Deep Saline Aquifer 222

10.5 Discussion 222

10.6 Summary 224

10.7 Figures 225

11 Geomechanical Performance Assessment of Caprock Systems in CO_2-EOR Storage Projects 232

11.1 Introduction 232

11.2 Performance Assessment: Transparency and Elements 232

11.3 Methodology 234

11.3.1 Objective 234

11.3.2 Time Frame 234

11.3.3 Uncertainty 235

11.3.4 Pre-CO2 Injection Performance Assessment 236

11.3.4.1 Scenario Analysis 236

11.3.4.2 Model Development 237

11.3.4.3 Evaluation Against Performance Criteria-Scenario Adjusment 238

11.3.5 Short-Term Performance Assessment 239

11.3.5.1 Scenario Analysis 239

11.3.5.2 Model Development 239

11.3.5.3 Evaluation Against Performance Criteria 239

11.3.5.4 Monitoring and Verification 240

11.3.6 Long-Term Performance Assessment 240

11.4 Geomechanical Performance Assessment of Weyburn 240

11.4.1 Scenario Analysis 240

11.4.2 Uncertainty 241

11.4.3 Model Development 241

11.4.4 Compliance with Performance Criteria 242

11.4.5 Implications for Weyburn's Risk Assessment 242

11.5 Summary 243

11.6 Figures 244

12 Conclusions and Recommendations 245

12.1 Summary 245

12.2 Conclusions 247

12.3 Recommendations and Future Work 251

13 References 254

A. Appendix A – Instruments Calibration 272

B. Appendix B – Stress and Displacement Contours for Base Case Scenario 275

List of Tables

Table 2-1. Estimate of the volumes of CO_2 that can be sequestered below surface [18] 8

Table 5-1. Properties of the permeability measurement system developed. 65

Table 6-1. Mechanical properties of the different anhydrites included in the database 102

Table 6-2. Mechanical properties of anhydrites 104

Table 6-3. Summary of geomechanical tests carried out in Midale Evaporites 106

Table 6-4. Mineralogical Components of Different Midale Evaporite Samples. 109

Table 7-1. Hydrogeological description of the reservoir units 150

Table 7-2. Dynamic elastic properties from dipole sonic logs at Weyburn Phase 1A 151

Table 7-3. Mechanical properties of the caprock system formations 154

Table 7-4. Elastic Modulus of the caprock system formations 155

Table 7-5. Poisson's Ratio of the caprock system formations 155

Table 7-6. Scenarios for geomechanical performance assessment 158

Table 9-1. Elastic properties used for the geomechanical model 207

Table 10-1. Thermal and hydraulic properties for the formations used in the models 220

Table 10-2. Mechanical properties for the formations used in the models 220

List of Figures

Figure 2-1. Trapping mechanisms for geological storage, modified after Benson et al. [12] 13

Figure 2-2. Geological storage options, courtesy of ARC 13

Figure 2-3. Weyburn location, courtesy of EnCana 14

Figure 2-4. Miscible flood roll-out, courtesy of EnCana 14

Figure 3-1. Performance assessment methodology for NWD, modified after Howard et al. [61]. 35

Figure 3-2. Risk management decision making process and the context of performance assessment within it (outlined region), modified after Standards Australia [37] 35

Figure 3-3. The scenario approach for CO_2 storage safety assessment, modified after Wildenborg et al [38] 36

Figure 3-4. Regional pressure-depth plot. Notice the numerous pressure gradients parallel to the hydrostatic pressure gradient, suggesting the presence of multiple pressure cells and the compartmentalization of the basin fluids, modified after Darby et al. [47] 36

Figure 3-5. (a) Lithostratigraphy of the Viking Graben; and (b) Distribution of fluid pressures, minimum horizontal stress, and vertical stresses in the Snorre area, modified after Caillet [50] 37

Figure 3-6. (a) Three-dimensional block diagram including the fault that may have reactivated; (b) Mohr circle during fault reactivation. Failure envelope calculated from shales at ~1800 m that are used as analogues; (c) Pressure and stress versus depth as specific gravity, modified after Grauls and Baleix [54] 37

Figure 3-7. Map of the Leroy Storage facility showing the wells with early leaks and the first tracer survey, modified after Araktingi et al. [56] 38

Figure 3-8. Injection curves for 1978, 1979, and 1980 in the Leroy Storage facility, modified after Araktingi et al. [56] 39

Figure 4-1. Geomechanical mechanisms that affect the hydraulic integrity of caprocks 47

Figure 4-2. Consequences of reservoir production and depletion that may affect the hydraulic integrity of bounding seals 48

Figure 5-1. Schematic of the laboratory equipment developed to evaluate the hydromechanical and seismic properties of caprocks 68

Figure 5-2. High-pressure, high-temperature triaxial cell. The cell is 70 cm tall 69

Figure 5-3. Detailed of the 2.5" (6.35 cm) platens. Notice the connectors for acoustic measurements 69

Figure 5-4. Loading frame and servo-controlled pump for constant strain rate testing 70

Figure 5-5. Close-up view of the internal LVDTs system mounted on a sample. Two LVDTs are mounted parallel to the sample to measure axial displacements, and one LVDT mounted in a change measures radial displacements 71

Figure 5-6. Stability of internal LVDT readings. The LVDT 0198 measures axial displacements while the LVDT 0245 radial. The fluctuations account to $5*10^{-4}$ and $6*10^{-4}$ mm respectively 72

Figure 5-7. Contrast between internal and external LVDT readings 72

Figure 5-8. Contrast between internal and external LVDTs during an entire test 73

Figure 5-9. Side bottoms used to shot and measure travel time of radial seismic waves 73

Figure 5-10. Detailed view of side bottom mounted in the sample for radial acoustic measurements 74

Figure 5-11. Pulse pressure transient technique 74

Figure 5-12. Graphical solution to the TPT, modified after Hsieh et al. [97] 75

Figure 5-13. Upstream pressure decay for different values of specific storage 75

Figure 5-14. Downstream pressure increase for different values of specific storage 76

Figure 5-15. Upstream pressure decay for different permeabilities 76

Figure 5-16. Downstream pressure increase for different permeabilities 77

Figure 5-17. Example of two readings and evaluation of permeability using the pulse pressure technique. Only upstream data were acceptable for calculations 77

Figure 5-18. Downstream readings during a pulse pressure tests. Because of the low pulse applied and the instantaneous jump in pressure, it is impossible to use these readings to calculate permeability 78

Figure 5-19. Change in deviatoric stress and deformation induced by pulsing 78

Figure 5-20. Pressure and flow measurements during constant flow permeability measurements 79

Figure 5-21. Average flow rates for different gradients, and permeability values measured. Notice how stable the measurements are once the flow is more than 0.05 ml/min 79

Figure 6-1. Classification of stiff clays and shales, modified after Morgenstern and Eigenbrod [109]. C_u is unconfined compressive strength and w is moisture content 112

Figure 6-2. Sedimentation compression curves for natural clays, modified after Skempton [118] 112

Figure 6-3. Intact, intrinsic and post-rupture failure envelopes as well as residual strength for Todi Clay, modified after Burland [116] and Burland et al. [129] 113

Figure 6-4. Stress-strain behaviour of mudstones: (a) generalized picture; and (b) London clay, modified after Petley [127] and Johnston and Novello [107] 114

Figure 6-5. Idealized failure envelope for stiff clays, modified after Petley [127] 115

Figure 6-6. Schematic representation of the development and evolution of shear zones, modified after Skempton and Petley [132] 115

Figure 6-7. Permeability of argillaceous material from both laboratory and inversion of flow systems, modified after Neuzil [156]. The range of permeabilities and porosities measured measured in the laboratory for the Midale Evaporite in this thesis and by Dong et al. [70] are included 116

Figure 6-8. North to south cross section of the Cretaceous shales and underlying Dakota Sandstone showing regional vertical permeabilities of the shales. (a) Initial analysis; and, (b) the conceptual model presented by Neuzil and Belitz [71]. Here the shaded and blank area of shales indicate depths of less than and more than one kilometre respectively, modified after Neuzil [184] 117

Figure 6-9. Permeability at large pressures for different argillaceous materials 118

Figure 6-10. Permeability change during shear and consolidation for (a) normally consolidated sample; and, (b) overconsolidated sample. Notice the increment in permeability during shear for OC samples, modified after Zhang and Cox [161] 119

Figure 6-11. Diagrammatic illustration of the different structures observed during the geotechnical cycle, and interpreted fluid pressure relative to hydrostatic. Dots on the respective graphs indicate the fluid pressure at the onset of shear, modified after Bolton and Maltman [163] 120

Figure 6-12. Permeability evolution with mean stress for the overconsolidated sample. Notice the permeability dependence on the mean effective stress post-shear, modified after Bolton and Maltman [76] 120

Figure 6-13. Permeability evolution during triaxial compression in Swiss Alps shales, modified after Renner et al. [164] 121

Figure 6-14. Permeability- mean effective stress relationship for a friable claystone retrieved during ODP Leg 170, modified after Bolton et al. [185] 121

Figure 6-15. (a) Dilation vs. shear displacement for four samples sheared at different effective normal stress; and., (b) change in fracture permeability after shearing the fractures, modified after Gutierrez et al. [77] 122

Figure 6-16. Deere classification updated with the Geological Strength Index (GIS) by Martin et al. [186] for the anhydrite database 123

Figure 6-17. Unconfined compressive strength as a function of anhydrite content 124

Figure 6-18. Relation between elastic properties and unconfined compressive strength for the anhydrite database 124

Figure 6-19. Mohr-Coulomb envelope for anhydrites 125

Figure 6-20. Hoek-Brown envelope for anhydrites 125

Figure 6-21. Summary of triaxial tests carried out in the both the Three Fingers and Midale Evaporite 126

Figure 6-22. Test No. 1, unconfined compression of a Three Fingers sample 127

Figure 6-23. Test No. 1, brittle failure of a Three Fingers sample in an unconfined compression test 127

Figure 6-24. Test No. 2, triaxial compression of a Three Fingers sample carried out under a confining stress of 8 MPa and a pore pressure of 3 MPa 128

Figure 6-25. Test No. 2, brittle failure of a Three Fingers sample sheard under a confining effective stress of 5 MPa. Notice the well-defined shear plane at 32° with the axis of the sample, and the damage induced throughout the sample. The rule measures 15 cm 129

Figure 6-26. Test No. 2, permeability in the fractured Three Fingers sample compared with average intact values for anhydritic samples 130

Figure 6-27. Test No. 2, photograph of the shear plane. Notice the roughness of the faces and the contrast in mineralogy in the Three Fingers unit 131

Figure 6-28. Test No. 3, triaxial compression of a Midale Evaporite sample carried out under a confining stress of 30 MPa and a pore pressure of 3 MPa. It was not possible to achieve failure due to equipment limitations 132

Figure 6-29. Test No. 3, evolution of permeability and specific storage during shear of a Midale Evaporite sample carried out under a confining stress of 30 MPa. The lack of significant change in properties is due to the inability to induce damage in the sample with the experimental equipment available at such a large confining stress 133

Figure 6-30. Test No. 4, cyclic shear of a Midale Evaporite sample carried out under a confining stress of 3 MPa and a pore pressure of 1 MPa 134

Figure 6-31. Test No. 4, evolution of elastic properties of a Midale Evaporite sample sheared cyclically under a confinig effective stress of 2 MPa 135

Figure 6-32. Test No. 4, permeability evolution of a Midale Evaporite sheared cyclically under a confining stress of 3 MPa and a pore pressure of 1 MPa against axial strain 135

Figure 6-33. Effective permeability and minimum capillary displacement pressure for different argillaceous materials using N2 and CO2, modified after Hildenbrand and Krooss [66] 136

Figure 6-34. Breakthrough pressure test history from similar samples from Weyburn caprock samples using N_2, pure CO_2, oil-saturated CO_2/brine system and pure CO_2/brine system, modified after Dong et al. [70] 137

Figure 7-1. Stratigraphic and hydrostratigraphic column at Weyburn, after Khan and Rostron [192] 159

Figure 7-2. Detailed geology of the Madison Group at Weyburn, courtesy of EnCana 160

Figure 7-3. Centres and inflection ellipses of the modeled sequences during the tectonostratigraphic evolution of the Williston Basin, modified after Redly [193] 160

Figure 7-4. Areas of massive salt dissolution around the risk assessment area at Weyburn, after Kreis et al. [223] 161

Figure 7-5. Influence of salt dissolution and erosive periods in the in-situ stresses at the Weyburn Field, Phase 1A 161

Figure 7-6. Pressure versus depth profile (a) in the Weyburn Fiel, and (b) east of the Weyburn Field, after Khan and Rostron [192] 162

Figure 7-7. Water Cut profile at the Midale Field (Beliveau [201]) and water cut profile at the Weyburn Field (Ko et al. [205]). Notice how both fields follow a NE trend similar to the fractures in both fields........ 162

Figure 7-8. Fractures in the Midale Evaporite: (a) synsedimentary cracks, (b) dewatering fractures, (c) fracturing, and (d) long-elongated fractures; after Nickel [197]........ 163

Figure 7-9. Fractures in Late Cretaceous to Late Pleistocene sediments in the Williston Basin, modified after Stauffer and Gendzwill [207] 164

Figure 7-10. Model used to analyze the change in stresses in formations with different stiffnes due to shortening in one direction........ 165

Figure 7-11. Change in stresses perpendicular to shortening direction. The two top lines are the stiff Midale and Frobisher Evaporite, and the lower line is the Midale Beds. Notice how the stresses in the softer bed tend towards tensional values........ 165

Figure 7-12. Location of dipole sonic logs, density logs, and geophysical picks used for geological information to correlate with dynamic elastic properties of the caprock system 166

Figure 7-13. Elastic properties of the stratigraphic column at Weyburn 167

Figure 7-14. Relation between dynamic and static Young's modulus for various sedimentary rocks, data from different authors [224-226] 168

Figure 7-15. Variation of field over dynamic moduls against rock quality for dams built in different lithologies, modified after Deere [175] 169

Figure 7-16. Elastic and mechanical properties of the caprock system at Weyburn, Phase 1A .. 170

Figure 7-17. Estimated in-situ stress regime at Weyburn 170

Figure 7-18. Maximum horizontal stress at the Western Canadian Sedimentary Basin. Data from Bell and Babcok [194] 171

Figure 8-1. Nine-pattern spot at Phase 1A used for geomechanical modeling with the location of the wells used to track displacements 185

Figure 8-2. Displacements in the west-east direction for different "buffer zone" sizes. A buffer zone of 6 km was used for the geomechanical modeling as displacements were becoming insensitive to the size of the buffer 185

Figure 8-3. Displacements in the west-east direction for both constant stress and fixed boundary conditions 186

Figure 8-4. FLAC 3D grid used for the geomechanical modeling. The grid honors the geological structure as much as possible 186

Figure 8-5. Reservoir pressure history at Phase 1A depicted through maximum, minimum and average pressure. Notice how the reservoir pressure has been maintained in average above the in-situ pressure since the waterflood 187

Figure 8-6. Histograms of pressure at four different points in the reservoir's history 187

Figure 8-7. Change of horizontal stress with pressure during depletion for multiple oilfields worldwide, data from Teufel [237] 188

Figure 8-8. Change of both horizontal and vertical effective stress during depletion for multiple oilfields worldwide, data from Teufel [237] 188

Figure 8-9. Change in horizontal stress due to depletion in the Upper Vuggy at Weyburn from the geomechanical simulations 189

Figure 8-10. Change of horizontal and vertical effective stresses at Weyburn from the geomechanical simulations 189

Figure 8-11. Theoretical relation between horizontal stress and pore pressure as a function of Poisson's ration and Biot's coefficient. Notice that the chalk reservoirs presented large subsidence while the sandstone reservoirs did not 190

Figure 8-12. Principal stresses for the Rulison (before and after depletion), and the McAllen field (after depletion). Notice that in both cases the final state of stresses is belowe the damage line. Strength data from Lin [240] and Salz [241] 190

Figure 8-13. Principal stresses for the Weyburn field (before and after CO_2 injection) for the base case scenario. Notice that the final state of stresses is below the damage line during the history of the reservoir. However, once injection pressures are increased around 16% from actual pressures the boundary is crossed 191

Figure 8-14. Stress results from the geomechanical models and pressure evolution. Plots (a), (c), (e), (g), (i), (k) illustrate pre-CO_2 injection results and plots (b), (d), (f), (h), (l) illustrate post-EOR CO_2 storage results where injection pressures have been elevated above operating pressures to test performance limits of caprock. 193

Figure 8-15. Displacements at every formation in the Well 101-14-14-006-14W200 (location shown in Figure 8-1) for the base case cenario.......194

Figure 8-16. Displacements at every formation in the Well 191-10-12-006-14W200 (location shown in Figure 8-1) for the base case scenario.......195

Figure 8-17. Displacements at every formation in the Well 101-16-13-006-14W200 (location shown in Figure 8-1) for the base case scenario.......196

Figure 8-18. Influence of stiffness in deformations, Well 101-14-14-006-14W200 (location shown in Figure 8-1).......197

Figure 8-19. Influence of initial state of stress in deformations, Well 101-14-14-006-14W200 (location shown in Figure 8-1).......198

Figure 8-20. Displacement at each well location showed in Figure 8-1 at the Midale Evaporite for the base case scenario.......200

Figure 8-21. Pressure to induce fault reactivation for base case scenario in a strike slip regime 201

Figure 8-22. Pressure to induce fault reactivation in a reverse fault setting.......201

Figure 8-23. Pressure to induce fault reactivation in a normal fault setting.......202

Figure 8-24. Maximum friction angle at which it is possible to induce normal fault reactivation at Weyburn.......202

Figure 9-1. Modes of salt dissolution [250]: suprajacent dissolution resulting from groundwater penetration; subjacent dissolution resulting from groundwater flow along sub-salt aquifer units; and, lateral dissolution resulting from circulation along the lateral margins of the salt body.......212

Figure 9-2. (a) Minor salt dissolution feature east of Phase 1A, below Phase 1B. This feature has been observed in (b) seismic, and (c) there is a fault that pass by the dissolution zone, after Kreis [223], and Bunge [202].......213

Figure 9-3. Schematic of the geomechanical model.......214

Figure 9-4. Results from elastic analysis for salt dissolution.......215

Figure 9-5. Elastic and plastic analysis for 50 m of salt dissolution, K_0=1.0.......216

Figure 9-6. Subsidence profile and terminology, modified after Whittaker and Reddish [269]..216

Figure 10-1. Model of carbonate reservoir used as a potential CO_2-EOR storage sink.......225

Figure 10-2. Temperature and pressure profiles along the centerline of the carbonate reservoir from 17 days to 208 days of injection 226

Figure 10-3. CO_2 enthalpy at different pressures and temperatures 227

Figure 10-4. Horizontal stresses along the centerline of the reservoir for isothermal and non-isothermal cases, after 208 days of CO_2 injection 228

Figure 10-5. Horizontal stresses from top to bottom of the model at a distance of 7.5 m from the injector, after 208 days of CO_2 injection 229

Figure 10-6. Temperature and pressure profile along the centerline of the formation after 20years of CO_2 injection, deep saline aquifer 230

Figure 10-7. Horizontal effective stress and zone that has failed in tension due to CO_2 injection after 20 years, deep saline aquifer 231

Figure 11-1. Methodology to assess the geomechanical performance of caprock system in CO_2-EOR storage projects 244

Figure A-1. Calibration of internal LVDTs, axial (L) and radial (R). 272

Figure A-2. Calibration of external LVDT. 272

Figure A-3. Calibration of pore pressure gauges. 273

Figure A-4. Calibration of cell pressure gauge. 273

Figure A-5. Calibration of load cell. 274

Figure A-6. Displacement rate vs. flow rate for loading system pump. 274

Figure B-1. West-East stresses in the Watrous Formation. 275

Figure B-2. West-East stresses in the Midale Evaporite Formation. 275

Figure B-3. West-East stresses in the Marly Formation. 276

Figure B-4. West-East stresses in the Upper Vuggy Formation. 276

Figure B-5. West-East stresses in the Lower Vuggy Formation. 277

Figure B-6. West-East stresses in the Frobisher Evaporite Formation. 277

Figure B-7. North-South stresses in the Watrous Formation. 278

Figure B-8. North-south stresses in the Midale Evaporite Formation. 278

Figure B-9. North-South stresses in the Marly Formation 279

Figure B-10. North-South stresses in the Upper Vuggy Formation 279

Figure B-11. North-South stresses in the Lower Vuggy Formation. 280

Figure B-12. North-South stresses in the Frobisher Evaporite Formation 280

Figure B-13. Vertical stresses in the Watrous Formation. 281

Figure B-14. Vertical stresses in the Midale Evaporite Formation 281

Figure B-15. Vertical stresses in the Marly Formation 282

Figure B-16. Vertical stresses in the Upper Vuggy Formation 282

Figure B-17. Vertical stresses in the Lower Vuggy Formation. 283

Figure B-18. Vertical stresses in the Frobisher Evaporite Formation 283

Figure B-19. Pore pressures in the Watrous Formation 284

Figure B-20. Pore pressures in the Midale Evaporite Formation 284

Figure B-21. Pore pressures in the Marly Formation 285

Figure B-22. Pore pressures in the Upper Vuggy Formation 285

Figure B-23. Pore pressures in the Lower Vuggy Formation. 286

Figure B-24. Pore pressures in the Frobisher Evaporite Formation 286

Figure B-25. West-East displacement in the Watrous Formation 287

Figure B-26. West-East displacement in the Midale Evaporite Formation. 287

Figure B-27. West-East displacement in the Marly Formation. 288

Figure B-28. West-East displacement in the Upper Vuggy Formation. 288

Figure B-29. West-East displacement in the Lower Vuggy Formation 289

Figure B-30. West-East displacement in the Frobisher Evaporite Formation. 289

Figure B-31. North-South displacement in the Watrous Formation. 290

Figure B-32. North-South displacement in the Midale Evaporite Formation 290

Figure B-33. North-South displacement in the Marly Formation 291

Figure B-34. North-South displacement in the Upper Vuggy Formation 291

Figure B-35. North-South displacement in the Lower Vuggy Formation. 292

Figure B-36. North-South displacement in the Frobisher Evaporite Formation. 292

Figure B-37. Vertical displacement in the Watrous Formation. 293

Figure B-38. Vertical displacement in the Midale Evaporite Formation. 293

Figure B-39. Vertical displacement in the Marly Formation. 294

Figure B-40. Vertical displacement in the Upper Vuggy Formation. 294

Figure B-41. Vertical displacement in the Lower Vuggy Formation. 295

Figure B-42. Vertical displacement in the Frobisher Evaporite Formation. 295

List of Symbols

A	Area, Depletion stress path
c'	Cohesion
C_b	Bulk compressibility of the sample
C_e	Fluid compressibility time total volume of the flow pump system
C_f	Compressibility of the pore fluid
c_p	Specific heat
C_r	Rock compressibility
C_w	Volume compressibility of the permeating fluid
D	Disturbance factor (Hoek-Brown failure criteria)
E	Young's Modulus
G	Shear modulus
GSI	Geological strength index
H_D	Hydraulic head downstream
H_U	Hydraulic head upstream
K	Hydraulic conductivity
k	Permeability
K_0	Coefficient of earth pressure
K_b	Rock bulk modulus
K_g	Rock mineral bulk modulus
k_t	Thermal conductivity
l	Length of the sample
$1/M$	Specific storage coefficient at constant strain (Biot's modulus)
m, s	Rock mass parameters (Hoek-Brown failure criteria)
P	Pressure
P_D	Downstream pressure

P_U	Upstream pressure
Q	Flow rate
S_u	Unconfined compressive strength
T	Tensional strength
V_f	Total volume of the flow pump system
V_P	Compressional velocity, Pore volume
V_S	Shear velocity
B_d	Storage capacity of the flow system downstream
B_S	Storage capacity per unit volume of the fluid-sample system
B_U	Storage capacity of the flow system upstream
α	Biot's coefficient, Linear coefficient of thermal expansion
ε	Strain, Error
ε_f	Strain at failure
ε_{kk}	Bulk strain
ϕ	Porosity, Friction angle
η	Dynamic viscosity
λ	Lamé constant
μ	Pore pressure, Average friction coefficient
ν	Poisson's Ratio
ρ	Density
σ'	Effective stress
σ'_1	Major principal effective stress
σ'_3	Minor principal effective stress
σ_{ci}	Unconfined compressive strength (Hoek-Brown failure criteria)
σ_f	Deviatoric stress at failure

σ_H	Maximum horizontal total stress
σ_h	Minimum horizontal total stress
σ_{ij}	Stress tensor
σ_n	Normal stress
σ_v	Vertical total stress
τ	Shear stress

1 Introduction

1.1 Statement of the Problem

The natural greenhouse effect is a well-understood phenomenon whereby gases such as methane, ozone, carbon dioxide, and water vapor contribute to the warming of the earth's atmosphere by absorbing and re-emitting the infrared or heat radiation [1]. Without this, global mean annual temperature would be about -6°C instead of the current 15°C [2]. Among the different greenhouse gases (GHG) CO_2 is not the most effective, with one molecule causing 0.13 times the effect of one molecule of CH_4, however, CO_2 accounts for around 56% of the anthropogenic greenhouse effect at present [3], and although hotly debated, there is growing acceptance that increasing CO_2 emissions are contributing to the rise of global temperature. The possible consequences of such climate change are causing international concern.

Geological storage can serve a powerful role as an emissions reduction technology but the acceptance of this new "paradigm" will require a view of geological storage as safe and environmentally sound. Caprock and reservoir integrity as well as an adequate understanding of the possible leakage mechanisms through the caprock is one of the technical development issues of critical importance to the safe and effective implementation of geological storage. The IEA[1] Weyburn CO_2 Monitoring and Storage Project offers one of the best opportunities to conduct a performance assessment of a caprock system overlying a large scale storage project.

The IEA Weyburn CO_2 Monitoring and Storage Project is an enhanced oil recovery (EOR) project, where CO_2 injection is used to carry out a miscible flood. The Weyburn field is a matured reservoir, and although depleted oil and gas reservoirs are regarded as safe sinks for geological storage of greenhouse gases, the depletion of reservoirs can give rise to a variety of coupled physical and chemical processes, which may affect the hydraulic integrity of bounding seals, both caprocks and wellbores. Therefore, the project presents not only the opportunity to carry out a performance assessment of a caprock system, but to gain a better understanding of safety issues associated with the history of the reservoir for storage projects.

---

[1] International Energy Agency

1.2 Objectives and Scope

Geological storage of CO_2 is a promising novel technology to reduce emissions of CO_2 into the atmosphere. However, such a technology has many particularities, such as large scales and long timeframes that make it different from any other waste disposal technique. Consequently, there is the need for performance assessment of the system to gain confidence that CO_2 storage is a safe and sound process. The IEA Weyburn CO_2 Monitoring and Storage Project is the first large-scale project in CO_2-EOR storage in the world, and as such a prime opportunity to addresse many of the scientific and technical concerns that CO_2 storage raises.

This thesis will put into context the geomechanics implications of injecting CO_2 into deep geological formations and it will carry out the geomechanical performance of Weyburn's reservoir and caprock. The main research objectives are:

i. Develop an understanding of the impact that geomechanics has in the performance of the reservoir and its caprocks, with particular attention to caprock integrity.

ii. Carry out a geomechanical performance assessment of the caprock system at Weyburn. This task will be accomplished through the following research tasks:

    a. Utilize the available information of the Weyburn reservoir to characterize it as well as its caprock, in order to build a realistic model for geological storage. Such a task will include geomechanical testing on Weyburn's anhydrites, gathering and interpretation of data such as geological studies, geophysical surveys, reservoir modeling and others.

    b. To build an earth model that will put "numbers" to the caprock system geological model for the most relevant hydraulic, mechanical and seismical parameters, as well as any other relevant information for performance assessment.

    c. Develop a geomechanical model, where the influence of the history of production and exploitation of the reservoir will be studied through geomechanical modeling. Such modeling will also include a sensitivity analysis of parameters such as in-situ stresses and material properties.

    d. Analyze the specific scenario of salt dissolution, a phenomenon that has occurred extensively in the Williston Basin. Such analysis will include the influence of salt dissolution on the actual integrity of the reservoir, and the possible influence of future dissolution in the basin.

iii. Using the geomechanical performance assessment of Weyburn's caprock system, a methodology will be developed and generalized to evaluate the geomechanical performance assessment of the sink and its caprock for geological storage projects.

1.3 Organization of Thesis

The concept of geological storage is presented in Chapter 2. It provides an overview of the trapping mechanisms, the different types of geological sinks, and introduces the IEA Weyburn CO_2 Monitoring and Storage Project. In Chapter 3 an overview of the concept and general methodology of performance assessment is given, a working performance criterion is developed, and the particularities that geological storage of CO_2 projects have for performance assessment are reviewed. Chapter 4 develops specific considerations for disused oil and gas reservoirs, focusing on the geomechanical issues that may affect the suitability of these formations as safe storage sites.

Chapter 5 details the laboratory work, presenting the triaxial testing apparatus developed for this project, and finally gives an overview of permeability techniques for low permeability geomaterials. Following Chapter 5, Chapter 6 presents the laboratory testing results, and contextualizes them with a literature review of behavior of anhydrites and shales as caprocks.

Chapter 7 develops the mechanical earth model at Weyburn, which includes a review of the geology and hydrogeology of the site. Chapter 8 presents the results of the geomechanical modeling carried out to assess the reservoir integrity both during exploitation and production, and when the volume of CO_2 injected is going to be maximized. Chapter 9 addresses the issue of what geomechanical impact salt dissolution in the Williston Basin may have in the reservoir and its hydraulic integrity. Then Chapter 10 studies the thermal effects associated with CO_2 injection in the integrity of the reservoirs and its bounding seals.

Chapter 11 develops a methodology to assess the performance of a caprock for geological storage projects. Such a methodology encompasses all the knowledge and understanding gathered from the Weyburn project in a pragmatic methodology that can be applied elsewhere. Finally, Chapter 12 presents the conclusions and recommendations based on study of the geomechanical performance assessment of the Weyburn Field.

2 Geological Storage

2.1 Introduction

In 1958 the AAPG[2] acceded to a request from the atomic energy industry to assist in the evaluation of geologic basins as possible sites for the safe subsurface disposal of radioactive wastes [4]. Likewise, in the early history of the petroleum industry operators injected salt-water wastes into shallow and deep permeable sandstones, until it became obvious that the brine was contaminating fresh-water sands, and subsequently became a regulated practice [4]. Moreover, in the 1960's different industries found in deep-well injection a possible solution for disposal of wastes, and by August of 1968, the first proceedings on "Subsurface Disposal in Geologic Basins –A Study of Reservoir Strata-" were published by the AAPG [5].

By 1968 there were more than 110 deep industrial-waste injection wells in the United States, which were used for a large variety of wastes and in quite different conditions [6]. From previous experience Warner [6] compiled a set of general considerations for carrying out waste-injection successfully. Among these considerations were:

- an injection zone with sufficient permeability, porosity, thickness, and areal extent to act as a reservoir;
- an injection zone that is vertically below the level of fresh-water circulation and is confined vertically by rocks that are, for practical purposes, impermeable to waste liquids.

By the 1990's the concept of geological sequestration of GHG began to be explored. In 1992, Koide et al. [7] stated: "there exist huge volumes of unused aquifers in the earth due to high salinity of the groundwater. Deep aquifers can contain large amounts of CO_2 in the form of compressed gas, liquid or aqueous solution under formation pressure". Moreover, Koide et al. [7] raise concerns about the ideal geological setting that could act as a trap sequestering large volumes of CO_2, limiting the risk of leakage out of the trap through a caprock to avoid the contamination of the sea or aquifers used for other purposes. In 1994 Hangebrauck [8] analyzed different options to mitigate carbon emissions into the atmosphere, including geological disposal. He posed some complex questions associated with capacity, rates of injection, and suitability of this option; as well as how the process may deteriorate the mechanical condition of the geological structures involved, and even what is the potential for catastrophic release of CO_2.

---

[2] American Association of Petroleum Geologists

Therefore, the idea of waste storage in deep geological formations has been around for some time, and for geological storage of CO_2 the concept has evolved into reality with the actual operation of CO_2 storage facilities such as the Sleipner Field in the North Sea, and the IEA Weyburn CO_2 Monitoring and Storage Project.

2.2 The Concept of Geological Storage of GHG

In order to mitigate the effects of global warming seen recently, a reduction of carbon dioxide emissions must be accomplished by either using alternative sources of energy, capture and re-utilization of carbon dioxide, or the long-term disposal of carbon dioxide [9]. In 1999, the Department of Energy (DOE) of United States published "Carbon Sequestration Research and Development"[10], a road map to develop the scientific understanding of carbon sequestration to make this option environmentally acceptable. DOE defines carbon sequestration as: "the capture and secure storage of carbon that would otherwise be emitted to or remain in the atmosphere. The idea is; (1) to keep carbon emissions produced by human activities from reaching the atmosphere by capturing and diverting them to secure storage, or (2) to remove carbon from the atmosphere by various means and store it". The concept of geological storage of GHG falls into the first idea, where a geological formation is used as a container to store large volumes of GHG that otherwise will be emitted to the atmosphere. GHG are captured at large point sources such as power plants or natural gas reservoirs, and injected into geological formations. The most likely sinks are deep saline aquifers, disused oil and gas reservoirs, unmineable coalbeds or salt caverns.

Four primary mechanisms of trapping have been proposed for geological storage, Figure 2-1:

- Physical or hydrostratigraphic trapping, which results from CO_2 migration driven by regional-scale flow velocities (most likely a few centimetres per year). Such low flow velocities would allow sufficient time for CO_2 to dissolve into the formation water and become subject to diffusion, dispersion and convection [3, 9, 11].
- Solubility and ionic trapping in which CO_2 is dissolved into the in-situ reservoir fluids [12].
- Geochemical trapping, which involves geochemical reactions that sequester CO_2 in the form of carbonate minerals. The advantage of this trapping mechanism is that the minerals are stable and CO_2 is effectively immobilized for geologically important

timescales [3, 9, 11]. Over very long timescales, mineral trapping is likely to be the dominant trapping mechanism for CO_2 [13].

- Irreducible saturation, which is that portion of the porosity from which residual CO_2 cannot be physically displaced. Its value is a function of the pore size and structure (strictly speaking, the CO_2 can always be chemically removed by flowing undersaturated water around it).

Over time the dominance of these mechanisms changes. In the short-term or injection stages, the physical trapping where a competent caprock will provide the containment for the injected CO_2 whether it goes into solution or not, and before any geochemical reaction that can fix large volumes of CO_2 for geological times can occur. The time scale and rate of each mechanism is site specific and depends on the type of formation used for storage and the fluids in the formation [12]. However, the caprock will see large injected volumes of CO_2 that will dramatically increase near wellbore pressures, change the flow regime, the temperature, and the chemical environment in the sink. One primary concern in the short-term is the stability of the caprock seals, the integrity of the reservoir, and the sink reaction to a rapidly changing environment, which in turn affects their geomechanical, geochemical, and hydrogeological properties.

2.3 Geological Sink: What it is

A geological sink for CO_2 storage is a system composed of a suitable porous medium for injection of large volumes of CO_2 and competent bounding seals that will provide physical trapping. However, the porous medium and the caprock must have certain conditions as different authors have stated [3, 14-16], and these are compiled below.

2.3.1 The Porous Medium

The characteristics of the porous medium are a significant porosity and permeability, proximity to any anthropogenic CO_2 source, and being located in a stable geological setting [3, 16]. Ideally, such a medium will be deeper than 800 m, a depth where temperature and pressure will guarantee that the CO_2 is in supercritical state. CO_2 in supercritical state has an average density of 700 kg/m^3, and as a consequence much less volume (<0.3%) compared to its gaseous form under surface conditions [16]. However, in the case of CO_2-EOR storage projects shallower depths may be considered because the economics from oil recovery may drive the project.

2.3.2 Bounding Seals

Bounding seals constitute the barrier against migration of CO_2 in geological storage projects. Bounding seals are compromised of two elements; the overlying (and possible underlying) caprocks and the wellbores used for reservoir access. The concept of seal or caprock is normally used in the evaluation of a potential hydrocarbon accumulation [17]. In this case, a seal is a sediment, rock or immobile fluid with a high to very high capillary entry pressure. Seal capacity is the capillary pressure at which hydrocarbon will leak into a seal. Therefore, when evaluating a seal as a component of a hydrocarbon accumulation, the two properties that characterize the seal are its capillary entry pressure and the hydrocarbon column height.

However, for geological storage the concept of seal or caprock is different. A seal or caprock is a geological formation capable of hydraulic sealing over geological times, that is it will maintain its sealing properties despite geomechanical, geochemical, and hydrogeological changes. Such a definition is vastly different from that of petroleum applications, making the performance assessment of caprocks rather complex because, essentially, a caprock is no longer a capillary seal at certain points in time and conditions, but a hydraulic seal in a changing environment over time.

The other bounding seals are wellbores used for reservoir access. A wellbore is a potential flow path for leakage because it is a channel through the overburden that connects the surface with the reservoir. It is important to note that a wellbore does not have to penetrate the reservoir to be a potential leakage path. As long as there is hydraulic communication between the well and the reservoir, CO_2 can escape.

2.3.3 The Concept of Hydraulic Integrity

Hydraulic integrity is used qualitatively to describe whether a bounding seal -either a caprock or a wellbore- is performing adequately i.e., its transport properties are low enough that allows them to serve as hydraulic seals for geological storage. The hydraulic integrity of bounding seals can potentially change during the lifetime of a project, and in order to make CO_2 storage viable, there must be enough knowledge and understanding as to how both exploitation and production (in the case of disused hydrocarbon pools), and the injection of CO_2 affect hydraulic integrity, how that effect can be quantified, how it can be predicted and if the effect is detrimental, how it can be avoided or mitigated.

2.4 Possible Geological Sinks

Among the different options for geological sequestration of GHG are: depleted oil and gas reservoirs, abandoned salt caverns, the ocean, unmineable coal beds, and deep saline aquifers, Figure 2-2. Each of these has its own advantages and disadvantages, and even objectives, as will be seen below. Also, it is important to be aware that the volumes of carbon that can be sequester in each of these formations is substantially different, Table 2-1.

Table 2-1. Estimate of the volumes of CO_2 that can be sequestered below surface [18]

Sequestration Option	Worldwide Capacity[3]
Oceans	1000s GtC
Deep saline formations	100s-1000s GtC
Depleted oil and gas reservoirs	100s GtC
Coal seams	10s-100s GtC

2.4.1 Geological Storage in Deep Saline Aquifers

Deep saline aquifers have received a lot of attention because they are the most promising option for sequestration of GHG. First of all, there are deep saline aquifers almost everywhere, which means that usually there will be one of these formations near any source of GHG. Secondly, significant volumes of GHG could be stored within the porous space of deep saline aquifers, far more that can be stored in the other formations. Finally, as many authors have suggested, storage over geologically long time periods is likely in these formations [10, 13, 16, 19]. Lateral containment in deep aquifers may not be necessary due to hydrodynamic and geochemical trapping within the aquifer, which could ultimately trap the CO_2 over geologically long periods [20, 21]. However, there is not economical profit in sequestering in deep aquifers as there is in enhanced oil recovery (EOR) or enhanced gas recovery (EGR); although if a carbon tax for emitting GHG to the atmosphere is implemented, sequestration in deep aquifers may become very attractive as it is the case of the Sleipner West Field[4] [22].

---

[3] Worldwide total anthropogenic carbon emissions are ~7GtC per year (1 GtC=1 billion metric tons of carbon equivalent).

Bounding seal integrity in deep saline aquifers will likely be governed by the presence of pre-existing discontinuities and the induced buoyancy driven flow of CO_2 through those discontinuities. Concerns about leakage due to hydraulic fracturing or shearing of caprocks are minor because the facilities will be designed such that pressure build-up is minimized through injection of CO_2 in "sweet spots" of large permeability, leading to minimal geomechanical impact on caprock integrity. However, an appropriate characterization of the reservoir will be challenging and unexpected issues may come along during operation.

The Sleipner Field is the first commercial sequestration project in the world, which is operated by the Norwegian company STATOIL [22, 23]. In this project STATOIL exploits the Sleipner gas field in the North Sea, but the CO_2 content of the gas is between 4 to 9.5%, and Norway has in place an emissions tax. The project has been in operation since 1996, a million tonnes of CO_2 are injected every year, and the project is planned to operate for 20 more years. STATOIL separates and injects the CO_2 from the gas field into the Utsira Formation, a sandstone formation at 800 m depth, of excellent quality that allows high rates of injection, and where bottomhole pressures due to CO_2 injection have changed very little [22, 23]. Aquifer thickness ranges from 150 to 250 m, and is overlain by the thick Hordaland Shale Formation.

In deep saline aquifers it is likely the only wellbores present will be those related with storage of GHG, which are boreholes for site investigation, injection, and monitoring. Therefore, there is reasonable certainty that these wellbores will be drilled and completed with state of the art techniques. However, this does not guarantee its integrity both in the short- and especially in the long-term, so wellbores must be included in the performance assessment of the bounding seals.

2.4.2 Disused Oil and Gas Reservoirs

When an oil field ceases production it is because the field has become uneconomic, not because most of the oil has been produced. Disposal of CO_2 in depleted oil reservoirs is used usually as an EOR technique, where CO_2 is injected into mature reservoirs, and additional oil is recovered. CO_2 reduces the oil viscosity and interfacial tension (capillary pressure), increases the field pressures and improves the sweep efficiency resulting in the recovery of up to 40% of the residual oil [24].

---

[4] Norway has a $38 carbon tax in place per tonne of CO_2 emitted into the atmosphere.

It is more attractive to consider the project as an EOR operation than purely storage of CO_2. Moreover, the CO_2 injected will eventually breakthrough at the producing wells with the recovered oil, making the residence time very short, and the amount of CO_2 sequestered uncertain, although it is thought that much of the injected CO_2 will remain stored [24].

On the other hand, storage of CO_2 into gas reservoirs can be done either in abandoned fields, or in depleted but still active fields where gas recovery could be enhanced by CO_2 injection [10]. The use of depleted gas reservoirs as waste repositories is not uncommon in petrochemical and oil and gas industries, and therefore the investigation into their ability as potential receptors for GHG is a natural extension. The amount of gas that is produced from the reservoir will determine the volume of pore space available for CO_2, minus a few percentage points [21]. Ideally, depleted gas reservoirs should be utilized soon after abandonment to maximize the amount of pore space available for CO_2 storage; otherwise, the available pore space will become occupied with water, resulting in less pore space for CO_2 [21].

The integrity of bounding seals in disused oil and gas reservoirs presents many geomechanical challenges because of the history of the field, which will be addressed throughout this thesis, and presented in detail in Chapter 4.

2.4.3 Salt Caverns

Salt caverns have been used in the petroleum and petrochemical industries as underground storage vessels for oil and gas, and waste repositories. Bachu [16] suggested that a single salt cavern is capable of holding 500000m^3, at up to 80% of the fracturing threshold pressure. However, because of the small volumes that can be stored and the scarce presence of salt deposits, this option is not practical for geological sequestration of GHG where the volumes to be stored are quite large, and the transport of GHG can be very expensive and risky.

2.4.4 Unmineable Coal Beds

The Western Canadian Basin is home to a large amount of coalbeds suitable for methane production. Coal Bed Sequestration (CBS) involves injection of CO_2 into deep unmineable coalbeds. Within the microstructure of the coalbed there is adsorbed methane, the amount of methane stored is based on the confining pressure, temperature and microporosity of the coal bed surface area. CO_2 can be used as an EGR technique where for every molecule of CH_4 desorbed, two molecules of CO_2 will be adsorbed, based on adsorption isotherms [24]. The storage capacity for sequestering CO_2 could potentially be similar to that of deep aquifers, with the added benefit of producing CH_4 as a fuel source. Bachu et al. [24] suggest that CBS can potentially sequester CO_2 for mid to long residence times, depending on the geological conditions. This technology appears to be promising, and research into this area is on going.

2.5 The IEA Weyburn CO_2 Monitoring and Storage Project

The IEA Weyburn CO_2 Monitoring and Storage Project is a major research project that has as an overall objective of understanding the mechanism of and extent to which greenhouse gases, particularly carbon dioxide, can be permanently and safely sequestered/stored in geological formations [25]. The project will focus on the direct injection of CO_2 into a partially depleted oil reservoir as part of a large-scale, commercial, enhanced oil recovery operation at Weyburn, Saskatchewan, Figure 2-3. The CO_2 is transported via pipeline from a gasification plant in Buelah, North Dakota. The goal is to confirm the ability of an oil reservoir to geologically contain, isolate and permanently store a significant amount of CO_2. Furthermore, results will be applicable to other reservoir situations where permanent CO_2 storage is contemplated. The ultimate deliverable is a credible assessment of the permanent containment of injected CO_2 determined by long-term predictive simulations and formal risk analysis techniques [25]. Such assessment will help answer questions by regulatory bodies as to the safety and robustness of storage of large volumes of CO_2 not only in the Williston Basin but also in other areas where geological similarities exist.

2.5.1 History of the Weyburn Field

The Weyburn Field is a major oil field in southeastern Saskatchewan, Canada. The Weyburn Field was discovered in 1954. The oil is located in a carbonate reservoir of Mississippian age with an upper seal of anhydrite. Initial oil in place is estimated at approximately 1.4 billion barrels (221000000 m^3) [26]. The Weyburn Field covers an area of about 180 km^2 and produces 22 to 33° API gravity crude oil from Mississippian shallow-water carbonates at a mean depth of 1450 m [27]. Pay thickness ranges from 5 m to over 30 m with an average of about 10 m. Following its discovery in 1954, the Weyburn Field was exploited by primary depletion for about 10 years. Production declined and in 1964 the reservoir was waterflooded, achieving maximum rates of more than 7000 m^3/day by 1966. Production then decreased to 2000 m^3/day by 1985. An aggressive vertical infill program began in 1986, bringing back the production to almost 4000 m^3/day. Horizontal drilling was introduced in 1991, becoming the favored production strategy for over 10 years. By the mid 1990s, planning for CO_2 miscible flood was well underway and CO_2 injection began in the fall of 2000, Phase 1A area, Figure 2-4 [28, 29].

The Weyburn Field has undergone an aggressive scheme of production and stimulation, which raises certain concerns about the integrity of the reservoir to store CO_2. Therefore, it is necessary to evaluate the risk of loss of hydraulic integrity in the Weyburn project in order to ensure that any volume of stored CO_2 will be contained, and the rate of leakage is within acceptable limits. Any performance assessment for an EOR project must be divided in two components: (i) evaluate the evolution of the hydraulic integrity of the reservoir from the moment production is initiated, until injection of CO_2 begins (pre-CO_2 injection). These results will allow identification of critical areas for leakage, and will help with the design of the facilities and the monitoring scheme. (ii) Assess hydraulic integrity during injection and closure (CO_2 injection and abandonment). The two phases of the approach are a necessity. If the state of the bounding seal prior injection of CO_2 is unknown, it will be next to impossible to defend the integrity under the ensuing CO_2 flooding conditions.

2.6 Figures

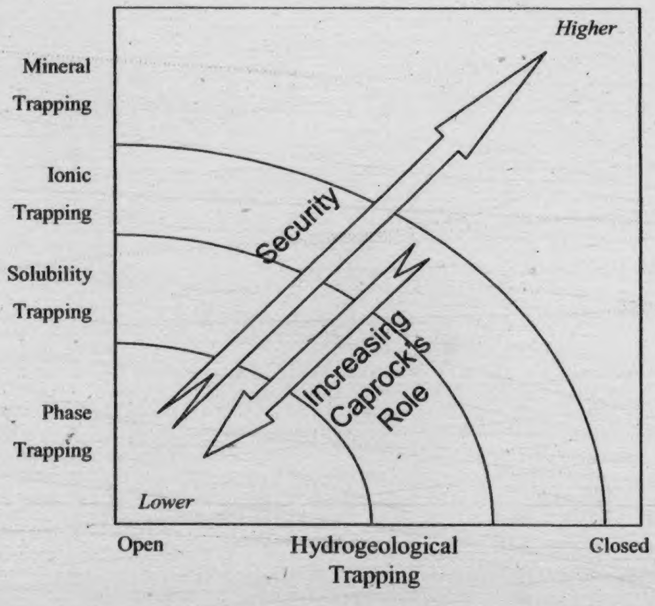
Higher
Mineral Trapping
Ionic Trapping
Solubility Trapping
Phase Trapping
Security
Increasing Caprock's Role
Lower
Open
Hydrogeological Trapping
Closed

Figure 2-1. Trapping mechanisms for geological storage, modified after Benson et al. [12]

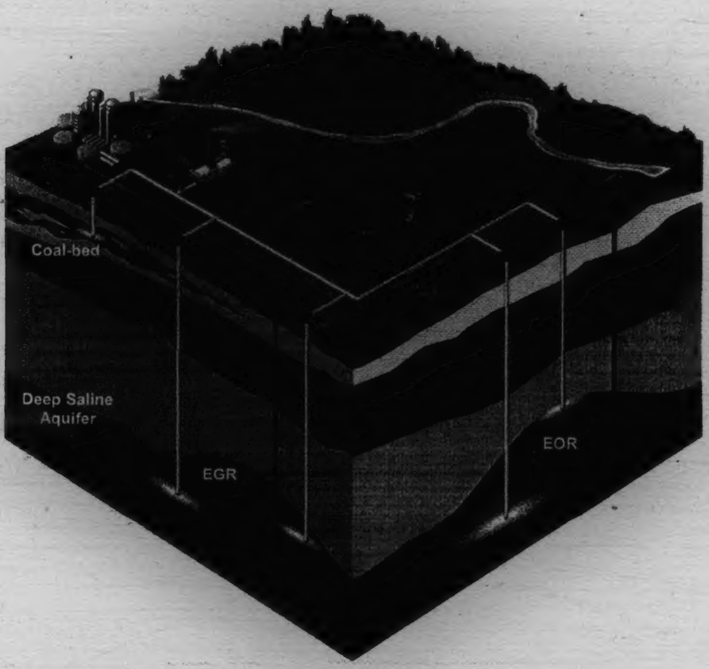
Coal-bed
Deep Saline Aquifer
EGR
EOR

Figure 2-2. Geological storage options, courtesy of ARC

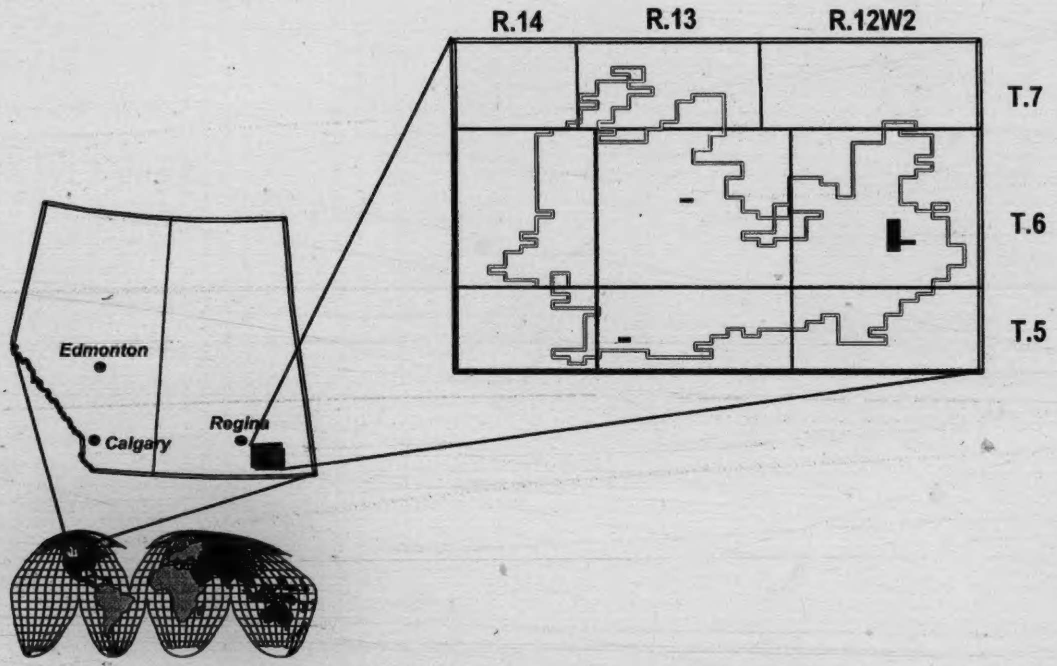
R.14
R.13
R.12W2
T.7
T.6
T.5
Edmonton
Calgary
Regina

Figure 2-3. Weyburn location, courtesy of EnCana

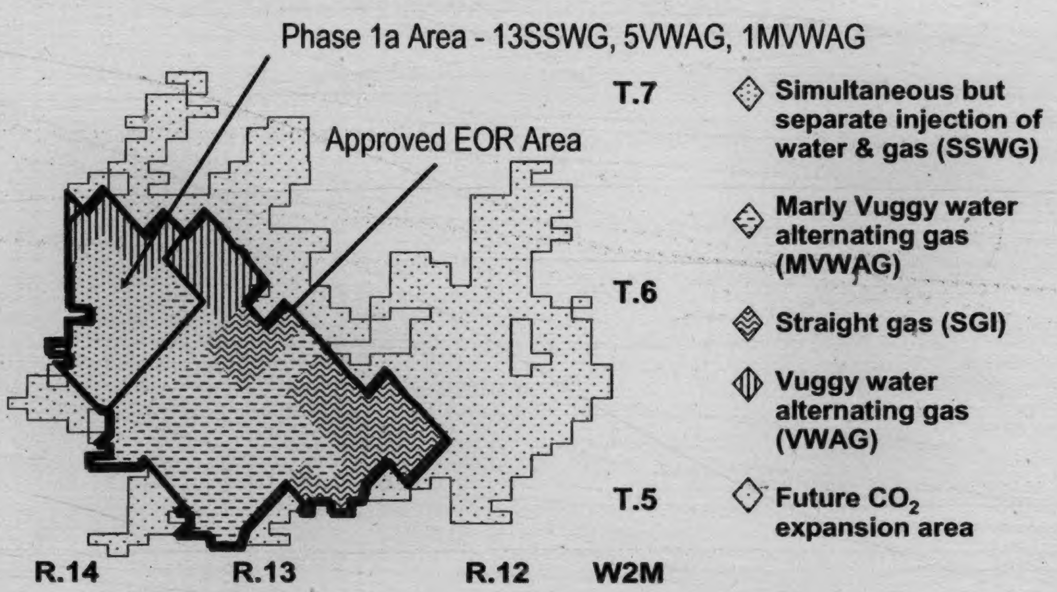
Phase 1a Area - 13SSWG, 5VWAG, 1MVWAG
Approved EOR Area
T.7
T.6
T.5
R.14
R.13
R.12
W2M
Simultaneous but separate injection of water & gas (SSWG)
Marly Vuggy water alternating gas (MVWAG)
Straight gas (SGI)
Vuggy water alternating gas (VWAG)
Future CO2 expansion area

Figure 2-4. Miscible flood roll-out, courtesy of EnCana

3 Performance Assessment for CO_2-EOR Projects

3.1 Introduction

CO_2 storage, as any other engineered waste disposal system must be designed to ensure that the risks of harmful waste release to the environment is so low that it is acceptable to the regulatory authorities and the public. A waste disposal system is considered successful when it performs, where performance requires considerations of safety, serviceability and affordability [30]. The ultimate goal of a performance assessment for geological storage of CO_2 is to determine whether the CO_2 will remain in the reservoir over an extended period of time, or it will migrate into the overburden and eventually the ecosystem. However, there are clear differences between the requirements for both short- and long-term storage, which may be addressed considering each situation independently.

As was mentioned in Chapter 2, in the short-term or injection stages the main trapping element is a competent caprock, and in the long-term solubility and ionic, geochemical and/or irreducible saturation trapping will be the basic trapping mechanisms that will keep CO_2 from reaching potable water sources and/or the biosphere, Figure 2-1. When the main mechanism is hydrostratigraphic trapping, the movement of the CO_2 plume and the continuity and stability of the bounding seals will determine its performance. When solubity or geochemical trapping are the main mechanisms, the fluid properties, environmental conditions and chemical reactions between the plume and the rock will control its performance, and when irreducible saturation trapping is the control mechanism, its performance will be given by the pore structure of the porous media and the regional flow. Nonetheless, in the short-term the caprock and its performance assessment become critical to the successful implementation of geological storage of CO_2.

Consequently, a CO_2-EOR storage project must undergo a rigorous safety assessment to guarantee the optimum performance of the overall waste disposal system, and the performance of the different systems and subsystems. The present work is concerned specifically with the performance assessment of the caprock system at the Weyburn Field; hence the basic concepts for performance assessment are reviewed in this chapter, highlighting the most relevant issues for CO_2-EOR storage, and developing a preliminary methodology for the performance assessment of caprocks, which is developed in more detail in Chapter 10.

3.2 Performance and Safety Assessment

Performance assessment (PA) for waste disposal systems has its origins in the management of nuclear wastes and the seeking for approval of nuclear repositories. The Nuclear Energy Association (NEA) and the Organisation for Economic Co-operation and Development (OEDC) [31] define performance and safety assessments as "an analysis to predict the performance of a system or subsystem, followed by comparison of the results of such analysis with appropriate standards and criteria. A performance assessment becomes a safety assessment when the system under consideration is the overall waste disposal system and the performance measure is a global measure of impact on safety". The major goals of a performance assessment are [31]:

- developing a sufficient understanding of the physical and chemical behavior of a disposal system;
- quantifying this understanding in order to allow predictions of future system behavior;
- assessing the uncertainties in the predictions; and
- convincing all relevant groups of the adequacy of the analyses.

From this definition it is clear that a performance assessment can be used for a variety of systems at different levels, while safety assessment is reserved for the overall system and its impact. A safety assessment consists of a number of interrelated elements, and there is constant feedback and iteration through the safety assessment, Figure 3-1 [31-33]:

- broad identification of the possible future evolution of the selected disposal system. This process is called scenario development;
- development and application of appropriate models;
- evaluation of potential consequences of release (leakage) and migration in an integrated assessment;
- uncertainty and sensitivity analysis;
- validation and review of all components of the assessment; and
- comparison of the results with criteria.

The U.S. Environmental Protection Agency (EPA) has a similar definition, but it is explicit about the use of probabilistic techniques within PA. PA is defined as "… an analysis that: (1) identifies the processes and events that might affect the disposal system; (2) examines the effects of these processes and events on the performance of the disposal system; and (3) estimates the cumulative releases of radionucleides, considering the associated *uncertainties*, caused by all significant processes and events. These estimates shall be incorporated into an overall probability distribution of cumulative releases to the extent practicable" [34].

In the case of geological storage of CO_2 performance assessment is defined as "…the process of evaluating the behavior or "performance" of an element of a geological storage project ***relative to one or more performance standards***. Performance has both engineering and safety aspects incorporated in the assessment. Thus, performance may be expressed in terms of the ability of the reservoir to retain the CO_2 as a function of time. In order to assess such performance, the long-term fate of CO_2 initially injected into a geologic formation must be determined. Ultimately, if the CO_2 migrates far enough to the environment, and the flux of CO_2 to the environment is sufficiently low, that this does not pose a potential safety hazard" [35].

It is clear that the three definitions presented above for PA are in essence quite similar, and the differences are more methodological than anything else. In general terms the approach to performance and safety assessments includes the following interrelated steps [31, 32]:

- the wastes that require disposal need to be identified and characterized;
- the potential repository site must be identified and characterized;
- the engineering design for the repository must be specified;
- the main processes determining the leakage and migration of the waste from the disposal system to the ecosystem must be identified;
- the behavior and evolution of the disposal system must be studied;
- the disposal system's overall behavior has to be evaluated. This step only applies to safety assessments, not performance assessments; and,
- the assessment result has to be compared with the design goals and the regulatory criteria. This step only applies to the safety assessment. However, for performance assessment working criteria to different systems must be enforced, but they do not necessarily have to come from a regulatory body.

Also, it is important to undestand that PA is an iterative process [36]. Initially, PA can be primarily exploratory and relatively simple. It provides opportunity for:

- uncertainty and sensitivity analysis;

- gainining insight to the problem in hand;
- an external review and engagement of regulator and stakeholders, and initiation of a quality assurance (QA) program;
- setting the foundation for experimental programs and data development, as well as model development; and
- a computational structure for a fully integrated analysis to be developed.

Intermediate stages of PA are typically more complex, and usually present the best opportunity to push the limits in model complexity. Intermediate PA has the following qualities:

- there are improvements in the physical understanding of the problem and the models used to simulate systems;
- there is a better gathering of information and knowledge from the different parties involved;
- it allows the identification of errors in both analysis and models;
- it gives more weight to uncertainty and sensitivity analysis, and external reviews are more comprehensive; and
- there is a continuation in the engagement and education of stakeholders and regulators.

The final PA benefits from the experiences of the prior analyses. This iterative process pays dividends through:

- a well-defined and well tested analysis system;
- an analysis focused on recognized needs and requirements;
- the use of models that meet the requirements of the analysis, as well as accepted simplified models;
- continuing to build its soundness on QA procedures emplaced and employed throughout the process; and,
- a more constructive and stronger interaction with reviewers, stakeholders, and regulators that have been involved throughout the PA.

3.2.1 Performance Assessment and Risk Management

Performance assessment forms a key component of a risk assessment for any geological storage project, and ultimately feeds into the entire risk management process. The risk management process provides a comprehensive decision process that aids decision-makers in identifying, analyzing, evaluating and controlling all types of risks, including risks to health and safety. The objective of risk management is to ensure that significant risks are identified and that appropriate action is taken to minimize these risks. Such actions are determined based on a balance of risk control strategies, their effectiveness and cost, and the needs, issues and concerns of stakeholders. Communication among stakeholders throughout the process is a critical element of this risk management process. Decisions made with respect to risk issues must balance the technical aspects of risk with the social and moral considerations in the project. The activities associated with performance assessment within the context of a full risk assessment are outlined in Figure 3-2 [37].

3.3 Performance and Risk Assessment Methodology for Geological Storage of CO_2

Wildenborg et al. [38] have developed a methodology for safety assessment of CO_2 sequestration that consists of three major steps, scenario analysis, model development and consequence analysis, Figure 3-3. This method is based on risk assessment studies on the storage of radioactive waste, but it has been adapted to the particularities and challenges that geological storage present.

3.3.1 Scenario Analysis

The core of the methodology is the systematic development of a limited number of scenarios that describe the risk sources, migration and impact routes relevant to health, safety and environment (HSE) [39]. A scenario consists of an assemblage of interdependent features, events and processes (FEPs). Thus, scenario development is the conception and definition of all possible futures to be considered in the subsequent modeling and consequence calculations [31, 32]. Systematic approaches to the development of scenarios are done currently through brainstorming sessions, databases, and many other engineering systems.

As was mentioned before, PA can be carried out either in a sub-system or the whole system. Leijnse et al. [40] recognize this fact, and split the system into what they call spatial compartments:

- CO_2 containment zone consisting of the CO_2 reservoir and the overlying seal. This thesis focuses on this sub-system, and it is called the ***caprock system*** in this work.
- Overburden in between the containment zone and exposure zone.
- CO_2 exposure zone comprising the shallow saturated and undersaturated zone, fresh or marine surface water, and atmosphere.
- Preferential CO_2 migration paths like the well zone or fault zone.

3.3.2 Model Development and Application

Once the scenarios have been defined, they need to be evaluated through mathematical modeling. A complete analysis of each scenario requires simulations by using individual models for different compartments that govern the transport of CO_2 from the geosphere to the biosphere [38]. These models should be verified and validated, preferably using field data from natural or industrial analogues. Predictive models are necessary to assess possible consequences due to underperformance of different systems or subsystems in a waste disposal system. There are general procedures for the development and validation of such models. Nonetheless, a firm understanding of the relevant properties of the system's constituents and their evolution remains a main prerequisite for successful modeling [31].

In general the input parameters, the geometry of the system, and the process operating the system are inherently uncertain. One method to cope with these uncertainties is to perform the assessment in a probabilistic manner [40]. However, computational limitations lead to a simplification of the model. Such simplifications must still capture the important physical and chemical processes that are intrinsic to the system, and the effect of simplification must be an overestimation of the consequences of CO_2 leakage.

3.3.3 Consequence Analysis

The modeling results must be translated into consequences with respect to health, safety, and environment (HSE) [39]. The ultimate goal of data gathering, scenario development, and predictive modeling is an integrated assessment describing the characteristics of the system and quantifying the performance of the overall system as a function of time [31]. Such integrated assessments can be based in either detailed research models or simplified system models. The first ones are used to analyze different design and engineering options, and to provide defensible arguments as to whether certain processes are relevant or not. On the other hand, simplified system models are used to conduct a more robust or bounding analysis [31, 32]. The analysis of the consequences of the scenarios can be done either deterministically or probabilistically.

3.3.4 Confidence Building and Performance Criteria

Two aspects that need to be considered through this process are confidence building and the regulatory criteria in place. In the case of confidence building it is necessary to anticipate that the ultimate goal of a safety assessment is to provide a basis for well-founded decisions about a waste disposal system [31]. Consequently, the decision makers need to have confidence in the information, insights, and results provided by safety assessments. Such confidence is built through model validation, thorough documentation, and sound judgment. The final step in a safety assessment is to evaluate the results in the context of the established regulatory standards and criteria. The safety of a waste disposal system is judged after a clear presentation of the information obtained in an integrated assessment, consideration of the uncertainties associated with the assessment results, and a critical review by the decision-makers [31]. However, at present, there is not a regulatory criterion in place for geological storage of CO_2.

3.4 The Observational Method

The observational method is a performance assessment tool and an integral part of risk management in geotechnical and geoenvironmental engineering. The method is effective for coping with uncertainty, especially from ground conditions, and it has been proven beyond a doubt [41]. Peck [42] embodies the following ingredients to the application of the method in soil mechanics:

- exploration to establish the general nature and properties of the deposit, but not necessarily in detail;
- assessment of the most probable conditions and the most unfavorable conceivable deviation from these conditions;
- establishment of design premised on the most probable conditions, with performance predictions for both this and the most unfavorable case;
- selection, in advance, of actions or modifications to be implemented for every foreseeable significant deviation from the design premise; and
- measurement of predicted quantities as construction proceeds, with planned modifications as necessary to suit the values obtained and conditions revealed.

Summarizing, one hopes for the best, but plans for the worst, using measurements and observations to distinguish the two as events unfold [43]. Its principal limitation is that it can only be used if the design can be altered during construction. Morgenstern [41] reviewed its use in environmental geotechnics, where the method has been successfully applied but found new limitations in highly regulated issues, the nature of decision-making related to environmental matters, and the issue of longevity (long-term predictions).

Nonetheless, the method has been applied successfully in mine waste management, ground remediation, landfill design, and even nuclear waste disposal (NWD). In NWD, despite the strict regulations, the complex decision-making process and the long-term requirements, a study by the Board on Radioactive Waste Management, U.S. National Research Council [44], advocated a strategy based on the following premise:

- Surprises are inevitable in the course of investigating any proposed site, and things are bound to go wrong on a minor scale in the development of a repository.
- If the repository design can be changed in response to new information, minor problems can be fixed without affecting safety, and major problems, if any appear, can be remedied before damage is done to the environment or the public health.

Morgenstern [41] clearly states that this approach is the observational method, and sees this as a recognition of the realities in geotechnical engineering. The strategy from the Board embodied key components of the observational method such as [41]:

- Start with the simplest description of what is known, so that the largest and most significant uncertainties can be identified early in the program and given priority attention.
- Meet problems as they emerge, instead of trying to anticipate in advance all the complexities of a natural geological environment.
- Define the goal broadly in ultimate performance terms, rather than immediate requirements, so that increased knowledge can be incorporated in the design at a specific site.

3.5 Approach to Geomechanical Performance Assessment of CO_2-EOR Storage Projects

First, it is prudent to examine the characteristics and particularities that geological storage of CO_2 present, and that make its performance assessment different from other injection/disposal techniques. These include [14]:

- The volume, rates and duration of injection are anticipated to be orders of magnitude larger than any other similar injection that has been carried out to date.
- The residence time is on the order of hundred of years, which raises a set of scientific challenges from the point of view of modeling, monitoring, and performance assessment.
- The CO_2 plume will cover a very large area; therefore the heterogeneities in the reservoir and its caprock will play a key role in CO_2 migration, pressure build-up, geochemical reactions, and potential leakage flow paths.
- CO_2 density and viscosity are lighter and lower, respectively, than surrounding fluids resulting in buoyancy driven flow, fingering, larger mobility and other related effects.
- Chemical reactions between CO_2 and the existing rock mass can affect their hydromechanical properties, i.e. decrease permeability near the injection wells, or affect the hydraulic integrity of the caprock.
- In-situ effective stresses will change, resulting in consolidation (or swelling) and deformation. Such changes will affect the hydraulic integrity of the caprock because the permeability of geomaterials is strongly dependent on its mechanical behavior.
- Abandoned wells must remain sealed for very large periods of time with current estimates being 1,000 years. Short- and long-term mechanisms may cause leakages like improper sealing practice, reservoir and overburden deformation leading to shear of wellbores, unanticipated and unpredictable subsurface conditions, intersection with conductive discontinuities, and long-term degradation of seals.

As was seen in the first part of this chapter, the NWD 'establishment' has worked extensively through the years to establish a basic and reliable approach to performance assessment. Such an approach is very useful in the development and use of models of the different systems and subsystems. However, NWD and CO_2 storage are two very different disposal systems, therefore the approach from NWD is not directly applicable in CO_2-EOR storage because of the following reasons:

- Nuclear wastes are much more harmful to humans, and the ecosystem in general.
- The NWD 'industry' can engineer its barriers. The bounding seals (barriers) in geological storage of GHG are the caprock and the wells. Caprocks cannot be engineered, and only preventive measurements like maximum injection pressures and temperature ranges can be specified. On the other hand wells can be engineered, but there are numerous uncertainties associated with the long-term performance of wellbores, and in EOR activities usually there is a large amount of existing wells in place already, which were not designed and abandoned considering long-term stability. Moreover, ***wells are a direct path to the biosphere***.
- Site characterization is the most cumbersome activity for CO_2 storage because of the large volume that a CO_2 plume will cover. Moreover, in the case of CO_2-EOR storage there is no luxury of choosing the most convenient storage site, and all efforts must focus on site characterization.
- There currently are no regulator criteria in place for geological storage of CO_2.

On the other hand, in geotechnical and geoenvironmental engineering the observational method has been the preferred tool for risk management and performance prediction. However, the methodology was envisioned for the design and construction of risky projects, while in CO_2-EOR storage projects there is not design *per se* (except for wellbores and its abandonment), but the focus of the projects shift towards efficient operation, optimization of the EOR process, and long-term storage of CO_2. Considering the focus on geomechanical performance of the present work, a combination between the performance assessment methodology developed for NWD, and the geotechnical observational method would produce the best results.

From the foregoing discussion a geomechanical performance assessment approach for CO_2-EOR projects must have the following steps:

Scenario Analysis

- Identification and characterization of the waste: in this case CO_2 is the waste, which has been extensively studied [9, 45, 46], and is beyond the scope of this thesis. Clearly, geological storage of CO_2 has been considered as an option for management of GHG because of the large volumes of CO_2 emitted, and properties of CO_2 such as mobility and density.

- Identification of potential geomechanical effects that can lead to leakage and migration of CO_2 outside the caprock system: all the interactive processes between reservoir exploitation and production, EOR activities, and CO_2 storage with the mechanical earth model (MEM), and CO_2 itself that may lead to geomechanical failure must be identified. This is addressed in Chapter 4.
- Site characterization: the development of a MEM (Chapter 7) that collects and organizes all the geological, hydrogeological, and geomechanical information relevant, as well as the information gathered through reservoir characterization. This step will establish the most likely condition of the caprock system, as in the observational method, and identify the gaps in information and uncertainties of the system. In the case of CO_2-EOR projects, usually the geological model and reservoir characterization are well developed, but the hydrogeological and geomechanical models can be relatively simple.

Model Development

- Evaluate the geomechanical performance: prediction of performance and sensitivity analysis must be conducted to evaluate the integrity of the reservoir pre- and post-CO_2 injection. This step has two components, a performance assessment of the reservoir during years of exploitation and production, and performance predictions for the CO_2-EOR storage project, Chapter 8.
- The performance of the caprock system must be evaluated against alternative scenarios such as faulting, tectonic activity, salt dissolution, drilling in the future and other. These scenarios can be evaluated using analytical tools but human intrusion. Chapter 9 will evaluate the effect of salt dissolution in the caprock system, considering the large amounts of salt that have been dissolved in the Williston Basin.

Evaluation against Regulatory Criteria

- Comparison of the assessment with performance criteria: the performance assessment and performance prediction carried out in the preceding step must be validated against performance criteria. Such criteria are developed later on in this chapter.

Monitoring and Observation

- Monitoring and verification: the predicted performance must be validated through monitoring, as in the observational method, to see if there is the need to implement an already developed contingency plan, that will establish clear safeguards as to what measures to undertake in the event of leakage.

3.5.1 The Caprock System

Following the definition of performance assessment, it is clear that PA can be carried out either in the whole system or components of the system. In the present thesis, the focus is on what it is called the caprock system, a component of the whole system that is made of the reservoir itself or primary sink, and its caprock.

3.6 Performance Criteria

A performance assessment cannot be carried out without criteria to establish whether the system is performing or underperforming. Therefore, it is necessary to establish these criteria for the caprock system. A review of caprock systems that have leaked or performed in an unexpected way due to geomechanical and hydrogeological issues, either in natural conditions or man-made facilities such as gas storage facilities, will serve as the base to establish the criteria. The following sections present a brief overview of these caprock systems and how they lost hydraulic integrity or performed unexpectedly.

3.6.1 Natural Analogues

Some oil and gas fields throughout the world have been found highly overpressured making them an excellent analogy for geological storage of GHG such as many fields in the North Sea, the Uinta Basin, fields in the Gulf of Mexico and so on. Some of these fields have been the subject of extensive studies to understand the cause of overpressuring, the hydrodynamic regime, the caprock properties, the process of oil generation and migration, and other matters. Likewise, leakage has been identified in some of these fields; therefore a review from the point of view of deep-well injection of CO_2 will give insight as to the possible causes of leakage and underperformance of caprocks.

3.6.1.1 The UK Central Graben

At the Central Graben of the North Sea, high levels of overpressuring are observed --up to 40 MPa overpressure at 4500 m depth--, Figure 3-4 [47]. The distribution of overpressure is controlled by the low vertical permeability of thick Cenozoic mudstones, which inhibit vertical escape of fluids as the shales undergo compaction. A potentiometric map of the central section of the Central Graben shows that the heads in the graben coincide aerially with structural features.

The axial Forties-Montrose High and marginal "Puffin" horst represent unexpected zones of low energy or head. It suggests that fluid escapes through the caprock at specific points. These zones or "Leak Points" are associated with low heads, high sandstone fluid pressures, and thin seals. The most likely mechanism that enhanced permeability in these zones is hydraulic fracturing, although that does not mean that is the only one. Leakage through these leak points is evidenced by heat flow anomalies, which unfortunately do not provide any information about how the leakage occurs, and the mechanical conditions of the caprock.

3.6.1.2 The Uinta Basin

The Altamont oil field in the deep Uinta Basin has been known for its large reservoir pressures, which approach lithostatic pressures. There have been an important number of studies about how these pressures are generated, and its evolution with time. Among these studies, the ones by Bredehoeft et al. [48] and McPherson and Bredehoeft [49] provide useful insight into this geological phenomenon. Through numerical modeling and permeability adjustments due to overpressuring, they were able to reproduce the existing conditions in the basin. A detailed examination of the results suggests that a trade-off between induced fracturing and oil generation must occur for the final value of overpressure to be consistent with the observed value [49].

3.6.1.3 The Snorre Field, Norway

The Snorre Field is an overpressured reservoir, which has a caprock formed by a thick shale of Cretaceous and Paleocene age [50, 51]. Gaseous and liquid hydrocarbons are present in the caprock up to a few hundred meters above the reservoir, which have the same origin as the ones in the reservoir, and have likely been introduced from the underlying reservoir. Lieth et al. [51] suggested that the distribution of hydrocarbons in the caprock succession hints that they were largely emplaced through a bulk flow mechanism, which may be buoyancy driven where major faults apparently did not play an important role. The distribution and concentration of hydrocarbons in the caprock suggests a relationship with the occurrence of undercompaction or overpressuring or both, in a relatively dynamic system.

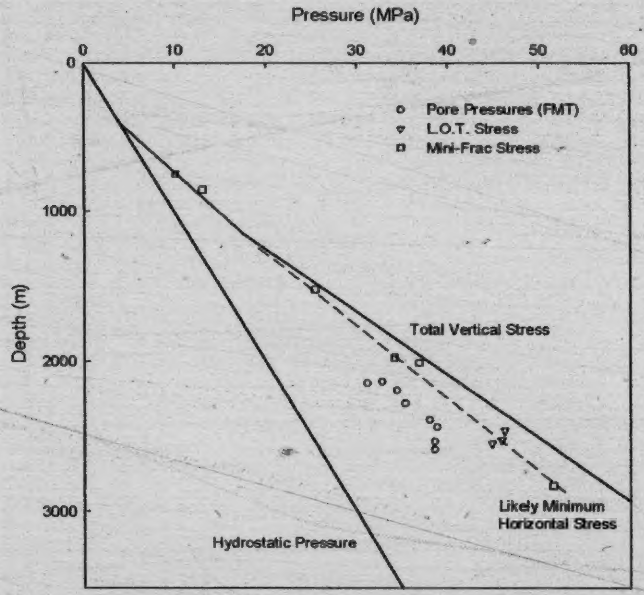

Figure 3-5 shows that the present pressures are about 82% of the vertical effective stress, which is about 90% of the fracture pressure from minifrac and leak-off tests, suggesting that leakage occurs through existing fractures instead of the formation of new ones [50]. Therefore, it appears there is a critical pressure at which these fractures open as flow channels.

3.6.1.4 Microfractures at the Frio Formation

Capuano [52] showed evidence of microfracturing and fluid flow in geopressured shales at depths of 3-5 km in the Frio Formation of the Texas Gulf Coast. He based his conclusions on the paragenetic relationship between the calcium sulfate structure fill and the later deposited organic material, and the more extensive alteration of the fracture margins, which indicates that these fractures were developed in-situ, and there was fluid flow and mineralization through them. Thin sections of shales at 3725 m showed that the sides of the fractures match so their origin must be tensional.

3.6.1.5 The Gullfaks Area, North Sea

Pore fluid pressure gradients in Lower Tertiary to Upper Jurasic mudrocks in the Gullfaks show significant variations, with a hydrostatic regime in the shallower formations, and large overpressures in Jurasic formations [53]. The presence of oil and gas in the shaly caprock seal, and post-Jurasic sediments has been frequently recorded, indicating hydrocarbon leakage.

Pressure gradients in the Gullfalks field approach the lithostatic pressure gradient, therefore overpressure release by a combination of hydraulic fracturing and flow through a network of fractures could explain the presence of hydrocarbons above the caprock.

3.6.1.6 Fault Reactivation in a Tertiary Basin in south-East Asia

Multiple wells drilled in a Tertiary basin showed accumulation of hydrocarbons at depths between 1900 and 2000 m [54]. Likewise there is a thermal anomaly at the same depth, and nearby wells showed the same anomaly at depths between 1800 to 2500 m. The properties of the hydrocarbons, and the thermal regime seem coincident with the hydrocarbons and thermal regime from an overpressured sandstone pool at a depth of 3000 to 3200 m. The confirmed deep source of these fluids and the amounts that have migrated during a short time interval can only be explained by active fluid migration along faults and fractures. A review of the stress-regime and structural geology of the basin indicates the presence of normal faults bounding the hydrocarbon pools. Such a geological setting combined with the overpressured pools seems to indicate episodic reactivation of the faults and a significant increase in the fault permeability, leading to leakage of hydrocarbons from the sandstone pools, Figure 3-6.

3.6.1.7 South Eugene Island 330 Field, Gulf of Mexico

A set of pools in the Gulf Mexico present different degrees of overpressuring [55]. The field is in a Pliocene-Pleistocene salt-withdrawal minibasin bounded to the north and east by a regional growth fault system and to the south by an antithetic fault system. Sand lenses embedded in shales, and bounded laterally by faults largely dominate the stratigraphy. The pools with larger overpressures have smaller oil columns, and their pressure at the top of the pool is close to the critical pressure to either reactive the bounding faults or induced hydraulic fracturing. On the other hand, reservoirs with large hydrocarbon columns are well below the critical pressure. Consequently, fault reactivation and hydraulic fracturing appear to be the mechanisms that control the amount of oil present in the largely overpressured pools.

3.6.2 Deep Storage and Disposal

Natural gas is stored in depleted gas and oil reservoirs, aquifers, and mined salt caverns to help meet cyclic seasonal and/or daily demands for gas. This activity has been carried out for almost a century, with a peak between the 1950s and 1980s. Consequently, the experience gathered from this technology can provide useful insight as to the performance of underground storage facilities. However, the information on performance of these projects seems limited, althougth there are some cases worth mentioning and reviewing, which will provide a better idea of the implications of injection and storage in geological formations.

3.6.2.1 Leroy Storage Facility

The Leroy gas storage facility is an aquifer storage development by Mountain Fuel Supply Co. in Uitna County [56]. This is a complex problem of gas storage in an aquifer because of uncontrolled migration of gas to the surface through both the wells and the caprock. Injection was carried out into the Thaynes Formation, although the Nugget Formation presented excellent potential for storage but was rejected due to the questionable integrity of the caprock.

The field was approved to initiate storage operations by the end of 1972 and by the end of 1973 gas began flowing out around the surface casing of Well 3. Studies proved that the failure had occurred in the Twin Creek formation at approximately 415 m in the Well 4 with subsequent gas migration to Well 3. Corrosion seemed to be the reason for leakage, but it is still unknown how the gas migrated from Well 4 to Well 3, Figure 3-7.

Subsequent wells were drilled in the following years, Well 4 could not be repaired and a new well (4A) was drilled to replace 4, but by November of 1978 gas migration was confirmed on the surface by bubbling in the adjacent creek and pond. A survey during that month indicated that gas was bubbling to the surface at two areas, one in the vicinity of Well 11 and other near Well 7. On June 1980 a tracer was injected into the Well 4A, while the other wells were shut down, the tracer was identified in the surface nine days later close to the Well 11, Figure 3-7. A workover program in Well 4A was carried out, and by July of 1982 another tracer was introduced. In this instance, the tracer showed up 163 days after injection, indicating a longer path and reduced extent of migration.

All these problems lead to simulation and history matching of the leaky reservoir. The results suggested that the behaviour of the aquifer simulated a ‘valving’ effect, where a pressure threshold exists below which the aquifer storage had a proper seal, and above which the loss and continued migration of gas occurred. Figure 3-8 shows the pressure into the reservoir for three consecutive seasons (1978 to 1980) against the volume stored. It is clear how after the pressures exceed 1800 psi (12.4 MPa), the slope flattens indicating the valving behaviour. The reservoir is located approximately 1000 m below the ground level. The results indicate that there was leakage not only through the wells but also through the caprock, and that a pressure of 1850 psi should not be exceeded into the reservoir, otherwise leakage would be triggered.

It is interesting to notice that the 'valving' pressure was substantially below the hydraulic fracturing pressure, which for a depth of 900 m assuming 1.8 MPa/100 m is 16.2 MPa. Again, as was seen with some overpressured reservoirs, large amounts of leakage can occur when the pressure in the reservoir is below hydraulic fracturing in an apparently competent caprock.

3.6.2.2 Suffield Upper Mannville I (Gas Storage Project)

This is a massive project of gas storage in Alberta, which is operated AEC Oil and Gas Company, a Division of Alberta Energy Company Ltd [57]. Gas storage is carried out in a Lower Cretaceous pool, the Suffield Upper Mannville I Pool. The I Pool, is a north/south trending Lower Cretaceous linear sand body draped over a Mississippian high. The sand is relatively clean and homogeneous with well-sorted medium to coarse quartz and chert grains. Only a small quantity of clay is present.

During production of the field, build-up tests conducted showed an excellent pressure communication in the three producing wells. Usually these tests were run for short periods of time (72 hours) due to the high permeability and apparent rapid stabilization. During the evaluation of the storage project, simulations of the producing stage of the reservoir were carried out. These simulations could not explain the production history using the geological model previously constructed. To obtain a good match to the production and pressure data, a permeability barrier had to be placed in the reservoir between one of the wells and the other two.

Early during the first injection cycle, some anomalous pressure behaviour was observed at the gas storage wells, as the pool appeared to be pressuring up much faster than was anticipated. Based on this behaviour, it was theorized that the I Pool was composed of several interconnected lobes. Due to the low average production rate the pressure difference between regions was small; however, after injecting at high rates for only a few months, the pressure difference between the main lobe and the poorly connected regions became quite large as the gas could not migrate into the poorer areas as fast as it was being injected into the main body of the pool.

As a result of such anomalies a new 3D seismic program, as well as the drilling of new wells was carried out to perform further reservoir simulation studies. These studies provided a new interpretation of the I Pool as a longer and narrower reservoir, where the performance of the project was dramatically affected by reservoir heterogeneities along the length of the pool, and the location of the injection/withdrawal wells. This example is a clear case of compartmentalization of the reservoir, where an unexpected pressure response of the reservoir put in jeopardy the integrity of the caprock system. Its effects can be even more dramatic on a sequestration project, where the injected volumes and duration of the injection process are much larger than in any other storage project, and large pressures can have detrimental effects on the integrity of caprocks.

3.6.2.3 Well Problems in Natural Gas Storage

In natural gas storage, wells are the most likely places for operating accidents to occur [58]. These accidents are related to improper well design, construction, operation and maintenance, resulting in damaged casing, leaking pipe joints, and inadequate cementing of casings.

Thus, in the West Montebello oil and gas field, improperly plugged oil wells allowed the migration of natural gas into an overlying zone [59]. The wells that created the problem were plugged again, and at present the storage project is inactive. In the McDonald Island gas storage field, California, the operators lost control of an injection/withdrawal well, which then caught fire. The well had to be plugged and abandoned [59].

A recent case was an eruption of natural gas built up under the city of Hutchinson, Kansas, killing two people [59]. The gas apparently escaped from an injection/withdrawal well in the Yaggy natural gas storage field (a mined salt-cavern) located about seven miles northwest of the city. This case also shows how mobile a gas can be, and how quickly it can reach far distances. By plugging the damaged well, the problem was solved but 143 million cubic feet of gas had leaked from the facility.

3.6.3 Criteria

After reviewing the underperfomance or unexpected performance of caprock systems, a criterion made of three parts was established to evaluate the performance assessment of caprock systems:

i. the caprock has conductive features that can allow the migration of CO_2 through, or that can easily become conductive with stress changes;

ii. the caprock fails mechanically due to either the processes of exploitation and production, or the process of CO_2 injection. It will be considered that mechanical failure leads to permeability enhancement and underperformance of the caprock system; and,

iii. there is a potential external event (different from those presented in Chapter 4) that can lead to the mechanical failure of the caprock system. Events such as salt dissolution or tectonic activity.

The second criterion may be controversial because it is well known that permeability begins increasing before reaching peak stresses and having a failure (in the mechanical sense) in brittle materials. However, as it will be seen in Chapter 6, the permeability enhancement pre-failure is rather small compared with the post-failure one. Likewise, permeability is not always enhanced by mechanical failure, but to assume that it is always enhanced is a conservative assumption. Nonetheless, further examination of this topic in caprock materials such as shale and anhydrite deserves further investigation.

3.7 Uncertainty and its Management

Uncertainties are always present in performance assessment of complex systems. Although the methods to evaluate and quantify uncertainty may vary, there is agreement on the types of uncertainties that need to be considered [31, 60, 61]:

- Parameter uncertainty, such as incomplete datasets, sampling artifacts, or simply measurement uncertainty. It arises where single values cannot be defensively derived or defined for these parameters.
- Conceptual model uncertainty, which is due to incomplete system understanding, the use of an inadequate conceptual model, an overly simplified mathematical description; or because there may be more than one way of describing a process or system within a particular context and in accordance with the data available.
- Scenario uncertainty, which is caused by the possible omission of important events or processes, a faulty description of the system, or uncertainty in the evolution of the system.

There are several approaches to cope with uncertainty such as [31, 60]:

- systematic sensitivity analysis;
- use of geostatistical and/or stochastic models;
- use of conservative assumptions and/or parameters;
- integration of data from many geosciences and engineering areas;
- use of simplified models, underlain by detailed system understanding;
- use of a set of alternative conceptual models to investigate model uncertainty; and,
- use of independent expert judgment.

However, a combination of judgment, redundant designs, monitoring and verification, and flexible designs is still the best tool to manage uncertainty. The observational method has been an advocate of these concepts, and in the specific case of CO_2 storage, redundant barriers design or the concept of "belt and suspenders" must be seen as a principle of design as Peck advocates for dams [62]. Thus, if the caprock system underperforms, further regional aquitards must act as defensive elements against leakage. Moreover, analytical work must be used as decision-making and uncertainty management tools rather than the final performance indicator. Whitman [63] states about that "… the true value of the analysis often lies in the insights and understandings that come from careful formulation of the problem….Engineers use analyses to sharpen their judgment…". On the other hand, the biggest challenge that CO_2-EOR storage projects faces is that lack of "belt and suspenders" when wellbores are the system under scrutiny.

Uncertainty and its management will be addressed throughout this thesis where considered necessary.

3.8 Summary

A combined approach of performance assessment techniques and the observational method provides the most efficient approach to evaluate the geomechanical performance of the caprock system for geological storage of CO_2. The methodological approach of these techniques can potentially build on the soundness and robustness of the performance of the caprock system, as well as indicate the path to follow considering that an underperforming caprock system does not necessarily mean that CO_2 cannot be stored safely in a given geological setting. Moreover, this process must be accompanied by good judgment and decision-making, as it is well recognized in geotechnics that actual failures result far more often from incorrect diagnosis of the processes operating in the field than from incorrect parameters used in their analysis [43].

3.9 Figures

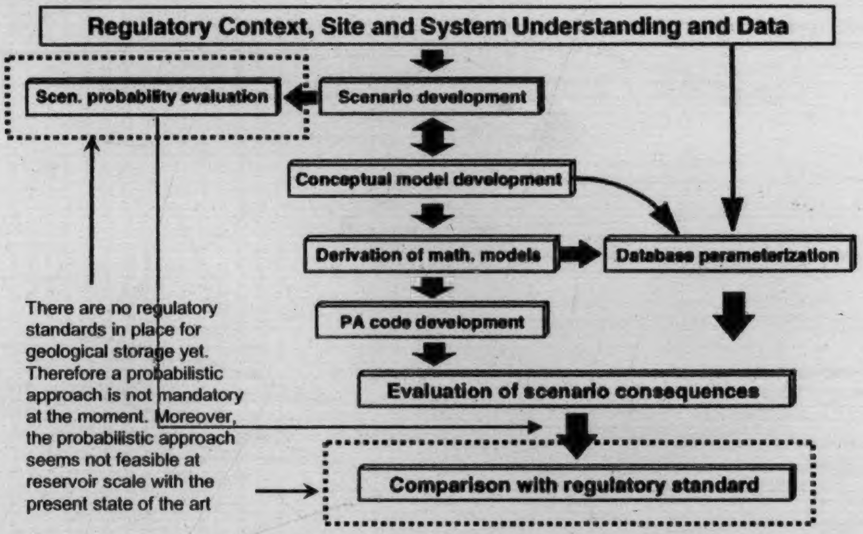
Regulatory Context, Site and System Understanding and Data
Scen. probability evaluation
Scenario development
Conceptual model development
Derivation of math. models
Database parameterization
PA code development
Evaluation of scenario consequences
Comparison with regulatory standard

There are no regulatory standards in place for geological storage yet. Therefore a probabilistic approach is not mandatory at the moment. Moreover, the probabilistic approach seems not feasible at reservoir scale with the present state of the art

Figure 3-1. Performance assessment methodology for NWD, modified after Howard et al. [61]

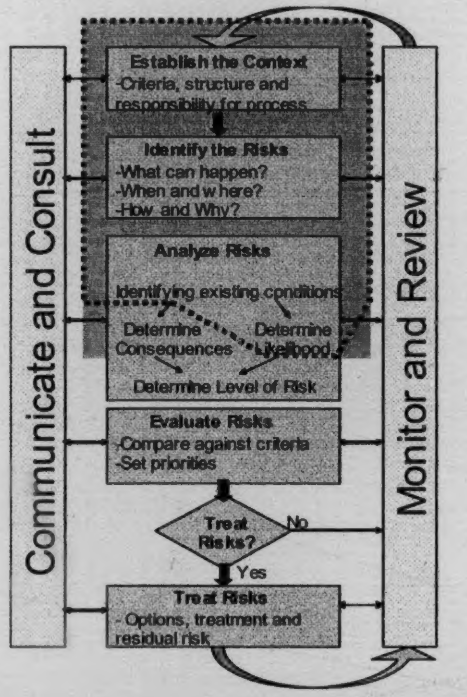
Communicate and Consult
Establish the Context
-Criteria, structure and responsibility for process
Identify the Risks
-What can happen?
-When and where?
-How and Why?
Analyze Risks
Identifying existing conditions
Determine Consequences
Determine Likelihood
Determine Level of Risk
Evaluate Risks
-Compare against criteria
-Set priorities
Treat Risks?
No
Yes
Treat Risks
- Options, treatment and residual risk
Monitor and Review

Figure 3-2. Risk management decision making process and the context of performance assessment within it (outlined region), modified after Standards Australia [37]

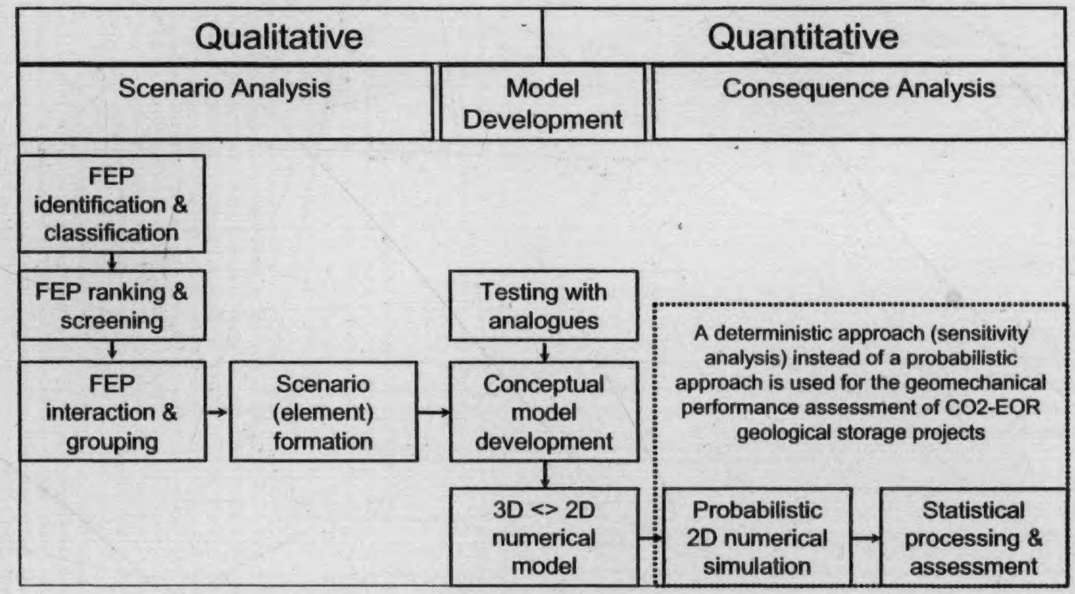
Qualitative
Quantitative
Scenario Analysis
Model Development
Consequence Analysis
FEP identification & classification
FEP ranking & screening
FEP interaction & grouping
Scenario (element) formation
Testing with analogues
Conceptual model development
3D <> 2D numerical model
A deterministic approach (sensitivity analysis) instead of a probabilistic approach is used for the geomechanical performance assessment of CO2-EOR geological storage projects
Probabilistic 2D numerical simulation
Statistical processing & assessment

Figure 3-3. The scenario approach for CO_2 storage safety assessment, modified after Wildenborg et al [38]

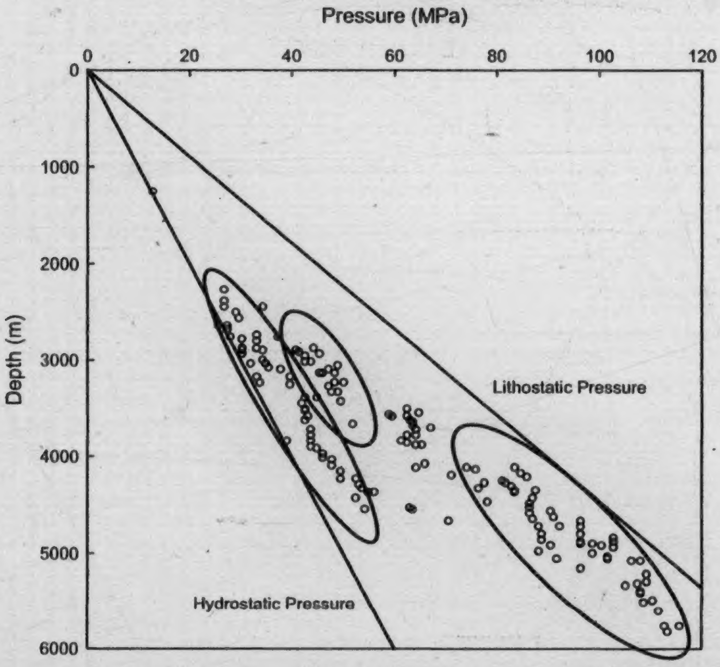

Figure 3-4. Regional pressure-depth plot. Notice the numerous pressure gradients parallel to the hydrostatic pressure gradient, suggesting the presence of multiple pressure cells and the compartmentalization of the basin fluids, modified after Darby et al. [47]

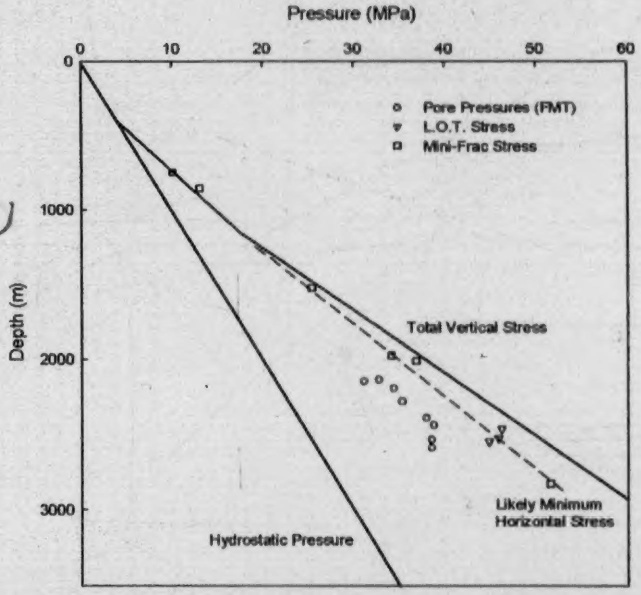

Figure 3-5 (a) Lithostratigraphy of the Viking Graben; and (b) Distribution of fluid pressures, minimum horizontal stress, and vertical stresses in the Snorre area, modified after Caillet [50]

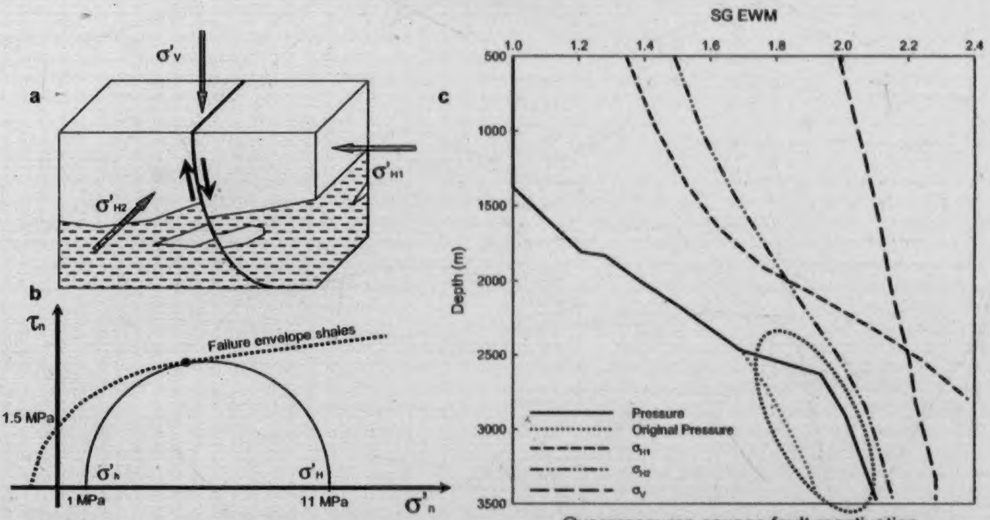
a
σ'V
σ'H1
σ'H2
b
τn
Failure envelope shales
1.5 MPa
σ'h
σ'H
1 MPa
11 MPa
σ'n
c
SG EWM
1.0
1.2
1.4
1.6
1.8
2.0
2.2
2.4
500
1000
1500
2000
2500
3000
3500
Depth (m)
Pressure
Original Pressure
σH1
σH2
σV

Overpressures causes fault reactivation

Figure 3-6. (a) Three-dimensional block diagram including the fault that may have reactivated; (b) Mohr circle during fault reactivation. Failure envelope calculated from shales at ~1800 m that are used as analogues; (c) Pressure and stress versus depth as specific gravity, modified after Grauls and Baleix [54]

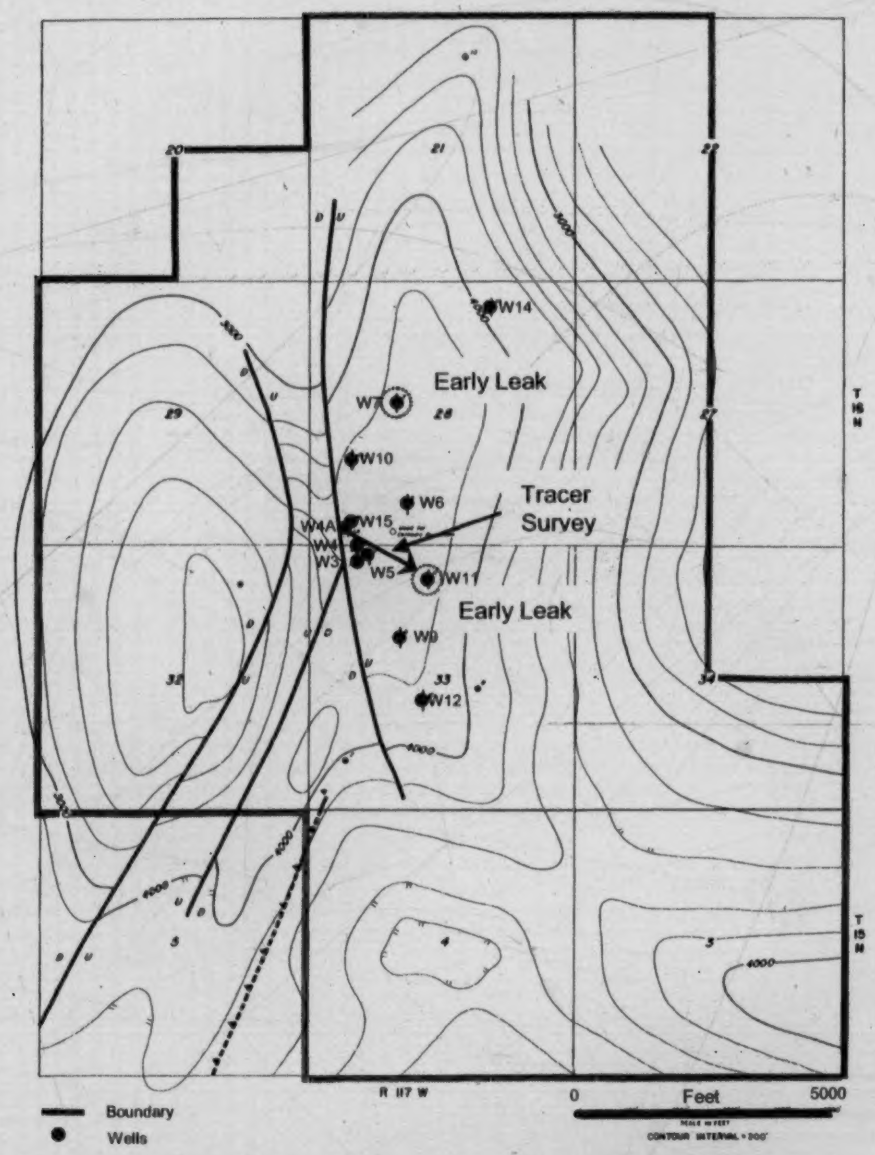

Early Leak
W7
W14
W10
W6
Tracer
Survey
W4A
W15
W4
W3
W5
W11
Early Leak
W9
W12
20
21
22
27
28
29
32
33
34
3
4
5
3000
4000
T 16 N
T 15 N
R 117 W
0
Feet
5000
CONTOUR INTERVAL = 200'
Boundary
Wells

Figure 3-7. Map of the Leroy Storage facility showing the wells with early leaks and the first tracer survey, modified after Araktingi et al. [56]

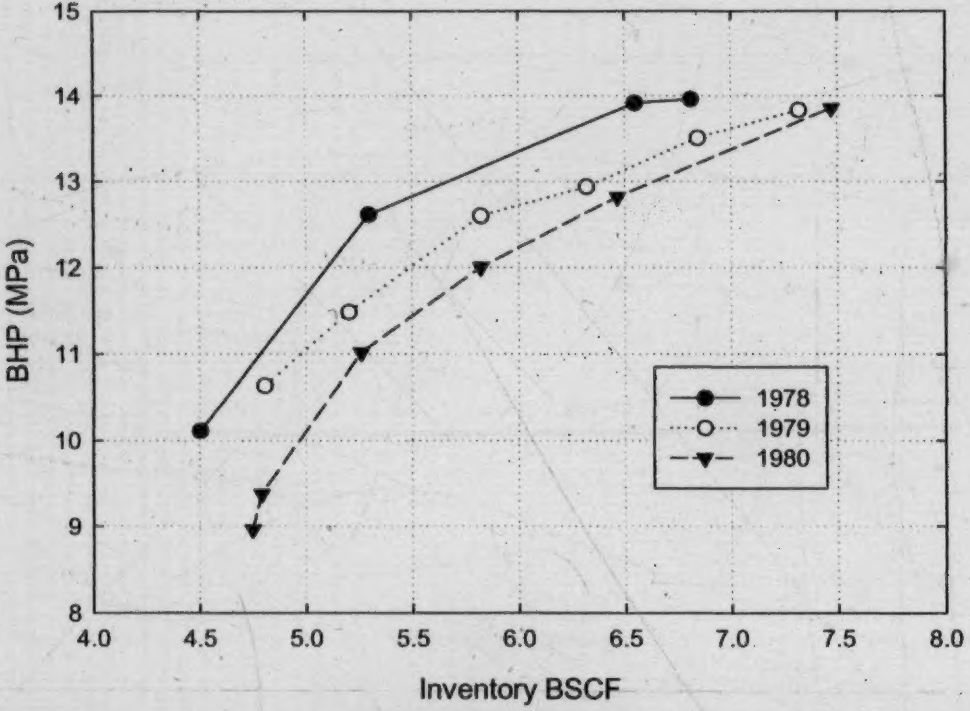

Figure 3-8. Injection curves for 1978, 1979, and 1980 in the Leroy Storage facility, modified after Araktingi et al. [56]

4 Disused Oil and Gas Reservoirs as Sinks for Geological Storage of CO_2

4.1 Introduction

Within the current options undergoing investigation for suitability as geological sinks for CO_2, disused oil and gas reservoirs are included along with salt caverns, coal beds, saline aquifers and EOR activities within hydrocarbon reservoirs. This chapter focuses specifically on the performance assessment issues associated with the use of disused oil and gas reservoirs as geological storage sites for the storage of CO_2. Recent investigations to identify the barriers to overcome in the implementation of CO_2 storage in disused oil and gas reservoirs has identified the following [64]:

- high costs of capturing, processing and transporting anthropogenic CO_2 ;
- incomplete understanding of reservoir processes and storage methods;
- monitoring, verification and environmental safety of CO_2 storage;
- lack of functioning emission trading system and storage regulations; and
- conflicts between CO_2 sequestration and EOR or natural gas recovery.

This study and others [16] have concluded that disused oil and gas reservoirs can be considered as safe sinks for geological storage of CO_2 because hydrocarbon reservoirs have existed within structural and stratigraphic traps over geological time and that this uniquely demonstrates their suitability for CO_2 storage. From a performance assessment perspective, it will be shown that this is a simplified approach from the viewpoint of ensuring effective CO_2 containment within the reservoir. Oil and gas reservoirs have usually undergone a variety of processes during primary recovery and may have been subjected to secondary and tertiary recovery processes. These reservoir production processes imply that the reservoir and the bounding sealing horizons (caprock) have undergone physical and/or chemical changes such as changes in in-situ effective stresses, consolidation, depressurization, repressurization and temperature. This chapter discusses how these various processes may impact the hydraulic integrity of the reservoir and caprock to the point where the initial hydraulic integrity prior to depletion may be sufficiently deteriorated. Understanding these processes is critical in the performance assessment of any disused oil and gas reservoir for geological storage.

4.2 Caprock (Seals): Petroleum Approach vs. Storage Approach

Caprocks or seals –as commonly referred to in the petroleum literature—are a critical element for successful exploration and production, because in order for a hydrocarbon accumulation to exist there must be a seal or trap, and hydrocarbon charge. The recognition of this fact has lead to extensive study of seals to gain an insight of what makes a seal, what properties define a seal, which characteristics make an efficient seal, how faults, fractures and other discontinuities affect the seal, and what effect geomechanical, thermal, hydrogeologic, and geochemical changes have in its performance.

There are a number of distinctive geomechanical mechanisms that can affect the hydraulic integrity of caprocks, leading to leakage and/or failure of the seal, Figure 4-1 [65]. Effects from the initial massive injection can be classified as those that are storage-induced, and those that are storage-activated. Capillary leakage, hydraulic fracturing and shear deformation/fracturing of caprocks are considered as storage-induced; flow through faults, fractures and fissures are considered storage-activated. Tectonically active regions are considered separately. Moreover, an additional transport mechanism is diffusion, but it occurs independently of geomechanical changes. It is important to recognize in the case of disused oil and gas reservoirs how the history of exploitation and production may trigger and/or affect these mechanism, and lead to the loss of hydraulic integrity in bounding seals, Figure 4-2 [15].

4.2.1 Capillary Leakage

The dominant trapping mechanism is a combination of the 'sealing forces' [66], which are the entry capillary pressure and the intrinsic permeability of the caprock. Capillary leakage under hydrostatic conditions takes place when the CO_2 columns build up beyond the equivalent entry pressure (EEP), and once the EEP has been overcome, the rate of movement is controlled by the intrinsic permeability of the caprock [66]. Shales and evaporites are the seals of the 25 largest oilfields and 25 largest gasfields worldwide [67] and in general account for most of the caprocks worldwide. Mudstones and shales can hold very large hydrocarbon columns [67, 68]; however, recent experiments on capillary entry pressure with CO_2 on both shales [69] and anhydrites [70] have shown that the entry pressure for CO_2 is substantially lower than from N_2, and it can be expected that it is lower than that of water. It reflects the difference in wettability and interfacial tension of CO_2 and other fluids [69]. Therefore, there is the need for more research as to what are the transport properties of caprocks when the flowing fluid is CO_2. Nonetheless, the "sealing forces" and diffusion will likely be the controlling mechanisms for leakage through the caprock in the long-term.

4.2.2 Hydraulic Fracturing

If the capillary pressure is too high, seal fracture may occur by fracturing of the caprock. These fractures result from increased pore fluid pressures in the reservoir, and its contact with the caprock that will reduce the minimum effective stress below zero, and overcome the tensile strength of the rockmass. Once the fracture is formed, it will allow highly pressurized fluids to escape. This mechanism seems to be a constant for hydrocarbon leakage and migration in basin development due to overpressures [67, 68].

From the basin evolution perspective, generation of overpressures is a very slow and gradual process which may take geological times to occur and can cover large areas. Moreover, it is very likely that formed fractures may self-heal with time through precipitation of newly formed minerals. On the other hand, depleted reservoirs usually have gone through a series of aggressive processes both in magnitude and intensity that may have lead to localized hydrofracturing of the reservoir and its propagation through the caprock. Among those processes are changes in in-situ stresses or fluid pressures due to production, stimulation or thermal changes, and pressure build-up due to changes in permeability inside the reservoir due to compaction, formation damage, and development of flow barriers among others. Furthermore, these fractures may self-seal (seal due to increase in stress) but the time scale is usually too short for self-healing, so they can re-open fairly easy with new changes in stresses and/or pressures during storage of CO_2.

4.2.3 Pre-Existing Fissures and Fractures

The presence of fissures and fractures in an otherwise intact rock mass may enhance its permeability. It depends on the aperture and infilling of these joints, as well as their interconnectivity. Neuzil and Bleitz [71] found in studies of regional flow in the Cretaceous shales of mid North America that transmissive vertical to subvertical fractures connected by a network of horizontal to subhorizontal fissures and fractures control and allow the easy flow of fluids at a certain level of effective stress. However, the presence of such fractures does not always imply that the flow will be enhanced. Apparently other parameters may play a role, such as porosity, water content, and mineralogical composition, as shown by work on the Tournemire shales in France [72], and Opalinus clay in Switzerland [73-75].

Healed fissures, in contrast, may have a lesser impact on permeability. Self-healing is associated mainly with two mechanisms. First, an increase in effective stress large enough to close the fissure will reduce its transmissivity to values similar of the intact rock mass in what is called self-sealing. Second, precipitation of newly formed minerals can heal the fissure --self-healing-. One concern is that the properties of a rock mass containing self-healed fissures and fractures are virtually indistinguishable from those of the same rock with no fractures, including its geophysical properties. It makes such fissures almost impossible to detect, still these fractures may re-open easily.

4.2.4 Shear Deformation/Fracturing

Dilatant shear deformation and fracturing may occur in top seals, and thus it is not always necessary to have extensional fractures (hydraulic fracturing) forming in response to high fluid pressure for leakage to take place. Such a mechanism of deformation and failure usually is associated with permeability enhancement. On the other hand, if the mechanism of deformation and fracturing is contraction, permeability might not be enhanced and may be reduced. Such a phenomenon has been studied in recent years for a variety of materials such as shales [76, 77], and salts [78]. It has been shown that where dilation is the mechanism of pre-failure deformation, permeability can be enhanced through the development of shear bands, microfractures, and ultimately creating a preferential flow path in the form of shear fractures.

This mechanism of failure has been often overlooked during basin modelling because of a series of reasons that comes from lack of appreciation, confusion with hydrofracturing, or modelling complications. Furthermore, in very slow processes, deformations and shear stresses can be "accommodated" easily causing minor impact, which is why its exclusion in basin modelling does not significantly influence the final result. Nonetheless, shear failure has been observed as the mechanism of seal failure and leakage during basin evolution [79]. On the other hand, in fast aggressive processes such as the ones in depletion, the impact of shear fracturing can be quite important for reservoir modelling and storage of CO_2. In these cases, shear failure will be the principal and most frequent failure mechanism for the rock mass, as it has been observed in many reservoirs [80, 81] where dilatant shear failure has resulted in constant permeability despite decreasing porosity. Similarly, shear failure has been observed in caprocks [82], especially in reservoirs where subsidence has been significant, and as hydrofractures, usually the time frame is too short for self-healing, and the fractures may only self-seal.

4.2.5 Fault-Related Flow

Faults have a strong influence in patterns of regional flow, therefore there are extensive studies in fluid flow through faults and what parameters control such flow [83]. Faults usually act as barriers to flow in sedimentary basins because faults are planes where the maximum pore throat diameter is very small. This may result from several different mechanisms such as cataclasis, clay smear and diagenetic healing. However, faults can also act as flow conduits when the infill is highly permeable, the normal stresses are low. Moreover, there can be episodic fluid expulsion from overpressured basins, fault-valve behaviour, which is a function of the magnitude and direction of the in-situ effective stresses [84].

Basin modelling has mostly concentrated its efforts on the features of the fault and its infill, considering that mainly these parameters control the fault permeability in regional scales for basins where stresses are developed slowly. However, normal stress controlled-permeability and episodic fluid are the most likely mechanisms to stimulate fluid flow through faults in a depleted reservoir where the in-situ stresses have been changed significantly from its virgin state. The same mechanisms will be the most critical for fault leakage during storage of GHG.

4.2.6 Molecular Transport (Diffusion)

Diffusion refers to the migration of solute from areas of high solute concentration to areas of low solute concentration. Diffusion depends on the solute and geological media properties, and can be influenced by geochemical changes but not by geomechanical changes. CO_2 diffusion is expected to be a very slow but unavoidable process in shales and evaporites [4]. Consequently, the influence of reservoir depletion in this process might not be large because most of the changes inside the rock mass are geomechanical, but still there is the need for more research, especially for the long-term assessment of storage of CO_2 where diffusion can be the controlling mechanism for leakage.

4.2.7 Tectonic Failure

The primary reason for seal failure in an otherwise adequate caprock configuration is tectonic deformation, which leads to extensive faulting and fracturing, both in compressional and tensional systems [85]. Tectonic failure will not be considered in this work.

4.3 Wellbores and Their Hydraulic Integrity

Wellbores provide access between the surface and the reservoir, which makes them a preferential flow path for leakage outside the reservoir. Additionally, wellbores may cut through overlying faults and discontinuities that may be in communication with the reservoir. Wellbores are composed mainly of four elements: (1) the borehole itself; (2) the annular space between borehole and casing; (3) the casing, including hydraulic connections and (4) the internal space within casing (which would contain an abandonment seal). The integrity of this wellbore system is affected by many of the same geomechanical, geochemical, and hydrogeological processes influencing the integrity of the caprocks.

Because wellbores are man-made "discontinuities" in the caprock, their propensity to leak depends mainly on the quality of the wellbore system and its operational history. The first concern rises during drilling, where borehole failures are not unusual. Completion configuration following drilling also has a bearing on the long-term integrity of the wellbore system. The operational history of a wellbore reflects the production/injection/stimulation processes that have occurred within that wellbore. These processes may affect its hydraulic integrity and in most cases is an onerous task to evaluate because of all the possible scenarios and interactions between wellbore operations, casing types, and lithologies. Moreover, the interaction between the wellbore and reservoir as a system must be considered. It includes compression failures within the reservoir due to consolidation, tensile failures in the deformed overburden, shearing of wellbores due to shearing of reservoir and/or its overburden, shear failures along weak overburden planes or pre-existing discontinuities.

Finally, well abandonment is one of the main concerns for two main reasons. First, the long-term integrity of seals is not well understood; what is the long-term degradation of their transport properties? There is no evidence for long-term stability of seals, and how the seal performance changes with time. A second concern for EOR projects relates to what the conditions for abandoned wells are, how the wells were sealed, and how those seals can be evaluated. Abandonment is a critical and rather complicated topic that needs more research before it can be included with confidence in any performance assessment strategy.

4.3.1 Casing Shear

Shear displacement in weak layers in the overburden, faults, discontinuities and at the top of the producing interval is a common cause of casing failure during reservoir production [86, 87]. Whether it will lead to a leak depends on the amount of displacement and the properties of the casing. When the displacement occurs through a weak layer, a fault or a discontinuity is always associated with changes in the in-situ stresses. If the displacement occurs at the top of the producing interval, the driving mechanism is a combination of vertical movement of the payzone, and differential lateral contraction (or expansion) between the producing interval and the caprock.

4.3.2 Compression and Buckling Damage

A mechanism of casing failure observed in a number of fields is buckling due to axial compression within the producing interval [86, 87]. This has been observed to occur most frequently near perforated intervals and is related to formation consolidation induced by pressure decline. This occurs near perforated intervals because pressure drawdown is larger close to this zone and the eventual solids production in this area leads to a loss of lateral support.

Although this mechanism is observed mainly in the payzone, it could occur in the overburden due to significant subsidence or heave in reservoirs that are sensitive to pressure changes. The effects will be more pronounced in the caprock, which implies that the hydraulic integrity may be affected right above the CO_2 plume.

4.4 Summary

Although oil and gas reservoirs have held hydrocarbons for geological times, and are considered safe sinks for geological storage of CO_2, the depletion of such reservoirs may have damaged the hydraulic integrity that used to make these geological settings traps. Even though the sealing properties of these caprocks have been studied from the basin evolution perspective, time scale, rate, intensity, and magnitude of the dominating processes during depletion is so aggressive that equivalent processes can have different consequences regarding the hydraulic integrity of caprocks. Moreover, wellbores, being preferential flow paths, are critical elements for geological storage of CO_2. Wellbore integrity is strongly affected by wellbore depletion as well. Therefore, a performance assessment of a depleted reservoir must include a careful study of how depletion may have affected the hydraulic integrity of the bounding seals.

4.5 Figures

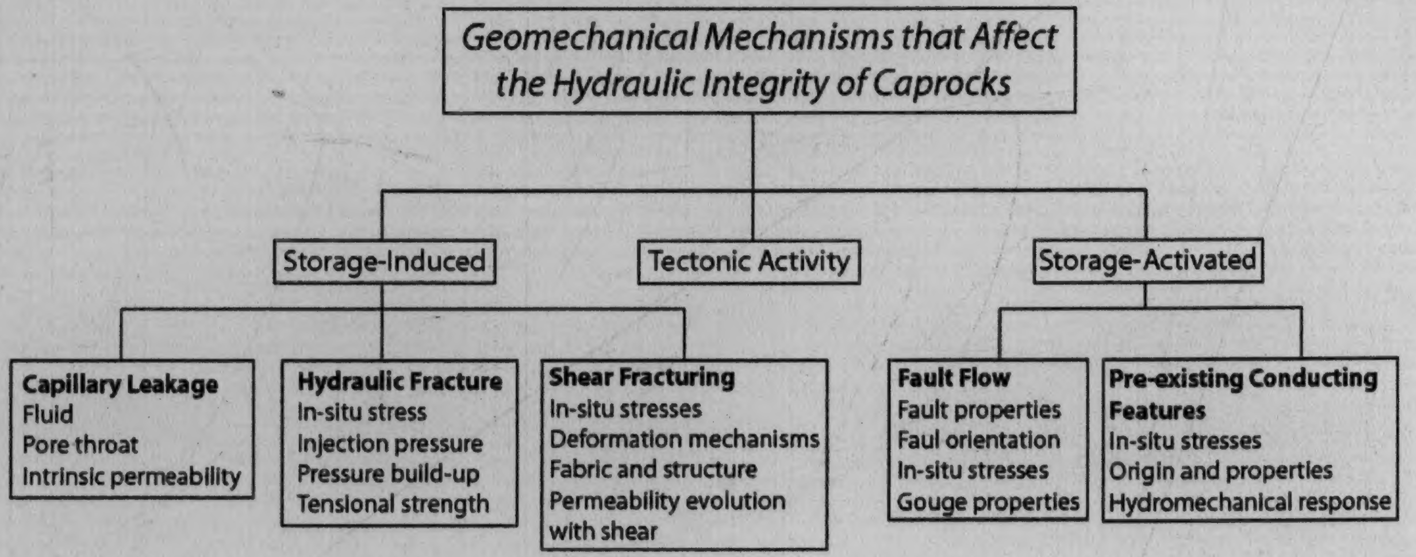
Geomechanical Mechanisms that Affect the Hydraulic Integrity of Caprocks
Storage-Induced
Tectonic Activity
Storage-Activated
Capillary Leakage
Fluid
Pore throat
Intrinsic permeability
Hydraulic Fracture
In-situ stress
Injection pressure
Pressure build-up
Tensional strength
Shear Fracturing
In-situ stresses
Deformation mechanisms
Fabric and structure
Permeability evolution with shear
Fault Flow
Fault properties
Faul orientation
In-situ stresses
Gouge properties
Pre-existing Conducting Features
In-situ stresses
Origin and properties
Hydromechanical response

Figure 4-1. Geomechanical mechanisms that affect the hydraulic integrity of caprocks

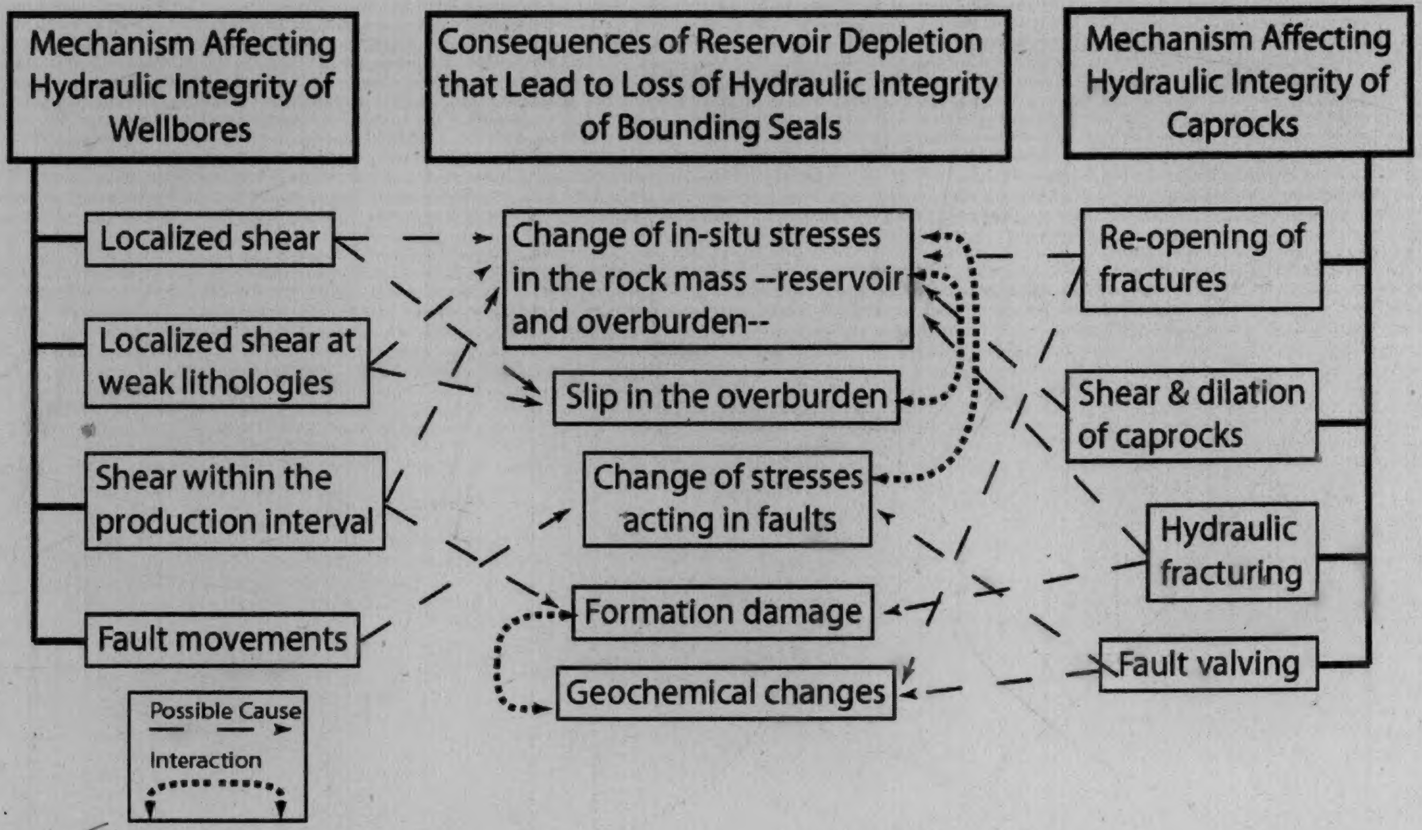
Mechanism Affecting Hydraulic Integrity of Wellbores
Consequences of Reservoir Depletion that Lead to Loss of Hydraulic Integrity of Bounding Seals
Mechanism Affecting Hydraulic Integrity of Caprocks
Localized shear
Localized shear at weak lithologies
Shear within the production interval
Fault movements
Change of in-situ stresses in the rock mass --reservoir and overburden--
Slip in the overburden
Change of stresses acting in faults
Formation damage
Geochemical changes
Re-opening of fractures
Shear & dilation of caprocks
Hydraulic fracturing
Fault valving
Possible Cause
Interaction

Figure 4-2. Consequences of reservoir production and depletion that may affect the hydraulic integrity of bounding seals

5 Experimental Facilities and Permeability Measurements

5.1 Introduction

The need for accurately predicting the hydro-mechanical behavior of either fine grained materials and tight geologic deposits has increased dramatically in past years as a consequence of the utilization of these materials and deposits to control and contain hazardous wastes for long periods of time. The hydro-mechanical properties of a caprock help define its competency as a seal for geological storage of CO_2. Consequently, as a part of the decision-making process while evaluating possible host formations for CO_2, it is necessary to measure the hydro-mechanical properties of potential caprocks.

5.2 Experimental Facilities

Considering that CO_2 is stored at large depths where pressure and stresses are high, a system capable of high-pressure testing was implemented, Figure 5-1. The system comprises a high-pressure high-temperature triaxial cell, an axial loading device (load frame), a local strain measurement system, a hydraulic system that is used for both pore pressure control/measurement and permeability measurement, and a logging system. The calibration of the different systems is provided in Appendix A.

5.2.1 High-Pressure Cell

The cell is constructed from high-yield 316 stainless steel, and can test samples with diameters up to 2.5" (6.35 cm), and lengths of up to 6" (15.24 cm). The cell can withstand pressures up to 70 MPa and temperatures up to 180° C. The cell is confined at the top and bottom by a thick steel plate which is held in place by six steel bolts, Figure 5-2. The water pressure inlet and outlet valves are connected to the bottom of the cell as well as the internal strain meter connections. Internally, the water inlet and outlet are connected to the platens by 1/16" (0.158 cm) high-pressure tubing. The cell is filled with silicon oil to avoid short-cutting and misreading in the internal LVDTs. Oil is pumped into the cell using a container with an air pressure connection to displace the oil, Figure 5-1. The overflow valve for expelling air from the cell is located at the top plate of the cell.

The bottom platen screws into the bottom plate, while the top platen sits on top of the sample, with the ram sitting on top of the platen. The platens have two slots, the top one to place the o-rings that firmly holds the thick latex membrane (1.5 mm) and the bottom one to hold the ring that holds the internal LVDT's, Figure 5-3. A servo-controlled pump provides constant cell pressure throughout the test. Cell pressure is logged by the pump pressure gauge at one of the cell outlets.

5.2.2 Loading System

A load frame that can withstand loads of up to 100 kN was employed to apply the axial load to the specimens. The load is applied using a constant flow-rate hydraulic pump, making the system constant-strain rate, Figure 5-1 and Figure 5-4. The load is measured through an external load cell placed between the ram and the piston of the frame. Moreover, the displacement of the load ram is measured externally through an LVDT, but as discussed below, this external LVDT must not be used to calculate the strains occurring in the test specimens.

5.2.3 Local Strain Measurements

As was mentioned above, the cell includes a system to measure local deformations by the use of two LVDTs that run parallel to the sample, and a chain device to measure radial strains, Figure 5-5. Unfortunately, the chain device does not yield high-quality reading in hard rocks in the pre-peak range, but the measurements are excellent in the post-peak range (Martin, personal communication).

The use of local strain measurements has become increasingly popular due to the awareness that geomaterials exhibit a nonlinear stress-strain behavior --especially weak rocks— therefore local strain measurements are necessary for accurate deformation measurements. In the present system, the LVDT's run parallel to the sample, are diametrically opposed, and are mounted in two rings held by the platens. This system provides excellent resolution and accuracy, good stability, and a linear calibration curve, Figure 5-6. However, it requires a non-conductive cell fluid, it is an expensive system, and it makes the set-up of the test cumbersome.

Figure 5-7 and Figure 5-8 show the contrast between local and external strain measurements for this experimental setup. Figure 5-7 clearly shows that local strain measurements are more stable and facilitate recognition of the actual initiation of loading in the test, while external readings can be misleading, and this discrepancy between readings is accentuated during the test and can lead to miscalculation of elastic properties, and identification of yielding stresses, Figure 5-8.

5.2.4 Acoustic Measurements

Initially acoustic measurements during sample shearing were planned as an integral part of the testing program. However, two primary and fundamental difficulties that worked against this effort were the poor wiring in the Civil Building that resulted in serious electrical noise problems, which I were unable to overcome. Also, the lack of grounding causes the cell to act as a huge antenna instead of as a shield. Bench measurements with both rocks and slurries provided good results, backing up the conclusion that a lack of proper 'electrical infrastructure' in the building was the cause of this unsuccessful effort.

However, techniques to measure acoustic waves not only in the axial direction, but in the radial direction were developed. Figure 5-9 shows the bottoms developed to install on the side of the sample through the membrane, Figure 5-10. These were going to be used for radial measurements. Pressure tests in the bottoms up to 30 MPa were successful and readings carried out outside the building without pressure were encouraging (the systems was taken to the West side of the city to make sure it was the building and not our design, or the design of the cell itself that was the cause of our inability to obtain acoustic measurements).

5.2.5 Hydraulic System

The hydraulic system is made up of two high-pressure, high-accuracy hydraulic pumps, one an ISCO® Pump, the other a Quizix® Pump. Both pumps can work in either constant flow-rate or constant pressure mode and they can measure both pressure and volume changes with high-precision, high-resolution, and high-accuracy.

Pressure gauges were installed at the inlet and outlet valves of the pump in order to minimize the volume stored in the system, which affects the precision and resolution of transient techniques for permeability measurements. The lowest permeabilities measured in this system (using transient techniques) were as low as 10^{-21} m^2. Moreover, standard techniques such as constant flow-rate or constant head can be used with the same system. A more detailed review of the different techniques to measure permeability of tight materials will be given in Section 5.3.

5.2.6 Logging System

The readings of the cell pressure transducer, pore pressure transducer, axial and lateral strains, and load cell are monitored and displayed continuously using a DataTaker® logging system. The system allows logging of up to 10 analog or digital channels and sampling rates up to a second. The Quizix Pump comes with its own in-house software to continuously monitor the multiple readings from the pump.

5.2.7 Procedure and Preliminary Results

5.2.7.1 Sample Preparation

Test specimens are right circular cylinders having an ideal height to diameter ratio of 2.0. However, in the present case where samples come from deep formations like Midale evaporites, the height to ratio diameter can vary from 1.0 to 3.0, considering how expensive and sparse these samples are. Evaporites were cored from samples of 3½" (8.89 cm) to 2½" (6.35 cm) in diameter using a water lubricated diamond-coring barrel.

5.2.7.2 Test preparation

Samples are submerged in distilled water for a period or 1 or 2 weeks in a pressure cell at 10 MPa to accelerate the process of saturation. Unfortunately, because of the stiffness of the samples, a B test cannot be used as indicator of saturation [88]. Once a sample is ready to be used in the actual test, its height, diameter, number, depth and location must be recorded.

A thick latex membrane with side bottoms for the ultrasonics is prepared. In order to do so, two sets of orthogonal holes at medium height are made in the membrane (maximum of 4 holes) using 1/8" (0.317 cm) inches tubing. The membrane is perforated by impacting the membrane with the tubing. Once the holes are made, the bottoms that carry the crystals are mounted, and an O-ring is put at the back of every bottom, wrapping the membrane to avoid any leakage, and applying a generous amount of vacuum grease, Figure 5-10.

The membrane is mounted in the sample making the flat spots in the sample coincide with the bottoms that carry the crystals. The flat spots are to guarantee that the waves travel orthogonally and there is no influence from reflecting waves. Then, the sample is mounted in the platens and sealed by an O-ring in the platens with generous amounts of vacuum grease. The platens must be aligned because the crystals mounted in the platens have to be aligned, so the same energy is applied in either the top or bottom platen.

Once the sample is mounted, all the LVDTs are connected. The axial LVDTs must be vertical and equidistant from the sample. The radial LVDT must be mounted in a way that does not interfere with the ultrasonics and vice versa. If side crystals are not being used, the radial LVDT must be mounted at the medium height of the sample. Once everything is mounted inside the cell and working properly, it can be closed. To do so, the piston must be moved upwards before hand to avoid touching the sample. Then the piston is lowered gently until it touches the top platen. The cell is placed in the load frame and all the flow lines and logging devices are then connected.

5.2.7.3 Test Procedure

Once the cell is filled with silicon oil and all the reading systems are working properly, a minor confining pressure is applied to adjust the position of the sample, LVDTs, and platens, of around 100 kPa.

From this point the procedure of the test depends on the desired results. As was mentioned before, the B test does not provide an effective measurement of saturation, so it was not conducted. However, once the pore pressure that will be used as backpressure is achieved, a waiting period of 48 hours was used in all the tests to assist with both specimen saturation and to provide a period for identifying possible leaks.

The strain-rate is adjusted by adjusting the flow rate of the pump that feeds the ram. The test is stopped for permeability measurements (whose procedure is described in the following section). Unfortunately, because the load frame is not stiff enough, failure of the samples lead to massive release of energies and no possibility of taking meaningful post-peak readings.

5.3 Permeability Measurements

Researchers have developed a wide range of techniques to measure the permeability in the laboratory of different materials. These different techniques and their applicability depend on how permeable the material is. Among the most popular tests for measuring permeability in geotechnical engineering are the constant head and variable head, which have been studied extensively for years throughout the geotechnical literature [89]. However, when the permeability is very low these techniques can take very long periods of time and the measurements are unreliable; hence, researchers have seen the need to develop more efficient and reliable techniques.

Among these techniques, the flow pump is the most popular for soil mechanics, where for rock mechanics applications transient techniques are better. These techniques can measure lower permeabilities, but are more demanding on the laboratory equipment and the quality assurance.

5.3.1 Flow Pump

A flow pump can be used to control fluid movement to and from the ends of a test specimen, which allows its use for measurements of equipment compliance, constant-rate-of-deformation consolidation, permeability, coefficient of consolidation [90]. The flow pump is especially useful for soils with low permeability that must be tested at low confining stresses to simulate the in-situ conditions. The method can be used with high confining stresses as well. In this method a constant-rate flow pump is used to precisely control the flow through a sample. The initial transient hydraulic head is recorded versus time, and eventually stabilizes to a steady state with a constant head gradient imposed across the specimen. Permeability can be evaluated from either the transient phase or the steady state condition, the latter option is prefered, but not always the most convenient in materials with very low permeabilities. The specific storage of the sample can be evaluated as well.

Morin and Olsen [91] developed a theoretical formulation of the constant flow rate hydraulic conductivity test, which allows evaluation the hydraulic conductivity, K, of the specimen during the transient response of the test. Such a formulation is given by:

$$K = \frac{FL}{H_1}(1.900 - 0.857P - 0.023P^2 - 0.012P^3 - 0.006P^4)$$

where

$$F = \frac{Q}{A}$$

$$P = \frac{H_1}{H_2}$$

Thus a value of hydraulic conductivity can be determined at early times during the transient response part of the flow pump test by choosing t_2 to be twice t_1 (to use this solution the relation between times must be 2 to 1 always) and by inserting the corresponding values of head difference into the equation [91]. When the steady state condition is reached (long times) $H_1=H_2$ and P=1.0, which makes the bracketed term practically 1.0, and the expression simplifies to Darcy's law:

$$K = \frac{QL}{AH}$$

Results on real tests showed that this analysis gives a close agreement with conductivity values determined at steady state conditions [91], but its accuracy and resolution of early time estimates of specific storage is limited.

Esaki et al. [92] carried out a rigorous analysis of the flow permeability test considering that the analysis by Morin and Olsen [91] did not take into account the storage capacity of the experimental system. They solved their formulation using a numerical method based on the parameter identification theory, where the parameters can be calculated minimizing the following error function:

$$\varepsilon = \left\{ \sum_{i=1}^{M} \left[H(L,t_i)_{(K,S_s,C_e)} - H(L,t_i)^{*} \right] \right\}^{1/2}$$

where

$$H(L,t_i) = \frac{qL}{AK} \left\{ 1 - 2\sum_{n=0}^{\infty} \frac{\exp(-\frac{K}{S_s}\beta_n^2 t)}{L\delta^2 \beta_n^2 \left[L\left(\beta_n^2 + \frac{1}{\delta^2} \right) + \frac{1}{\delta} \right]} \right\}$$

$$\delta = \frac{C_e}{AS_s}$$

$$C_e = C_w V_f$$

C_w = volumtric compressibility of the permeating fluid

V_f = total volume of the flow pump system

and β_n are the roots of

$$\tan(\beta L) = \frac{1}{\beta\delta}$$

This expression represents a least squares reduction of the discrepancies between the *M* hydraulic differences *H(L,t_i)** measured at time t_i and the corresponding data $H(L,t_i)$ obtained by the theoretical analysis. They found that the early time evaluation of the permeability and the storage of both the sample and the system can be measured accurately, which is very convenient for specimens with very low permeability. Olsen et al. [90], Esaki et al. [92], and Zhang et al. [93] found that the results of transient analysis are very sensitive to small changes in temperature.

5.3.2 Transient Pulse Technique

5.3.2.1 Brace's Solution

In 1968 Brace et al. [94] introduced the transient pulse technique (TPT) to measure the permeability of 'tight' rocks, in their case granite at high confining pressures. In the TPT two reservoirs are connected through a sample, a sudden increase of pressure is induced in one of the reservoirs and the decay of this small pulse is observed, Figure 5-11. The equations describing such a situation are [95]:

$$\frac{\partial^2 p}{\partial x^2} - \frac{\beta_s \eta}{k}\frac{\partial p}{\partial t} = 0 \quad \text{for } 0 < x < L \text{ and } t > 0$$

$$p = 0 \quad \text{for } 0 < x < L \text{ and } t = 0$$

$$p = p_d(t) \quad \text{for } x = 0 \text{ and } t > 0$$

$$p = p_u(t) \quad \text{for } x = L \text{ and } t > 0$$

p = the pressure in the sample

x = the distance from the downstream face of the sample

l = the length of the sample

k = the permeability of the sample

η = the dynamic viscosity of the pore fluid

β_s = the storage capacity per unit volume of the sample - fluid system.

where *d* and *u* subscripts refer to the downstream and upstream reservoirs respectively.

The storage capacity per unit volume is given by:

$$\beta_s = C_b + \phi C_f - (1-\phi)C_r$$

C_b = the bulk compressibility of the sample

C_f = the compression of the pore fluid

C_r = the mean compressibility of the rock - forming minerals

ϕ = the porosity of the sample

The boundary conditions are defined by:

$$\left(\frac{\partial p}{\partial x}\right)_{x=0} - \frac{\beta_d \eta}{kA}\frac{dp_d}{dt} = 0 \quad \text{for } t > 0$$

$$p_d = 0 \quad \text{at } t = 0$$

$$\left(\frac{\partial p}{\partial x}\right)_{x=L} + \frac{\beta_u \eta}{kA}\frac{dp_u}{dt} = 0 \quad \text{for } t > 0$$

$$p_u = P_0 \quad \text{at } t = 0$$

P_0 = the initial pressure pulse applied on the sample

Brace et al. [94] assume that the term that considers storage capacity was negligible, which implies that both the rock and the fluid are incompressible. Such an assumption leads to acceptable errors in low porosity stiff rocks. This reduces the expression to:

$$\frac{\partial^2 p}{\partial x^2} = 0$$

indicating that the pressure gradient in the sample is constant along its length, although it will vary with time. They found a solution in the form:

$$p = P_0\left(\frac{V_d}{V_u} + V_2\right)e^{-\alpha t} + P_f$$

where

$$\alpha = \left(\frac{kA}{\eta\beta_f L}\right)\left(\frac{1}{V_u} + \frac{1}{V_d}\right)$$

$A =$ the cross - section of the sample

$V_u =$ volume of the upstream reservoir

$V_d =$ volume of the downstream reservoir

$P_f =$ the final equilibrated pressure

$\beta_f =$ the fluid compressibility

The permeability is determined from the slope of *ln* $(P_t\text{-}P_f)$ versus *t*, which is equal to α, as the rest of the terms are known constants.

5.3.2.2 Finite Differences Solution

Considering that there is not an analytical solution when the storage of the sample is not neglected, Lin [95] and Trimmer [96] use numerical solutions to solve the equations. Both solutions modeled the problem using a finite difference approach, which divides the sample in *n* zones, with reservoirs at the 0th and *(n+1)* zones. The code assumes that the flow across each zone interface is steady state for the increment time used, thus calculating the pressure of the sample-reservoir system as a function of time and position only.

Comparing the numerically generated reservoir pressure-time histories with the experimental data, permeability is evaluated. To compare the different pressure-time histories, it is assumed that there is a ‘critical region’, the middle part of the curve (Figure 5-12), which is given the most weight in determining permeability. This because the transient effects induced by the initial pressure pulse has disappeared by this time, the slope is greatest, allowing maximum resolution, and this portion of the curve is relatively insensitive to the water-storage system [96].

The downside of this method is that it assumes that the specific storage of the sample is known, or it must be estimated. To determine the specific storage it is necessary to independently measure the porosity and bulk compressibility of the sample.

5.3.2.3 *Analytical-Graphical Solution*

Hsieh et al. [97] developed an analytical solution for the problem and showed how to apply the method to different tight rocks. The initial-boundary value problem was solved by the Laplace transform method. The solution (which is beyond the scope of this work) for the hydraulic head in the upstream and downstream reservoirs contain a dimensionless variable:

$$\alpha = \frac{Kt}{L^2 S_s}$$

and two dimensionless parameters:

$$\beta = \frac{S_s AL}{S_u}$$

$$\gamma = \frac{S_d}{S_u}$$

In the above definitions α is the dimensionless time, β is the ratio of the compressive storage within the sample to the compressive storage in the upstream reservoir, and γ is the ratio of the compressive storage of the downstream reservoir to the compressive storage of the upstream reservoir.

The solution is presented in the form of plots of dimensionless hydraulic head in the upstream and downstream reservoirs, h_u/H and h_d/H, and the above dimensionless parameters mentioned in the form of the following expressions:

$$\frac{h_u}{H} = \frac{1}{1+\beta+\gamma} + 2\sum_{m=1}^{\infty} \frac{\exp(-\alpha\phi_m^2)(\beta+\gamma^2\phi_m^2/\beta)}{\left[\gamma^2\phi_m^4/\beta^2 + (\gamma^2\beta+\gamma^2+\gamma+\beta)\phi_m^2/\beta + (\beta^2+\gamma\beta+\beta)\right]}$$

$$\frac{h_d}{H} = \frac{1}{1+\beta+\gamma} + 2\sum_{m=1}^{\infty} \frac{\exp(-\alpha\phi_m^2)(\beta-\gamma^2\phi_m^2/\beta)}{\left[\gamma^2\phi_m^4/\beta^2 + (\gamma^2\beta+\gamma^2+\gamma+\beta)\phi_m^2/\beta + (\beta^2+\gamma\beta+\beta)\right]}$$

where ϕ_m are the roots of

$$\tan\phi = \frac{(1+\gamma)\phi}{\gamma\phi^2/\beta-\beta}$$

Since γ depends only on experimental parameters, it can be measured in the laboratory. Using the family of type curves for the appropriated value of γ, the following procedure permits calculation of the hydraulic properties of the sample. The dimensionless changes in hydraulic head in the reservoirs, h_u/H and h_d/H, are plotted against the logarithm of time on graph paper at the same scale used for the type curves to give the solution, Figure 5-12. The sheet with the test data is overlaid on the type curve plot and moved horizontally, keeping the abscissa of both plots superposed, until the data points fit a particular type curve. After obtaining a fit, a convenient match point is chosen. At this match point, the value of $\alpha\beta$ or $\alpha\beta^2$ is taken from the type curve plot and t is taken from the data plot. Using t and the value of $\alpha\beta$ or $\alpha\beta^2$ the permeability K, or the product of permeability times specific storage $K\,S_s$, can be calculated. Since β depends on a single unknown, specific storage S_s, the value of S_s can be computed from the value of β for the curve fitted by the data [98].

However, to be able to calculate both K and S_s, β must be larger than 0.01 and less than 10. Otherwise, only the product KS_s can be calculated. β depends on the sample dimension, the compressive storage of the upstream reservoir, and the specific storage of the sample, so the sample dimensions and design of the apparatus can be adjusted within limits, to try to get in the range needed. Moreover, in order to minimize the time for the test, the same parameters can be adjusted, where the adjustment of β being most easily accomplished by changing the volume and consequently the compressive storage S_u, in the upstream reservoir. When β is less than 0.01 either Brace's [94] solution or the solution presented above can be used.

5.3.2.4 Oscillation method

A sinusoidal pressure oscillation is induced at one end of the specimen and the pressure response is monitored at the other end. The response downstream is another sinusoidal oscillation, which is attenuated and phase-shifted relative to the applied oscillation. Kranz et al. [99] and Fischer [100] developed solutions that related the magnitudes of the attenuation and the phase shift to the values of permeability and specific storage of the specimen tested. The basic equations and boundary conditions are shown below, however, the development of this solution is rather cumbersome and beyond the scope of this work.

$$\frac{\partial^2 p}{\partial x^2} - \frac{\beta_s \eta}{k}\frac{\partial p}{\partial t} = 0 \quad \text{for } 0 < x < L \text{ and } t > 0$$

$$p = 0 \qquad \text{for } 0 < x < L \text{ and } t = 0$$

$$p = p_d(t) \qquad \text{for } x = 0 \text{ and } t > 0$$

$$p = p_u(t) \qquad \text{for} = L \text{ and } t > 0$$

p_d and p_u are functions of time and obey the conditions

$$\frac{\beta_d \eta d}{kA}\frac{dp_d}{dt} - \left(\frac{\partial p}{\partial x}\right)_{x=0} = 0 \quad \text{for } t > 0$$

$$p_d(0) = 0$$

$$p_u = P_A \sin(\omega t + \delta)$$

$P_A =$ the amplitude of the generated oscillation

The solution of the equation and its boundary conditions [100], consists of the sum of a transient term and a steady-state term, the value of the steady –state term at the downstream face being of the form:

$$p_d = \alpha P_A \sin(\omega t - \delta)$$

$\alpha =$ the attenuation factor

$\delta =$ the phase lag

$\omega = 2\pi / T$

$T =$ the period of the generated oscillation

Following Fischer's solution, permeability and storage capacity per unit volume are then implicitly described by the functions α and δ, which are given by the expressions:

$$\alpha = \left| \frac{\kappa(1+i)\cosh[\kappa x(1+i)] + \dfrac{\beta_d i\omega}{KA}\sinh[\kappa x(1+i)]}{\kappa(1+i)\cosh[\kappa L(1+i)] + \dfrac{\beta_d i\omega}{KA}\sinh[\kappa L(1+i)]} \right|$$

$$\delta = \arg\left\{ \frac{\kappa(1+i)\cosh[\kappa x(1+i)] + \dfrac{\beta_d i\omega}{KA}\sinh[\kappa x(1+i)]}{\kappa(1+i)\cosh[\kappa L(1+i)] + \dfrac{\beta_d i\omega}{KA}\sinh[\kappa L(1+i)]} \right\}$$

where

$$\kappa = \sqrt{\frac{\beta_s \pi \eta}{Tk}}$$

$$K = \frac{\kappa}{\eta}$$

Alternatively, one can express α and δ in term of two graphically determined parameters γ and ψ (see Fischer and Paterson [101] for the Figure):

$$\alpha = |R(\gamma,\psi)| = \left| \frac{1}{\cosh[\psi(1+i)] + \gamma\psi(1+i)\sinh[\psi(1+i)]} \right|$$

$$\delta = \arg[R(\gamma,\psi] = \arg\left[\frac{1}{\cosh[\psi(1+i)] + \gamma\psi(1+i)\sinh[\psi(1+i)]} \right]$$

where

$$\gamma = \frac{\beta_d}{AL\beta_s}$$

$$\psi = L\left(\frac{\pi\eta\beta_s}{Tk}\right)^{1/2}$$

From the measurements of α and δ, the values of the dimensionless parameters γ and ψ can be evaluated and thence:

$$\beta_s = \frac{\beta_d}{LA\gamma}$$

$$k = \frac{\pi\eta\beta_s}{T}\left(\frac{L}{\psi}\right)^2 = \frac{\pi\eta\beta_d L}{TA\psi^2\gamma}$$

5.3.2.5 Parameter Identification Solution

Zhang et al. [102, 103] used a parameter identification technique from systems engineering to develope a technique that permitted to evaluate both permeability and specific storage with confidence, and without the hazards that graphic pressure-time history matching present. The components of a parameter identification technique are:

- a system, in this case the testing device and procedure itself,
- a mathematical model of the system, which was developed in the preceding sections,
- an input imposed on the system boundaries and simulated by the model, the pressure pulse,
- a set of experimental data defined as the system output and a corresponding set of theoretical values obtained from the model output, the latter values presented as functions

of the parameters to be determined. In this case the pressure decay as a percentage of the initial pulse,

- an error function, sometimes called "loss criterion," suitably defined in order to assess quantitatively the discrepancy between measured and theoretical output values; and,
- an algorithm designed to minimize the error over a feasible domain[5] in parameter space and, hence, to identify the parameters that characterize the "best model" within the model class selected.

The mathematical model and error function are defined as:

$$\varepsilon = \left\{ \sum_{i=1}^{M} \left[\frac{h(l,t_i)_{(K,S_s,C_e)} - h(0,t_i)_{(K,S_s,C_e)}}{H} - \frac{h(l,t_i)^{*}{}_{(K,S_s,C_e)} - h(0,t_i)^{*}}{H} \right] \right\}^2$$

where

H = initial pulse

* = theoretical solution

l = upstream

x = 0 = downstream

$$\frac{h(x,t)}{H} = \frac{1}{1+\beta+\gamma} + 2\sum_{m=0}^{\infty} \frac{\exp(-\alpha\phi_m^2)[\cos\phi_m\xi - (\gamma\phi_m/\beta)\sin\phi_m\xi]}{\left[(1+\beta+\gamma-\gamma^2\phi_m^2/\beta)\cos\phi_m - \phi_m(1+\gamma+2\gamma/\beta)\sin\phi_m\right]}$$

and

$$\xi = \frac{x}{l}, \beta = \frac{S_s AL}{S_u}, \gamma = \frac{S_d}{S_u} \text{ and } \alpha = \frac{Kt}{l^2 S_s}$$

ϕ_m are the roots of

$$\tan\phi = \frac{(\gamma+1)\phi}{\gamma\phi^2/\beta - \beta}$$

Thus, the minimization of this solution for both permeability and specific storage keeping the other value constant at its 'real value' gives an optimum solution. Ideally both upstream and downstream pressures are used to have a better constraint of the solution, but depending on the permeability and length of the sample, only the upstream record can be used. The error function is highly nonlinear and very sensitive to changes in permeability. Therefore, the permeability can be determined more accurately using this technique than the specific storage [102, 103].

---

[5] A feasible domain in this case means a test duration long enough to obtain reliable measurements of permeability and storage, see Figure 5-17.

5.3.3 Which Technique to Use

Although there is not a unique answer for which technique to use in measuring permeability in 'tight' materials, aspects such as test conditions (pressures and sample lengths), gauge resolutions, hydraulic properties of the material, and time constrains must be taken into consideration. Usually the flow pump test is recommended where the confining stresses during the test have to be very low, and hydraulic conductivities are around 10^{-19} m^2. Transient techniques are more appropriate for very low permeabilities and high confining stresses, and especially for rocks. Brace [104] provides some guidelines as to what laboratory technique must be used depending on the type of material.

In the case of transient techniques the ideal 'variation' to use is case specific. Thus, the lower permeability that can be measured will depend on the equipment available, the compliance of the system, and the resolution of the pore pressure transducers used, as well as how good the temperature controls are. Moreover, the purpose of the test plays a very important role. If the test is only to evaluate transport properties short samples can be used, and the oscillation method can give very reliable, accurate and fast answers. On the other hand, if mechanical measurements are being done as well, the sample will be too large, and the pulse decay technique solved by the parameter identification method is prefered. However, if porosity is very low, specific storage will be very low as well, and Brace's solution may be accurate enough, and quicker.

Trimmer [105] and Lin [95] analyzed the assumption of no storage in the sample and found that it can produce significant errors when the storage is considerable. Trimmer found that the error was a function of the ratio R of the effective sample pore volume and the reservoir volume:

$$R = \frac{AL\phi_e}{V}$$

Trimmer found that R must be less than 0.25 for systematic errors of 0.1 or less, i.e. the value of R for the work of Brace et al. [94] was 0.02. Lin [95] introduces the concept of fluid storage, which is given by:

$$\delta = \frac{AL\left[\phi\beta + \beta_r - (1+\phi)\beta_s\right]}{\beta(V_1 + V_2)}$$

which he compared against a systematic error in the measurements of permeability and found that the value should of δ should be less than 0.01, otherwise Brace et al. [94] approach must not be used.

5.3.3.1 Application Considerations

As was mentioned before, transient techniques require temperature control environments for stability and comparison considerations. Likewise, the pulse induces poroelastic effects on the sample including deformations, and a non-uniform pressure distribution inside the sample. Applying a pulse that is less than 10% of the current pore pressure in the sample can minimize these effects. Large pulses may led to misinterpretation of the results, and in particular, underestimation of permeabilities by a factor perhaps as large as 2 [106]. Likewise, the downstream volume must be as small as possible.

Moreover, shear tests will usually need to be stopped to avoid a combination of poroelastic effects that may affect both the mechanical and hydraulic measurements. However, the oscillation technique could potentially be used in undrained triaxial tests, where if the rate of load/strain is kept very small, the measurements may be acceptable. However, this option needs to be explored in more detail and it may not be practicable in many cases because of the attenuation caused by large samples as those use in triaxial testing. If the oscillation technique is chosen, it is important to note that:

- the upstream volume must be kept as small as possible; if dilatancy and permeability are to be measured there must be enough fluid to flow toward the sample,
- the initial pulse of the oscillation pressure must not be more than 10% of the pore pressure inside the sample. Otherwise secondary effects like consolidation or weakening of the sample can play an important role on the test and affect the whole triaxial/permeability test,
- a Fast Fourier Transform (FFT) data processing technique offers a powerful signal to noise ratio enhancement due to its filtering effect, resulting in an increased resolution/sensitivity and consequently in the possibility of measuring very low permeabilities and storage capacities. Owing to its steady-state character, systematic combinations such as leaks and modulations can easily be recognized and often removed from the data record [101]; and,
- the optimum oscillation frequency will depend on both the hydraulic character of the rock and the fluid pressure system parameters [99].

5.3.4 Procedure and Preliminary Results

Considering the foregoing discussion on permeability measurement, the equipment was developed trying to meet the majority of the requirements and features described above. Volumes of both upstream and downstream reservoirs were minimized, pressure gauges with excellent resolution and accuracy were used, and the temperature was controlled as closely as possible within certain limitations.

The volume of the downstream reservoir was limited by placing a pressure gauge and a valve as close to the outlet of the cell as possible. The upstream reservoir volume included the tubing from the outlet of the cell up to the pump. Fortunately, the Quizix pumps use pneumatic valves after their internal reservoir, so each time a pulse was applied, the valve was closed and the reservoir volume was not part of the system. This facilitated the measurement of system compliance. Volumes of both the upstream and downstream reservoir were measured using nitrogen compressed at a given pressure in a known volume, which was connected to the reservoir. Once there was an initial measurement of pressure, the connection was open, the pressure registered, and using the law of ideal gases the new volume was evaluated. This was repeated a limited number of times and the average was the volume of each reservoir. The compressibility of the system, C_e, was measured by pressurizing each of the reservoirs and measuring the volume added in each pressure increment. Table 5-1 shows the properties of the system developed for permeability measurements.

Table 5-1. Properties of the permeability measurement system developed.

Parameter		Value
Upstream volume	V_u (cm^3)	17.78
Downstream volume	V_d (cm^3)	8.67
Compressibility	C_e (m^{-1})	1E-4
Upstream storage	S_u (m^2)	1.7780E-09
Downstream storage	S_d (m^2)	8.6700E-10
γ	-	0.48763

For temperature control it was necessary to rely on the temperature control of the room, which was acceptable. Unfortunately, the system is too large to isolate and have a strict control of temperature at the moment.

The oscillation technique was considered initially because of its simpler processing, its ability to detect leaks, and the potential of being used without stopping the shear test. However, because of the length of the samples, the results were unsatisfactory and its application was disregarded. Consequently, the pulse decay technique was used, using the parameter identification technique to evaluate the values of permeability and specific storage. However, because of the length of the sample, the error function had to be constrained to use only upstream pressure measurements, as the experimental pressures downstream were very low, and no reliable enough to be used in the calculations. Moreover, to get a good record of pressure downstream, a longer testing was needed.

Figure 5-13, Figure 5-14, Figure 5-15 and Figure 5-16 show theoretical analysis for a variety of permeabilities and specific storages for a sample of 10 cm length. Clearly from the pressure analysis downstream, attenuation is quite large for permeabilities lower than 10^{-19} m^2, as was the case with the Midale Evaporite, and permeability had to be evaluated only with upstream readings. Figure 5-17 shows two results for two different tests and it clearly shows how quickly the technique can obtain results with a good precision. Figure 5-18 shows the downstream readings for one of the tests in Figure 5-17, where the pressure is adjusted because there is a slight jump at time zero due to the compression of the downstream fluid volume as a response to the pulse. Still, the adjusted readings were of insufficient quality to measure permeability, as the head increase is less than 2% of the pulse applied, which in this case was 2 MPa. Consequently the increase in pressure downstream after half an hour is less than 40 kPa, making these readings beyond the accuracy of the instruments. The data analysis was carried out in a spreadsheet where the error function was minimized for both specific storage and permeability in an iterative manner, until the error was considered acceptable.

Poroelastic phenomena can affect transient techniques as deformation is induced during the test by the pulse, but the consequences in permeability measurement are small as long as the pulse is kept below 10% of the pre-pulsing pore pressure [106]. However, these results were obtained in tests at very high pressures, so this criterion may be more flexible at low pressures as in the case of the tests reported here. Figure 5-19 shows the very small deformations induced by an 800 kPa pulse in a test where pore pressure was 3 MPa.

The flow pump technique was used to measure permeability in sheared samples. Considering the significant enhancement in permeability due to shear, it was not necessary to use the transient analysis because steady state was reached easily. Figure 5-20 and Figure 5-21 shows the application in one measurement using different flow rates. Notice the stability and accuracy of the readings. However, it is advisable to carry out a multiple readings with different gradients, as very low gradients can lead to erroneous permeability values. In this case, the readings are from a failed sample, where permeability was controlled by a very rough fracture with gouge, Figure 6-27, which may have affected the low pressure reading.

5.4 Summary

The experimental capabilities developed at the University of Alberta to carry out hydro-mechanical characterization of caprocks were presented and the capabilities shown. This system is a high-pressure, high-temperature triaxial cell for rock mechanics testing capable of measuring low permeabilities in short periods of time with precision. Likewise, the different techniques for measuring low permeabilities precisely and quickly were reviewed.

5.5 Figures

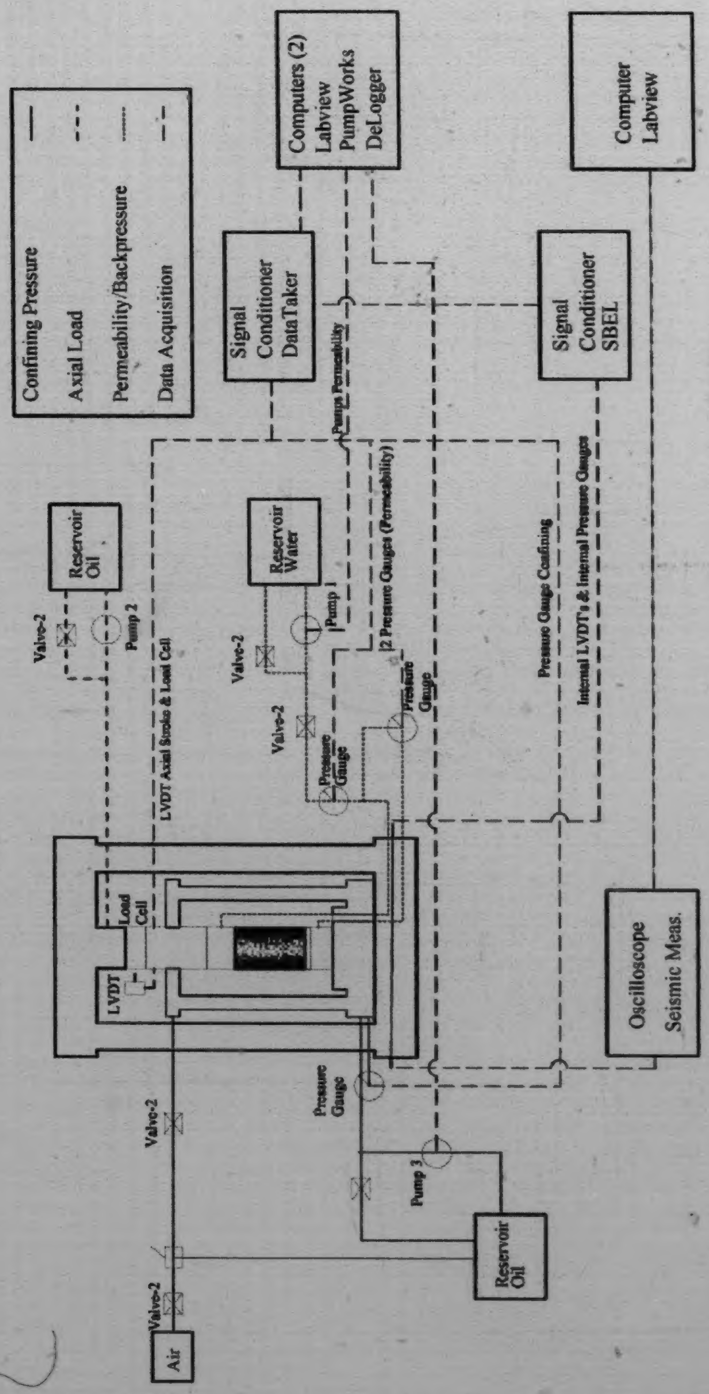
Confining Pressure
Axial Load
Permeability/Backpressure
Data Acquisition
Computers (2) Labview PumpWorks DeLogger
Computer Labview
Signal Conditioner DataTaker
Signal Conditioner SBEL
Reservoir Oil
Pump 2
Valve-2
LVDT Axial Stroke & Load Cell
Reservoir Water
Pump 1
Pumps Permeability
2 Pressure Gauges (Permeability)
Valve-2
Pressure Gauge
Pressure Gauge
Pressure Gauge Confining
Internal LVDT's & Internal Pressure Gauges
LVDT
Load Cell
Oscilloscope Seismic Meas.
Pressure Gauge
Valve-2
Pump 3
Reservoir Oil
Valve-2
Air

Figure 5-1. Schematic of the laboratory equipment developed to evaluate the hydromechanical and seismic properties of caprocks

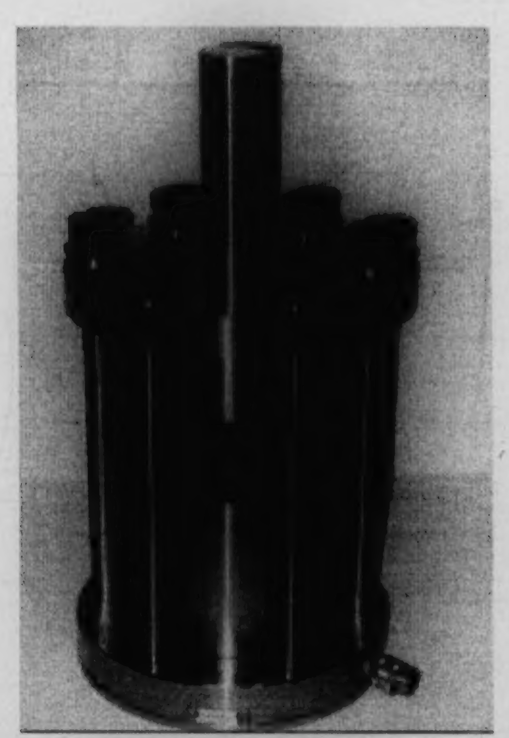

Figure 5-2. High-pressure, high-temperature triaxial cell. The cell is 70 cm tall

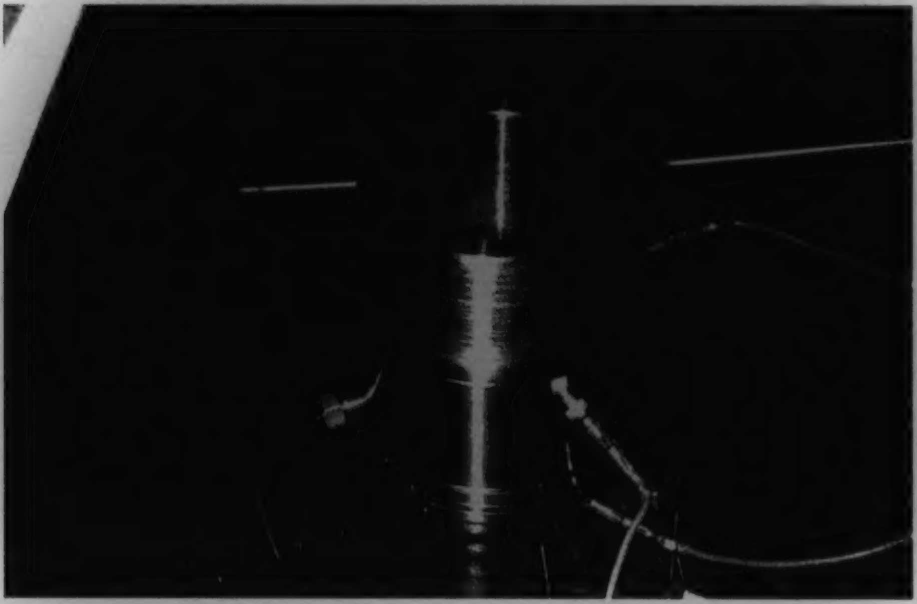

Figure 5-3. Detailed of the 2.5” (6.35 cm) platens. Notice the connectors for acoustic measurements

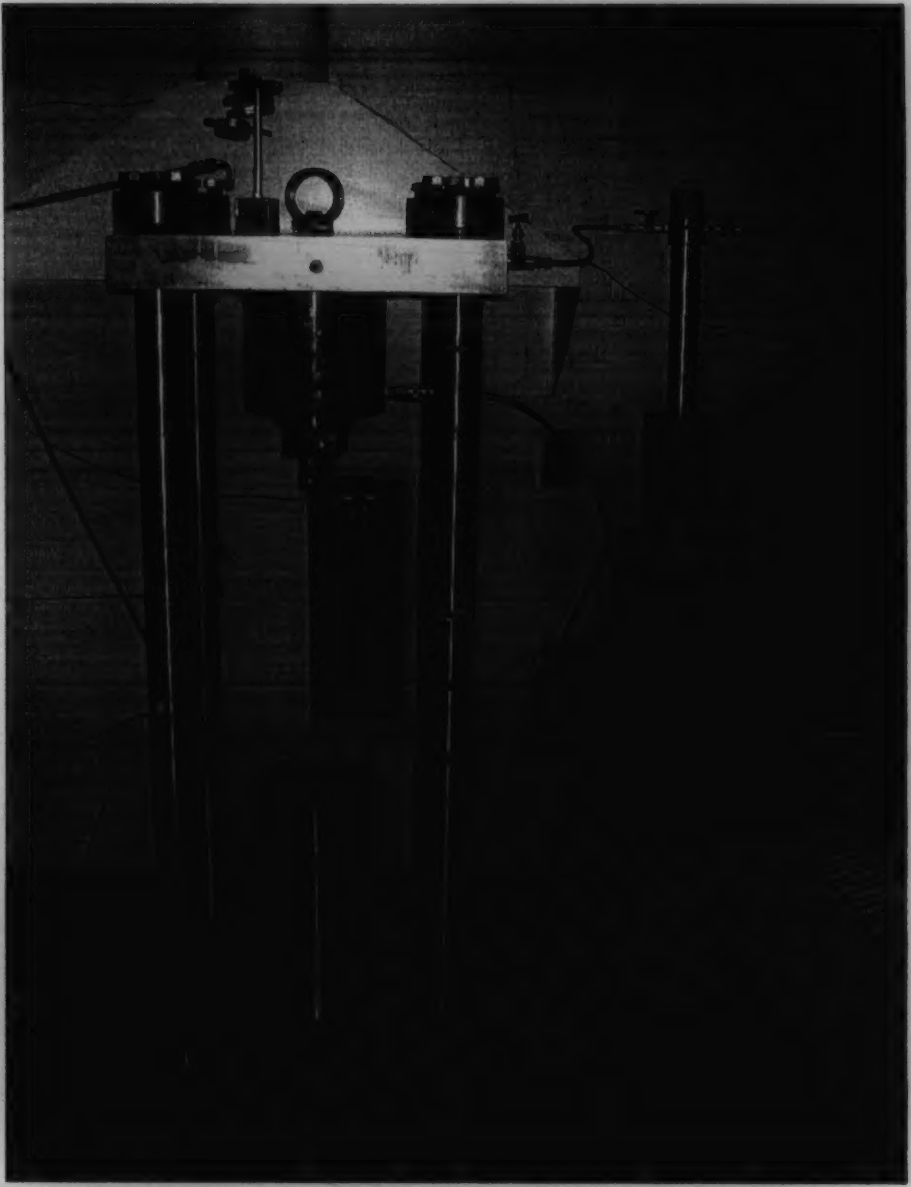

Figure 5-4. Loading frame and servo-controlled pump for constant strain rate testing

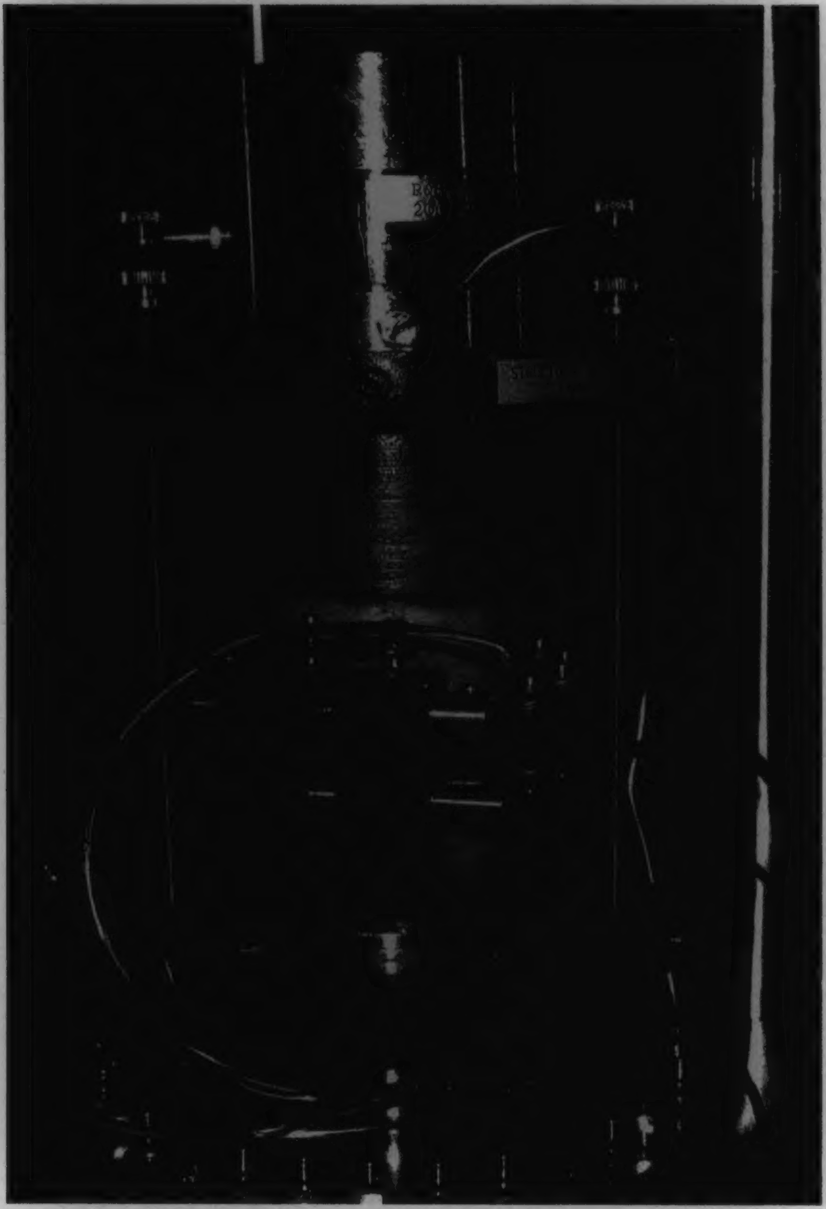

Figure 5-5. Close-up view of the internal LVDTs system mounted on a sample. Two LVDTs are mounted parallel to the sample to measure axial displacements, and one LVDT mounted in a change measures radial displacements

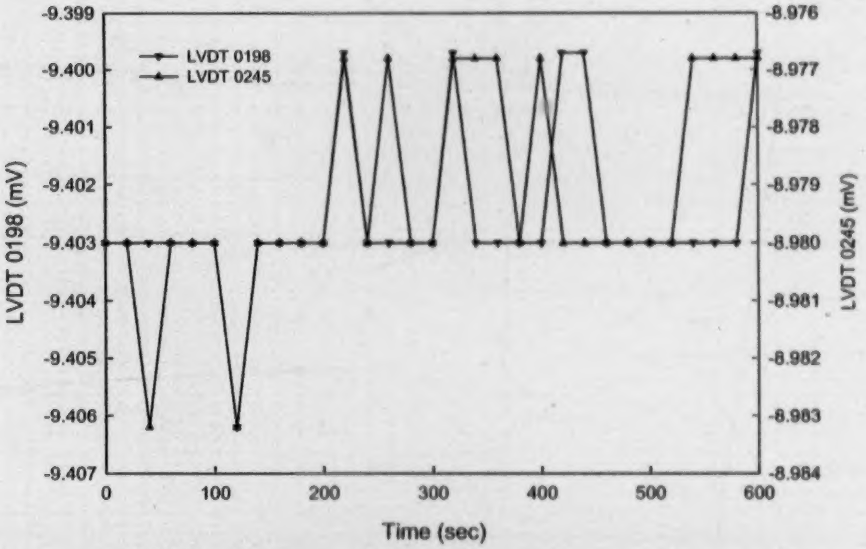

Figure 5-6. Stability of internal LVDT readings. The LVDT 0198 measures axial displacements while the LVDT 0245 radial. The fluctuations account to 5*10^{-4} and 6*10^{-4} mm respectively

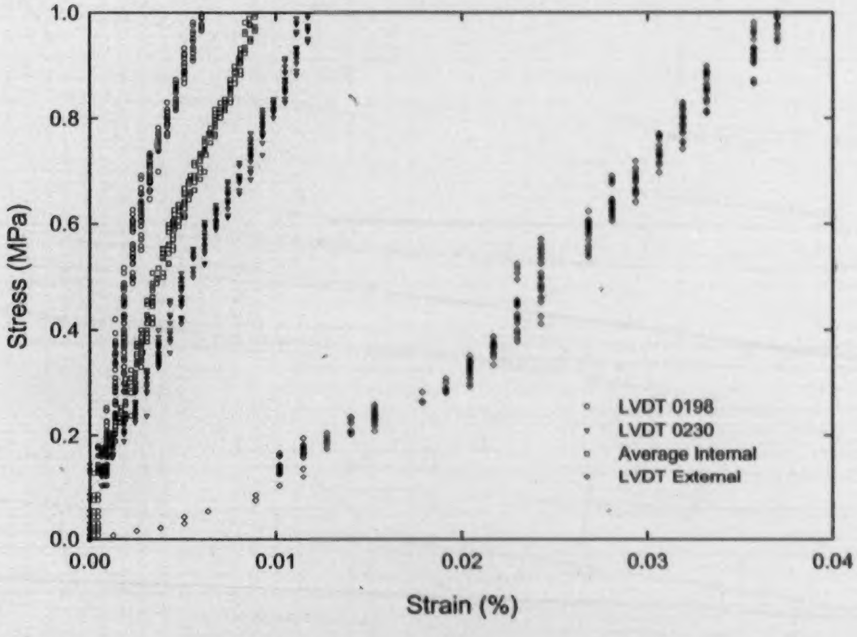

Figure 5-7. Contrast between internal and external LVDT readings

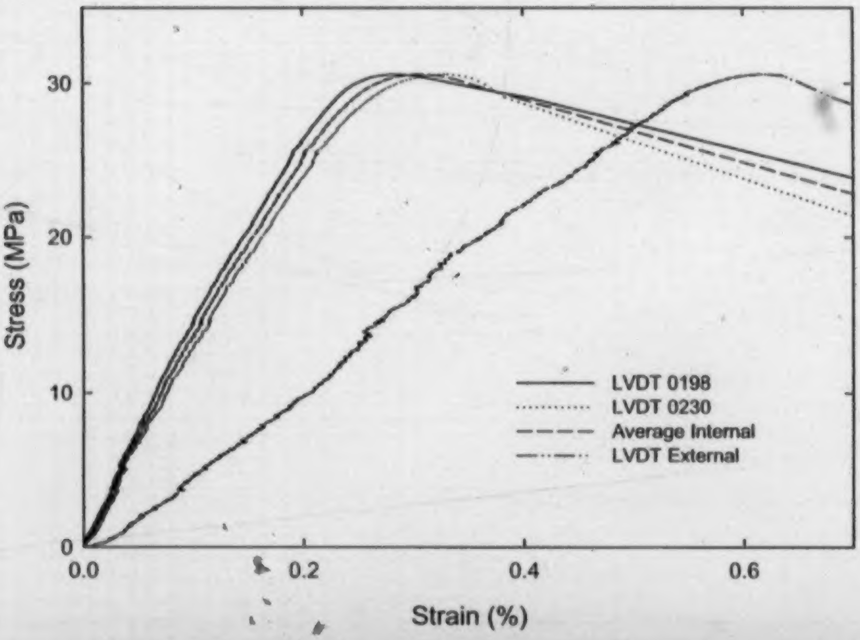

Figure 5-8. Contrast between internal and external LVDTs during an entire test

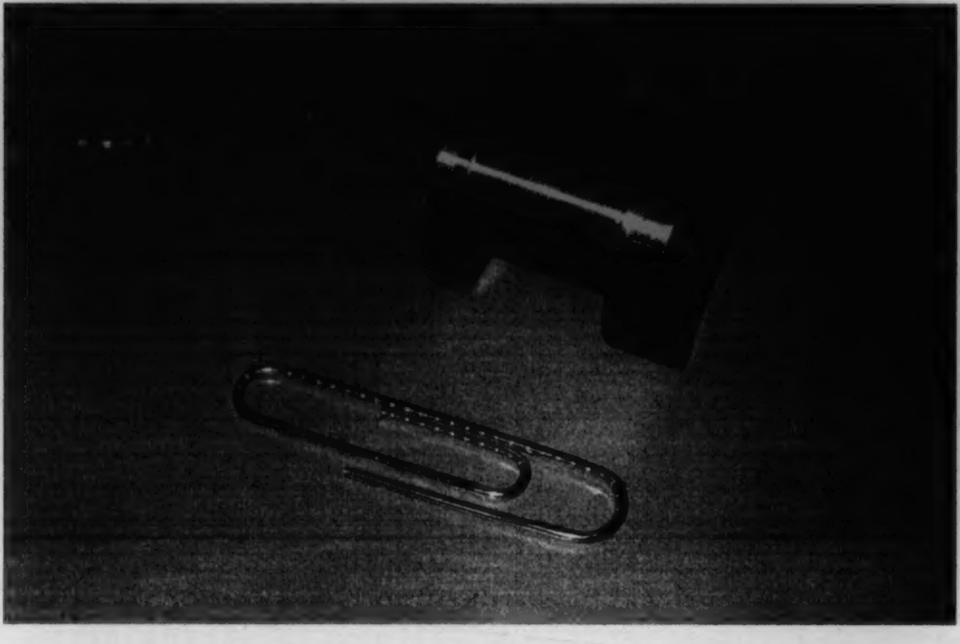

Figure 5-9. Side bottoms used to shot and measure travel time of radial seismic waves

Figure 5-10. Detailed view of side bottom mounted in the sample for radial acoustic measurements

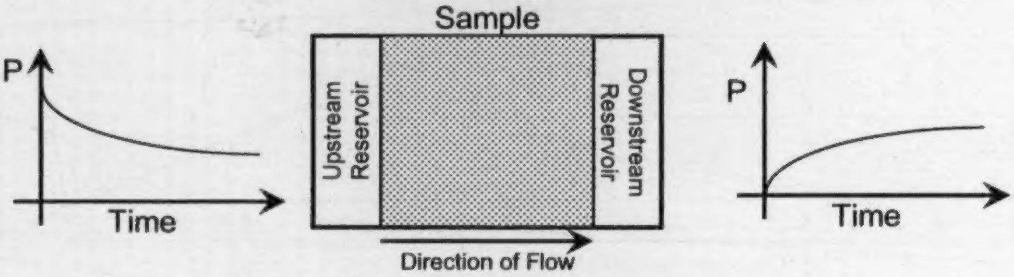
Sample
P
Time
Upstream Reservoir
Downstream Reservoir
Direction of Flow
P
Time

Figure 5-11. Pulse pressure transient technique

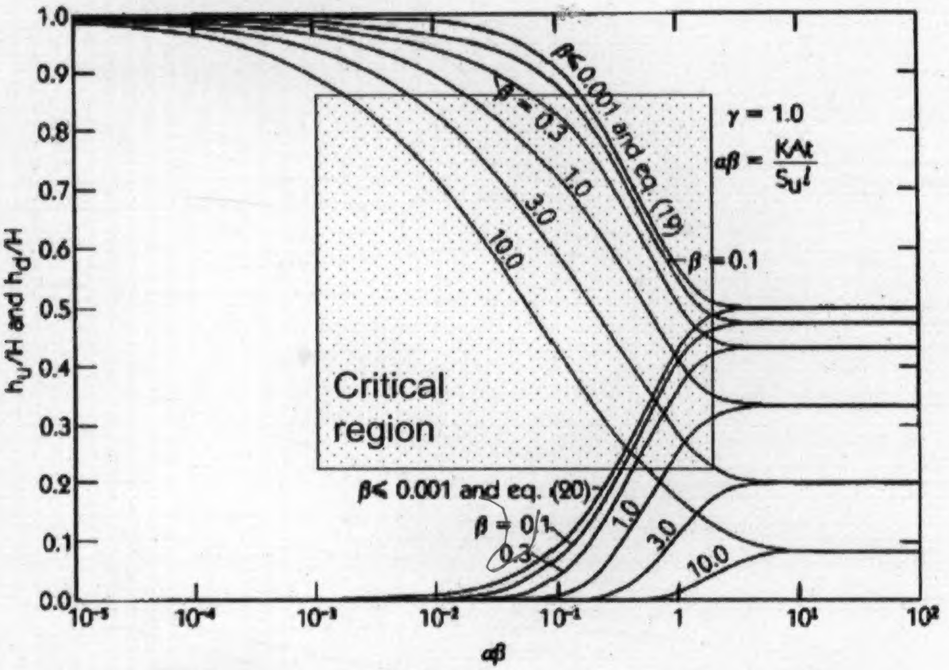

Figure 5-12. Graphical solution to the TPT, modified after Hsieh et al. [97]

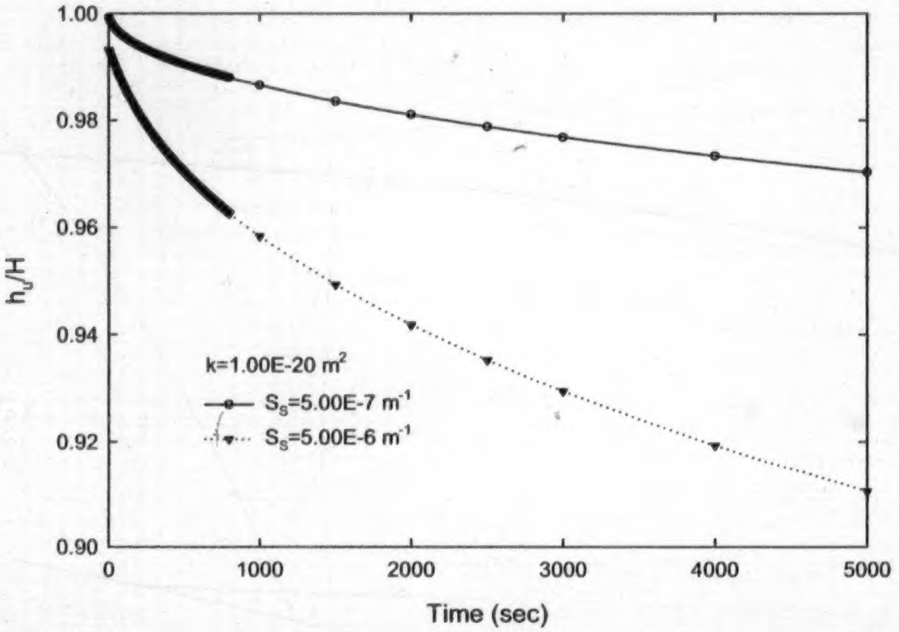

Figure 5-13. Upstream pressure decay for different values of specific storage

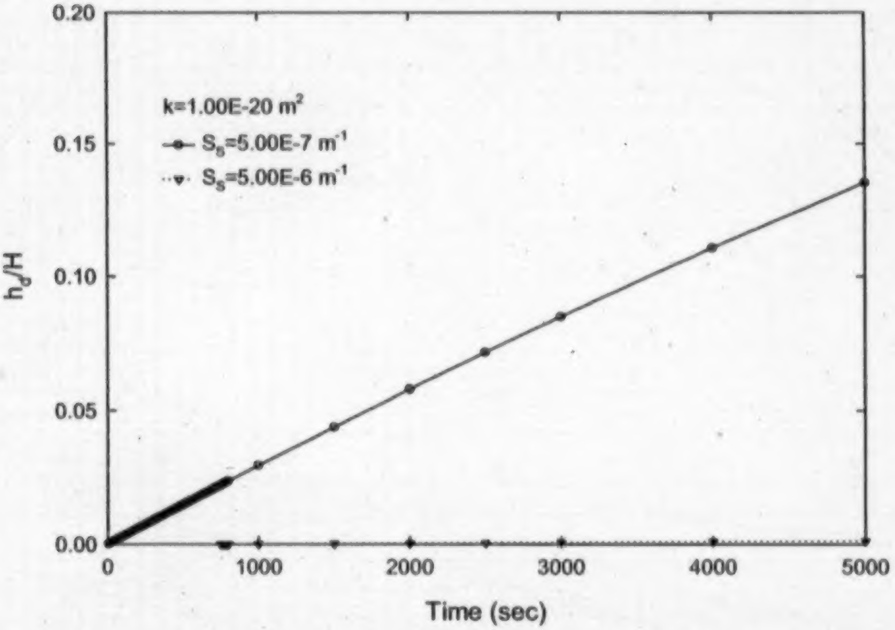

Figure 5-14. Downstream pressure increase for different values of specific storage

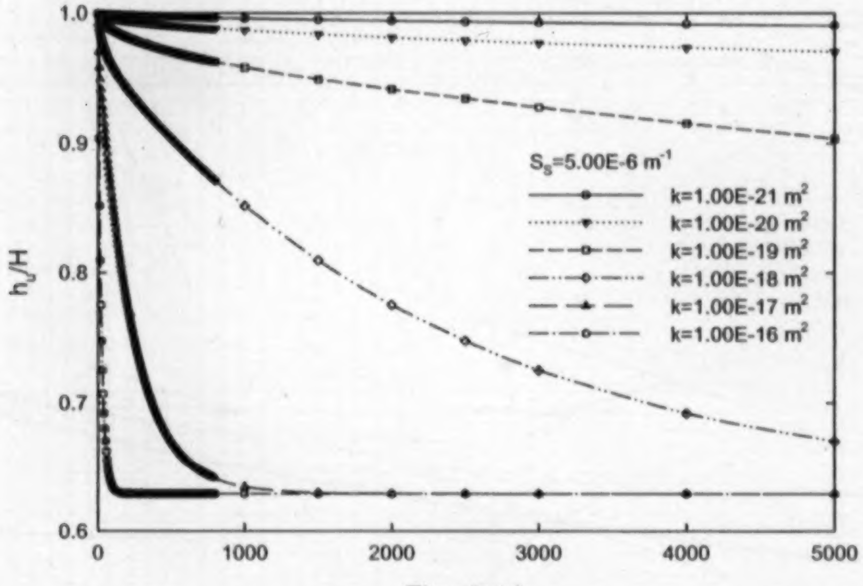

Figure 5-15. Upstream pressure decay for different permeabilities

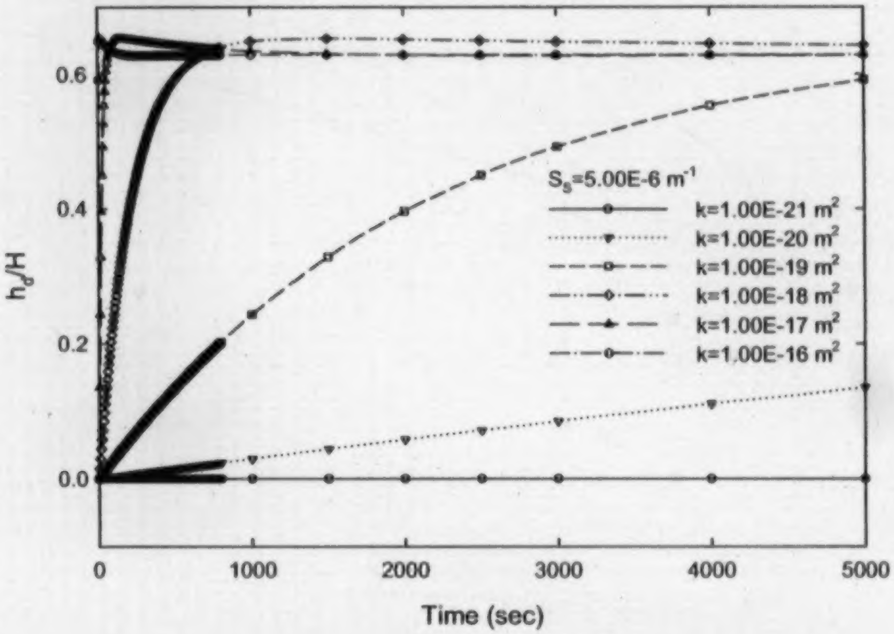

Figure 5-16. Downstream pressure increase for different permeabilities

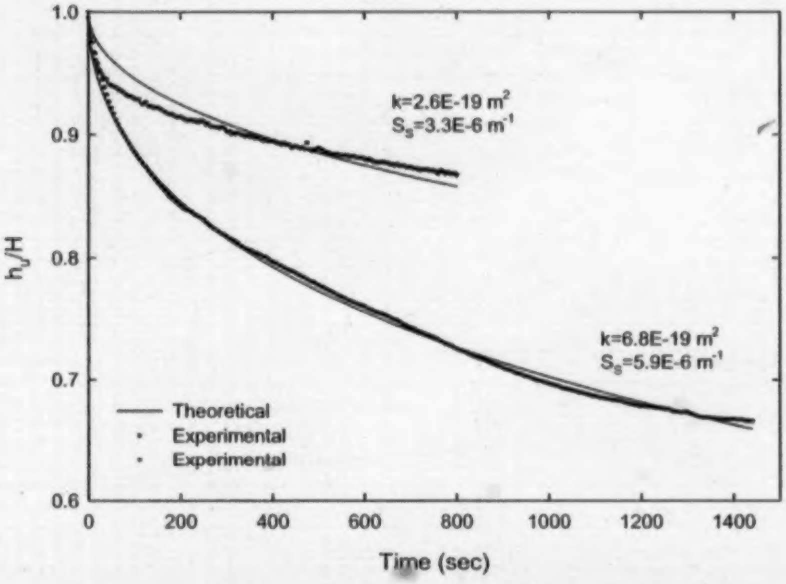

Figure 5-17. Example of two readings and evaluation of permeability using the pulse pressure technique. Only upstream data were acceptable for calculations

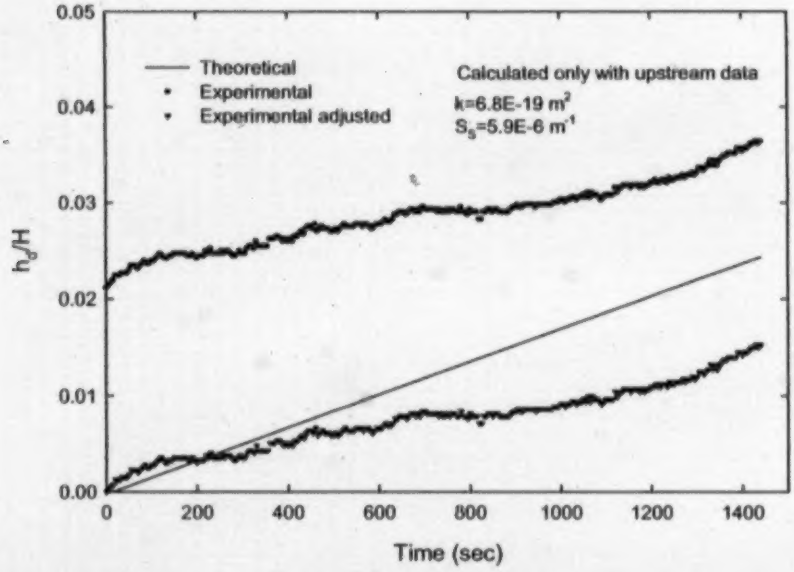

Figure 5-18. Downstream readings during a pulse pressure tests. Because of the low pulse applied and the instantaneous jump in pressure, it is impossible to use these readings to calculate permeability

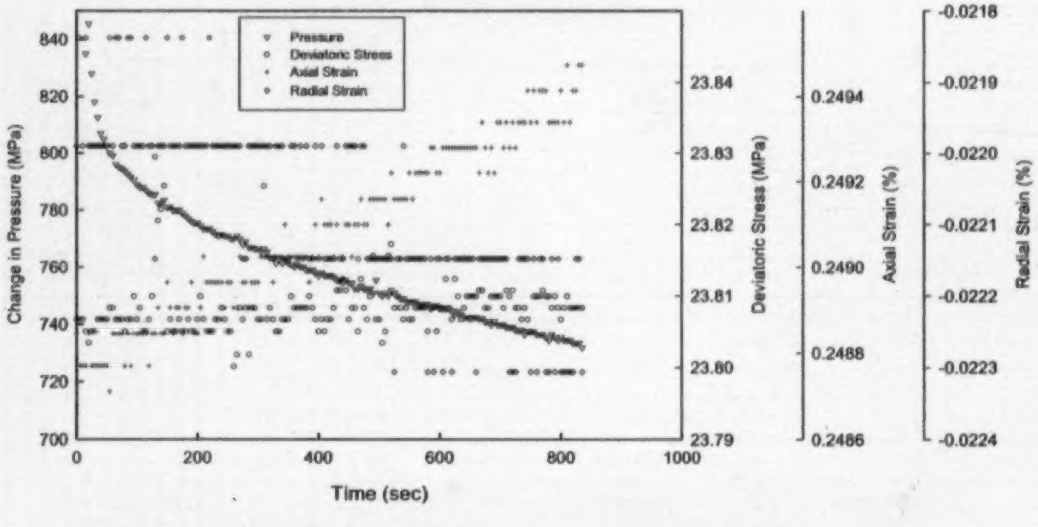

Figure 5-19. Change in deviatoric stress and deformation induced by pulsing

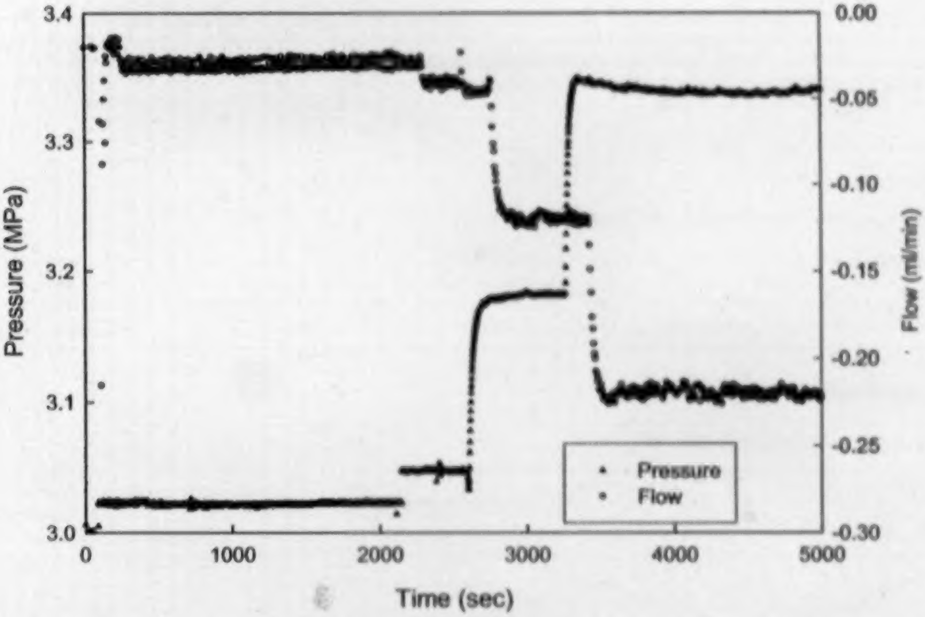

Figure 5-20. Pressure and flow measurements during constant flow permeability measurements

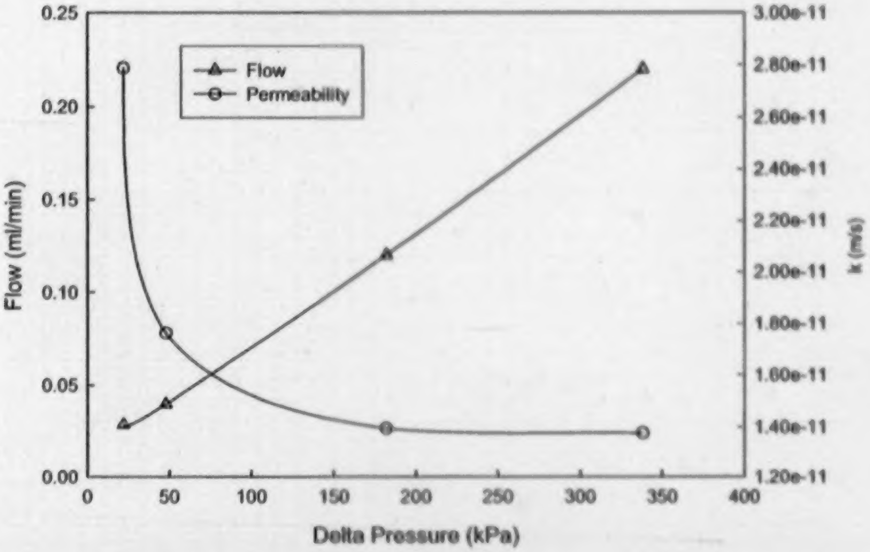

Figure 5-21. Average flow rates for different gradients, and permeability values measured. Notice how stable the measurements are once the flow is more than 0.05 ml/min

6 Behavior of Shales and Anhydrites as Caprocks

6.1 Overview

As was mentioned in Chapter 4, anhydrites and shales constitute the caprocks of the 25 largest oil fields and the 25 largest gas fields in the world. Therefore, they are ideal materials to act as caprocks for CO_2. However, the geomechanical implications of CO_2-EOR storage make necessary a comprehensive understanding of the hydro-mechanical behavior of these rocks. Likewise, the experience with these two materials at the depths, pressures, and temperatures that deep storage is carried out is limited. Consequently, a literature review in the hydro-mechanical behavior of shales and anhydrites will improve the understanding on the response of these materials to CO_2-EOR storage activities and it will help to identify and address knowledge gaps, as well as it will contribute to the confidence in their performance as caprocks.

6.2 Shales: Hard Clays and Mudrocks

6.2.1 Classification of Argillaceous Stiff Soils and Soft Rocks

Stiff clays, clay shales and mudstones are a type of hard soil-soft rock, which forms more than 50% of the materials on the earth, and are one of the most problematic from an engineering point of view. Weak rocks, soft rocks, hard soils are the most common names used for this class of materials that occupy the central part of the geotechnical spectrum with characteristics intermediate between the soft soils and the hard rocks [107]. The compressibility and the generation of high porewater pressures, which can be of the same order as the strength of the soil and consequently have a major effect on strength, control the behaviour of the materials toward the side of soft soils in the spectrum. On the hard-rock side of the spectrum, the same principles apply but rock compressibility is much smaller than soil compressibility, the porewater pressures generated are much smaller and because of the large strength of hard rocks, these pore pressures generally become insignificant. Thus, soft rocks in the brittle range behave like overconsolidated soils and soft rocks in the ductile range behave like normally consolidated soils [108]. However, the rock mass performance can be heavily influenced by the presence of defects. Exactly the same principles apply to soils, but because the properties of intact material are so much closer to the properties of the defects, the influence of the defects is not nearly as marked [107].

There has been an important number of contributions to define and classify stiff clays, shales and mudrocks, with some associated parameters that define the limits for the different materials. Morgenstern and Eigenbrod [109] developed a classification for argillaceous soil and weak rock that is in widespread use, Figure 6-1. Such a classification is based on the idea that a soil will disintegrate when exposed in an unconfined manner to water and that a rock will not. Thus, the distinction between clay and a mudstone is a function of relatively stability when immersed in water. Clays can be further subdivided according to the rate at which strength is lost upon immersion. Most clay-shales fall under the heading of hard clays. Clays and mudstones can further be characterized in terms of slaking properties. However, this classification does not consider the presence or absence of fissibility and anisotropy, two of the main properties that control the behaviour of these materials. The classification states the following definitions for mudstones, clay and clay shales:

- Mudstone: softens slowly over a period of weeks, the strength loss during softness is less than 40% of the original material strength, and this correlates with an unconfined compressiver strength (C_u) of the original material greater than 1.8 MPa.
- Clay shale: softens over a few days to lose more than 60% of the original material strength, such a material has a shear strength between about 300 kPa and 1.8 MPa.
- Clay: softens within hours to lose more than 60% of the original material strength. The original unconfined compressive strength is less than about 300 kPa.

Grainer [110] developed an alternative classification of mudrocks, which is more detailed and complex than the one by Morgenstern and Eigenbrod, but its downside is that it requires a more complex set of tests like X-ray diffraction and index properties, the latter being highly dependant of procedure in these materials. Despite these limitations, it is interesting to mention a few points such as fissile or anisotropic rocks are termed shales, whether they are durable or not; clay shale are considered as a non-durable mudstones; and mudstones with an unconfined compressive strength greater than about 1.8 MPa can be thought of as durable.

6.2.2 Mechanical Behaviour of Stiff Clays and Shales

6.2.2.1 Mechanics of Shear Resistance in Mudstones and Stiff Clayes

The most important features that characterize clayey materials are mineralogy, particle size and shape, and platyness. Aggregation of clay particles due to diagenetic bonding increases the effective particle size and decreases platyness [111]. Clay particles and water are associated by either hydration of the particle surfaces or hydration of ions surrounding the surfaces. The former constitutes adsorbed water and the latter double layer water. Due to the adsorbed water, the minerals are not in intimate contact when in a face-to-face orientation. Consequently, water participates in the transmission of normal stress, but reduces interparticle contact and the ability to transmit shear stress [112].

Although at a particulate level the nature of frictional and cohesive strength is not well understood, it is thought that the main bonding mechanism in frictional resistance is primary valence bonds, where surface atoms at interparticle contacts are joined by sharing and transferring electrons. The number of these bonds increases with contact area, and so an increase in normal stress leads to a larger contact area, and larger shearing resistance [113]. Such a mechanism is reflected in the higher shear strength in overconsolidated clays than in normally consolidated clays at a given normal stress, where the overconsolidated clay has a lower void ratio. This is the so-called "true cohesion" that represents a mechanism of shear strength resulting from interparticle bonding [114]. However, such a cohesion in natural soils is not only due to chemical bonding, but may be the end result of other processes as it will be seen in the next section.

6.2.2.2 Sedimentation, Diagenesis and Bonding

The geological stages during which the soil structure is formed, and then modified, are part of a cycle: (1) subaqueous sedimentation, typically in a reducing, oxygen-deficient environment; (2) consolidation (geological compaction) under the increasing stresses of continuing deposition, followed by (3) uplift relative to sea-level, which leads to (4) erosion, with consequent unloading of the remaining clay, accompanied by subaerial weathering. The eroded material is then transported to another area of deposition, signalling the start of the next cycle. Diagenesis is embedded during every stage of the process that Chandler [115] calls the Geotechnical Cycle.

The Geotechnical Cycle commences with deposition: sedimentation of individual clay or silt particles, and often flocs of particles, at the mudline of the seabed. The considerable range of water content, even at this early stage in the history of the sediment, shows that there must be a corresponding range of soil structure. The original soil structure is retained as the soil element is buried, though with some modification with increasing depth and stress [115].

The most significant depositional factors are likely to be the mineralogy of the sediments, the rate of deposition and the stillness of the water. Slow deposition in still water leads to an open random fabric with high values of void ratio. On the other hand rapid deposition from a dense suspension, possibly with significant currents, will give rise to a more oriented fabric which is consequently more compact with a lower void ratio [116]. The fabric of soft sediments formed under different physicochemical environments is highly dependent on the clay mineralogy, i.e. the volume change undergone by the kaolinitic soils during settling and the shearing resistance at the particle level controls sediment formation, whereas for montmorillonitic soils it is governed by the diffuse double layer repulsion [117].

Skempton [118] examined the Sedimentation Compression Curves (SCC) of a range of natural clays in terms of water content, showing that the position of different SCCs depend on the liquid limit, Figure 6-2. The more or less constant position of each of the clays relative to the lines of equal liquid limit shows that each clay maintains its own basic structure with increasing depth of burial [115]. Expressing the water content as liquidity index (LI), Skempton [118] demonstrated that his data converged to a relatively narrow band, and noted the position occupied by the various clays appeared to depend on sensitivity, with the more sensitive clays lying to the right.

It is widely recognized that the fabrics and grain structures of clays, shales and mudrocks are highly sensitive to changes in both stress and chemical environments. These materials experience complex physical changes during diagenesis which can have a pronounced influence on their subsequent mechanical behaviour [107, 116, 118, 119]. During compaction diagenetic processes and chemical reactions that help turn a sediment into a rock (lithification) occur at the same time. The diagenetic reactions gradually increase the bonding between particles, whether or not the particles are being brought together physically. Cementation for bonding may be produced by dissolution of small, supersoluble particles and reprecipitation of calcium carbonate, precipitation of iron hydroxides or dissolved aluminun, recrystallization during alteration, changes in the absorbed water, and face and edge changes on clay particles [120]. The natural diagenetic and deformation history of a weak rock will therefore exert a pronounced influence on its mechanical characteristics when that material is subject to changes in its stress environment due either to engineering activities or geological processes [121]. As a result, natural clays can develop a structure stronger than that of the corresponding reconstituted clay in addition to the differences that result from sedimentation and normal consolidation processes [122]. Thus, oedometer tests in Boom Clay samples from 247 m depth showed a preconsolidation pressure of 6 MPa, which is not possible to reconcile with the geological history of the site [123]. Therefore bonding has to provide the additional strength of the material.

6.2.2.3 Peak Strength

The peak strength of stiff clays and mudstones is strongly influenced by the material fabric and structure, especially through diagenetic bonding. A combination of diagenetic bonding and/or overconsolidation increases the strength of intact material. At low to medium confining stresses peak strength is reached at low strains. Likewise, its strength envelope is curved at low to medium confining stresses due to dilation, as can be seen in results from testing in London clay, Bearpaw shale, Santa Barbara clay, or Todi clay, the latter in Figure 6-3. At large confining stresses the material behaviour is ductile, its strength envelope is linear, and it usually coincides with the intrinsic strength envelope due to partial destructuration during consolidation. Experiments on Vallerica clay [124] at low and high confining pressures showed a clear difference due to the structure. In the high pressure tests, the structure was partially destroyed before shear, while in the medium pressure tests, the structure controlled peak strength. However all the tests were heading toward a common unique critical state line.

6.2.2.4 Post-Peak Strength

At low to intermediate confining stresses, a failure plane develops at peak strength and the strength on this plane drops rapidly to a reasonably constant value after a relative displacement across the surface of only a few millimetres [116]. Burland called this value the 'post-rupture strength' and Skempton [118] the 'fully-softened'. Such an envelope is curved and it usually goes above the intrinsic one at low stress, and below it at medium stresses, as can be seen in triaxial tests carried out in Todi clay [116], Figure 6-3. Calabresi [125] found that the immediate post-peak strength is representative of the initial strength along a recently formed pre-existing discontinuity. This loss of strength is due to the breaking of diagenetic bonds, softening due to dissipation of dilation-induced pore pressure and increase in water content, and particle reorientation in the failure plane [126].

From tests on Todi clay with local measurements of strain and pore pressures it has been possible to see how the loss of strength occurs in stiff clays (see Figure 43 in Burland [116]). Initially there is a sharp drop immediately after the peak strength is reached due to the breaking of interparticle bonding. Dilation occurs as a response to the breaking of interparticle bonds and formation of a slip plane, along which clay can swell and soften due to moisture redistribution. Dilation stops once the post-rupture strength is achieved. Once interparcticle bonding has been destroyed, particles in the slip plane are realigned parallel to the movement direction with shear. Such a process requires large displacements to be completed and is responsible for the drop from fully-softened strength to residual strength.

Natural clayey materials have a partially random oriented structure, where a large amount of clay particles are aligned edge-to-face. Shear straining along a plane leads to a gradual a face-to-face reorientation of the particles, accompanied by a smaller interparticle contact pressure. As shearing continues there will be a plane where the particles are oriented parallel to the shear direction and the strength is at residual [111]. As the particle sizes decreases and the platyness increases, the interparticle contact pressure decreases, edge-edge interlocking is minimized, and residual strength decreases [111]. Such an evolution of structure has been observed by triaxial tests and SEM carried out in Kimmeridge Shale [121]. The Kimmeridge Shale shear failure is accompanied by the development of a single slip plane in the sample. The failure envelope is linear, except at low consolidation stresses, and resembles a critical state line at large pressures. The intact shale exhibits a 'house of cards' structure with many face-to-edge contacts between platy clay mineral grains. During consolidation, the fabrics of the shale was largely unaffected by the volumetric deformation, although some changes must have occurred to accommodate the volumetric strain. At failure the polished slip surface seems to be the centre of the shear zone, in which the original fabric is progressively reoriented so that platy clay minerals become aligned parallel to the shear direction. The degree of alignment increases with shear strain.

6.2.2.5 Brittle-Ductile Behavior

A conceptualized mechanism of failure for mudrocks and clay shales, Figure 6-4a [127] shows that the behaviour of mudrocks at low mean effective stresses is brittle, showing a distinct peak strength before undergoing failure and strain weakening to residual failure. At very high mean effective stresses they tend to behave in a ductile manner, with the maintenance of peak strength at large strains. In between, there is a 'transitional' regime, where undrained shear deformation leads to the maintenance of peak strength to a given axial strain in a manner that is similar to ductile deformation before the initiation of strain weakening to a residual strength. Such a behaviour has been observed in many stiff clays and shales, as can be seen for London clay in Figure 6-4b. Different soft rocks sheared at a large variety of confining stress show a similar behaviour [108].

This conceptualized model is similar to the one described by Malandraki and Toll [128], in which there are three modes of failure:

- Mode 1: when a bonded soil is sheared at low effective confining strengths; the soil sustains higher strengths than that of the destructured soil and yield (final yield) coincides with failure.
- Mode 2: a transitional zone where the soil yields in the initial stages of shearing, but achieves a higher strength than the destructured soil due to the post-yield influence of the bonds.

- Mode 3: the third mode of failure is defined when the bonded soil is sheared at higher effective confining pressures, yielding occurs under shear or in isotropic compression, and the soil's strength is similar to that of reconstituted soils.

However, a total loss of structure may require very large pressures, as was observed in the Pappadai clay [122]. The Pappadai clay is massive and regularly laminated, with a large content of carbonate, but it is largely concentrated in the sand and silt fractions. The clay fabric can be considered as a highly compressed 'bookhouse' type and overall has a medium orientation. The ratio of the yielding stress to the current vertical stress is twice the OCR, so there is a significant gain in strength due to its structure. The fabric beyond yield is more densely packed than the undisturbed clay, but less oriented as yield seems to result in extensive and chaotic change to the original fabric. In the undisturbed clay, the alteration of oriented and flocculated fabrics can be distinguished, whereas post-yield, the different particle arrangements seem to merge into each other so that the boundaries are ill defined. Post-yielded compression changes the structure to regular alternation of stacks and flocculated-honeycomb fabric. The honeycomb structure is very stiff and resistant to compression despite its openness, likely the result of electrostatic forces acting at the edge-to-face contacts between particles. This is probably the reason why the post-yielded clay can retain a higher void ratio and strength than the reconstituted clay.

The strength envelope also reflects the brittle-ductile transition that these materials go through, Figure 6-5 [127]. At low mean stresses a well-defined curved peak strength envelope is seen, with a fully-softened envelope near the intrinsic strength envelope, but usually above. Failure is brittle and the sample shows a distinct shear zone where it develops a slip plane and subsequent deformation is by rigid sliding across the shear plane [127, 129]. High shear stress represent a phase of brittle microfracturing, with the sample undergoing barrelling, and strain weakening leading to brittle failure due to coalescence of the microfractures [127, 129]. At medium mean stresses the peak envelope flattens and tends toward the intrinsic envelope, whereas the fully-softened envelope lies at or below the intrinsic line [129]. At large mean stresses, the structure is removed, the peak envelope coincides with the intrinsic envelope, and the failure is ductile. Deformation is through internal reorganization of the structure.

6.2.2.6 Residual Strength

Residual strength is the strength of a slip plane where the particles have been realigned and the particles are in face-to-face interaction. Consequently, it is difficult to establish short range contact and thus to generate shearing resistance [111]. Lupini et al. [130] recognized that there are three modes of residual shear behaviour; a turbulent mode, a transitional mode, and a sliding mode, each depending on dominant particle shape and on the coefficient of interparticle friction:

- The turbulent mode occurs when behaviour is dominated by rounded particles, or, possibly, in soils dominated by platy particles, when the coefficient of interparticle friction between these particles is high. Residual strength is high, no preferred particle orientation occurs, and brittleness is due to dilatant behaviour only. The residual angle depends on the shape and packing of the round particles and not on the coefficient of interparticle friction.
- The sliding mode occurs when behaviour is dominated by platy, low-friction particles. A low-strength shear surface of strongly oriented platy particles then develops. The residual friction angle depends primarily on mineralogy, pore water chemistry and on the coefficient of interparticle friction.
- The transitional mode occurs when there is no dominant particle shape, and involves turbulent and sliding behaviour in different parts of a shear zone. The properties of the soil in residual shear change progressively across the transitional range from those typical of turbulent shear to those typical of sliding shear. In this mode the residual friction angle is sensitive to small changes in grading soil, where the changes in grading required to cross this range entirely are typically small.

6.2.2.6.1 Shear Zones and its Structure

Shearing in clay generates changes in fabric and structure that become more important as the shear stress level increases. Such changes are often concentrated in a narrow soil layer (strain localization). If drainage is allowed, shear strain localization is associated to contraction in the case of normally consolidated clays and to dilation in highly overconsolidated clays [131].

Picarelli et al. [131] gave an excellent description of the process of shearing in clayey materials, and clarify any confusion with the use of terminology. They state that a shear surface represents a physical discontinuity in the material: this indicates the onset of rupture, but no shear displacements yet occur along this surface. Once the soil fails, it is physically separated into two adjacent bodies, moving along the newly formed interface, which is a displacement discontinuity or slip surface. According to Skempton and Petley [132] the mechanism of rupture is characterized by initial formation of single separate shear surfaces, called Riedel shears (R) that are slightly inclined to the direction of shear, and by some conjugate discontinuities. Then, another set of discontinuities, the thrust shears (P) are formed at location almost symmetrical to the R shears. All these discontinuities called minor shears do not allow for significant displacements [132]. Finally, the displacement discontinuities (D) are formed in the direction of the imposed shear. In the final stage, the latter link up to form a unique principal displacement discontinuity. Figure 6-6 shows the successive stages on the development of slip surfaces in clay and its relation with the behaviour of the material [133]. The described zone of discrete thickness including such a complex system of shear discontinuities is a shear zone. The shear zone structure is then characterized by the presence of various minor shears and slip surfaces, along which clay particles are more or less oriented (shear-induced microfabric) [134, 135].

Finally, the expression shear band has sometimes been used to indicate a soil layer subjected to intense shear strains without formation of discontinuitites [136]. Therefore, a shear band is what Turner and Weiss [137] call a strain discontinuity that does not physically separate the material in adjacent parts, as shear surfaces do.

6.2.2.7 Softening

Clay shales are typically characterized as a stiff, fissured clay or shale that is succeptible to significant deterioration as a result of interaction with water. They are usually highly overconsolidated clays with high plasticity, a high content of montmorillonite clay, and a tendency to undergo extreme slaking with wetting and drying cycles [138].

Both the presence of fissures and unloading are necessary for softening to occur. It is evident that softening can arise from both internal and external processes. There is considerable evidence that the end result of the softening process is essentially cohesionless clay behaving more or less like a normally consolidated material. Softening typically results in a greater reduction in effective cohesion than friction [139].

6.2.2.8 Fissures and Joints

A fissure is a discontinuity in a clay or rock, which may or may not have undergone shear displacement. Fissures are small scale (i.e. typically hand specimen size) while joints are medium- to large-scale discontinuities (i.e. best observed in field exposures) [140]. The most relevant issue with fissures and joints is whether displacement has occurred on them.

In clay shales there are three important effects of fissures in controlling the behaviour of the deposits. First, they provide inherent planes of weakness along which shear can occur. Second, the fissures greatly increase the permeability of clay shale deposits. Without the conduits provided by fissures, most clay shales would be virtually impervious. Third, fissures significantly increase the surface area exposed to weathering agents. No matter which softening mechanism is acting on a clay shale deposit, the rate and extent of softening is highly dependent on the presence of fissures [138].

Marsland [141] shows that for a particular clay the strength measured in the field and in the laboratory depends on the extent of fissuring, the size of the element of soil tested in relation to the spacing of the fissures; the inclination, orientation, shape, and surface roughness of the fissures; the stress change during sampling and testing, and the time associated with the stress change. Different clays will have different basic properties and previous stress histories, which will also vary with location and depth. These factors will affect the properties of intact clay and the nature of fissures, and the strength applicable to a particular engineering problem depends on some or all of these factors.

Fissures can also be responsible for the brittle failure observed in these materials. Vallejo [142] has found that if the water content in fissured clay samples reaches a value equal to or less than 20%, their behaviour under compression is similar to brittle materials. In compression, the tips of the crack concentrate both compressional and tensile stresses. The sample will always fail in the regions of tensile stresses. When the inclination of the cracks with respect to the axial load has low values, there is an absence of tensile stress at the tip of the cracks.

The widespread presence of fissures in stiff clays and shales has been widely documented. The most common causes of fissuring are briefly explained below.

6.2.2.8.1 Fissility

Fissility is the characteristic that causes a material to split into thin layers lying parallel in a particular direction, as for example, bedding planes [143], which is an intrinsic characteristic of many clay shales. As the degree of fissility decreases, the orientation of the clay minerals becomes more random. When fissility is completely lacking, as in clays, the orientation of the clay minerals is also lacking or random. The chemical environment at the time of sedimentation strongly influences the development of fissility. Consolidation serves to increase the degree of fissility by bringing already oriented clay minerals closer together. Fissibility can be caused not only by partcle orientation, but by destructuration, as was observed in oedometric tests in Pappadai clay [122]. The considerable compression is likely to have destroyed the calcite film bonding the particles, so that at high pressures bonding is mainly of an electrical nature. Thus, bonding is the weakest in the bands of oriented particles since there the particles are in face-to-face contacts. Thus on unloading these bands provide the sites of extension fractures or fissility planes.

6.2.2.8.2 Syneresis

Mitchell [89] defines syneresis as "… the mutual attraction of clay particles to form closely knit aggregates with fissures between them". Fookes [144] described syneresis cracks as "… fissures that develop in a suspension, where water is expelled from a clay/water system by internal forces". This process depends on the particle size of the sediment, and the concentration and type of cations present. Syneresis cracks are usually found in thin beds of clay between harder strata such as fissile shale, limestone, or sandstone. The clay minerals in the syneresis cracked bed are not oriented as in shales. The syneresis cracks are found in clays, which appear to have been deposited in a flocculated state. Syneresis cracks or fissures may develop during sedimentation and remain as closed cracks during normal consolidation but will open again by rebound, when a fresh face is exposed [143].

6.2.2.8.3 Desiccation

Desiccation results in shrinkage and cracking of clayey soils, particularly in those containing minerals with high swell potential, such as smecties [89]. Freezing and thaw cycles increase overconsolidation and desiccation by drawing water from soils towards the freezing front. With each cycle of freezing and thawing, the advance of the freezing front into the soil mass causes ice lenses to form in preexisting cracks, which draws water from the adjacent soil blocks and increases the overconsolidation of the blocks.

6.2.2.8.4 Tectonism

Tectonism is a deformational process responsible for the generation of faults and folds. Due to the strains resultant from tectonic processes, the mechanical properties can change. There are many examples in the literature on tectonic zones and its influence on clay shale material. D'Elia et al. [145] studied a Miocenic mudstone in Italy and found that tectonic stresses caused structural complexity in a twofold manner: (i) tectonics conferred completely different mechanical properties to materials slightly different in composition; and, (ii) tectonics caused an irregular heterogeneity due to the distribution of structurally different materials. Also, they compared the local tectonic structure and the principal structure characteristics during a tunnel excavation and found that: (i) the highly tectonized zones with sheared material were found where the distance from the faults is smallest; and, (ii) the average attitude of the bands of sheared material is close to that of the main faults and of the faults crossed by the tunnel.

6.2.2.8.5 Glaciotectonics

Glaciotectonics or ice-thrusting occurs when a glacier is forced into compressive flow by the underlying topography or during net ablation of the ice sheet, which involves recession of the ice front and thinning of the ice sheet. Elevated bedrock pore pressures are generated ahead of the glacial advance by basal freezing, which reduces the resistance of the bedrock to deformation by thrusting of the adjacent frozen bedrock. The sediments may be folded and sheared, and then re-deposited during ablation, forming complex structures including reversed stratigraphy sequences [146, 147]. Tsui et al. [148] described a 3.8 m thick shear zone found in bentonitic mudstones in the North Saskatchewan River valley, Alberta, where principal displacement discontinuities were present (Riedel) and thrust shears.

6.2.2.8.6 Erosion and Stress Relief

Studies of fissures on several Cretaceous clays of England [149] found that at every site that was studied, there was some indication that a set of fissures had developed parallel to the exposure orientation (a mechanism similar to bedding). Also, from these observations it is suggested that the process of fissure formation sympathetic to the topography is: (i) within a period of months after exposure a weakly concentrated uni-planar set of fissures is formed parallel to the slope surface, (ii) several years later a weakly concentrated major girdle of fissures becomes apparent perpendicular to the slope surface, making a right-angled combination with the uni-planar set. A similar development of sets of fissures was found on different glacial tills of Scotland [150, 151].

Another process of stress relief but on a larger scale is valley rebound [152, 153]. River erosion removes horizontal support from valley walls and vertical support from the valley floor. Valley walls deform inward and the valley floor upwards. Inward movement of valley walls concentrates in the weaker, more deformable beds, which usually develop shear zones. Stronger, stiffer beds develop vertical to subvertical tension joints, which typically do not extend across weaker beds. Most valley bottom deformation occurs between the valley walls but some deformation also occurs beneath relaxed zones in the valley walls. Lateral compression plus vertical load removal causes arching and buckling of beds in the valley bottom. Bedding planes open in strong, stiff beds while anticlines and thrust faults develop in weaker, more deformable beds. Shearing displacement along bedding planes produces shear zones commonly along weak bedding.

6.2.2.8.7 Relict Landslides

Previous landslides would have produced shear planes, as forensic labour in many landslides has proven [132, 135]. Barton [154] showed from a survey of the literature that compound shaped landslides are of common occurrence and of world-wide distribution in stratified over-consolidated clays and soft rocks with flat-lying bedding. The bounding shear surface of these landslides has a steep rotational part at the rear and a translational part parallel to the bedding at the front. The translational part is many times associated either with pre-sheared materials or progressive failure of the material.

6.2.3 Groundwater Flow and Permeability in Stiff Clays and Shales

6.2.3.1 Groundwater Flow

Groundwater flow in low-permeability environments is not well understood, although significant progress has been made in the last 20 years. The main reason for this lack of understanding is associated with the complications that arise measuring permeability both in the laboratory and in the field, the time that these tests can take, and the fact that even field tests only measure the permeability of very small volumes.

Studies about groundwater flow in these 'semipermeable' environments have shown that low permeabilities measured in the laboratory are representative and comparable with results backcalculated from regional studies [155, 156], Figure 6-7. However, Neuzil [155, 156] pointed out that as to now it is not possible to predict how and where heterogeneity will affect large-scale permeability in these media. Thus, it was found that some regions are often more permeable than small volumes of the same rock, owing to the presence of joints, fractures, and faults. However, there was evidence of many sizeable regions of low permeability where apparently either there are no fractures, or the fractures are not connected [71, 155-157]. Some examples of both "permeable" and "impermeable" groundwater flow regimes are presented below.

6.2.3.1.1 Regional Flow in the Cretaceous Shales of Mid North America

Different studies in the Cretaceous shales of mid North America [71, 155-157], which reaches more than two km in thickness and two million km^2 in areal extent, have been very useful to understand the groundwater flow regime of shales. Permeability measurement in the laboratory have given permeabilities of the order of 10^{-21} to 10^{-20} m^2. Studies in the Denver Basin, which is marked by strongly subhydrostatic fluid pressures in the Dakota aquifer, a regional sandstone aquifer below the Cretaceous shales, show no presence of secondary permeability, and the predicted values from modelling were similar to the ones measured in the laboratory [157].

On the other hand, Neuzil and Belitz [71] compiled and reanalyzed the data from different regional flow analysis in the Dakota Aquifer in South Dakota and North Dakota, Figure 6-8. Their conclusions suggest that intact clay shale material can be considered impermeable (permeabilities of the order of 10^{-21} to 10^{-20} m^2). However, on the regional scale, the secondary permeability controlled the flow and the average permeabilities were in the order of 10^{-18} m^2. Transmissive vertical to subvertical fractures or similar features were the central feature of this model, and the authors concluded "... such transmissive fractures control the regional vertical permeability of (and leakage through) the shales, but only at depths of less than approximately a kilometer".

Implicitly, Neuzil and Belitz [71] are providing an idea of the approximate state of stress at which the fissures and fractures ease the flow, and these features control the flow regime and movement rates. The absence of secondary permeability below approximately one kilometre depth means that either the fracture openings are lost with further increases in stresses, or there are no more fractures present in the media. Furthermore, the site study in South Dakota found no evidence of the vertical transmissive fractures. The nature of the study suggested the existence of a block of 'tight' shale that is at least a kilometre across. That led the authors to hypothesize that "... the fractures are very sparse and separated horizontally by a kilometre or more". In the early studies by Bredehoeft et al. [157] the hydraulic conductivity of the shales ranged from $5x10^{-12}$ m/s ($5*10^{-19}$ m^2) at depth to $2x10^{-9}$ m/s ($5*10^{-16}$ m^2) near surface. These regional values were as much as a factor of 10^3 larger than laboratory and in-situ determinations of permeability of the shale. This was interpreted as indicating fracture enhancement of the regional permeability [156].

This stress dependant behaviour of fractured rock mass has been observed in theoretical studies like the one carried out by Sanderson and Zhang [158], in which the fluid flow and deformation of a rock mass were simulated using the distinct element method. A series of numerical experiments on different rock masses with different fracture networks were carried out, where the increment in pressure led to a change in the flow regime from diffusive to highly localized once certain critical stress was reached. At the critical pressure at which permeability increases significantly all the principal effective stresses are still compressive, and the fluid pressure is sublithostatic.

6.2.3.1.2 Tournemire Tunnel, Southern France

In the context of an R&D program on nuclear waste disposal a 250 m thick argillaceous formation in southern France was studied for NWD purposes [72]. The argillite has a low natural water content (~3-5%) and very low porosity. Laboratory tests produced diffusion coefficient (tritiated water) from $2x10^{-12}$ to $2x10^{-11}$ m^2/s and hydraulic conductivities from 10^{-13} to 10^{-14} m/s (10^{-20} to 10^{-21} m^2). Field hydraulic conductivity tests produced permeability from 10^{-11} to 10^{-13} m/s (10^{-18} to 10^{-20} m^2). Because of the low values of permeability, it was concluded that fluid flow was essentially governed by diffusion. Fracture analysis from cores show the existence of planes with different types of fillings (mainly calcite) of various sizes. The fractures appeared to be perfectly sealed and impervious.

Also, a geochemical study was carried out using stable isotope from intersticial water, which gave some indications on the origin of the intersticial fluids and possible flow process [72]. From $\delta^{18}O$ and δ^2H contents of the pore water, the possible origins for the fluids were analyzed. By postulating diffusion processes as the main flow mechanism through the clay formation, an attempt at modeling travel time was made based on the deuterium profile. It was concluded that fluid-flow in this rock formation is most likely governed by diffusion processes.

6.2.3.1.3 Opalinus Clay, Fractured Jurassic Shale

As part of the Swiss programme for high-level waste disposal, a Jurassic claystone is being investigated as a potential host rock [75]. The measurements of hydraulic and geochemical properties of the shale were carried out in ten tunnels in the Folded Jurassic of northern Switzerland. Despite extensive faulting, only a few indications of minor water inflow were encountered in more than 6000 m of tunnel. All inflows were in tunnel sections where the overburden is less than 200 m, and are either associated with an intercalated series of fractured calcareous sandstone layers, or with faults, some with minor calcite veins. It seems that at stresses larger than the ones found at 200 m depth, fracture conductivity is null, which is similar to the results by Neuzil and Belitz [71] in Cretaceous shales. Hydraulic tests in deep boreholes (below 300 m) yielded a hydraulic conductivity lower than 10^{-12} m/s (10^{-19} m^2), even though joints and faults were included in some of the test intervals. It is important to note that this is a tectonized indurated clay with a total water content that ranges from 4 to 19%. Apparently, advective transport is not a critical issue in the Opalinus clay, and this conclusion was reinforced by hydrochemical and isotopic data [75].

On the other hand, hydraulic tests were carried out in the excavation disturbed zone (EDZ) of the Mont Terri Rock Laboratory, in the Opalinus Clay [73]. The EDZ was composed of two parts, the first one a meter into the walls, where there is a large density of fractures, which are well connected and unsaturated; and a second zone between one and two meters with a lower density of saturated, and poorly connected fractures. Permeability increases in the EDZ were between 2 and 4 orders of magnitude closer to the walls, quickly decreasing to in-situ values, usually between one and two meters from the wall. It is clear that both fracture connectivity and level of stress are very important for flow in argillaceous formations.

6.2.3.2 Hydro-Mechanical Response of Clays and Shales

Permeability of argillaceous materials, either soils or rocks have been extensively studied, but are still subject of controversy, and at a phenomenological level it is not well understood. However, it is clear that structure, mineralogy, porosity, and fluid chemistry are among the most important parameters that control permeability. In the case of geological storage, permeability measurements at large pressures are more relevant than the usual observations made in geotechnical engineering, so the following paragraphs will review some of these measurements.

Krooss et al. [159] investigated the molecular transport and fluid flow of unfaulted and faulted pelitic rocks form different regions and geological ages, Figure 6-9. Permeability was measured using the constant flow technique at very high temperatures and pressures in samples of 28.5 mm in diameter and 30 mm in thickness. The results show an exponential decrease (approximately linear in the semi-logarithmic plot) in permeability with effective stress and a power law for cemented silty claystone. Even more important, the authors found that neither of the tested samples showed a systematic dependence of permeability on fault frequency, intensity and orientation, which suggests that any increment in permeability due to faulting or fracturing seems reduced and eliminated by local secondary mineralization processes and/or ductile deformation of the shales. However, the effects of faulting and fracturing on the samples may have been masked by the small size of the samples, the high confining pressures and the very large gradients applied to the samples.

Faulkner and Rutter [160] evaluated the gas permeability of clay-bearing fault gouge from the Carboneras fault in Spain. The permeability was measured in the three main orthogonal directions using both the pulse transient and pulse pressure oscillation techniques with argon as a fluid. The sample was loaded and unloaded cyclically at effective stresses from 60 until 160 MPa. The results showed a dramatic decrease in permeability during the first cycle, due to both adjustment of the fracture walls, and compaction of the clay gouge. Still, decrease of permeability continued slowly with every cycle, due to compaction of the clay. The permeability perpendicular to the fault is up to three orders of magnitude lower than the one parallel to the foliation and Riedel shears, Figure 6-9. The permeability in the transport direction is intermediate between the others. Therefore, it is clear that the permeability of a highly structured rock like a clay-bearing fault is different in different directions due to its structure. These results –as will be seen later- are consistent with the ones by Zhang and Cox [161], showing that the anisotropy in permeability remains even at very large pressures.

Likewise, Faulkner and Rutter [162] compared the differences between the permeability measured with argon and with water during the same set of experiments. The results showed that permeability with water as a fluid is one order of magnitude lower than with argon. It is thought that this is due to physicochemical interactions between the fault gouge and the water, whereby layers of strongly adsorbed water on mineral surfaces reduce the effective pore throat apertures. Clearly the flowing fluid can have quite an impact in the permeability of these materials, as Lambe and Whitman [112] have shown.

Zhang and Cox [161] studied the permeability of a fault with flow parallel and perpendicular during shear, using a synthetic mud composed of 10% montmorillonite, 40% illite, and 50% silt-sized quartz, Figure 6-10. The tests were carried out in normally consolidated (NC) samples consolidated at 90 MPa, and in overconsolidated (OC) samples consolidated at 90 MPa and sheared at 30 MPa. The permeabilities parallel and across the fault are similar for the NC samples, and remain similar during shear. On the other hand, in the OC samples the combined effects of shear strain and reducing mean effective stress result in permeability enhancement of up to two orders of magnitude. The permeability parallel to the shear direction is one order of magnitude higher than that across the shear plane. Obviously the reorientation of particles during shear in OC sediments, and the development of a shear zone lead to the enhancement of permeability with shear in stiff clays and shales. Notice that larger confining stress will inhibit the development of shear zones and the permeability enhancement.

Bolton and Maltman [163] described the natural processes that fine-grained sediments go trough during compaction and tectonic evolution, and how permeability evolves. Moreover, consolidation, shear, and flow migration leave a distinct signature in the formation. The process can be summarized as, Figure 6-11:

- Sediment is initially deposited at conditions of minimal pore pressure and overburden. Open fabric is common in these sediments.

- If the sediment is buried and allowed to consolidate, there will be a loss of volume and the development of a 'consolidated' fabric.
- Shear starts at this stage. If flow is allowed, the material will compact and deform ductile. The excess of pore pressures generated during shear will depend on the strain rate and permeability.
- If any process like erosion, pressurized fluid or others induce overconsolidation on the material, deformation will proceed in a more brittle fashion, and localized shear zones could form. This could explain why ductile and brittle deformation fabrics have been observed in cores from modern convergent margins.
- If the overconsolidation ratio is further increased, future shear deformations will be brittle and strain will be concentrated in shear bands.
- Shear bands develop inside the material. The fabric will consist of aligned minerals in the shear band, which dilate with increase in pore pressures or shear strains, allowing cyclic fluctuation of pressure build-up and fluid release (valving).
- Large overconsolidation, shear strains and the dilation associated will end up in fracturing of the material and loss of pressure. Flow channels will be created several orders of magnitude more permeable than the matrix, which will dilate at low effective stress. The criterion for closure and opening of fractures depends not only on the mean effective stress but also on the relationship between the pore fluid pressure inside the cracks and the effective stress normal to the wall. If the pressure increases inside the crack more rapidly than it can dissipate into the surrounding sediment then the tendency for the cracks to open will increase. On the other hand, if the rate of pressure build-up is slow, the effective stress will be mobilized to close the crack and the enhanced concentrated flow will be less pronounced.

Bolton and Maltman [76, 163] provide evidence of this contrasting behaviour in NC and OC sediments. Tests were carried out on identical artificial samples made from a slurry of 80% kaolinite and 20% fine sand, both of them consolidated isotropically at 1 MPa; one of them being sheared at this isotropic stress, and the other sheared at 0.3 MPa. The tests were drained, at constant strain rate, and the permeability was measured through the tests by a constant-rate-of-flow permeameter. As was expected, the NC sample deformed by ductile barreling, and the permeability decreases with shear and porosity. An increase of permeability between 8% and 12% axial strain was due to the expulsion of fluid from the base of the sample because of the reduction in porosity. Post-shear hydraulic conductivity under varying conditions of effective stress indicated that any deformation fabrics that were produced had little influence on the fluid flow besides a small decrease in the hydraulic conductivity.

On the other hand, the permeability in the OC sample increased with strain as a result of dilation in the sample. The shear test was stopped a couple of times to evaluate the steady-state permeability, which showed the same results. This indicated that the shear zones are interconnecting creating a preferential flow path. Moreover, the post-shear permeability is controlled by the mean effective stress and the effects of the differential stress are negligible, Figure 6-12. The relationship between porosity and permeability are markedly non-linear. The permeability of the shear zone is a function of the effective normal stress acting on the shear plane. Thus, Figure 6-12 shows clearly how after decreasing the effective stress below a treshold pressure, in this case 250 kPa, the shear zones start to connect and prompt a definite increase in permeability. Although the shear zone walls at this stage are parting due to the reduction in effective stress, the small amount of porosity increase is sufficient to create a more interconnected pathway, and hence the permeability increases rapidly. The behaviour exhibited by the OC sample is similar to the Cretaceous shales of North America studied by Neuzil and Belitz [71], where fractures act as preferential flow paths below a certain threshold stress.

Renner et al. [164] carried out an investigation of the mechanical and hydraulic behaviour of foliated marls and shales from the Swiss Central Alps. Initially, the samples were loaded hydrostatically and the permeability decrease at least one order of magnitude from 5 to 40 MPa. The permeability was one order of magnitude lower on samples where the flow was perpendicular to the foliation (S samples) than where the flow was parallel to the foliation (P samples).

When the samples were sheared in a triaxial test, all exhibited brittle failures at small axial strains (0.1 to 0.3%), and the permeability decreased during axial deformation in accordance to the initial volume reduction, Figure 6-13. However, after failure, permeability of the samples rapidly increased, especially in the P samples because the fracture plane intersected both sample end faces. On the other hand the increment in the S samples is not as prominent because only one side of the fracture intersect the platens of the cell, but intuitively if both side would reach the end faces, the increment in permeability would have been in the same order (two orders of magnitude).

Moreover, Bolton et al. [165] tested some sediments from the Costa Rica convergent margin during the Ocean Drilling Program Leg 170, Figure 6-14. The material was a friable claystone from a fault zone, it was highly overconsolidated, and it contained intact shear fabrics. The results showed that at the lowest effective stress after shear (50 kPa) the permeability is two orders of magnitude greater for a given porosity than predicted by the pre-shear behaviour. Furthermore, post-shear permeability is more strongly dependent on effective stress changes than on porosity or deviatoric stress. It is interesting to note that other materials that behave in a brittle way (i.e. chalk) do not show an effective stress dependency on the post shear permeability. It is thought that this is due to the intrinsically high permeability of the matrix, and deformation fabrics in such lithology will only become important as barriers to fluid flow when they are oriented at high angles to the flow direction and porosities within the zone are significantly less than the matrix. The study of the Costa Rica convergent margin has lead to the identification of different stress and hydrogeological regimes, as well as the pattern of deformation in these regimes in the decollement zone. The upper zone behaves like an overconsolidated material, where flow is enhanced by the presence of a sheared, fractured silty clay, with the typical structure of shear zones in stiff clays. On the other hand, the underthrust section is a ductile, unfractured, low permeability silty clay.

Gutierrez et al. [77] studied the permeability of a 'de-mineralized' fracture in shale. 'De-mineralized' meaning that any cement on the surface of the walls of the fracture was washed out. The tests were carried out on the Kimmeridge shale, a naturally fractured shale from the Upper Jurassic, which is found throughout the North Sea as source, carrier or seal rock in several oil fields. Block samples were retrieved from the Isle of Purbeck, Dorset, UK. The fractures used for the tests were obtained by manually splitting the healed fractures in the block samples; the calcite cement was dissolved with a strong acid solution. The almost uniform thickness of the calcite cement and the apparent good match of the de-mineralized fracture surfaces are indications the fracture is a natural extensional fracture, likely a hydraulic fracture, which has never been subjected to shear deformation.

Initially, the samples were subjected to three loading and unloading cycles at 60% of the unconfined strength of the shale and the final permeability was assumed to be the one when the fracture was formed. The initial fracture permability was in the order of 10^{-10} m^2, while the matrix permeability was in the order of 10^{-19} m^2. The samples were tested in a direct shear machine, were permeability was measured across the fracture before and after shear. The sample was loaded and unlodaded cyclically, and a permeability function with respect to effective normal stress was fit with promising results. Also, it is important to notice that even after loading the sample to about 10 MPa --twice the unconfined strength--, the normal loading had not fully closed the fracture.

Permeabilities after shearing were related with the amount of dilation in the test, Figure 6-15. For low normal stresses (1 to 2 MPa) the permeability increased approximately by a factor of 10, and for shearing at large normal stresses (around 6 MPa) the permeability was 10^{-6} times the permeability before shearing. This reduction is due not only to the closure of the fracture by a larger normal stress, but by the gouge formation and transport of particles blocking the fracture. Notice that even with such a large decreasing in permeability, it is still larger than the matrix permeability by two to three orders of magnitude. It is interesting to note that this result is very similar to those in hard rocks, where it has been found that at normal stresses larger than the unconfined strength of the material, a reduction in permeability is experienced, and the parameter σ'_n/σ_c seems to be the key parameter for determining the permeability reduction [166, 167]. Likewise, during shear, permeability is controlled not only by the acting normal stress, but by the amount of shear, and the roughness and strength of the joint walls [166, 167].

6.3 Anhydrites

6.3.1 Origin and Formation

Anhydrites are evaporites, which are one of the mineral products of precipitation when brines are evaporated. The mineral anhydrite is a calcium sulfate like gypsum, and they are the two most common types of evaporite after halite by volume. It is believed that only gypsum is normally precipitated in nature from sea water, and that anhydrite forms secondarily by the dehydration process [168]. The dehydration of gypsum to anhydrite is represented by the following reaction:

$$\frac{CaSO_4.2H_2O}{\text{(gypsum)}} \Leftrightarrow \frac{CaSO_4}{\text{(anhydrite)}} + \frac{2H_2O}{\text{(water)}}$$

This process can occur under the influence of solar heating in the uppermost 1m or less of sediment supratidal areas [169]. Upon burial, the appropriate temperatures are reached at depths of 600-900 m, depending on the geothermal gradient [170]. The effect of the resulting volume change would be that a 10 m thick gypsum bed would reduce to 6.2 m thick bed of anhydrite [168]. Anhydrite exposed at the surface, or occurring at shallow depth, could hydrate to gypsum [168], however, large volumes of water would be required.

6.3.2 Mechanical Behaviour of Anhydrites

Experience with anhydrites and their mechanical behaviour is rather poor as an extensive literature review proved. Nonetheless, a database of experimental results was built, and reinterpreted to provide a better idea as to the mechanical properties and behaviour of anhydrites for use in the Weyburn project performance assessment. The primary basis of the database was the information collected in the Marker Bed 139, in the Waste Isolation Pilot Plant (WIPP) [171]. Yet, results from Blaine Anhydrite [172], Oklahoma, St. Bees evaporites from the Whitehaven mine, UK [173], the Northern Alps, France [174], and the Weyburn Field, Canada, are also included. Table 6-1 summarizes the properties gathered form the literature review.

Anhydrite can be considered a medium to low strength rock, with a high modulus ratio, following the Deere and Miller classification, Figure 6-16 [175]. This is due to the fabric (interlocking) and mineralogy (anhydrite). The mineral anhydrite is very strong, and the strength of anhydrites is largely dependant on the anhydrite content, Figure 6-17. Likewise, Young's modulus is linearly related with the unconfined compressive strength as was expected, whereas its Poisson's ratio seems to be independent of both Young's modulus and unconfined compressive, and consequently of anhydrite content, Figure 6-18.

Its stress-strain behavior in triaxial testing is that of brittle hard rocks, where damage through cracking and crack propagation develops once the load overcomes a certain threshold (0.4 σ_c from back analysis in tunnels and testing in Lac Du Bonnet granite [176, 177]). Once the cracks begin to coalesce the material weakens, finally developing a failure plane. At this point the material loses its cohesion, and its strength decreases significantly.

Failure in rocks can be described by either a liner Mohr-Coulomb criterion or the Hoek-Brown criterion. The more traditional Mohr-Coulomb failure envelope would be constructed based on results acquired from triaxial compression testing. The failure criterion is a linear locus drawn tangent to a series of Mohr's circles. The maximum stress (σ_1) and the minimum stress (σ_3) minus pore pressure (u) are plotted on the x-axis and shear stress (τ) is on the y-axis. A best-fit line would then be constructed tangent to the circles to give a failure envelope. Mathematically, the failure criterion can be expressed as:

$$\tau = c' + (\sigma_n - u)\tan\phi'$$

In the expression above c' is the effective cohesion; ϕ' is the effective angle of friction; σ_n is the normal stress on the failure plane; and u is the pore pressure. The Mohr-Coulomb criterion can represent adequately the rock properties in small stress ranges, but rocks in general present a non-linear behavior, where cohesion is small and friction large at low confining stresses, and vice versa at large confining stresses. However, the advantage of the Mohr Coulomb criterion is that it is well-known and consequently easy to communicate.

Table 6-1. Mechanical properties of the different anhydrites included in the database

Sample location	*Anhydrite Content (%)*	σ_c *(MPa)*	σ_t *(MPa)*	*E (GPa)*	ν	V_p *(m/s)*	*Reference*
Whitehaven		113	5.47	109			Bilgin [173]
Sandwith		102.9	8.2	56.7	0.25	3310	“
Newbiggin		97.5	7.1	67.1	0.31	3390	“
St. Jean Maurienne	98	62		50			Fabre & Dayre [174]
Moutiers	95	60		50			
Bramans	60	40		30			
La Coche		77		60			
Blaine		127					Handin & Hager [172]
Castillo Formation							
ERDA 9		117-120		73.1-74.8	0.35-0.39		Pfeifle & Hansen [171]
Room T		63.3		40.7	0.37		“
Room M		31.6, 35.2		21, 26.8	0.21, 0.48		“
MX05-12		35.6, 43.7		24.9, 32.2	0.31, 0.49		“
TV10-3		52.7		33.5	0.22		“
Salado Formation							
AEC7		73.9-105.8		56.3-87.6	0.35-0.39		“
AEC8		44.5-96		47.4-75.2	0.30-0.39		“

The Hoek-Brown failure criterion has been used to represent the failure envelope of jointed rock masses and also captures the non-linear strength behavior of a jointed rock mass [178]. Through the GSI (Geological Strength Index) associated with the Hoek-Brown envelope, the criterion has the ability to translate a failure envelope from an intact core in the laboratory, into the rock mass response of the same material with a different GSI value [179]. Also, the criterion includes a disturbance factor D, associated with the degree of excavation or drilling damage, which ranges from 0.0 for no damage to 1.0 for very poor control. The Hoek-Brown failure criterion can be expressed as [178]:

$$\sigma_1' = \sigma_3' + \sigma_{ci}\left(m_b \frac{\sigma_3'}{\sigma_{ci}} + s\right)^a$$

where σ_{ci} is the unconfined compressive strength, σ_1' and σ_3' are the major and minor effective principle stresses at failure, m_b is a GSI dependent, reduced value of the constant m_i ,given by:

$$m_b = m_i \exp\left(\frac{GSI - 100}{28 - 14D}\right)$$

and s and a are rock mass constants, dependent on GSI and D, through:

$$s = \exp\left(\frac{GSI - 100}{9 - 3D}\right)$$

$$a = \frac{1}{2} + \frac{1}{6}(\exp(-GSI/15) - \exp(-20/3))$$

Table 6-2 summarizes the properties of the different anhydrites for both Mohr-Coulomb and Hoek-Brown criteria. Friction, ϕ', is between 30° and 45° from most of the tests. The low friction of the Blaine anhydrite is due to the large confining stresses used in some of the tests, which accentuate the non-linearity of the rock response. Cohesion is between 13 and 20 MPa for most of the samples, with larger values for Whitehaven and Blaine anhydrites because of the larger confining stresses. The significant difference in properties between Castillo and Salado formations seems to be due to a difference in mineralogy, where the Salado formation results combine samples from two different areas in the same formation, while the Castillo samples come all from the same area. That also explains the scatter in the Salado results. Unfortunately, there are not specific mineralogical studies of any of these samples, but global results from the Marker Bed 139 showed a large scatter. When all the data are combined, the friction and cohesion are 44.8° and 18.1 MPa respectively, which are common values for a competent rock, Figure 6-19.

Hoek-Brown parameter results also show scatter, but it is less marked than in the Mohr-Coulomb parameters, because the criterion better reflects the response of rocks. It is interesting to notice the scatter in the value of σ_c due to different mineralogy and fabrics. However, when all the results are analyzed together, Hoek-Brown represents the rock behaviour quite well, with a value of σ_{ci} of 82.6 MPa. Hoek and Brown [178] reported average values of m_i of 13, substantially larger than the values of 5 to 6 that most of the results shown. However, when the results are combined and the large confining tests are included, m_i is 11.2, a comparable result to Hoek's, Figure 6-20, and a clear signal that Hoek-Brown parameters should be evaluated with results on testing with confining stresses that cover a range similar to the unconfined compressive strength of the material.

Table 6-2. Mechanical properties of anhydrites

Criterion	**Mohr-Coulomb**		**Hoek-Brown (Intact Core)**	
Formation	*Friction Angle*	*Cohesion (MPa)*	σ_{ci}	m_i
Castillo	31.4	20.2	72.4	5.2
Salado	46.9	15.6	102.9	6.3
Marker Bed 139[6]	46.7	13.0	94.2	5.2
Whitehaven	36.5	30.3	114.5	9.4
Blaine	17.1	57.9	165.3	2.0
All[7]	44.8	18.1	82.6	11.20

6.3.3 Hydraulic Properties

Anhydrites are a common caprock for oil and gas reservoirs, they have low permeabilities and high capillary entry pressures. However, actual measurements are scarce, and as with the mechanical behavior, the most extensive database of hydraulic properties comes from the WIPP [180]. An important series of hydraulic properties was produced for the Weyburn project by Dong et al.[70] and in this research.

Effective porosity measurements carried out in 42 samples of WIPP anhydrite samples ranged from 0.4 to 2.7%, and total porosity measurements ranged from 0.4 to 1.6% in three samples [180]. At Weyburn, porosity measurements were between 0.2 and 8.0% [70]. However, the large numbers were in the lower section of the formation that has substantially less anhydrite, and even some of the tests may have been carried out in the Three Fingers layer, a dolomite-anhydrite-gypsum formation. Gas permeabilitites measured at the WIPP ranged from a minimum of 5.0×10^{-20} m^2 at 10 MPa effective stress to a maximum of 8.3×10^{-16} m^2 at 2 MPa effective stress [180]. On the other hand permeabilities from Weyburn samples gave gas permeabilities (nitrogen) between 2.2×10^{-18} and 3.8×10^{-19} m^2, and liquid permeabilities (CO_2/brine) between 1.2×10^{-18} and 6.4×10^{-21} m^2 [70]. Likewise, permeability measurements using distilled water at the University of Alberta gave permeabilities between 4×10^{-19} and 1×10^{-20} m^2 (see Section 6.3.4).

---

[6] Marker Bed 139 includes both Castillo and Salado Formations

[7] No test with a confining stress larger than 40 MPa was considered for the Mohr-Coulomb parameters because the envelope becomes highly non-linear.

The results clearly showed that the correlation between porosity and permeability is rather weak. On the other hand, both porosity and permeability exhibit very small decrease with confining stress. Therefore, for a given specific project, permeability must be evaluated from both laboratory and field testing due to the lack of correlation with secondary parameters.

In-situ results from WIPP showed that the lowest permeability of anhydrites is 3 orders more than the lowest halite [181]. Moreover, at WIPP there was an intent to see the change in permeability with excavation of galleries, but the results were unsuccessful. Permeability values measured at different distances from the walls of different galleries showed no trend. However, the in-situ pore pressure was function of the distance to the galleries' walls. In most of the measurements within a diameter of the gallery the pore pressure was dissipated, it is clear that fracturing has occurred, and permeability, somehow, is a function of damage. Finally, hydraulic fracturing tests were carried out at the WIPP, and permeability was evaluated pre-treatment and post-treatment. The results show that newly opened fractures have a highly non-linear permeability that depends on fracture aperture and fluid pressure [182] where flow rates increased significantly. However, it was not possible to interpret the test to obtain fracture permeabilities, although residual apertures were estimated to be 0.2 mm.

6.3.4 Experimental Results

In order to establish more accurately the geomechanical and hydraulic properties of Weyburn's caprock, the Midale Evaporite and the transition unit between the Midale Evaporite and the Midale Beds[8], a laboratory testing program was carried out at the University of Alberta. Such a program included mechanical testing in the form of unconfined compressive strength and triaxial compression tests, cyclic triaxial loading, and permeability measurements before shearing, while shearing, and in one test, permeability after shearing. Also, the samples were sent for geochemical analysis. However, due to loading frame limitations the only samples that could be taken to failure were from the Three Fingers, a dolomite-anhydrite-gypsum layer that is the transition between the Marly and the Midale Evaporite. This formation has less than 30% anhydrite, and the test results must be carefully interpreted before considering them as representative of Midale Evaporite anhydrite, which has contents of anhydrite of more than 90%. These samples could not be loaded to failure because the load frame utilized for these experiments did not meet the load requirements.

---

[8] Test in the Three Fingers unit were included because their anhydrite content is in the order 0f 30% and it has low permeability.

6.3.4.1 Mechanical and Hydraulic Testing

A set of four tests was carried out, two in the Three Fingers and two in the Midale Evaporite. Table 6-3 and Figure 6-21 summarize the results obtained from the mechanical tests carried out in the Midale Evaporite. The results are fairly consistent, although as it will be seen in the next section, the mineralogy of the Midale Evaporite changes significantly throughout the reservoir, with anhydrite content being a critical value in the mechanical properties of the rock.

Table 6-3. Summary of geomechanical tests carried out in Midale Evaporites

Test No.	Well	σ_3 (MPa)	μ (MPa)	E_t[9] (GPa)	σ_f (MPa)	ε_f (%)	Unit
1	13-14-006-14W2	0	0	21.5	20.5	0.40	Three Fingers
2	13-14-006-14W2	8	3	12.9	30.6	0.30	Three Fingers
3	8-13-006-14W2	30	3	12.3	-	-	Anhydrite
4	8-13-006-14W2	3	1	12.0	-	-	Anhydrite

The failure mode in the unconfined compression test followed that of a brittle material, which is characterized by vertical failure planes, where columns are developed as can be seen from the 'jumps' in the radial strain measurements, Figure 6-22, and the picture of the failed sample, Figure 6-23. This sample had an unconfined compressive strength of 20.5 MPa with a tangent Young's modulus of 21.5 GPa.

---

[9] Tangent Young's Modulus

Two monotonic triaxial compression tests were carried out at confining pressures of 8 and 30 MPa. The test done at 8 MPa in a Three Fingers sample failed in a brittle manner, Figure 6-24. The sample developed a clear shear plane as a product of the coalescence of extensive microfracturing throughout the sample. Some of the extensive fracturing that occurred in the sample can be seen in Figure 6-25. The sample failed at a maximum deviatoric stress of 30.5 MPa, and its tangent Young's modulus was 12.9 GPa.

Once the sample failed, permeability was measured through the shear plane. As was expected in well-defined failure planes, the permeability becomes a function of the effective confining stress. However, the enhancement in permeability was very low because the plane of failure did not cut the sample at the end (which was expected), Figure 6-26. The plane was very rough, some gouge developed, and apparently, the contact area was still very large, Figure 6-27. All these factors have long been recognized as critical in the permeability of fractures.

The sample tested at 30 MPa confining stress (Midale Evaporite) unfortunately could not be failed because of limitations in the equipment available. The sample exhibited an elastic behavior through the entire test with a tangent Young's modulus of 12.3 MPa, Figure 6-28. Likewise, permeability and specific storage evolution were monitored during this test with limited change in their values, proving that during the test the sample was behaving elastically, Figure 6-29. The permeability of the sample was in the order of 10^{-20} m^2.

Finally, a cyclic triaxial loading was carried out at 3 MPa confining stress in a Midale Evaporite, which had as purpose to induce gradual damage in the sample. Figure 6-30 shows the stress-strain plot, where it is clearly seen how plastic strains are accumulated throughout the test. The gaps between cycles are interruptions in the test for a few days, which caused some minor creep in the sample. Figure 6-31 shows the evolution of elastic properties due to cycling. Such a plot is a clear indicator of mechanical damage occurring in the sample. However, the values tend to a constant, which means that the rate of induced damage is decreasing at every cycle. It is worth noting the Poisson's Ratio tends to its maximum possible value of 0.5, which can be due to the "destruction" of any anisotropy existing in the material due to the damage of the sample itself.

Permeability was monitored during the test with some interesting results. The results showed that permeability increases with incremental damage due to cyclic loading, the increase being in the order of one order of magnitude, Figure 6-32. However, measurements are also affected by the strain at which the measurement was taken. This clearly addresses the need of a better damage indicator such as acoustic velocities. Nonetheless, it is clear from this test that damage of the sample in the pre-failure range does not affect significantly the hydraulic properties of the anhydrite, which has positive implications inside a reservoir that has been exploited and stimulated for years such as Weyburn.

6.3.4.2 Geochemical Testing

The samples available for geomechanical and hydraulic testing at the University of Alberta were analyzed chemically using X-ray Fluorescence (XRF). The results were interesting because they exhibited mineralogical heterogeneity between samples from the same well but separated by only a few meters, Table 6-4. The proportions of the various minerals in a sample were estimated using a technique reported by Slaughter. This solution technique must be consistent with the mineralogy of the sample as determined by X-ray Diffraction, as the mineral proportions must reflect the bulk chemical analysis. The major oxides were determined using XRF. Sulphur content was determined using the uncalibrated UniQuant software technique (www.uniquant.com). The solution uses the simplex algorithm to minimize an objective function representing the difference between the measured elemental composition and that calculated from the estimated mineral proportions and the known mineral compositions [183]. The solution method requires that the calculated oxide content cannot exceed the measured value. A capability exists within the program to allow for the composition of the minerals to vary within prescribed bounds, although this was not needed for the samples analyzed here.

Table 6-4. Mineralogical Components of Different Midale Evaporite Samples.

Well	13-14-006-14W2		8-13-006-14W2		8-13-006-14W2		15-11-006-14W2	
Depth	1396.3-1397.5		1399.03-1400.25		1392.3-1393.2		1418.0-1420.0	
Unit	Three Fingers		Midale Evaporite		Midale Evaporite		Midale Evaporite	
Test No.	1 & 2		3		4		Not used	
	Mineralogical Assignment (%)							
Minerals	Dolomite	39.8	Dolomite	0	Dolomite	9.43	Dolomite	21.55
	Fe(OH)3	0.54	Fe(OH)3	0.04	Fe(OH)3	0.21	Fe(OH)3	0.25
	Kaolinite	2.6	Kaolinite	0	Kaolinite	1.44	Kaolinite	1.67
	Plagioclas	1.35	Quartz	0	Quartz	1.02	Quartz	0.2
	Quartz	7.18	Gypsum	3.01	Calcite	0	Gypsum	15.85
	Gypsum	15.06	Calcite	0	Anhydrite	81.48	Calcite	0
	Calcite	2.39	Anhydrite	92.08			Anhydrite	59.19
	Anhydrite	29.57						
	Total	98.49	Total	95.13	Total	93.58	Total	98.72
	X-Ray Fluorescence (mass fraction)							
Oxides	SiO2	9.32	SiO2	0	SiO2	1.69	SiO2	0.98
	TiO2	0.11	TiO2	0	TiO2	0.01	TiO2	0
	Al2O3	1.29	Al2O3	0.48	Al2O3	0.57	Al2O3	0.66
	Fe2O3	0.4	Fe2O3	0.03	Fe2O3	0.16	Fe2O3	0.19
	MgO	8.7	MgO	0	MgO	2.06	MgO	5.1
	CaO	30.53	CaO	38.91	CaO	36.43	CaO	36.1
	Na2O	0.16	Na2O	0	Na2O	0	Na2O	0
	K2O	0	K2O	0	K2O	0	K2O	0
	P2O5	0	P2O5	0	P2O5	0	P2O5	0
	SO3	24.39	SO3	59.55	SO3	53.24	SO3	42.18
	LOI	23.7	LOI	0.64	LOI	5.24	LOI	13.9

6.4 Transport Properties and CO$_2$

The flow of a non-wetting phase into a geological formation that is otherwise intact is controlled by its capillary displacement pressure and effective permeability. Both of these properties are fluid dependant, and storage of CO$_2$ has brought attention to the influence of CO$_2$ as a flowing phase into these properties. Hildebrand and Krooss [69] have carried out extensive research on these properties for argillaceous materials using fluids such as water, N$_2$, and CO$_2$. Among the materials tested by them were samples of Boom clay, Opalinus clay, and Tertiary mudstones from the Norwegian Shelf. Their results indicate that both the capillary displacement pressure and the capillary entry pressure are significantly lower when pure CO_2 is used instead of N_2, Figure 6-33. While no definitive explanation is given for this phenomenon, it was suggested that it is likely a result of the lower interfacial tension of CO_2. Clearly more fundamental research is needed to clarify these results. On the other hand, their results for effective permeability were inconclusive as there was not a clear contrast between effective permeabilities for different fluids.

Dong et al. [70] carried out similar experiments as part of the Weyburn project, using anhydrites from the Midale Evaporite. The results were similar to the ones in argillaceous materials where the breakthrough pressure using N_2 was three times the pressure using CO_2, Figure 6-34. Likewise, breakthrough pressures between oil-saturated CO_2/brine systems and pure supercritical CO_2/brine systems were compared for similar samples, and in this case the breakthrough pressures were similar, Figure 6-34. These results again pointed out that there are still questions as to the transport properties for CO_2 systems, and especially supercritical CO_2, which is expected at the in-situ conditions of most CO_2-EOR storage projects.

6.5 Implications for Geological Storage

The foregoing discussion has presented an intriguing picture of the ability of shales and anhydrites to provide hydraulic integrity for caprocks. These materials are the caprock of many oil and gas fields worldwide because of their low transport properties, but there is much uncertainty about their transport properties in the presence of CO_2. Moreover, hydro-mechanical effects can increase their transport properties significantly and both the identification of the conditions that can trigger this change, and prediction of the change are not easy matters, which are further complicated by the scale of the project.

The mechanical properties of shales cover a large spectrum of values, and their hydraulic properties are controlled by the presence of conductive discontinuities. These conductive discontinuities are usually of tectonic origin and their transport properties are functions of the acting effective stress and presence of cements. Moreover, when a shale deforms in a brittle manner, a distinctive shear plane develops where particles are aligned in the direction of displacement and permeability is enhanced by this new particle orientation and dilation. However, permeability is only enhanced by the full development of these shear planes. On the other hand, when shales deform in a ductile manner, there is no substantial change in their fabric and structure and permeability is not enhanced. The limit between brittle and ductile deformation is not clear and site specific hydro-mechanical testing is the best way to address this issue. Therefore, reservoirs capped by shales will require hydro-mechanical testing of caprock samples, and back calculation of caprock transport properties by hydrogeological modeling (which may identify the presence of conductive features).

Anhydrites are medium to hard rocks, and shear failure is unlikely to occur during a geological storage project. However, permeability in hard rocks is enhanced through microfracturing as the rock is stressed beyond its damage threshold, which is different from the ultimate strength, and this threshold could be overcome during a typical geological storage project. Such a threshold can be found generically by unconfined compression tests, and there is no need to fully characterize the material as in shales. However, more fundamental research in anhydrites is needed to establish the damage threshold and change in permeability before using a generic approach.

Among the critical issues that need to be addressed, there are the identification of conductive features in both shales and anhydrites, the influence of the change in the in-situ stresses in the transport properties of these features, as well as the transport properties of both matrix and fractures for CO_2.

6.6 Summary

The hydro-mechanical behaviour of both shales and anhydrites was reviewed, and the experimental results of the testing carried out in the Midale Evaporite were presented. It is clear that both materials can act as hydraulic seals under the right conditions, but certainly there are areas of uncertainty that need to be addressed to keep building confidence in geological storage as a safe option. The hydro-mechanical coupling is strong for both materials which implies that the hydro-mechanical behaviour of the caprock at any given CO_2 storage project must be evaluated and be an integral part of the safety assessment for such projects.

6.7 Figures

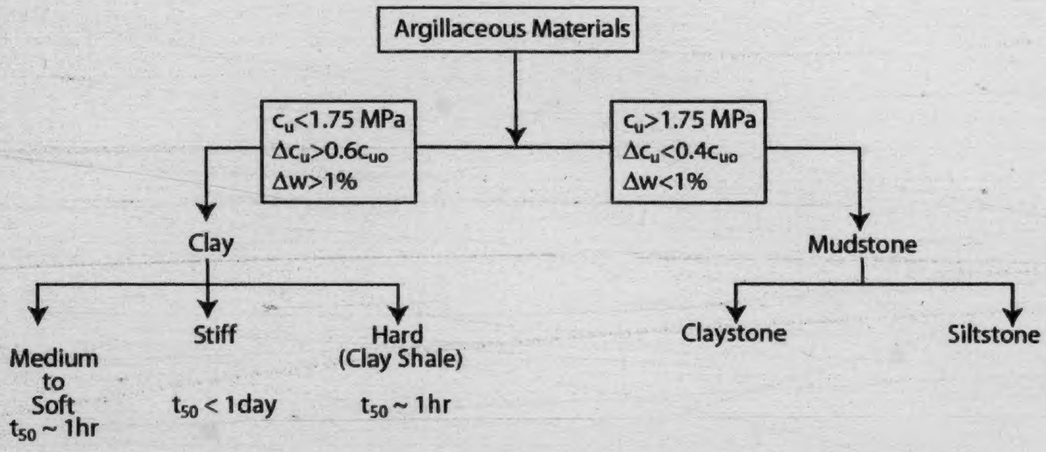
Argillaceous Materials
c_u<1.75 MPa
Δc_u>0.6c_{uo}
Δw>1%
c_u>1.75 MPa
Δc_u<0.4c_{uo}
Δw<1%
Clay
Mudstone
Medium to Soft
t_{50} ~ 1hr
Stiff
t_{50} < 1day
Hard (Clay Shale)
t_{50} ~ 1hr
Claystone
Siltstone

Figure 6-1. Classification of stiff clays and shales, modified after Morgenstern and Eigenbrod [109]. C_u is unconfined compressive strength and w is moisture content

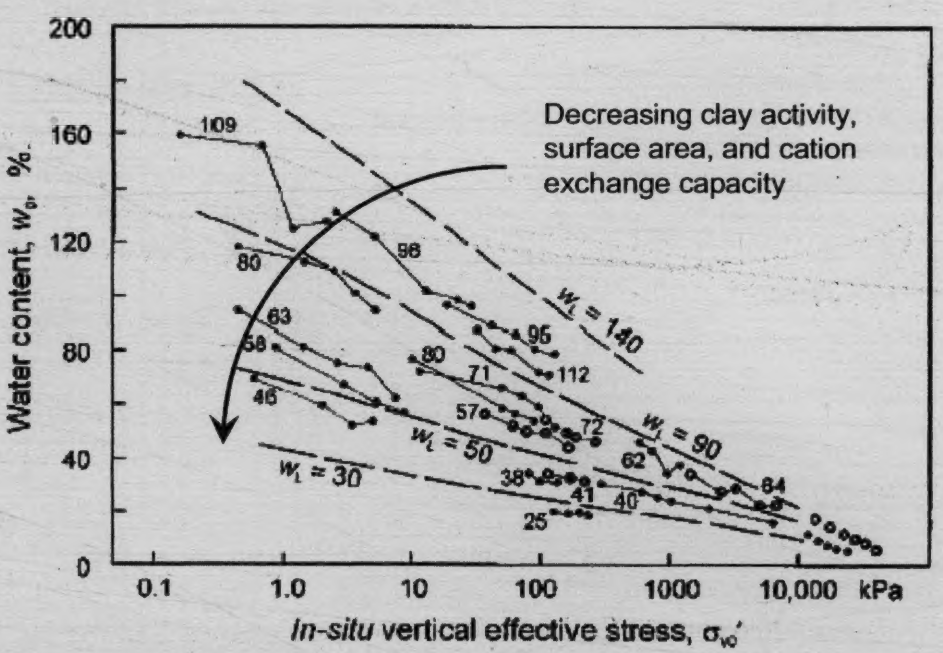

Figure 6-2. Sedimentation compression curves for natural clays, modified after Skempton [118]

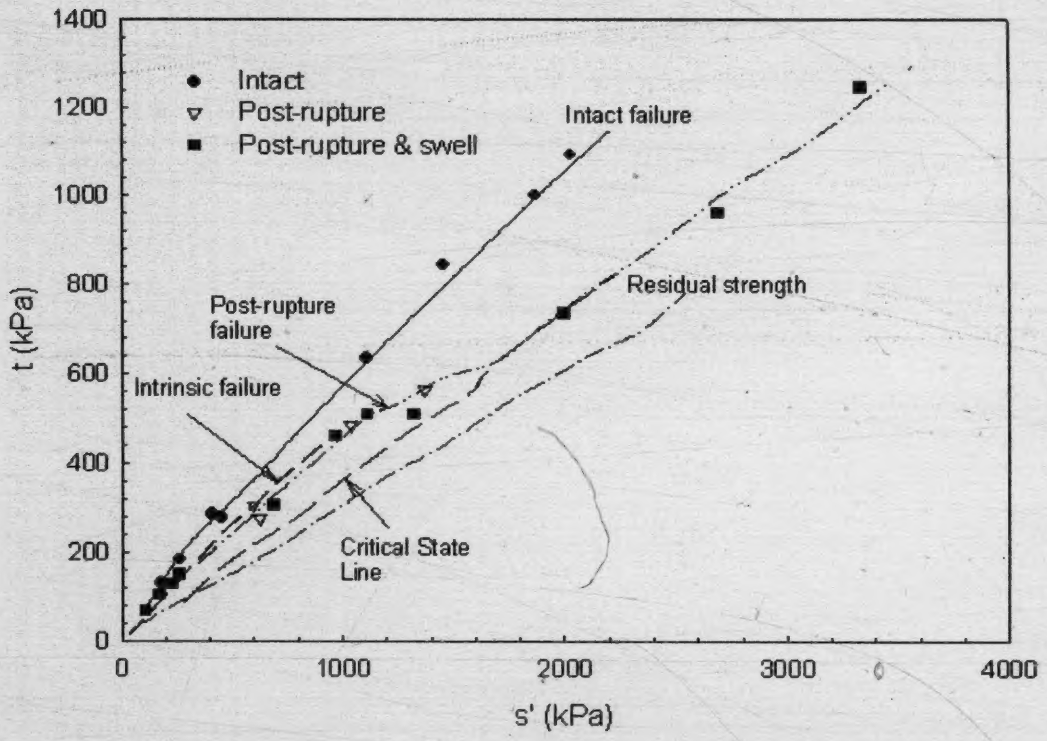

Figure 6-3. Intact, intrinsic and post-rupture failure envelopes as well as residual strength for Todi Clay, modified after Burland [116] and Burland et al. [129]

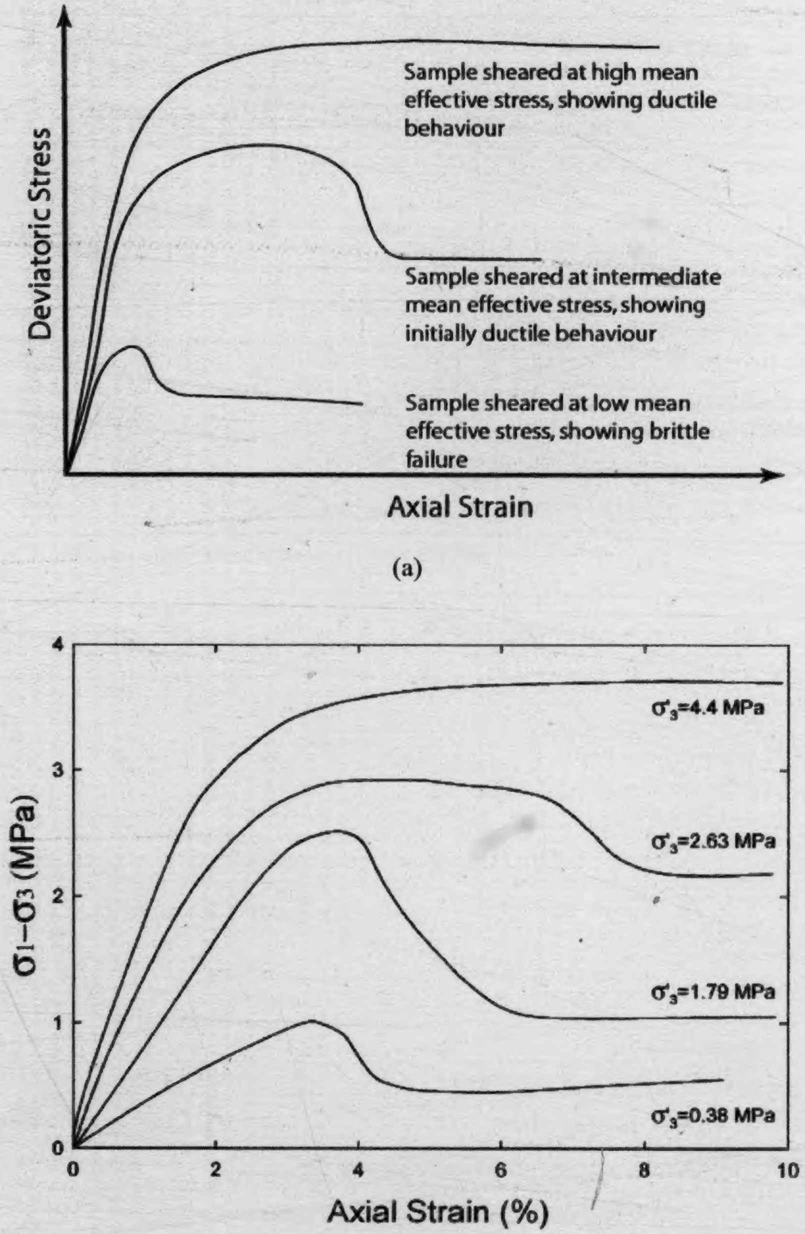

(a)

(b)

Figure 6-4. Stress-strain behaviour of mudstones: (a) generalized picture; and (b) London clay, modified after Petley [127] and Johnston and Novello [107]

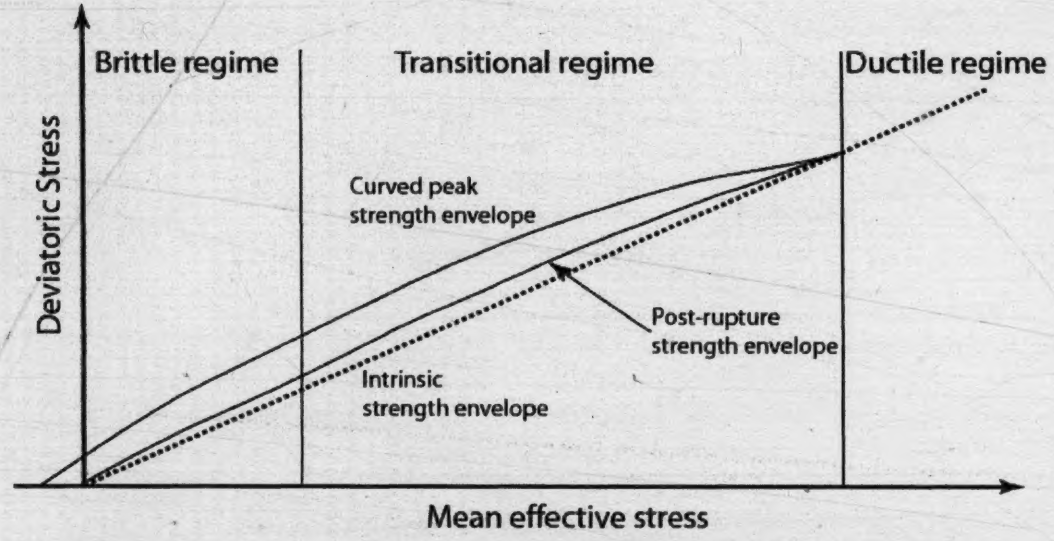

Figure 6-5. Idealized failure envelope for stiff clays, modified after Petley [127]

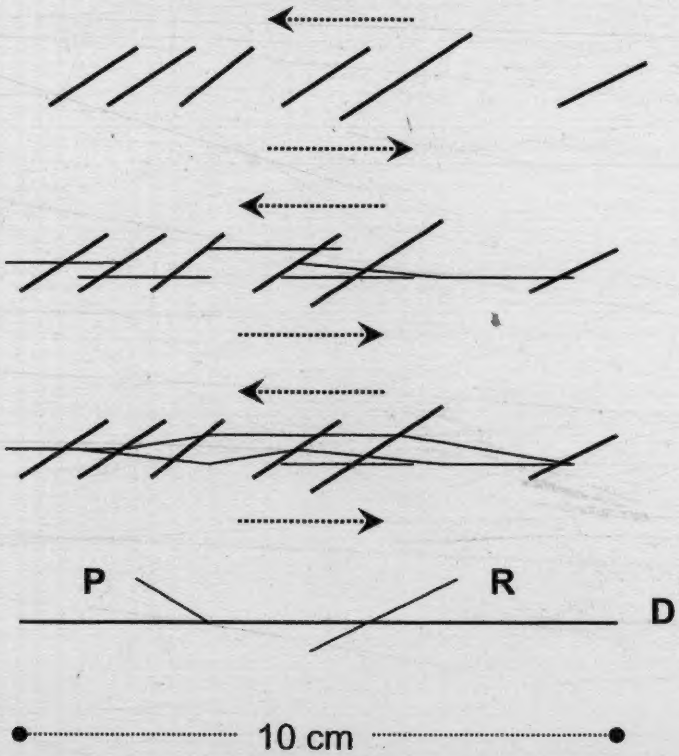

Figure 6-6. Schematic representation of the development and evolution of shear zones, modified after Skempton and Petley [132]

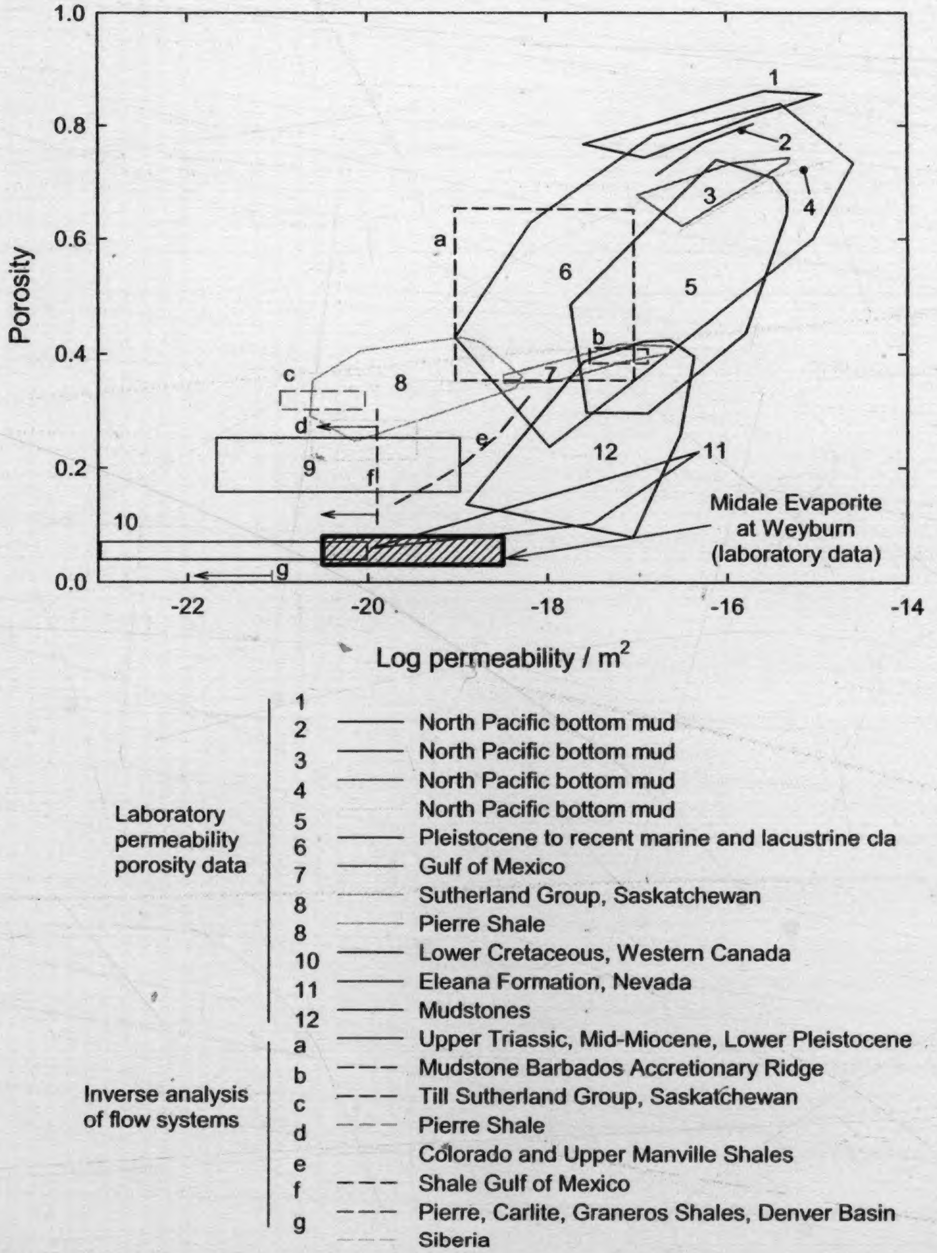

Figure 6-7. Permeability of argillaceous material from both laboratory and inversion of flow systems, modified after Neuzil [156]. The range of permeabilities and porosities measured measured in the laboratory for the Midale Evaporite in this thesis and by Dong et al. [70] are included

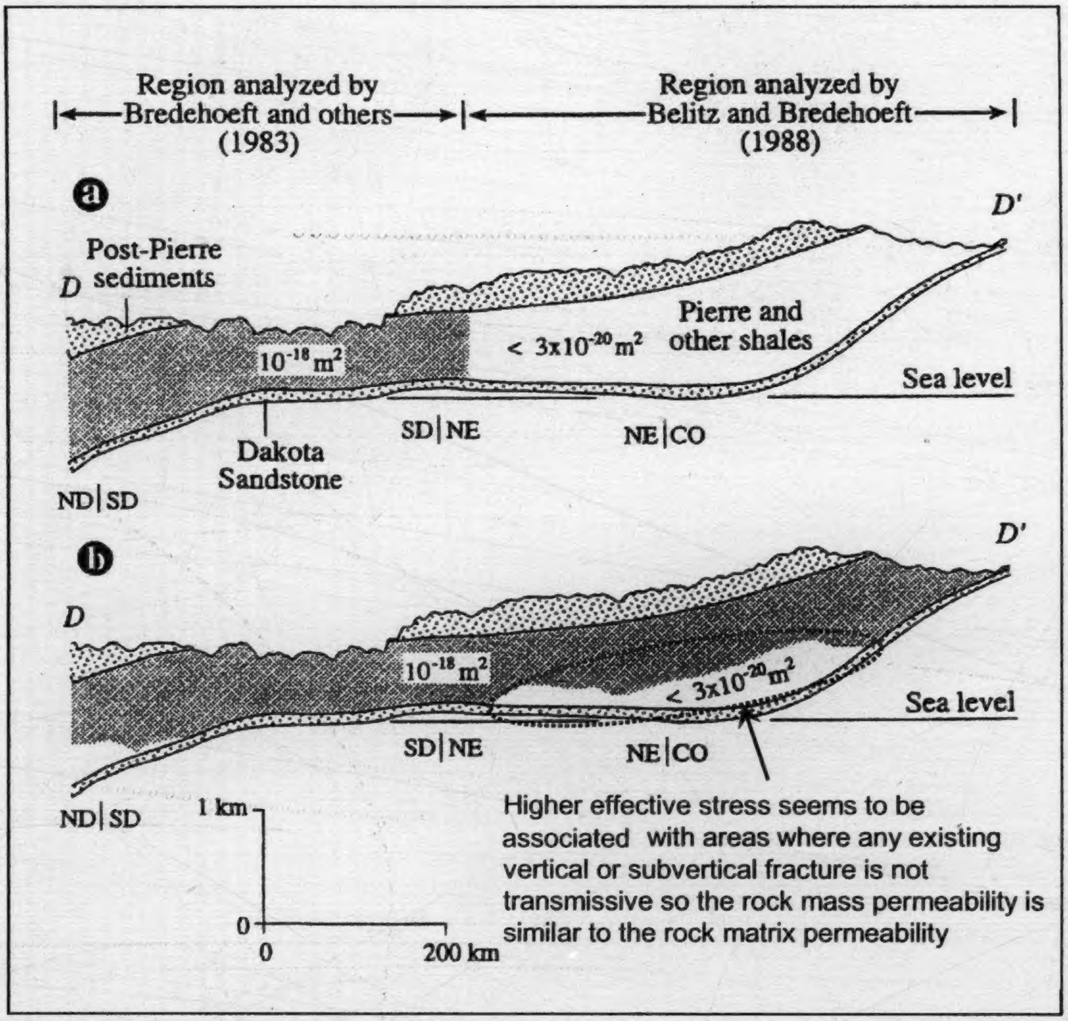
Region analyzed by Bredehoeft and others (1983)
Region analyzed by Belitz and Bredehoeft (1988)
a
D
D'
Post-Pierre sediments
10^{-18} m^2
< 3×10^{-20} m^2
Pierre and other shales
Sea level
Dakota Sandstone
SD|NE
NE|CO
ND|SD
b
D
D'
10^{-18} m^2
< 3×10^{-20} m^2
Sea level
SD|NE
NE|CO
ND|SD
1 km
0
0
200 km

Higher effective stress seems to be associated with areas where any existing vertical or subvertical fracture is not transmissive so the rock mass permeability is similar to the rock matrix permeability

Figure 6-8. North to south cross section of the Cretaceous shales and underlying Dakota Sandstone showing regional vertical permeabilities of the shales. (a) Initial analysis; and, (b) the conceptual model presented by Neuzil and Belitz [71]. Here the shaded and blank area of shales indicate depths of less than and more than one kilometre respectively, modified after Neuzil [184]

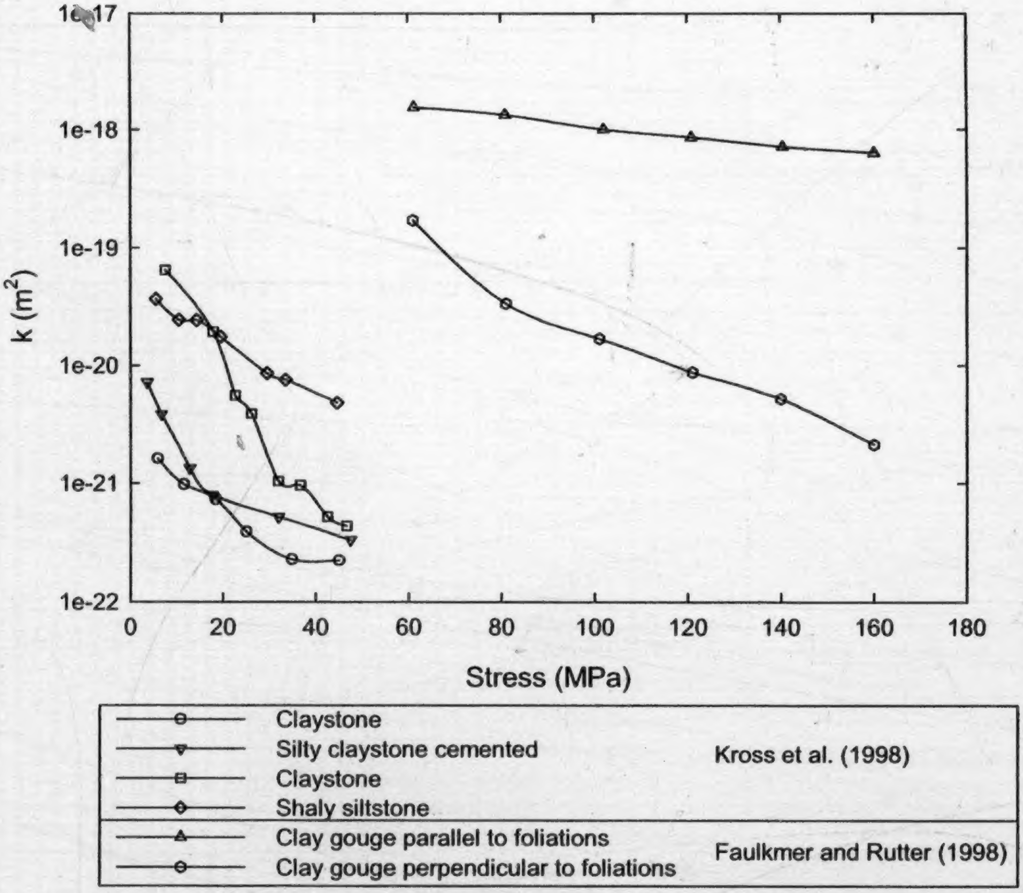

Figure 6-9. Permeability at large pressures for different argillaceous materials

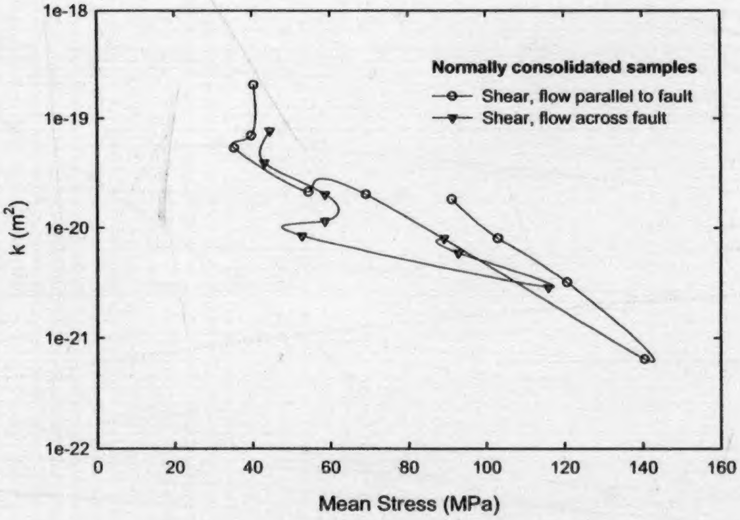

(a)

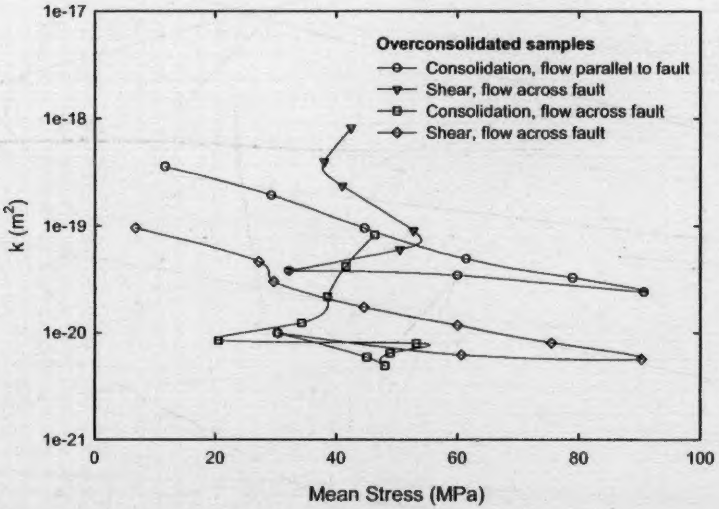

(b)

Figure 6-10. Permeability change during shear and consolidation for (a) normally consolidated sample; and, (b) overconsolidated sample. Notice the increment in permeability during shear for OC samples, modified after Zhang and Cox [161]

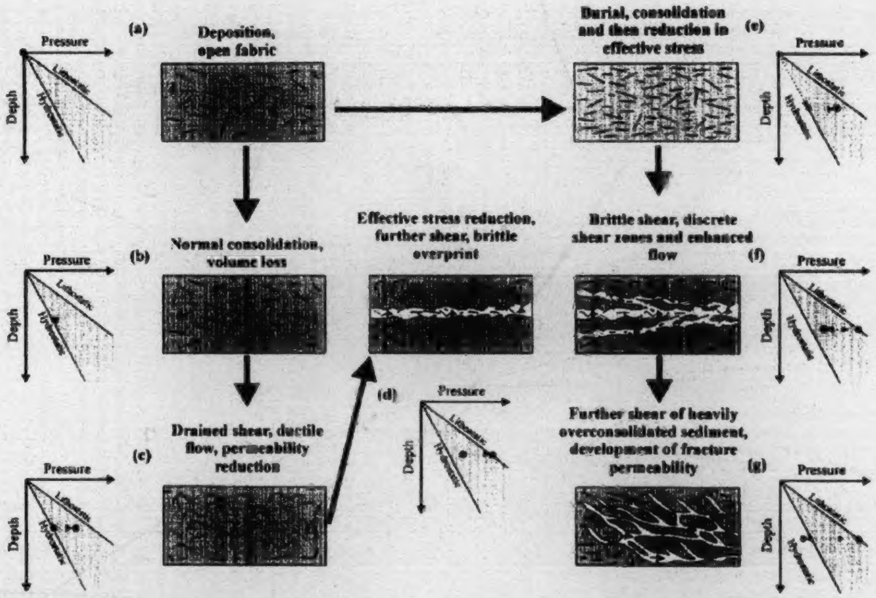
(a)
Deposition, open fabric
Pressure
Depth
Lithostatic
Hydrostatic
Burial, consolidation and then reduction in effective stress
(e)
Pressure
Depth
Lithostatic
Hydrostatic
(b)
Normal consolidation, volume loss
Pressure
Depth
Lithostatic
Hydrostatic
Effective stress reduction, further shear, brittle overprint
Brittle shear, discrete shear zones and enhanced flow
(f)
Pressure
Depth
Lithostatic
Hydrostatic
(d)
Pressure
Depth
Lithostatic
Hydrostatic
(c)
Drained shear, ductile flow, permeability reduction
Pressure
Depth
Lithostatic
Hydrostatic
Further shear of heavily overconsolidated sediment, development of fracture permeability
(g)
Pressure
Depth
Lithostatic
Hydrostatic

Figure 6-11. Diagrammatic illustration of the different structures observed during the geotechnical cycle, and interpreted fluid pressure relative to hydrostatic. Dots on the respective graphs indicate the fluid pressure at the onset of shear, modified after Bolton and Maltman [163]

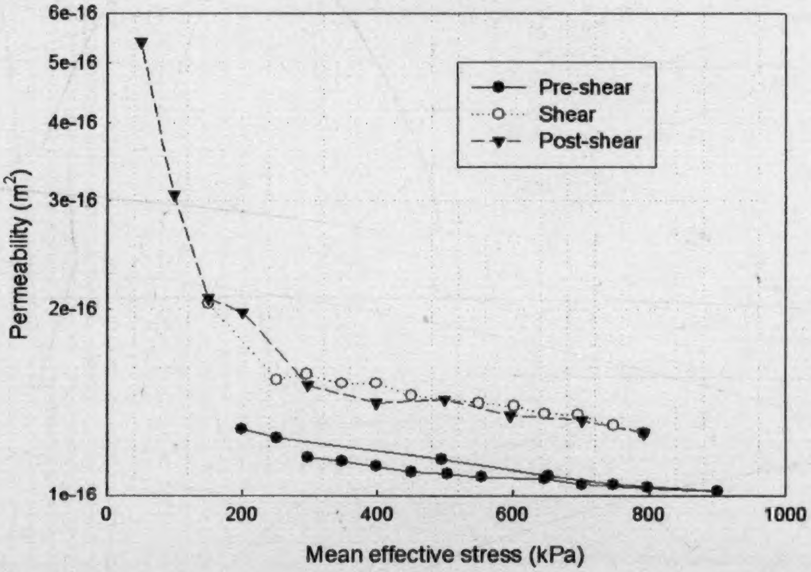

Figure 6-12. Permeability evolution with mean stress for the overconsolidated sample. Notice the permeability dependence on the mean effective stress post-shear, modified after Bolton and Maltman [76]

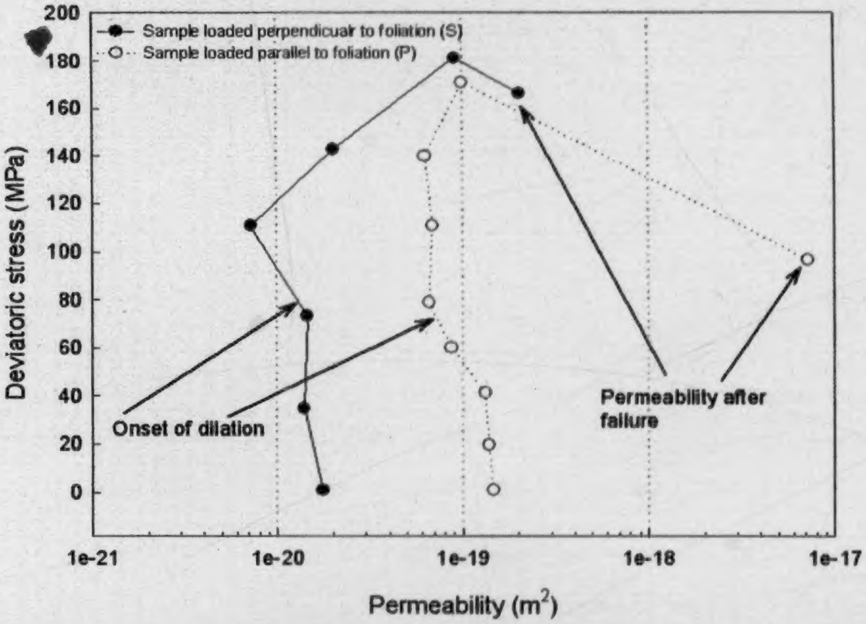

Figure 6-13. Permeability evolution during triaxial compression in Swiss Alps shales, modified after Renner et al. [164]

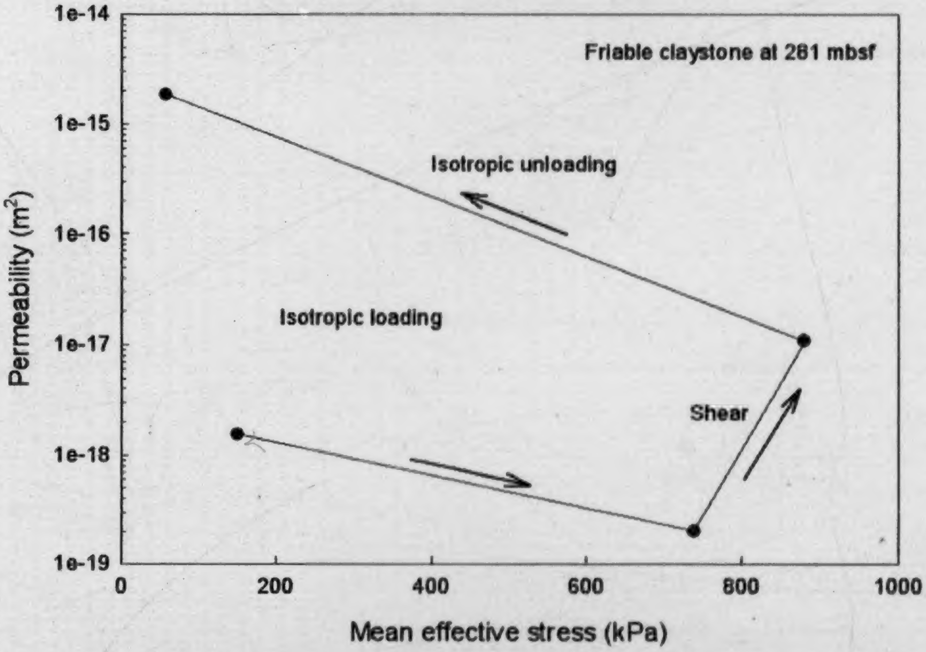

Figure 6-14. Permeability- mean effective stress relationship for a friable claystone retrieved during ODP Leg 170, modified after Bolton et al. [185]

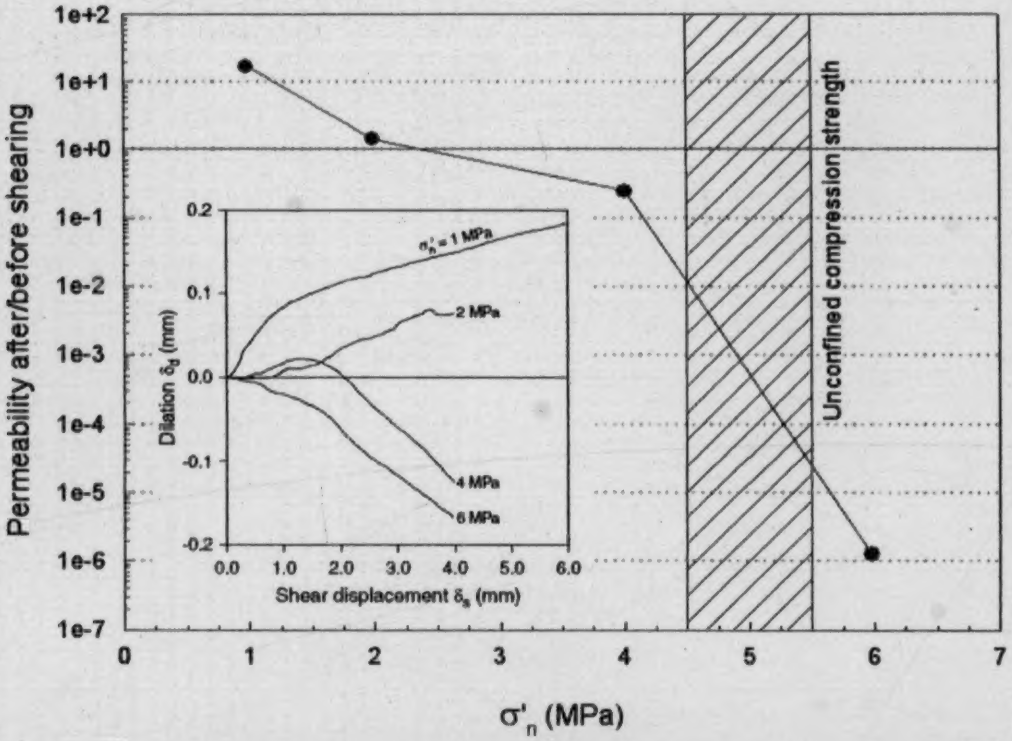

Figure 6-15. (a) Dilation vs. shear displacement for four samples sheared at different effective normal stress; and., (b) change in fracture permeability after shearing the fractures, modified after Gutierrez et al. [77]

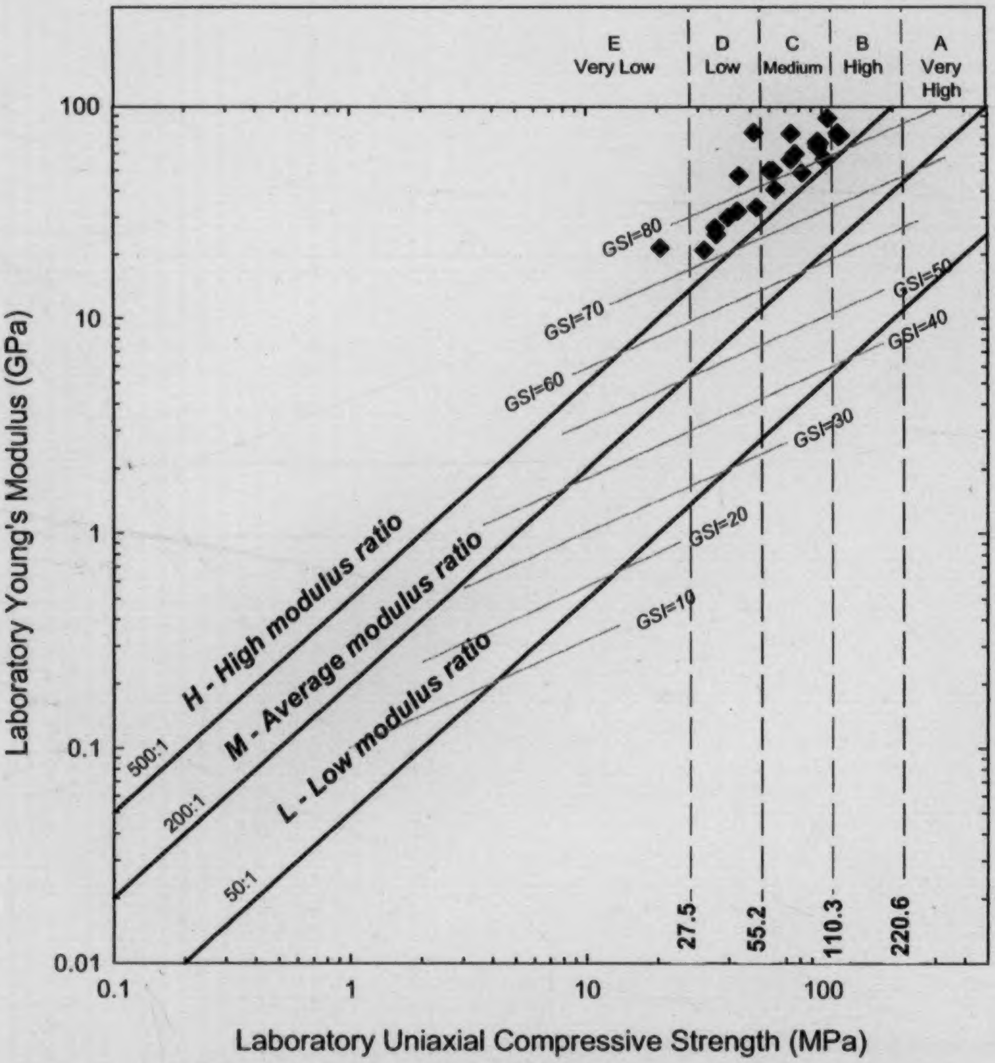

Figure 6-16. Deere classification updated with the Geological Strength Index (GIS) by Martin et al. [186] for the anhydrite database

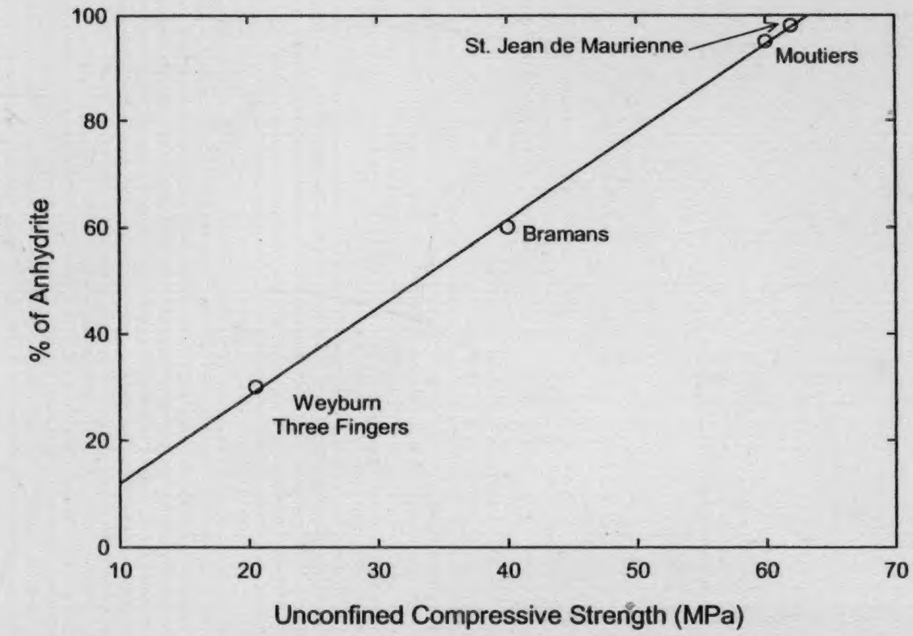

Figure 6-17. Unconfined compressive strength as a function of anhydrite content

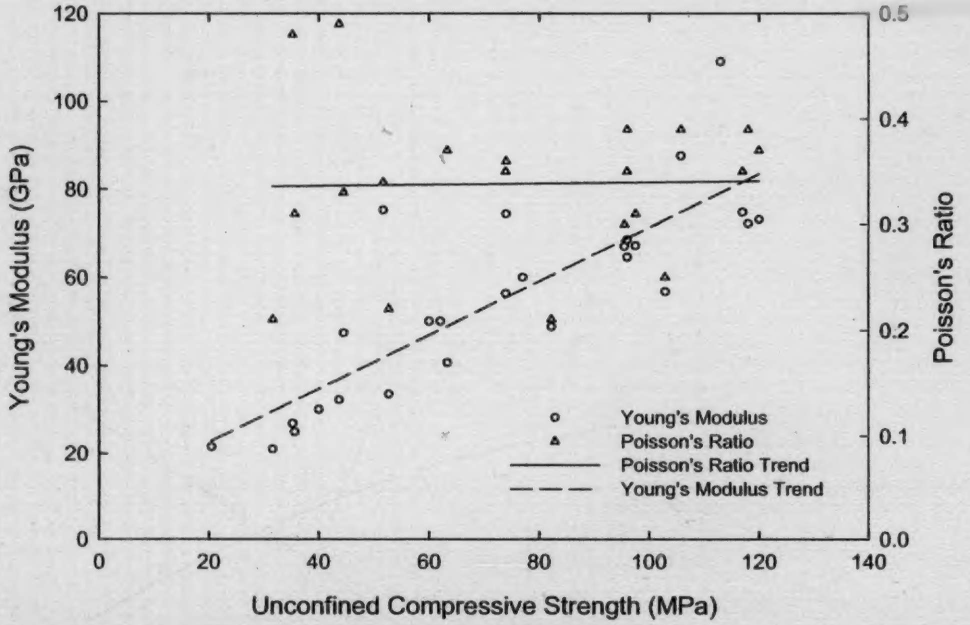

Figure 6-18. Relation between elastic properties and unconfined compressive strength for the anhydrites database

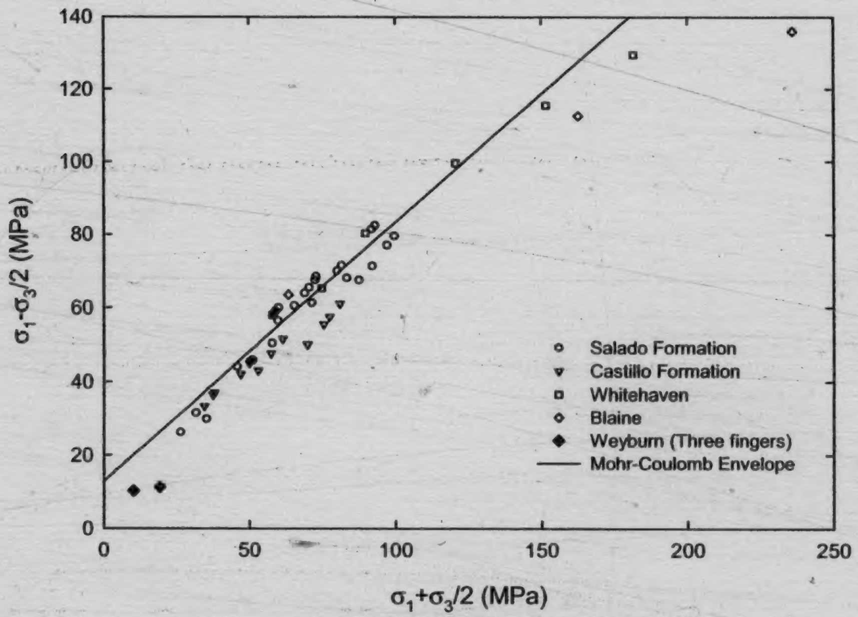

Figure 6-19. Mohr-Coulomb envelope for anhydrites

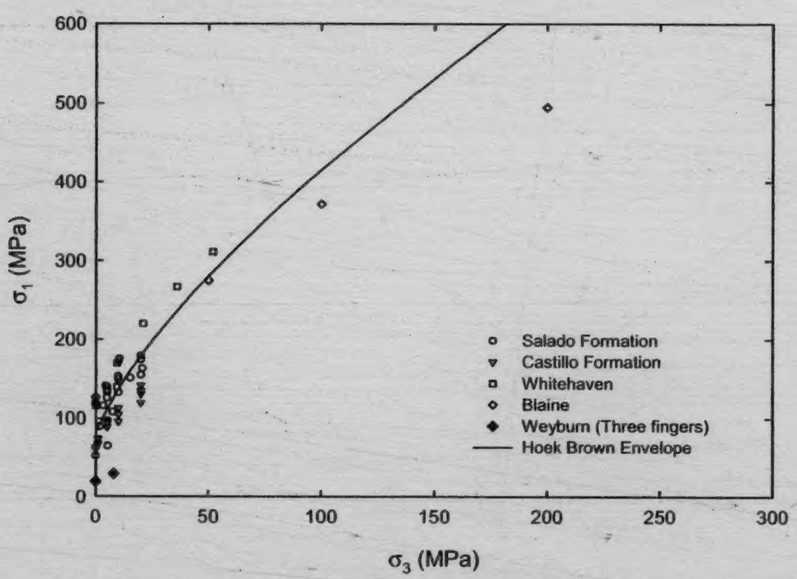

Figure 6-20. Hoek-Brown envelope for anhydrites

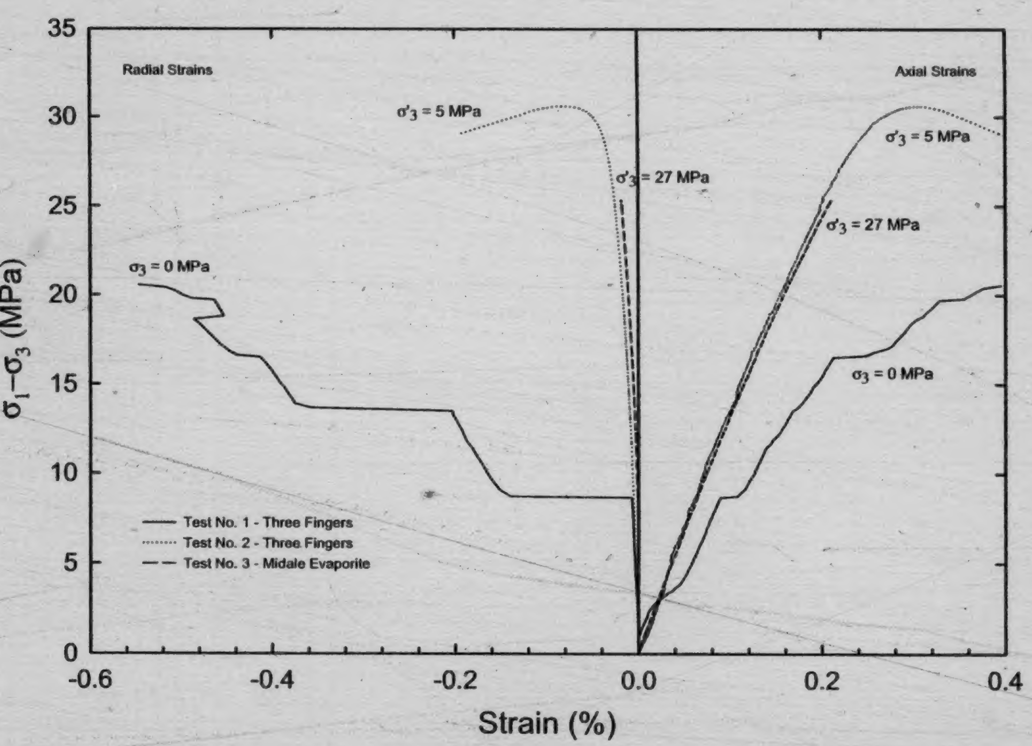

Figure 6-21. Summary of triaxial tests carried out in the both the Three Fingers and Midale Evaporite

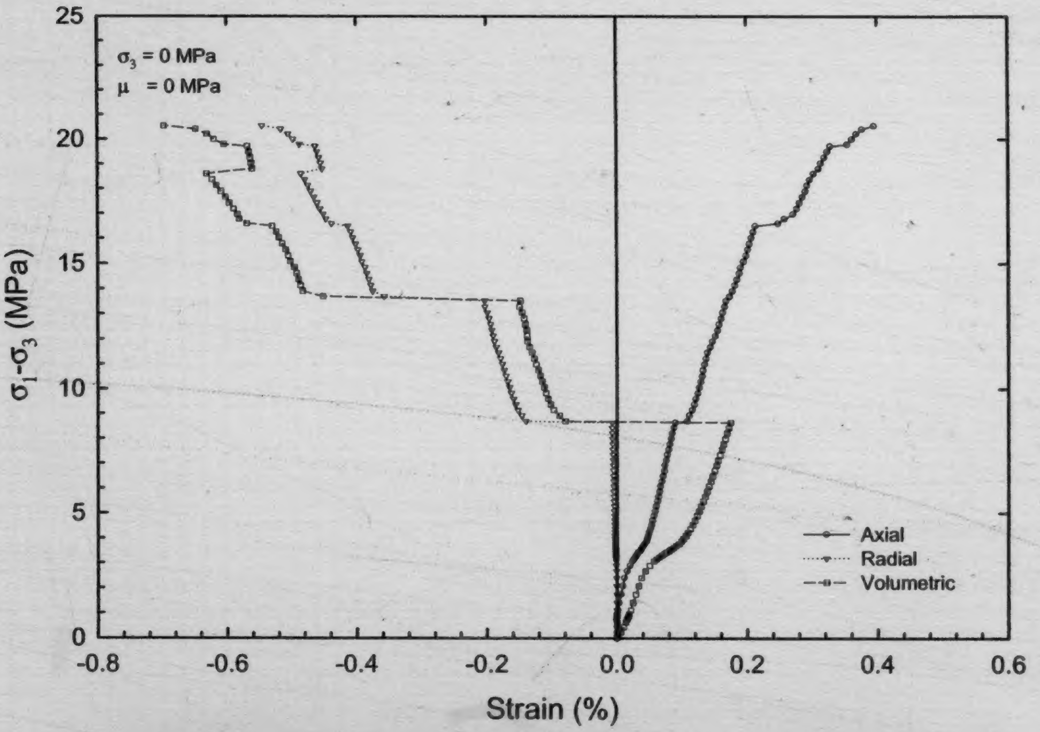

Figure 6-22. Test No. 1, unconfined compression of a Three Fingers sample

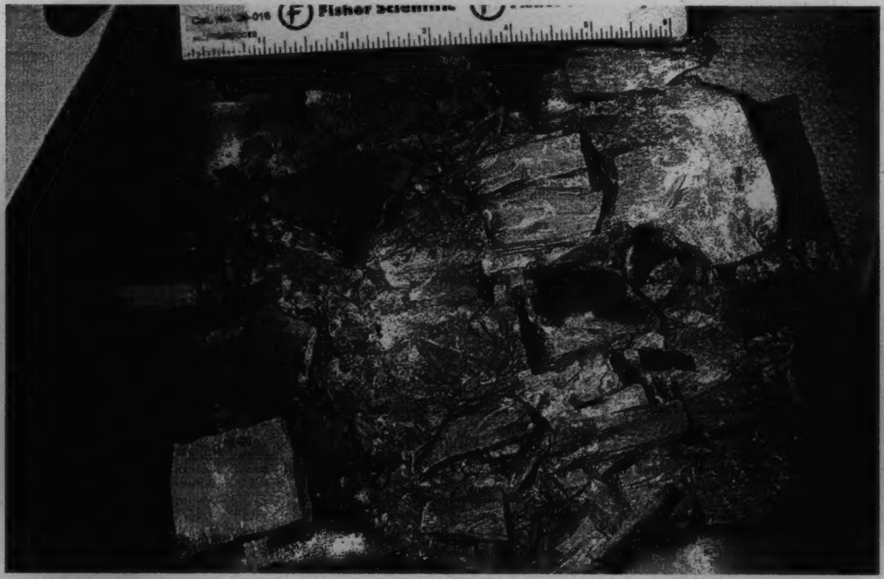
Fisher Scientific

Figure 6-23. Test No. 1, brittle failure of a Three Fingers sample in an unconfined compression test

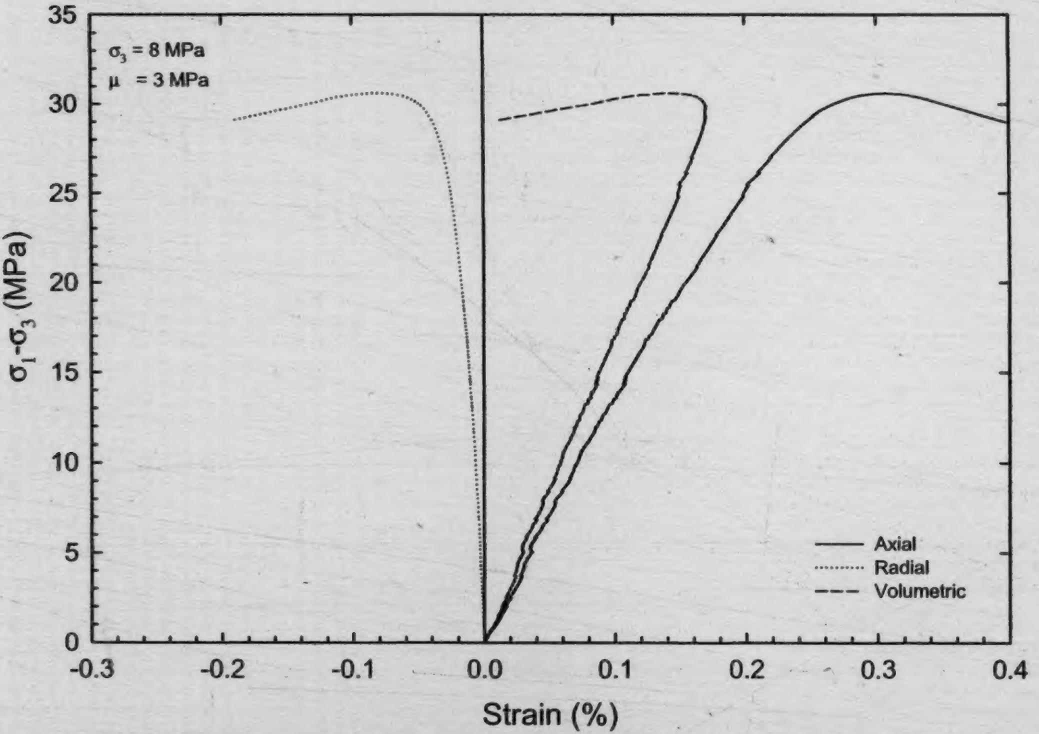

Figure 6-24. Test No. 2, triaxial compression of a Three Fingers sample carried out under a confining stress of 8 MPa and a pore pressure of 3 MPa

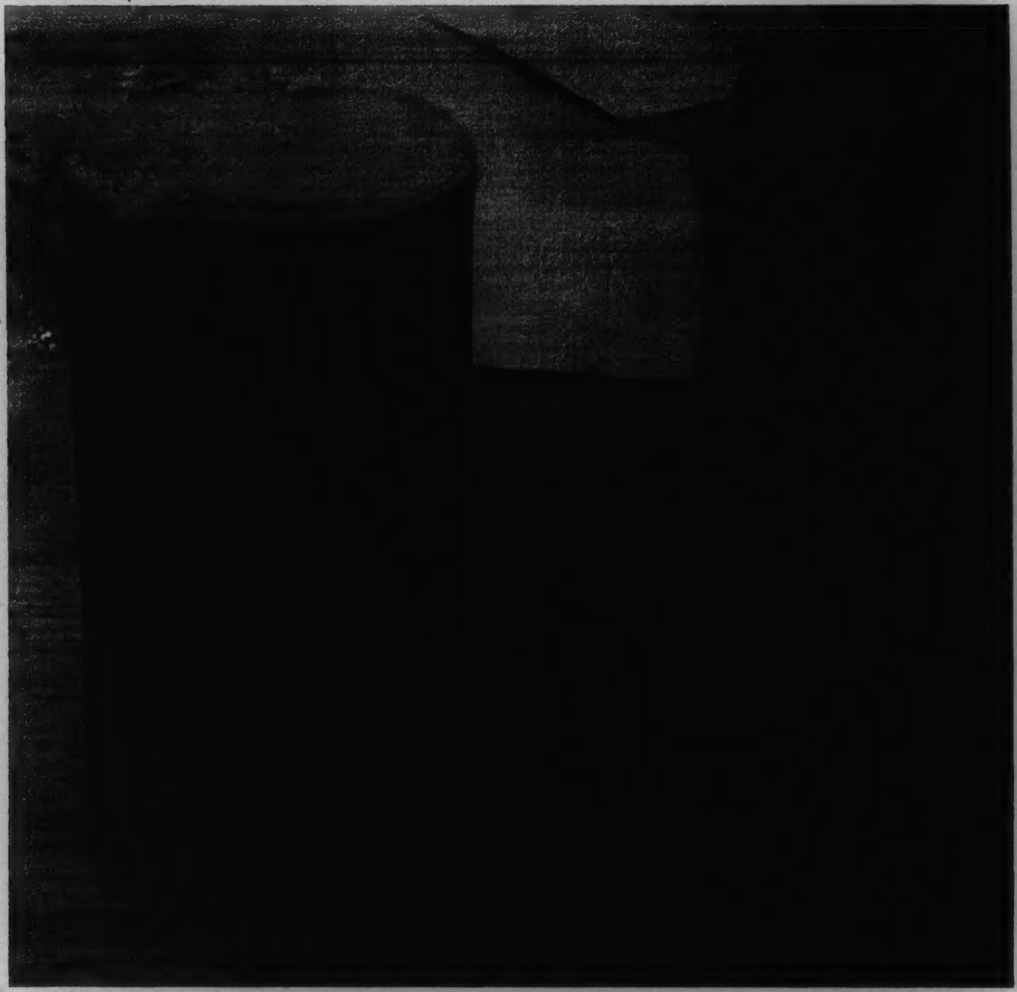

Figure 6-25. Test No. 2, brittle failure of a Three Fingers sample sheard under a confining effective stress of 5 MPa. Notice the well-defined shear plane at 32° with the axis of the sample, and the damage induced throughout the sample. The rule measures 15 cm

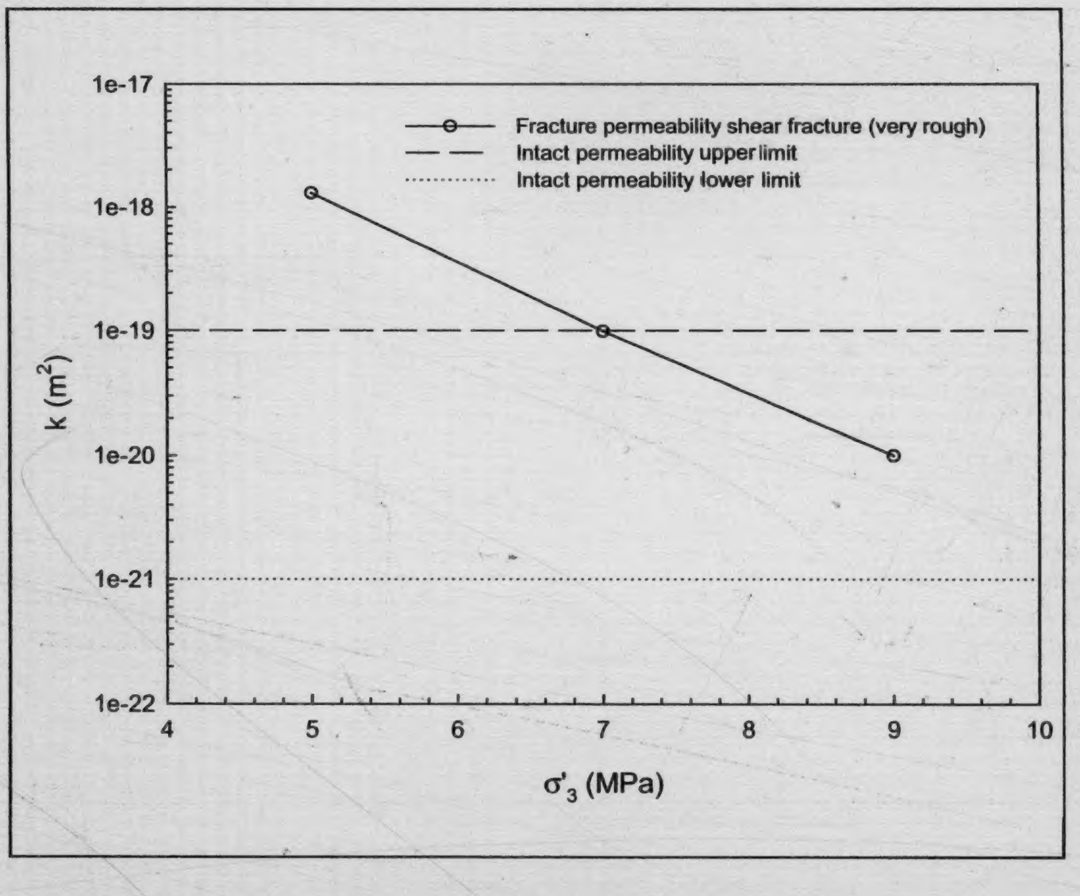

Figure 6-26. Test No. 2, permeability in the fractured Three Fingers sample compared with average intact values for anhydritic samples

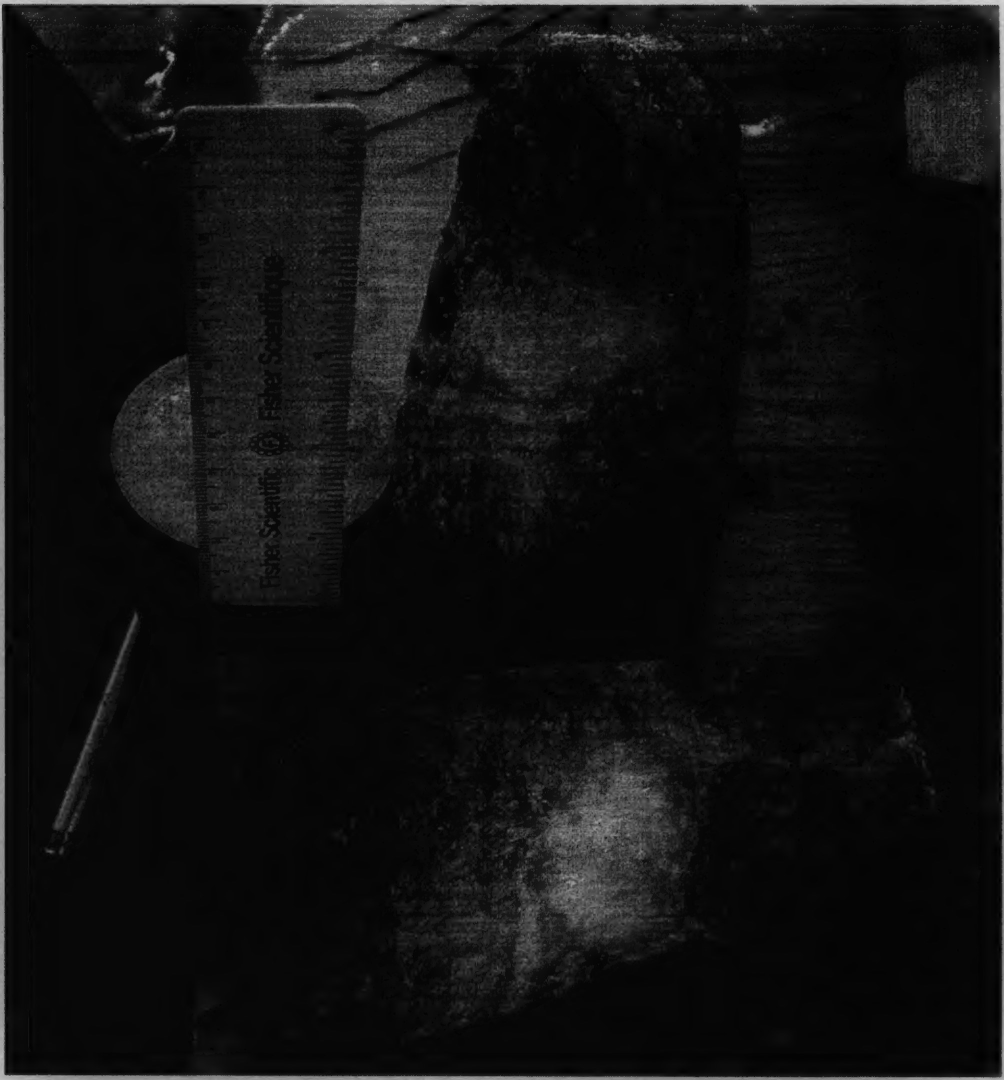
Fisher Scientific
Fisher Scientific

Figure 6-27. Test No. 2, photograph of the shear plane. Notice the roughness of the faces and the contrast in mineralogy in the Three Fingers unit

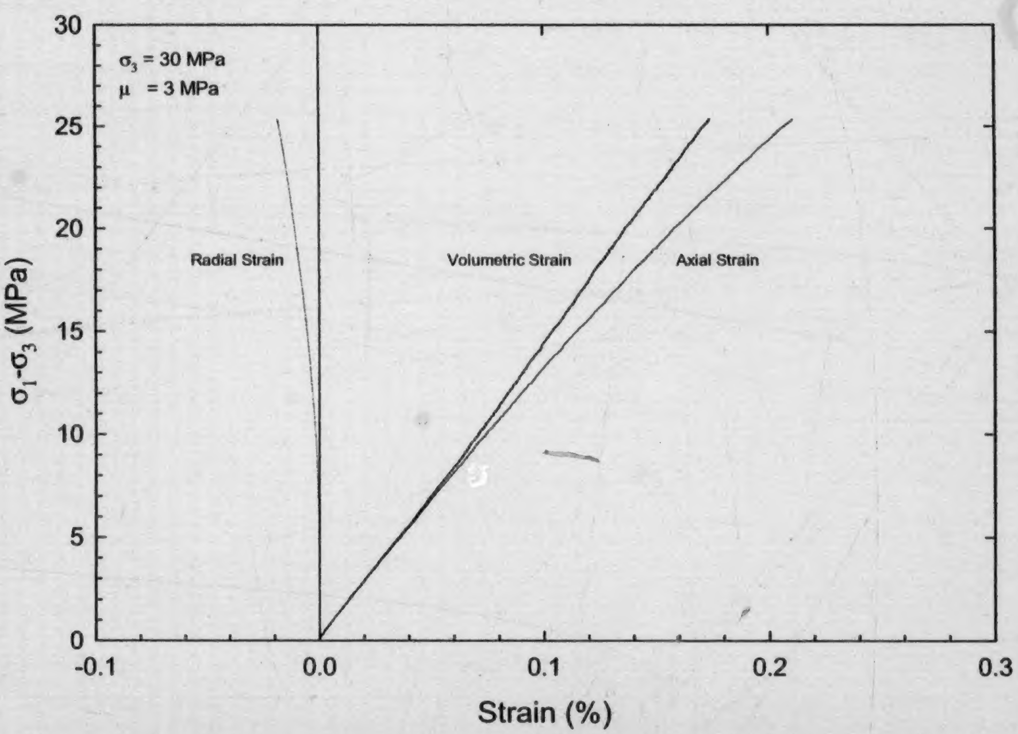

Figure 6-28. Test No. 3, triaxial compression of a Midale Evaporite sample carried out under a confining stress of 30 MPa and a pore pressure of 3 MPa. It was not possible to achieve failure due to equipment limitations

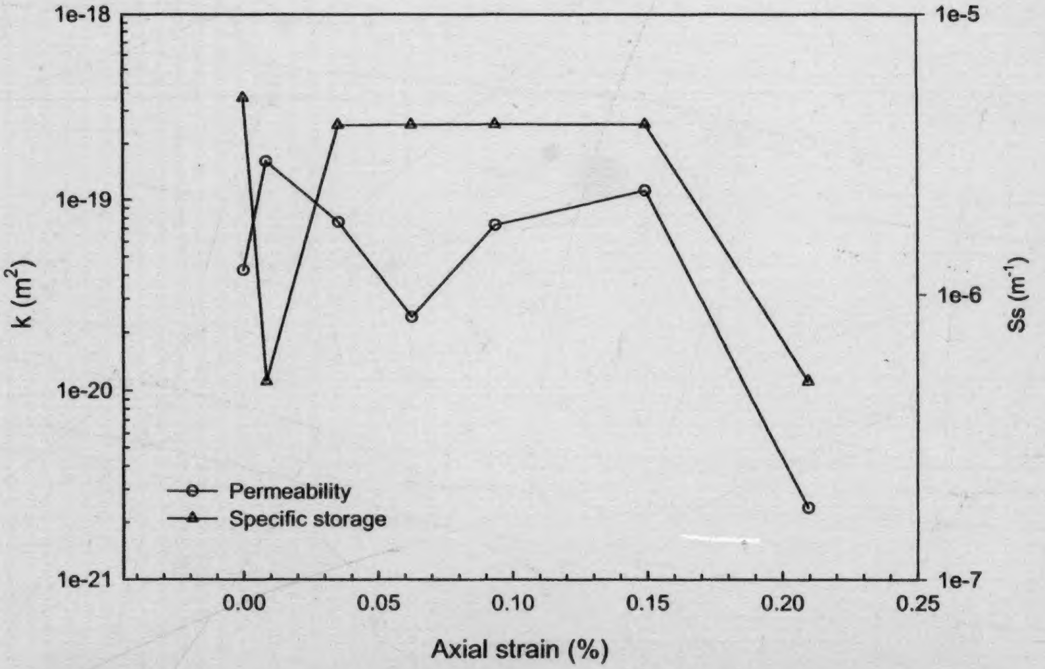

Figure 6-29. Test No. 3, evolution of permeability and specific storage during shear of a Midale Evaporite sample carried out under a confining stress of 30 MPa. The lack of significant change in properties is due to the inability to induce damage in the sample with the experimental equipment available at such a large confining stress

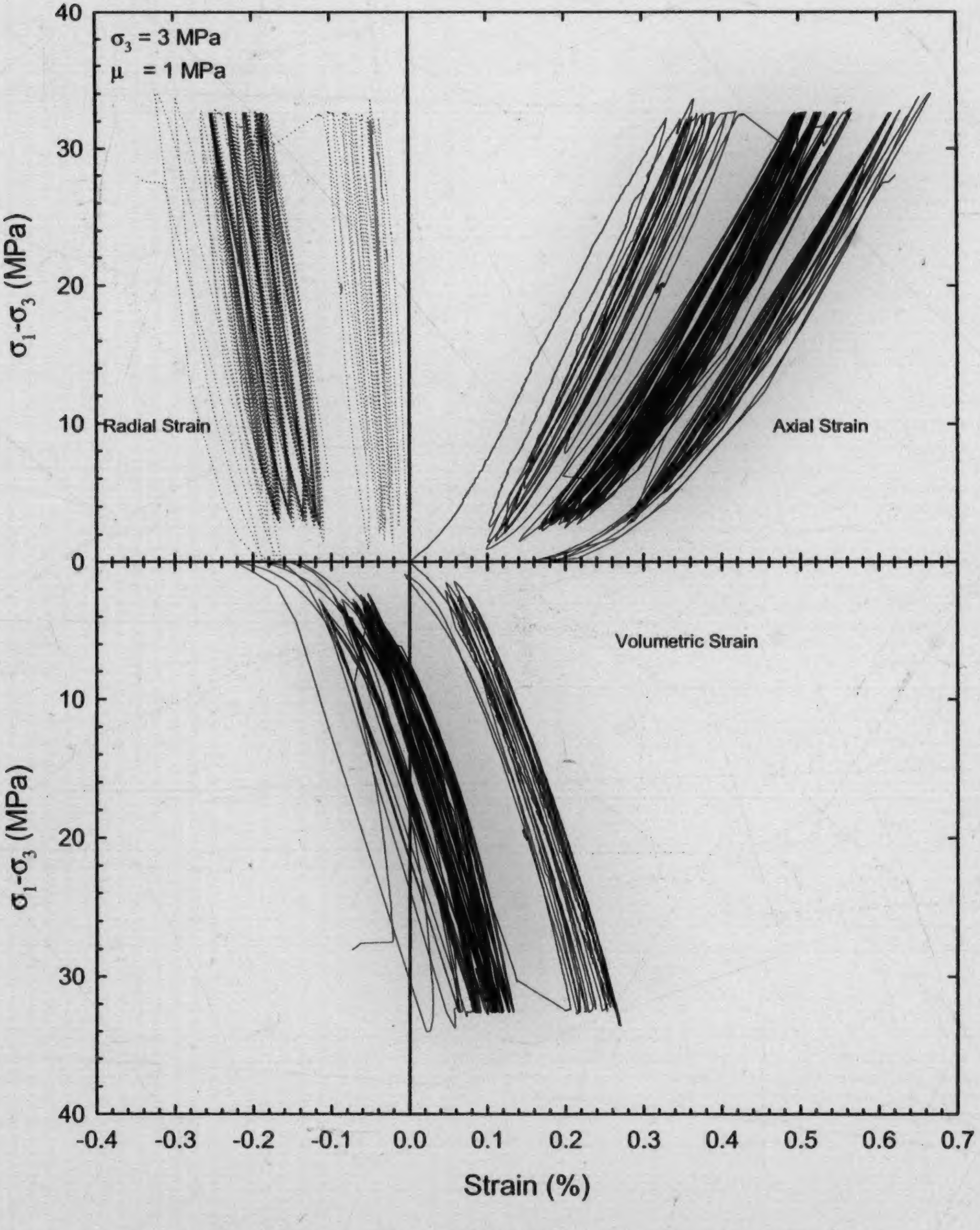

Figure 6-30. Test No. 4, cyclic shear of a Midale Evaporite sample carried out under a confining stress of 3 MPa and a pore pressure of 1 MPa

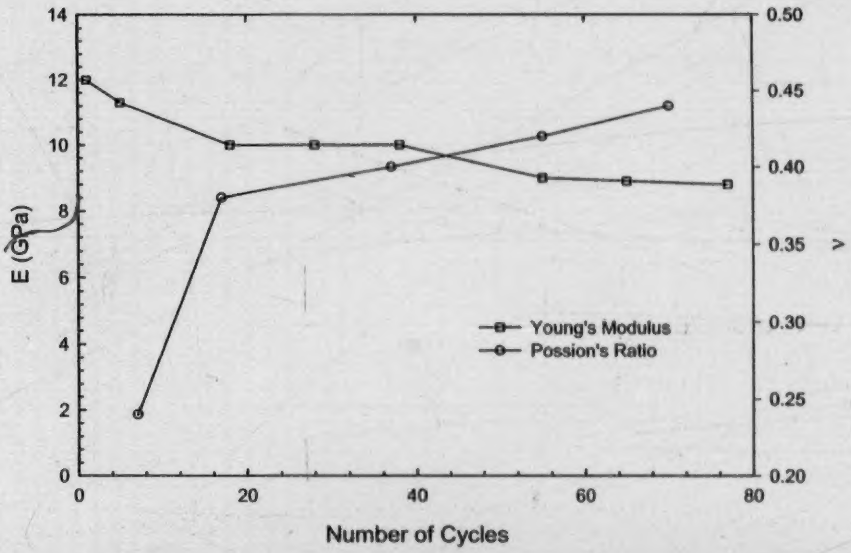

Figure 6-31. Test No. 4, evolution of elastic properties of a Midale Evaporite sample sheared cyclically under a confinig effective stress of 2 MPa

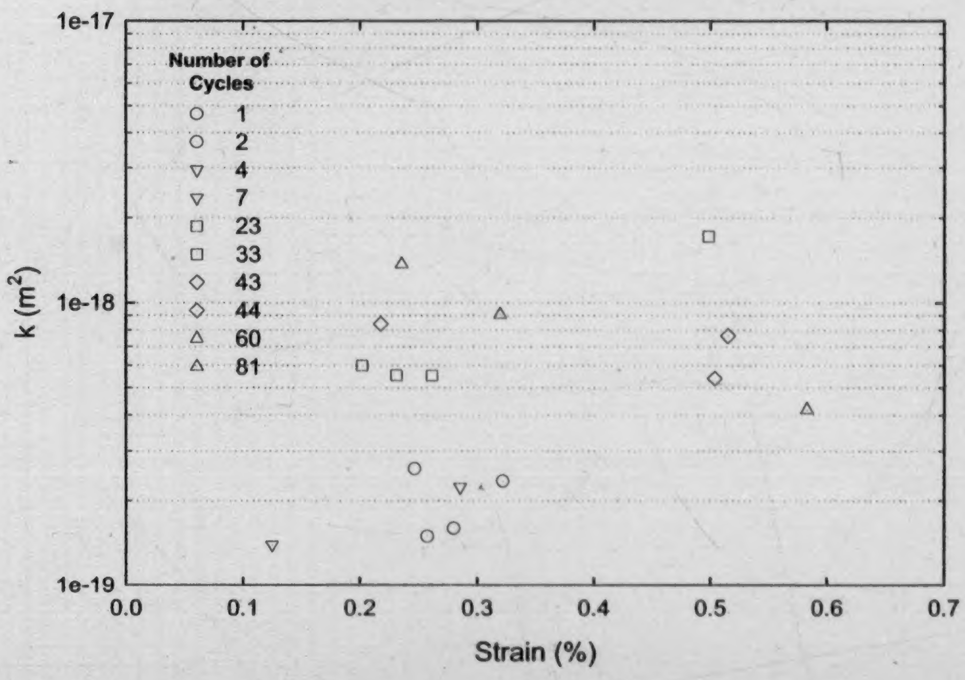

Figure 6-32. Test No. 4, permeability evolution of a Midale Evaporite sheared cyclically under a confining stress of 3 MPa and a pore pressure of 1 MPa against axial strain

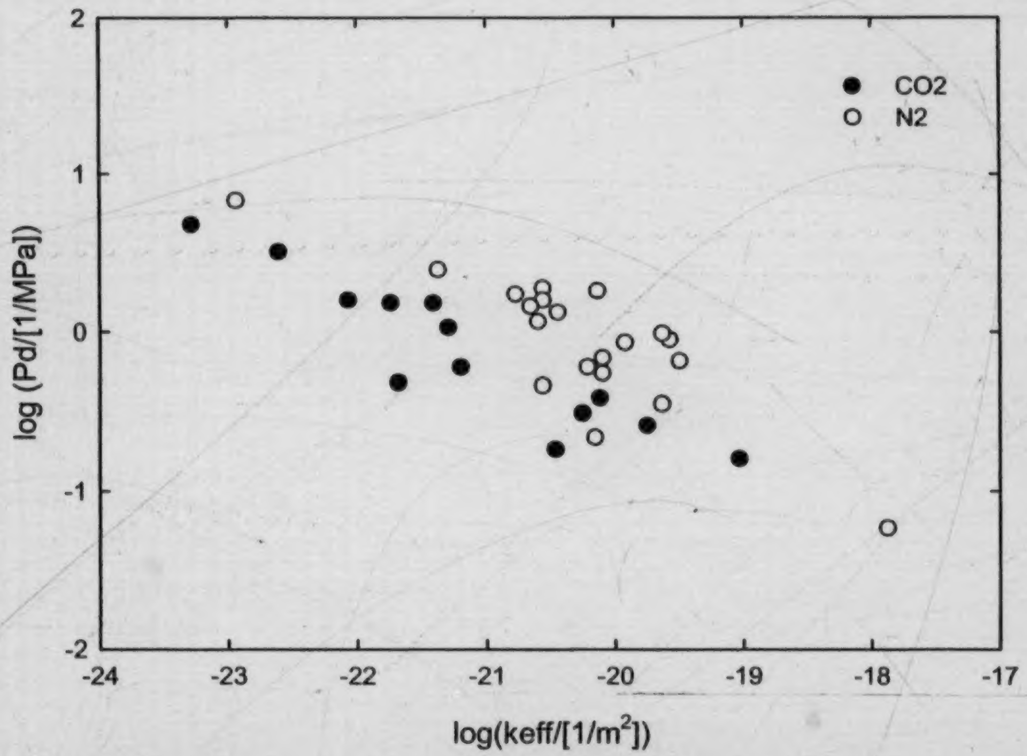

Figure 6-33. Effective permeability and minimum capillary displacement pressure for different argillaceous materials using N2 and CO2, modified after Hildenbrand and Krooss [66]

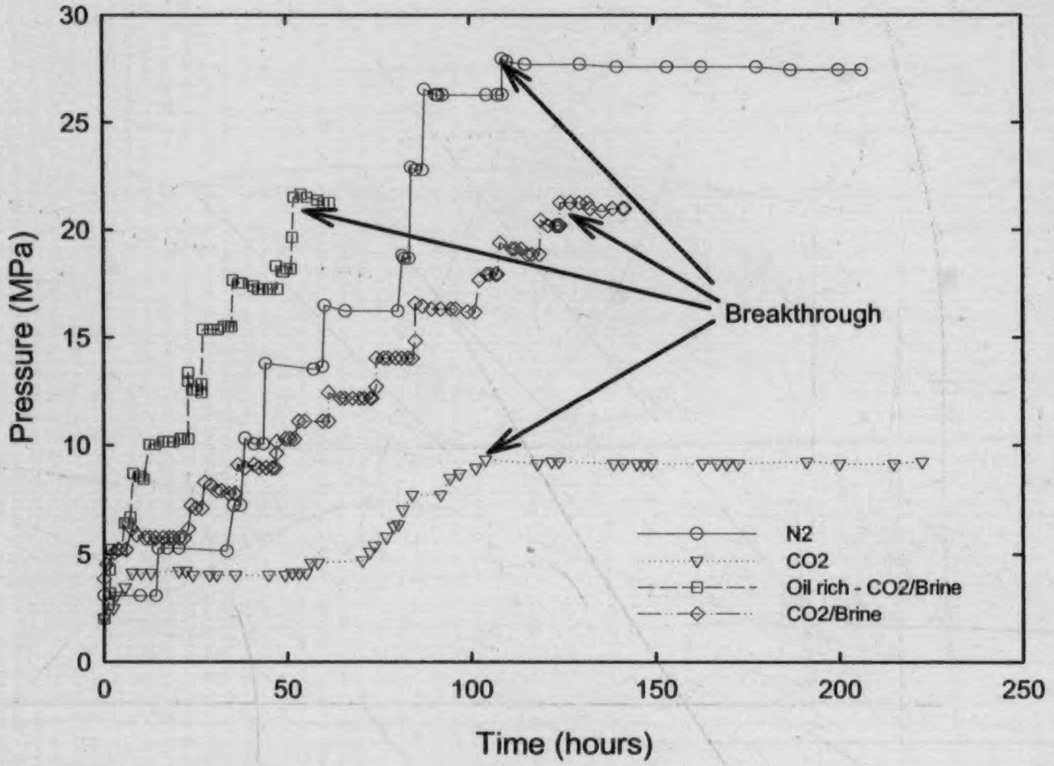

Figure 6-34. Breakthrough pressure test history from similar samples from Weyburn caprock samples using N_2, pure CO_2, oil-saturated CO_2/brine system and pure CO_2/brine system, modified after Dong et al. [70]

7 The Weyburn CO_2-EOR Storage Project: Mechanical Earth Model

7.1 Overview

Both performance assessment techniques and the observational method require a base case scenario or model that encompasses the most likely conditions of the site. This is achieved through the logical organization of all the relevant information gathered in a CO_2-EOR project. Collection and organization of such data leads to a clear picture of the in-situ conditions, and identifies the uncertainties and/or gaps in the base case scenario. In the case of geomechanical performance assessment for CO_2 storage, scenario development is efficiently accomplished by developing a mechanical earth model.

7.2 Mechanical Earth Model (MEM)

A MEM is a logical compilation of relevant information about earth stresses and rock mechanical properties based on geomechanical studies and geological, geophysical and reservoir engineering models [187]. Such a model is the base case scenario for geomechanical performance assessment, and is the ideal method to identify areas of uncertainty or lack of information. The recognition of uncertainty or lack of information will lead to the development of alternative scenarios.

7.2.1 Geological Model

7.2.1.1 Geological Setting

The Weyburn Field is a major oil field in southeastern Saskatchewan and is located in the northeastern part of the Williston Basin. The Williston Basin, where petroleum production is widespread, is an intercratonic basin located in central and western North Dakota, eastern Montana, northwestern South Dakota, and southern Manitoba and Saskatchewan [188]. The entire stratigraphic succession ranges from Middle Cambrian and Early Ordovocian sandstones that directly overlie the Precambrian basement to Quaternary rocks at surface [189]. The depositional history of the basin has lead to a clear division in two categories of rocks: Paleozoic rocks that are predominatly carbonates, evaporites, and minor shales; and Mesozoic rocks that are dominated by shales, siltstones, and sandstones [189]. The Basin has undergone successive erosional events, the most relevant being the Sub-Mesozoic Unconformity. During this event the sedimentation changed from marine and marginal marine environments during the Paleozoic to transport and deposition of siliclastic sediments in the Mesozoic. Figure 7-1 shows the stratigraphic column of the basin and differentiates between aquifers and aquitards.

The Weyburn Field is a carbonate reservoir of Mississippian age and part of the Madison Group, which ranges from 400 to 700 m in thickness of carbonate and evaporate deposition. The Upper Madison carbonates of southeastern Saskatchewan were deposited in a relatively broad, shallow marine environment [190]. Slight changes in sea level resulted in fairly uniform depositional changes [191]. Above the Weyburn Pool the thickness of the Mesozoic sequence is 1300 to 1400 m. The Mississipian rocks are capped by a regional aquitard, the Watrous Formation, a low permeability siliclastic shaly Triasic-Jurasic formation, Figure 7-2.

The Mesozoic units contain both the most important regional aquitards, and the aquifers with the largest transmissivity. The aquitards are the Watrous Formation, Vanguard Group, Joli Fou Formation, Colorado Group and the Bearpaw Formation. They are regionally extensive, and control the shallower flow regime as Khan and Rostron showed [192], and similar to what Neuzil showed for the Cretaceous shales of Mid North America [71, 155].

A detailed review of the tectonic evolution of the Williston Basin by Redly [193] indicates that the basin initially developed as a circular feature during the Sauk-Absakora (Paleozoic) cratonic sequences, and evolved to an oval asymmetric basin during the Zunji-Tejas (Mesozoic) sequences. This latter configuration of the basin, where the main axis is oriented NW/SE and the minor NE/SW, is a manifestation of the Sevier and Laramide orogenies that produced NW/SE and SW/NE striking faults and a southwest tilt to the basin, Figure 7-3. Consequently, the active stress regime in the Williston and Western Canadian Sedimentary basins [194] are expected to be similar as they were affected by the same regional tectonic events.

7.2.1.2 Salt Dissolution

Salt dissolution is a widespread feature in the Williston Basin especially in the Prairie Evaporite, and as such has played a very important role in the geological evolution of the basin, and the presence of hydrocarbon pools in it –the influence of salt dissolution in the reservoir's hydraulic integrity will be studied in more detail in Chapter 9. However, in the development of the MEM it is important to consider its influence on the in-situ stresses in the reservoir.

Consequently, modeling of the depositional history of the basin, including salt dissolution and erosional periods was carried out. The three depositional 'periods' included salt dissolution, which has been very active throughout the history of the basin. The Devonian and Mississippian erosional events were included in the model as both were significant (Whittaker, personal communication[10]). The modeling was carried out by simulating successive events of deposition and erosion, with dissolution occurring both during Devonian and Mississippian times but distant from the reservoir, salt free area in Figure 7-4. Thus, initially a model that included deposition up to Devonian was built, then 50 m were eroded, then deposition up to the Mississippian proceeded, followed by 200 m of erosion in what is the most significant unconformity of the depositional history of the basin. Finally, deposition up to the present was allowed, neglecting the more recent erosive events. The amounts of erosion were provided by Steve Whittaker[11]. The results of the model[12] show how the erosive events lead to a stress ratio (horizontal to vertical stresses), K_0, bigger than one, but still fairly close to one. There is evidence of thinning of the Prairie Evaporite by more than 30 m beneath part of the Weyburn Field, Figure 7-4 and Figure 9-2 in Chapter 9, as well as the absence of three other Devonian salt beds that are present elsewhere. However, anomalous thickening of the overlying Late Devonian and the earliest Mississippian strata indicates that compensatory deposition occurred before deposition of the Midale beds. Consequently, this localized dissolution below the reservoir could not affect the state of stresses in the reservoir. Figure 7-5 shows the results of the elastic modeling of these events at Phase 1A for the massive dissolution features that are distant from the reservoir. Clearly, salt dissolution has not influenced the stress state as it was induced into the model subsequent to each depositional event, and changes in K_0 were not observed due to salt dissolution. The erosional events had a larger influence at their time of occurrence, but the effect on the in-situ stresses was overwritten by massive depositional events. However, the erosion-deposition sequence must have affected the elastic and mechanical properties of the formations where K_0 increased significantly.

7.2.1.3 Reservoir Characterization

The Weyburn Field is a Mississippian carbonate reservoir where the oil is trapped in the Midale Beds of the Charles Formation at a depth of approximately 1450 m. The initial pressure and temperature of the reservoir was 14.5 MPa and 61°C respectively [28, 29]. The Mississippian strata in the Weyburn area dip southward at a rate of 8.3m/km, forming a broad homoclinal feature [191]. The reservoir is sealed by underlying low permeability dolostones and anhydrites of the Frobisher Beds and by an overlying 2 to 11 m thick layer of anhydrite of the Midale Evaporite. Although variably affected by erosion on the Sub-Jurassic Unconformity, the Midale Evaporite forms a regional top seal across the field [29]. The reservoir itself is subdivided into a lower limestone-dominated unit called the Vuggy, and an upper dolostone unit called Marly. These units have thickness ranging from 10 to 22 m and 1 to 11 m, average porosities of 15% and 26%, and average permeabilities of $2*10^{-14}$ m^2 (20 md) and 10^{-14} m^2 (10 md), respectively [28].

---

[10] Conversation on September 2003 with Steve Whittaker, Senior Research Petroleum Geologist at Saskatchewan Industry and Resources

[11] See footnote 8

[12] The parameters used in this model can be seen in Table 9-1 of Chapter 9

The Midale Evaporite is a band of anhydrite and anhydritic dolomite that makes the caprock of the reservoir. Formed during the latest phase of the brining-upward cycle of the deposition of the Midale Beds [189], the succession is made up of laminated to massive anhydrite at its base, grading upwards into nodular anhydrite with scattered dolostone interbeds.

The Midale Marly is divided into an upper non-reservoir low porosity zone known as the "Three Fingers". It is a thinly interbedded anhydrite, shale and cryptocrystalline evaporitic dolomite, of a thickness of 1.5 to 3.0 metres [190]. The porous Marly consists primarily of microcrystalline to chalky dolostone, whose porosity is limited to pin point vugs [190, 191, 195]. The chalky dolostones are often separated by less permeable interbeds of dolomitic limestone and limestone. These beds are usually less than a meter thick, with textures from mudstones to wackestones, with occasional anhydrite cemented grainstones [190].

The Vuggy zone is composed almost entirely of limestone. It consists of interbeds varying in texture from mudstone to grainstone [190, 195]. The rocks that make up the major portion of the reservoir consist of grainstones and packstones [190]. The name for this zone is derived from the open vuggy porosity that can be found in the coarser grained rock. The Vuggy zone was further divided into a lower and upper zone. The upper portion of the Vuggy unit consists of interbedded peloidal and bioclastic packstones and rare peloidal grainstones [191]. The lower portion is a thinly bedded, slightly argillaceous lime mudstone-wackestone, interbedded with occasionally porous bioclastics and/or peloidal packstones [191]. Marly-like dolomudstones occur locally in the lower part of the Vuggy section. These beds are generally thin, have poor porosity, poor oil staining, and are often anhydrite cemented [190].

The Frobisher Evaporite is a zone composed of massive, bedded and nodular anhydrite which is similar to the Midale Evaporite, but less massive [189, 190]. It forms a lower seal to the northern portion of the Weyburn Field but it is not present beneath the southern portion [189]. The Frobisher Evaporite is generally not fractured, although its nodular character makes it slightly prone to small-scale fractures [196].

The Frobisher Marly is lithologically analogous to the Midale Marly beds due to similar depositional environment and diagenetic processes [190]. Its thickness is from 1 to 6 meters. This horizon is considered to be in pressure communication with the overlying Midale Vuggy throughout much of the area, and has been productive in some areas of the field [190].

7.2.1.4 Depositional Environment

Four major shallowing upwards cycles have resulted in the deposition of the Frobisher and Midale beds [190]. The major components of a complete shallowing upwards sequence are an initial subtidal intershoal and subtidal shoal phase (the Vuggy), an intertidal lagoonal phase (the Marly), and a supratidal phase (the upper Marly and Evaporite) [190]. Initial lower Vuggy deposition occurred in response to the early phases of a major transgression over the Frobisher surface. The remainder of the cycle is dominated by a shallowing upwards sequence as the shoreline prograded seaward resulting in the deposition of the upper Vuggy and Marly; and finally the supratidal sediments of the upper Marly and Midale Evaporite. Each transgressive-regressive cycle contains smaller scale cycles which form the three primary stages of shoal development in the Vuggy [28, 190].

Shoals are characterized by bioclastic, oolitic, and pelloidal grainstones, which may or may not be anhydrite cemented. Packstone buildups are also locally present. Intershoal areas are characterized by tighter, fractured lime mudstones, wackestones and packestones. In general the Vuggy in the intershoal areas is thinner than the shoal areas, and is the thinnest in the Marly channel areas. The Marly dolostones are deposited as a drape over the pre-existing Vuggy topography and, consequently, are thinner over the shoal areas and thicker in the intershoal areas [28, 190].

The Midale Evaporite was not deposited in a sabkha environment like the Frobisher Evaporite, but rather in a broad flat salina setting. The majority was deposited subaqueously, which results in the laminated to massive anhydrite common in this formation. As the salina filled with bedded gypsum, the relative water level dropped, allowing for the deposition of nodular and elongate gypsum, later altered to anhydrite [197]. These anhydrite types are more abundant at the top of the formation, while the transition to massive/laminated deposition appears abruptly, suggesting a relatively sudden shallowing of the salina lake [197].

7.2.2 Hydrogeological Model

Khan and Rostron [192] built a comprehensive hydrogeological system for the Weyburn project. Their model showed that the Watrous aquitard separated the deep hydrogeological system from the shallow system, and thus this formation is the true hydraulic seal for the project. Moreover, they showed that all aquifer flow is predominantly laterally confined within regionally continuous aquifer units.

In the specific case in the Weyburn Field, the Midale aquifer has a uniform flow regime, but it is highly variable chemically (measured as Total Dissolved Solids, TDS). Within the field low gradients drive the flow slowly (<1 m/yr), and the flow is roughly parallel to the subcrop [192]. South and east of the Field, density driven flows drive formation water down dip and inward into the basin [192], which is positive for CO_2 storage. Vertical pressure profiles indicate slight overpressuring in the Mississippian beds, which may be due to either effects of water injection, minor isolation of that portion of the aquifer, or energy loss in the water phase due to lateral flow through the aquifer [192], Figure 7-6, indicating negligible vertical flow. Likewise, hydrochemistry differences between Mesozoic aquifers and Mississippian aquifers supports the lack of flow between these formations [192].

7.2.3 Role of Fractures

The Weyburn Field is a naturally fractured reservoir with a medium to low permeability matrix. Therefore, fractures are a main control in flow movement, production, and the design and/or operation of any EOR technique. This has lead to a large number of fracture studies in the Midale Beds [190, 198-202], and these results have been used to address geomechanical concerns with the caprock. Some of these studies have been carried out in the Midale Field, which is adjacent to the Weyburn Field and has similar geology.

7.2.3.1 Midale Field

Beliveau et al. [201] studied core from 100 vertical wells. About 20% of the core had fractures, 23% of the entire intershoal Vuggy, 16% of Marly, and 11% of shoal Vuggy. The Midale Anhydrite and Frobisher Anhydrite showed no fracturing. Additional information was gathered from three horizontal wells drilled orthogonal to the fracture system. The examination of this core showed the intershoal Vuggy fracture density was two to four times higher than the one in the Marly with a fracture trend of N45E. Based on these core examinations, a fracture spacing of approximately 0.6 to 0.9 m in the Marly, 0.3 m in the intershoal Vuggy, and 0.6 to 1.2 m in the shoal Vuggy was estimated. Among the most relevant features of the fractures are, that without exception the fractures are vertical to nearly vertical, predominantly open, and when there were two fractures in a core, no high-angle intersections were observed.

Fischer [199] studied the core from 48 vertical wells, and three Formation Microscanner logs (FMS) from the Midale Field. His results showed that the Vuggy is two to three times more fractured than the Marly. Moreover the Marly M2, which is a tight limestone, was more fractured than the rest of the more dolomitic Marly. The fracture density of the Marly was about one fracture every two meters for the Marly M1 and M3 (more porous crystalline dolomites), and four fractures per meter in the M2. The fracture density of the Vuggy was two to four fractures per meter, with the shoal having twice the fractures as the intershoal, but these results were anticipated [199].

From the FMS it was deduced that there were two sets of fractures. The dominant fracture set had a strike azimuth of 50° to 60° ± 30°. The remaining fractures were termed off-trend. Fracture length was not possible to quantify, but two wells 100 m apart did have simultaneous production response, indicating that they intersect on a single fracture trend. However, evidence was not found for wells in any injection pattern to be directly linked on trend, suggesting that fracture length is less than 560 m. Fracture heights of 28 cm and 47 cm with average apertures of 0.06 to 0.4 mm were measured for the Marly and Vuggy, respectively [199].

7.2.3.2 Weyburn Field

Churcher and Edmunds [190] carried out a fracture study for PanCanadian in 1994, where core from over 150 vertical wells was described, and five FMS logs from five horizontal wells as well as 51 Repeat Formation Tests (RFT) were used. The results showed a vertical to subvertical set of fractures oriented NE-SW, which controls the directional permeability of the field. The results show a fracture spacing of about 3 m for the Marly, 0.3 m for the intershoal Vuggy, and 2.5 m for the shoal Vuggy.

Bunge [202] analyzed three oriented cores originally collected by Core Laboratories Ltd. [198]. The study was more detailed than the previous ones, but the amount of core employed was less. Moreover the study included five electronic borehole images, four EMIs and one FMS, but not all of them were of good quality. His results found three sets of fractures, named A, B, and C, with strike azimuth of 40± 5°, 285± 7°, and 328±11° respectively. These fractures dip on average 80°, with fractures dipping 80° to 90° accounting for 69% of the total. Fracture height was about 30 cm and independent of the formation, which is different from the results in the Midale Field.

Apertures were between 0.004 mm and 0.2 mm. The fracture density (number of fractures per metre) in the Marly was 2.3, 1.5, and 1.0 for sets A, B and C respectively. Similarly, fracture density in the Vuggy was 3.8, 2.5, and 1.6 for sets A, B, and C respectively.

7.2.3.3 Fractures and Reservoir Performance

Considering the widespread fracturing in the reservoir, and the NE-SW trend of the fractures, it was expected that the reservoir performance was going to be dominated by these fractures. Thus, in the Midale Field, waterflooding was controlled by the fracture system as the water-cut distribution illustrates [201], Figure 7-7. Reservoir simulations showed a permeability anisotropy of 25 on average, a result similar to well testing in closely space wells, that allowed calculation of the dual-porosity parameters and area anisotropy in the Midale Field [203].

Likewise, the Weyburn Field showed a similar behavior during waterflooding [191, 195, 204, 205], Figure 7-7. Pressure buildup and falloff tests showed similar results as the Midale Field, but it was not possible to establish the permeability anisotropy, although history matches using 6:1 to 10:1 have given good results. However, there was not a test between closely spaced wells that allowed determining such a permeability anisotropy directly.

7.2.3.4 Fractures in the Caprock

Four types of fractures have been identified in core from the Midale Evaporite [197]. Synsedimentary cracks that were formed in and around the vertically growing gypsum crystals in the floor of the salina, Figure 7-8a [197]. Dewatering cracks were formed in the very early stages of compression and dewatering. These reflect upward water movement very early in the diagenetic history of the formation, Figure 7-8b [197].

Healed vertical fractures that occurred post lithification had taken place due to the angular pieces of the surrounding lithology within the fracture space, Figure 7-8c. There fractures are filled with another phase of anhydrite likely emplaced in the Tertiary, coincident with oil migration through the Midale beds [197]. These fractures appear to be completely healed. Anhydrite cementation is also present in fractures of the reservoir, and likely occurred the same time as oil was emplaced [190]. Therefore, the fractures in the caprock and the reservoir were most likely formed at the same time and as a consequence of the same events. Moreover, these fractures seem to coincide in age with structures formed during the change in orientation of the basin associated with the Laramide and Sevier orogenesis.

Finally there are late-stage cracks that are usually vertical, thin, and without infill or hydrocarbon residue. It is likely that these fractures are drilling-induced [197] or they could have been formed during the waterflooding of the field, Figure 7-8d.

7.2.3.5 Fractures in the Williston Basin

Fractures are not only present in the Midale and Weyburn fields within the Williston Basin, but are a widespread feature in different formations of different age. Many of these fractures share common azimuths, dips, and apparently formation time, which may lead to concluding they are the result of a common set of events.

Thin, vertical, planar fractures have been observed in the Mission Canyon Formation, at the Little Knife Field, North Dakota [206], which appear to be extension fractures. Fractures are present only in carbonate units, but within the carbonate units their occurrence is not lithology dependent. Fractures have a predominant East-West trend, with a density of 0.3 m of fracture per 0.7 m of core. Studies of aqueous and hydrocarbon fluid inclusions associated with the fractures revealed that the fractures formed after the strata were buried to at least their present depth of 2987 m, which indicates that their age is post-Mesozoic. Likewise, the pore fluid pressure gradient was hydrostatic immediately after (if not during fracturing), formation water salinity has remained fairly constant since fracture initiation, and migration of hydrocarbons into the reservoir preceded fracture genesis.

Likewise, fractures in Late Cretaceous to Late Pleistocene sediments have been observed in Saskatchewan, eastern Montana, and western North Dakota, Figure 7-9 [207]. Two sets of vertical fractures trending NE-SW and NW-SE are observed consistently, regardless of rock type or age. Both sets appear to be extensional in origin and are similar in character to joints in Alberta. The principal set of fractures has a trend NE-SW and the secondary set has a trend NW-SE, which matches the trend of modern lineaments observed in the Williston Basin area, Figure 7-9. The trend in sub-Mannville lineaments is similar, although more scatter is present and the principal and secondary trends are rotated 90° with respect to the modern lineaments. It seems that fracturing began at least by Late Jurassic time, as the sub-Mannville unconformity shows the same pattern of valleys as the modern topographic surface. Stauffer and Gendzwill [207] suggested that the fractures formed as a combination of tectonic stresses caused by westward motion of the North American Plate together with uplift of the sediments.

7.2.3.6 *Structural Features in the Williston Basin*

A fairly extensive study of the structural features, including basement structures, fracture zones, lineaments and faults was carried out as part of Phase 1A in Weyburn [189]. Results indicate that two phenomena are the cause of most of the structural features in the basin; salt dissolution and the movement of the North American continent during plate tectonics. Structures in the salt dissolution areas are probably connected with their surface expression and related intra-sedimentary structural features. Features due to plate tectonics are better seen as surficial expressions such as lineaments but can also cause deep-seated features such as the Souris River Fault. This is a strike-slip fault within the risk assessment area with a NNW-SSE trend, and no vertical displacement [189], and as such it is an expression of the actual stress field in the basin, as it will be seen later on in this chapter. Nonetheless, the risk assessment area is outside the salt dissolution area, and in general it shows the least disturbance from tectonism.

7.2.3.7 *Origin of the Fractures*

From the foregoing discussion it seems clear that the widespread presence of fractures in the Williston Basin has tectonic origins. The migration from a circular to elliptical basin, with the main axis oriented NW/SE and NE/SW due to the Seveir and Laramide orogenesis, lead to a new stress field in the basin. This stress field is common to the Interior Plains of United States [208] and the Western Canadian Sedimentary Basin [194]. The shortening in the NE/SW direction leads to fracturing perpendicular to the extension direction (NW/SE), as it is observed in the Williston Basin [209]. The direction of shortening became the direction of the maximum horizontal stress, and the minimum principal stress is orthogonal to this direction, parallel to the direction of elongation.

Systematic joints, such as the ones seen in the reservoir and other areas of the basin in the NE/SW direction began forming as a consequence of the NW/SE elongation of the basin by the time orogenic events had a larger manifestation in continental North America. Thus fractures such as the ones present in both Little Knife, and younger sediments in Saskatchewan, eastern Montana, and western North Dakota formed by the time of active plate tectonic movement reflected in the Nevada,. Sevier and Laramide orogenies, the earliest occur in Late Jurassic and the latest going up to Late Cretaceous/Paleocene. Differential stresses are observed up to 2000 km inland due to plate tectonic movement, as it has been recorded by twinned calcite in carbonate rocks in northwestern North America [210]. Thus, the fractures of Tertiary origin observed in the Midale Evaporite (section 7.2.3.4) are a consequence of these events as wells.

Likewise, a conjugate set in the NW/SE direction developed. These conjugate sets can form as a result of many different mechanisms such as the change of stress in the direction perpendicular to the systematic joints after their formation. Because the surface of open systematic joints is traction free, their formation will release the crack-normal tensile stress [211]. Another mechanism is fracturing development due to the elastic 'desire' of the basin to recover its original shape, once the shortening forces stop acting, which leads to fracturing perpendicular to the systematic joints [209]. The development of the conjugate set could be a result of bending or warping in the direction parallel to the systematic joints as well, considering that they formed long narrow bands of brittle material [209]. At Weyburn, the most likely causes of formation of this secondary set of fractures are the elastic stresses trying to bring the basin to its original circular shape, causing more fracturing between systematic joints, and the tilting of the basin that may have caused bending failure between systematic joints. Despite the possible multiple mechanisms acting to create the conjugate set, this set has a smaller density, and its influence on flow is masked by the fact that these fractures are contained between systematic joints, so their connectivity is poor compared with the main set. Also, those fractures are widespread, but not necessarily present between every systematic joint, and in that case, the 'off-trend' flow permeability would not be affected largely by this secondary set, as it is the case of Weyburn.

The mechanism of fracturing outlined above implies fracturing in the NE/SW direction in most of the stratigraphic column at the Williston Basin. However, many of these fractures may have self-healed through a combination of process and conditions such as mineralization, large pressures, and large temperatures. One of these events was the formation of metasomatic anhydrite, infilling not only the Midale Evaporite tectonic fractures, but also the reservoir fractures itself [190]. This cement was emplaced at the same time oil was emplaced. Therefore, fractures in the caprocks are not observed from core studies and well testing because most of them must have been cemented. Many reservoir fractures are cemented as well [190, 202], but it is likely that the density of fractures in the reservoir, and its vuggy nature did not permit complete cementation of the system, as the amount of anhydite needed may have been too large. This difference in volumes is a combination of larger porosity and higher fracture density in the reservoir than in the caprock. The lower fracture density in the caprock compared with the reservoir is due to the contrast in elastic properties between the Midale Evaporite and the Midale Beds, as they can lead to tensional fractures in formations with different stiffness, even in the presence of far-field compressional stresses [212]. A simplistic three dimensional simulation, Figure 7-10, assuming an isotropic state of stress as initial condition, and then applying a constant rate of displacement in one direction leads to much lower stresses in the direction of extension in the 'softer' formation

(Midale Beds) than in the 'stiffer' formations (Frobisher and Midale Evaporite), Figure 7-11. Once the displacement progresses, the stress in the softer formation tends toward higher tensional values, which would eventually lead to fracturing. Another factor to be mindful of is the presence of vugs in the Midale Beds that can act as 'defects', and create a lower effective area to resist the traction forces. Diederichs [213] showed how the critical crack intensity, critical extension strain, and the linearity crack interaction threshold in stress space are consistent in Brazilian tests, confined tension tests, and uniaxial tests when crack propagation is not permitted, which would lead to a very similar fracture density in both reservoir and caprock, but when crack propagation is permitted –which is more realistic-, isolated cracks propagate under tensile conditions resulting in instantaneous failure after initiation in direct tension tests [213]. These tensile stresses are developed despite an overall confined state [214]. Thus, it is possible to expect a faster crack propagation in the Midale Beds once the formations is under traction, while the Evaporites having less defects will have a slower crack propagation, and less tendency to crack. Granted this picture is rather simplistic, it helps to visualize how fracture density would be substantially larger in the Midale Beds, and therefore despite a cementing event later on, all the fractures were not sealed.

Table 7-1 summarizes the geological, hydrogeological, and fracture density information from the preceding sections for the caprock system formations. It is clear that before exploitation and production the caprock and the lower seal were very competent seals, with low transport properties and unknown fractures.

Table 7-1. Hydrogeological description of the reservoir units[13]

Reservoir Zone	Lithology	Porosity (%)	Matrix Permeability (m^2)	Heterogeneity	Fracture Density (spacing)
Midale Evaporite	Anhydrite	0.3 to 8	10^{-19} to 10^{-21}	Low	None-Low
Marly	Dolostone	20 to 37 (26)	$<10^{-16}$ to 10^{-13} (10^{-14})	Low	Low-Moderate (2-4 m)
Upper Vuggy	Limestone	2 to 15 (10)	$<10^{-17}$ to $2*10^{-14}$ (10^{-15})	Medium	High (<1 m)
Lower Vuggy	Limestone	5 to 20 (15)	$<10^{-15}$ to $5*10^{-13}$ ($2*10^{-14}$)	High	Moderate-High (<1-2 m)
Frobisher Evaporite	Anhydrite	NA	10^{-19} to 10^{-21}	Low	None-Low
Frobisher Marly	Dolostone	NA	NA	Low	Low-Moderate

7.3 Mechanical Earth Model for Weyburn

7.3.1 Mechanical Properties

A general model that covers the elastic properties from the Cretaceous Mannville Group down to the Mississippian Frobisher Beds was developed for this thesis. Such a model can be used for geomechanical studies on wellbores and/or faults as it includes most of the stratigraphic column. The Mannville Group was chosen as an upper limit because of its large flow velocity [192], as any CO_2 potentially leaking upwards would likely be carried away laterally by this aquifer. A more detailed model of the caprock system, with Mohr-Coulomb and Hoek-Brown parameters was built for the Midale Evaporite, the Midale Beds, and the Frobisher Evaporite for geomechanical modeling of the caprock system. In order to obtain properties for these models information from the geological model, geophysical logs, laboratory testing, and published information in similar materials was used.

---

[13] Values in parenthesis indicate averages

The dynamic elastic properties were evaluated using dipole sonic logs that were run in five different wells in the Weyburn area, Figure 7-12. This figure shows the location of wells used for density calculations, and to obtain the geological picks as well. For the case of the caprock system itself, the dynamic elastic properties were not only obtained from dipole sonic logs, but also from dynamic core studies carried out by Core Labs [215]. Static properties come from the results presented in Chapter 6 for the Midale Evaporite, and from tests in the Vuggy formation carried out by McLellan [216]. Compressional and shear wave velocities are related to elastic properties by the following equations[217]:

$$\nu = 0.5\left(\frac{(V_p/V_s)^2 - 2}{(V_p/V_s)^2 - 1}\right)$$

$$E = \rho V_s^2\left(\frac{3(V_p/V_s)^2 - 4}{(V_p/V_s)^2 - 1}\right)$$

where V_p is the longitudinal wave velocity; V_s is the shear wave velocity; E is the dynamic Young's modulus; and ν is the dynamic Poisson's ratio. Table 7-2 shows the dynamic elastic properties from dipole sonic logs for the whole stratigraphic column.

Table 7-2. Dynamic elastic properties from dipole sonic logs at Weyburn Phase 1A

Unit	*Unit Weigth kN/m*	*Vp km/s*	*Vs km/s*	*Young's Modulus GPa*	*Poisson's Ratio*	*Bulk Modulus GPa*	*Shear Modulus GPa*
Mannville	23.05	3.15	1.53	14.82	0.346	16.04	5.51
Rierdon	21.87	2.80	1.22	9.16	0.384	13.11	3.31
Upper Shaunavon	22.40	3.23	1.51	14.23	0.359	16.88	5.23
Upper Watrous	26.30	4.20	2.26	35.53	0.296	28.98	13.71
Lower Watrous	25.07	4.20	2.26	33.88	0.296	27.63	13.07
Poplar Beds	27.69	5.25	2.91	60.99	0.279	45.92	23.85
Ratcliffe Beds	27.62	5.25	2.91	60.82	0.279	45.79	23.78
Midale Evaporite	28.27	5.55	2.94	64.92	0.306	55.72	24.86
Midale Beds	24.21	4.13	2.32	33.78	0.268	24.23	13.32
Frobisher Evaporite	26.98	4.97	2.71	51.96	0.289	41.12	20.15
Frobisher Beds	25.55	4.97	2.71	49.20	0.289	38.94	19.08

There is a clear contrast between the post-Mississippian and pre-Mississippian formations, with shales and siltstones of the Triassic-Jurassic Watrous Formation serving as a transition possibly due to the presence of dolomitic and anhydritic cements, Figure 7-13. Unfortunately dynamic elastic properties are only strictly valid for very small strains, and the strains associated with geological deformations are large. Moreover, the relationship between strain and elastic properties is non-linear. However, an extensive review of dynamic and static measurements both in the laboratory and the field showed that in the worst-case scenario, static properties are generally never less than a third of dynamic properties, Figure 7-14 and Figure 7-15. Consequently, a 1/3 relation was used to determine the static modulus of the stratigraphic column. It is important to note that the contrast between elastic properties is more important than the actual value, and as such it is clear that the contrast of properties at the reservoir itself is very small. Therefore, the degradation in the elastic properties by three will affect absolute deformations mainly, but relative deformations between formations will not be affected significantly.

Information about mechanical properties of formations of the Weyburn's caprock system is limited to triaxial testing studies carried out at the University of Alberta on both the Three Fingers Unit[14] and the Midale Evaporite, and tests on the Vuggy at the Midale Field carried out by McLellan [216]. Properties of the Midale Evaporite are complemented by the review on anhydrites from Chapter 6. It is assumed that the Midale and Frobisher Evaporite have similar properties. However, intact core properties are not necessarily representative of rock mass properties. Therefore, the Hoek-Brown criterion is used as representative of the rock mass behavior, as the GSI is estimated considering the geological description and fracture density of each formation. Table 7-3 summarizes the mechanical properties of the caprock system.

Moreover, using the following, GSI can be used to evaluate the Young's modulus of rock masses [218]:

$$E_m(GPa) = (1-\frac{D}{2})\sqrt{\frac{\sigma_{ci}}{100}} * 10^{(GSI-10)/40}$$

---

[14] A transitional Unit between the Midale Beds and the Midale Evaporite whose anhydrite content is around 30% and has low permeability

where the different parameters are described in Chapter 6. This equation was established from near surface measurements, and at greater depth, particularly in massive to moderately jointed rock it may underestimate the rock mass modulus of virgin rock mass [186].

Table 7-4 and Table 7-5 summarize the elastic properties of the caprock system formations evaluated by the different techniques and correlations. Considering the uncertainty associated with both experimental and geophysical measurements, and correlations, two sets of values are chosen for the model: 'Soft' values which come from both static measurements and rock modulus evaluated using GSI; and 'Stiff' values which come from dynamic measurements and are meant to capture the upper limit to the value of these properties. Figure 7-16 shows both the elastic and mechanical properties for the caprock system.

Table 7-3. Mechanical properties of the caprock system formations

Criterion	**Hoek-Brown Parameters**						**Mohr-Coulomb**	
Unit	σ_{ci} *(MPa)*	m_i	m_b	*GSI*	*s*	*a*	ϕ *(°)*	*c' (MPa)*
Midale Evaporite	70-82	11.2	4.59	75	0.0622	0.5009	44.4	18.15
Marly	17-23	20.5	11.58	70	0.0357	0.5014	40.0	3.5
Upper Vuggy	16.7	20.5	4.91	60	0.0117	0.5028	46.8	3.5
Lower Vuggy			5.87	65	0.0205	0.5020		
Frobisher Evaporite	70-82	11.2	3.84	70	0.0357	0.5014	44.4	18.15

Table 7-4. Elastic Modulus of the caprock system formations

Young's Modulus	**Static / GPa**		**Dynamic / GPa**		**Model / GPa**	
Unit	*Lab*	*GSI Hoek*	*Lab*	*Log*	*Soft*	*Stiff*
Watrous				35.5	7.4	21.9
Midale Evaporite	21	38.3		65	22.7	61.3
Marly		12.9	25-38	34	10.3	33.4
Upper Vuggy	20	7.3	56		18.3	54.8
Lower Vuggy		9.7	48		15.4	48.7
Frobisher Evaporite		28.7		52	15.8	51.6

Table 7-5. Poisson's Ratio of the caprock system formations

Poisson's Ratio	**Static**	**Dynamic**		**Model**	
Formation	*Lab*	*Lab*	*Log*	*Soft*	*Stiff*
Watrous			0.296	0.227	0.219
Midale Evaporite	0.250-0.350		0.306	0.263	0.278
Marly		0.280-0.320	0.268	0.286	0.286
Upper Vuggy		0.333		0.309	0.306
Lower Vuggy		0.282		0.286	0.281
Frobisher Evaporite			0.289	0.313	0.290

7.3.2 In-situ Stresses

The information available for in-situ stress for the Weyburn Field is sparse and some is of questionable quality. To determine the direction of maximum and minimum horizontal stress, breakouts from nearby wells, including information from the Midale Field, and results from an anelastic strain recovery test performed in the Midale Field were utilized [219]. The directions are compared with the azimuth bearing of natural fractures as measured in core studies in the Weyburn and Midale fields reported in this chapter, Figure 7-17. The directions from breakouts measured in the Midale Field, anaelastic strain recovery tests, and the directions from natural fracture sets coincide. Breakouts that show a small azimuth angle are from poor quality measurements. The azimuth of the maximum horizontal stress is around 40-50°, whereas the minimum horizontal stress has an azimuth of 130-140°.

The vertical in-situ stress was obtained from density logs, with an average unit weight of 24 kPa/m. The magnitude of the horizontal stresses is difficult to establish because of the lack of direct measurements in the Weyburn Field. Measurements from Regina [220] and the Midale Field [219], both in southeastern Saskatchewan seem to indicate a minimum horizontal stress gradient of 18 kPa/m, where the lower values obtained from the Midale Field may be due to depletion of the reservoir (14 kPa/m). Measurements of Kindersley, southwest Saskatchewan, seem to show a slightly larger gradient, but they are fairly distant from the Weyburn Field. Currently, the only information available about the maximum horizontal stress is from the Regina area [220] about 100 km northwest of the Weyburn Field, but these measurements are right at the Precambrian basement of the basin and may not be representative of the maximum horizontal stress within the basin as there is a 90° re-orientation in the direction of stresses in the Precambrain basement [220]. Consequently, it becomes speculative to utilize these measurements for stress interpretations within the Weyburn Field. However, there is a corollary that the major principal stress will be in the NE/SW direction, as it is in the Western Canadian Sedimentary Basin. Therefore, the stress regime in the field is strike-slip, which leads to formation of faults such as the Souris River, which has not undergone any vertical displacement, as would be expected for this type of fault.

There was insufficient information available to evaluate the maximum in-situ stress, but clearly the stress regime is strike-slip and it was still necessary to bound the value of the maximum horizontal stress. Deep stress measurements carried out by Towned and Zoback [221] reveal that the average friction coefficient μ varies between 0.6 and 1.0 – which correpnds to friction angles of 30 to 45°-. Considering that the the Souris River fault that is present in the risk assement area seems to be in equilibrium, and assuming that the fault field friction coefficient is best reflected by a value of 0.6 with no cohesion it is possible to estimate σ_H. The state of stresses on a stike-slip regime is represented by [222]:

$$\frac{\sigma_1}{\sigma_3} = \frac{\sigma_H - P_P}{\sigma_h - P_P} \leq \left[\left(\mu^2 + 1\right)^{1/2} + \mu\right]^2$$

Solving for σ_H the equation above, a maximum stress gradient of 28 kPa/m would be expected. While this constitutes a gross estimate of σ_H other evidence exists to support that this value falls into the range of values expected in the Western Canadian Sedimentary Basin. Thus, Figure 7-18 summarizes the available data at the Western Canadian Sedimentary Basin for maximum horizontal stresses, and the average gradient is 25.6 kPa/m with a standard deviation of 3.4 kPa/m. Therefore a 28 kPa/m gradient is at the upper limit of the recorded maximum horizontal stress gradients. The use of the maximum gradient for the maximum horizontal stress is on the safe side, as the in-situ shear stress is the largest and shear failure is more likely to occur during both the history of the reservoir and the CO2 injection. Nonetheless a smaller horizontal stress gradient would be more likely because the Williston Basin is distant from the subduction zone that gave origin to the actual stress regime. Also while the maximum horizontal stress value is driven by this plate interaction, differential stresses decrease fairly as was shown by van der Pluijm et al. [210] in paleostress measurements recoded by twinned calcite in carbonate rocks.

7.3.3 Base Case Scenario and Alternative Scenarios

Thus far the geological, hydrogeological, geophysical, and geomechanical information at Weyburn, and especially with focus in Phase 1A, has been reviewed and analyzed. Following the performance assessment methodology discussed in Chapter 3, all this information has to translate into scenarios, a base case scenario or most likely model, and alternative scenarios. Table 7-6 presents the stress regime and mechanical properties use for the Base Case scenario, and the alternative scenarios to be analyzed. The Base Case is a geomechanical model in a strike-slip stress regime, with elastic properties named as 'soft' in

Table 7-4 and Table 7-5, where there are no faults. The rest of scenarios described in Table 7-6 address uncertainties with both in-situ stresses and mechanical properties because of the lack of information and/or reliable measurements for both aspects. None of the scenarios include a fault in Phase 1A as the extensive geological mapping combined with seismic measurements did not find any evidence of faulting in the reservoir area. Fractures were included in the manner of GSI values that affect the Hoek-Brown envelope, and the values estimated for the bounding seals were very conservative, so fracture densities were embedded in the properties for different scenarios. However, this does not mean that a scenario with a leaky caprock should not be considered for the flow simulation in the performance assessment of the whole system.

Table 7-6. Scenarios for geomechanical performance assessment

Scenario	σ_v kN/m	σ_H *kN/m*	σ_h *kN/m*	K_0	*Stress Regime*	*Elastic Properties*
Base Case SS-BC	24	28	18	0.93	Strike-slip	Soft
SS-BC-1	24	28	18	0.93	Strike-slip	Stiff
SS-BC-2	24	28	18	0.93	Strike-slip	Stiff in seals, soft in reservoir
Iso	24	24	24	1.00	Isotropic	Soft
RF-1	24	33	33	1.5	Compressional	Soft
RF-2	24	41	41	2.0	Compressional	Soft
NF-1	24	18	24	0.79	Extensional	Soft
NF-2	24	18	24	0.79	Extensional	Stiff
NF-3	24	18	24	0.79	Extensional	Stiff in seals, soft in reservoir

7.4 Summary

A MEM has been developed for Weyburn Phase 1A following the review and synthesis of all pertinent geological, hydrogeological, geophysical and geomechanical information. The issue of fractures in the caprock has been addressed, and it has been shown that the presence of fractures in the Midale Evaporite was minimal to absent before exploitation and production of the field began. All this information has been used to build a Base Case scenario and a set of Alternative scenarios to evaluate the geomechanical performance assessment of the caprock system for this CO_2-EOR storage project.

7.5 Figures

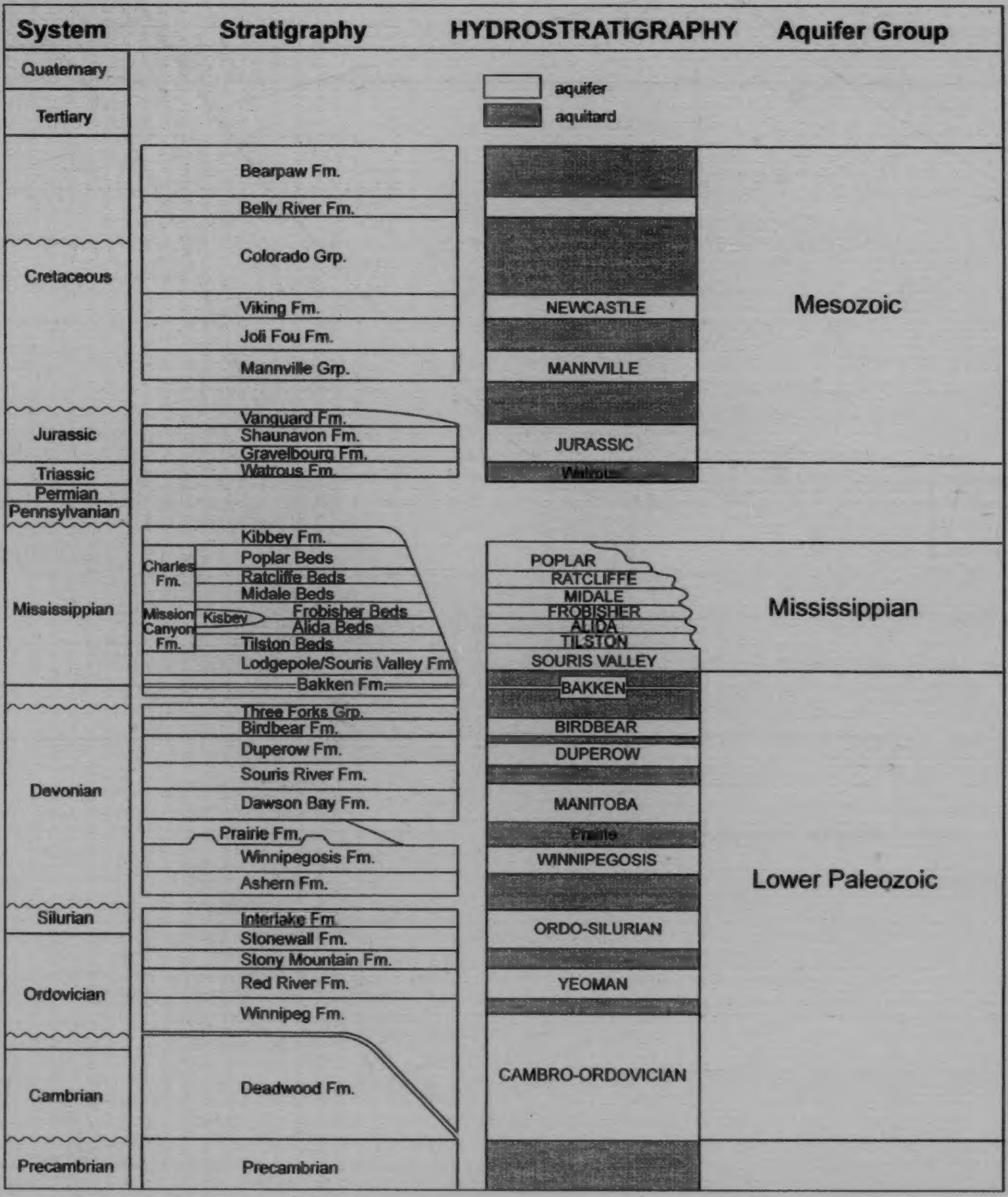
System
Stratigraphy
HYDROSTRATIGRAPHY
Aquifer Group
Quaternary
Tertiary
aquifer
aquitard
Cretaceous
Bearpaw Fm.
Belly River Fm.
Colorado Grp.
Viking Fm.
Joli Fou Fm.
Mannville Grp.
NEWCASTLE
MANNVILLE
Mesozoic
Jurassic
Vanguard Fm.
Shaunavon Fm.
Gravelbourg Fm.
JURASSIC
Triassic
Watrous Fm.
Watrous
Permian
Pennsylvanian
Mississippian
Kibbey Fm.
Charles Fm.
Poplar Beds
Ratcliffe Beds
Midale Beds
Mission Canyon Fm.
Kisbey
Frobisher Beds
Alida Beds
Tilston Beds
Lodgepole/Souris Valley Fm.
Bakken Fm.
POPLAR
RATCLIFFE
MIDALE
FROBISHER
ALIDA
TILSTON
SOURIS VALLEY
BAKKEN
Mississippian
Devonian
Three Forks Grp.
Birdbear Fm.
Duperow Fm.
Souris River Fm.
Dawson Bay Fm.
Prairie Fm.
Winnipegosis Fm.
Ashern Fm.
BIRDBEAR
DUPEROW
MANITOBA
Prairie
WINNIPEGOSIS
Lower Paleozoic
Silurian
Interlake Fm.
Stonewall Fm.
ORDO-SILURIAN
Ordovician
Stony Mountain Fm.
Red River Fm.
Winnipeg Fm.
YEOMAN
Cambrian
Deadwood Fm.
CAMBRO-ORDOVICIAN
Precambrian
Precambrian

Figure 7-1. Stratigraphic and hydrostratigraphic column at Weyburn, after Khan and Rostron [192]

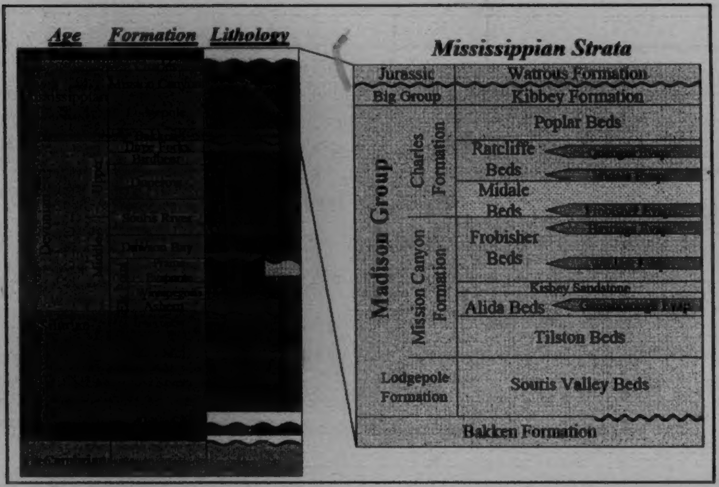
Age
Formation
Lithology
Mississippian Strata
Jurassic
Watrous Formation
Big Group
Kibbey Formation
Madison Group
Charles Formation
Poplar Beds
Ratcliffe Beds
Midale Beds
Mission Canyon Formation
Frobisher Beds
Kisbey Sandstone
Alida Beds
Tilston Beds
Lodgepole Formation
Souris Valley Beds
Bakken Formation

Figure 7-2. Detailed geology of the Madison Group at Weyburn, courtesy of EnCana

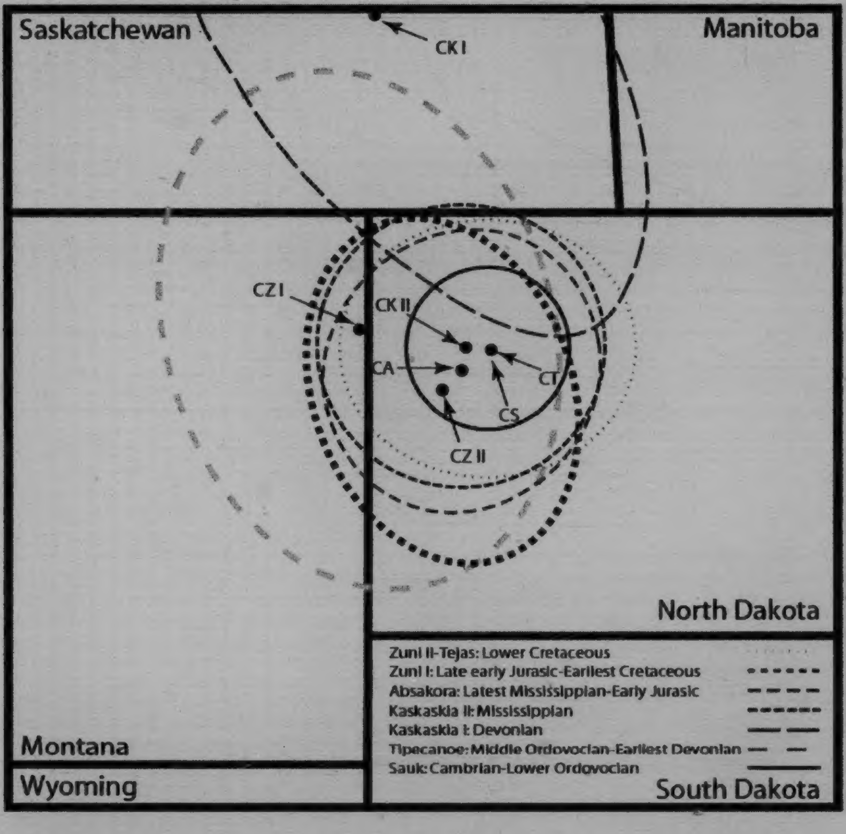
Saskatchewan
Manitoba
CK I
CZ I
CK II
CA
CT
CS
CZ II
North Dakota
Montana
Wyoming
South Dakota
Zuni II-Tejas: Lower Cretaceous
Zuni I: Late early Jurasic-Earliest Cretaceous
Absakora: Latest Mississippian-Early Jurasic
Kaskaskia II: Mississippian
Kaskaskia I: Devonian
Tipecanoe: Middle Ordovocian-Earliest Devonian
Sauk: Cambrian-Lower Ordovocian

Figure 7-3. Centres and inflection ellipses of the modeled sequences during the tectonostratigraphic evolution of the Williston Basin, modified after Redly [193]

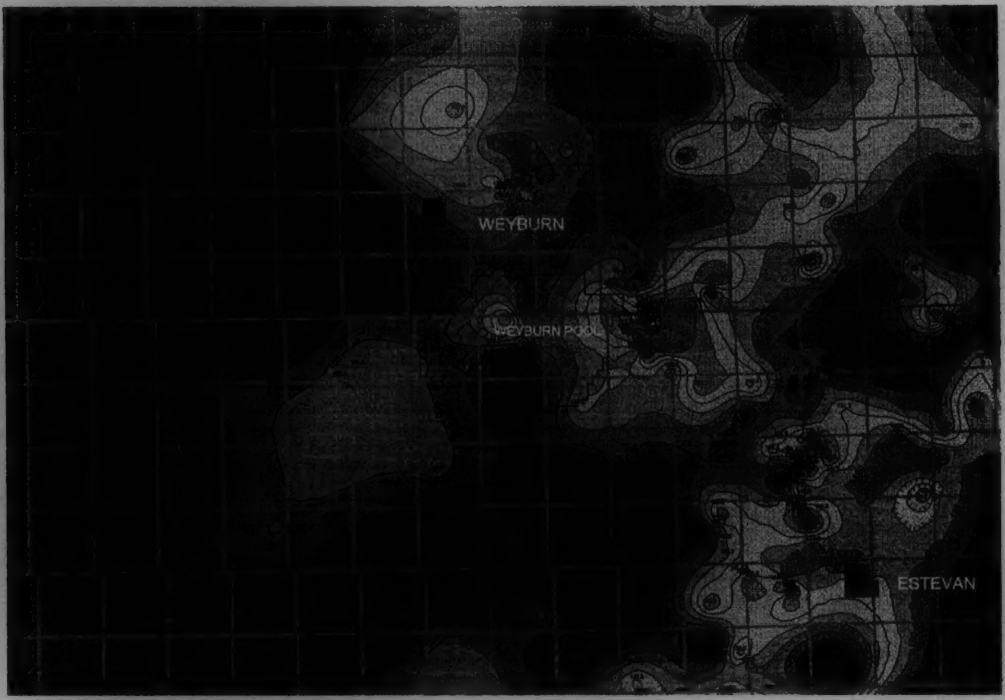
WEYBURN
WEYBURN POOL
ESTEVAN

Figure 7-4. Areas of massive salt dissolution around the risk assessment area at Weyburn, after Kreis et al. [223]

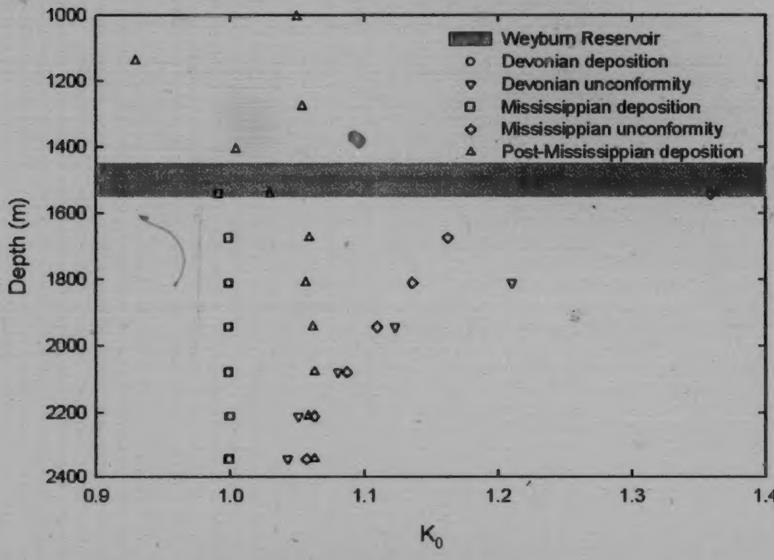

Figure 7-5. Influence of salt dissolution and erosive periods in the in-situ stresses at the Weyburn Field, Phase 1A

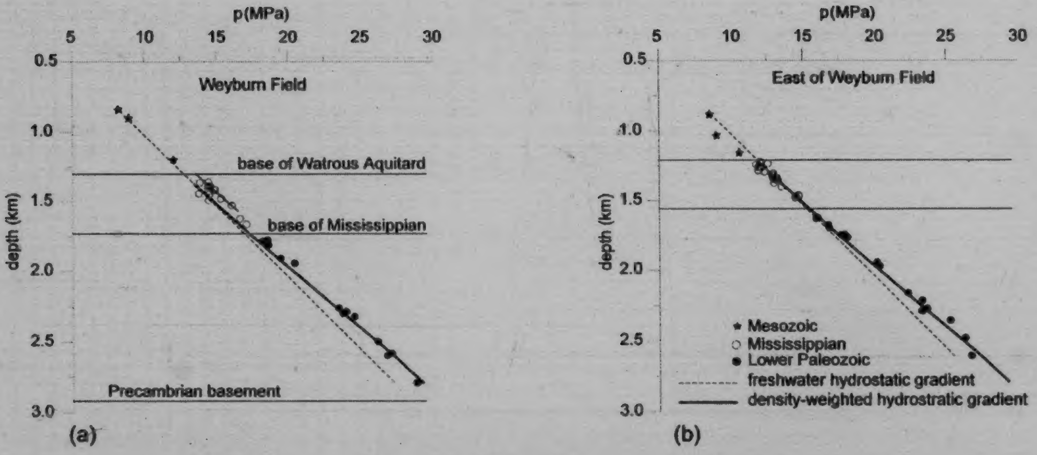

Figure 7-6. Pressure versus depth profile (a) in the Weyburn Fiel, and (b) east of the Weyburn Field, after Khan and Rostron [192]

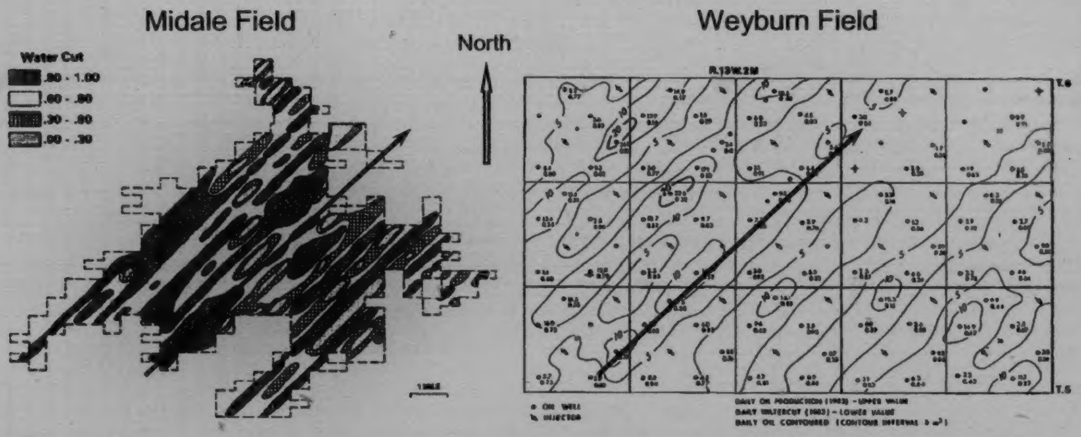
Midale Field
Water Cut
.80 - 1.00
.60 - .80
.30 - .60
.00 - .30
North
Weyburn Field

Figure 7-7. Water Cut profile at the Midale Field (Beliveau [201]) and water cut profile at the Weyburn Field (Ko et al. [205]). Notice how both fields follow a NE trend similar to the fractures in both fields

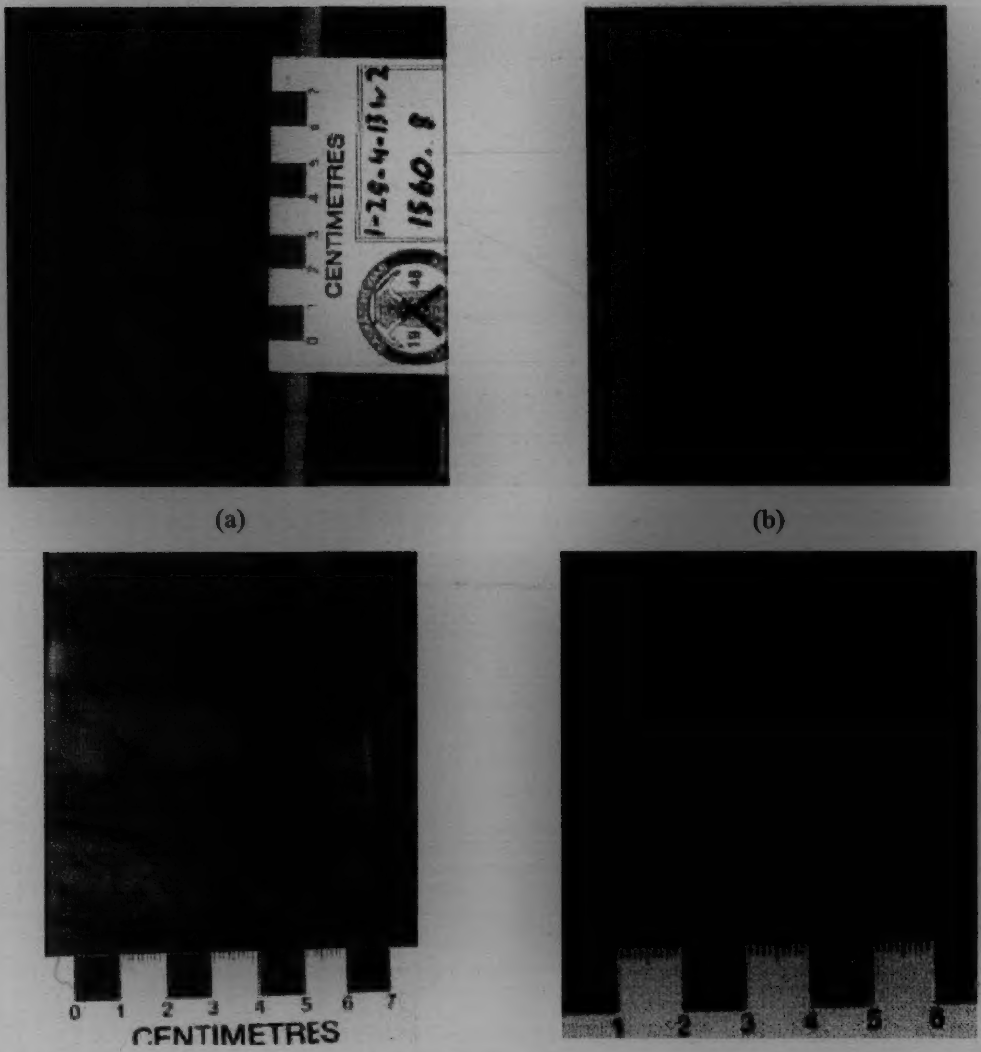
CENTIMETRES
1-29-4-13w2
1560.8
0 1 2 3 4 5 6 7
CENTIMETRES
1 2 3 4 5 6

(a)

(b)

(c)

(d)

Figure 7-8. Fractures in the Midale Evaporite: (a) synsedimentary cracks, (b) dewatering fractures, (c) fracturing, and (d) long-elongated fractures; after Nickel [197]

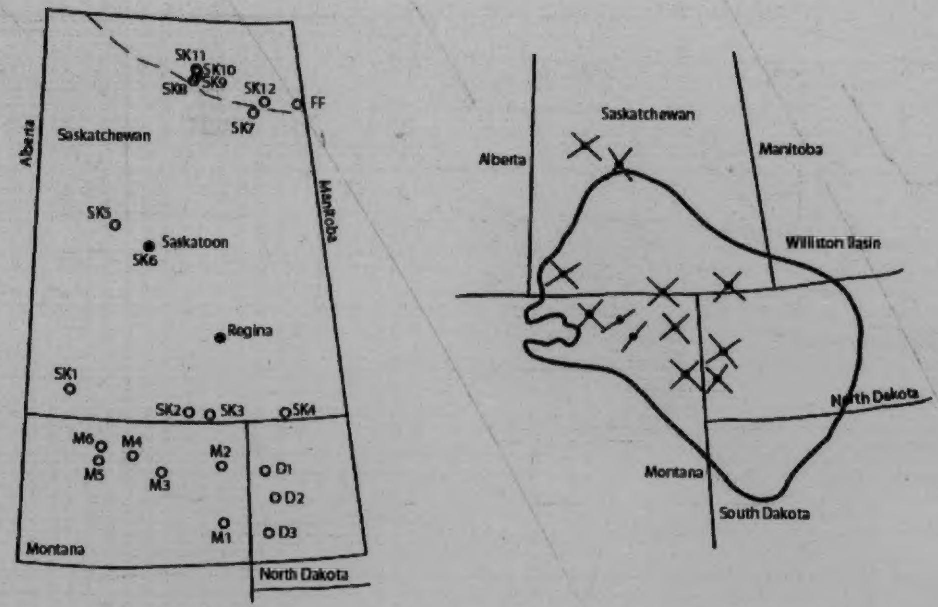

SK11
SK10
SK9
SK8
SK12
FF
SK7
Alberta
Saskatchewan
Manitoba
SK5
Saskatoon
SK6
Regina
SK1
SK2
SK3
SK4
M6
M4
M5
M3
M2
D1
D2
M1
D3
Montana
North Dakota
Saskatchewan
Alberta
Manitoba
Williston Basin
North Dakota
Montana
South Dakota

i. Fracture Studies

ii. Fractures in the Williston Basin

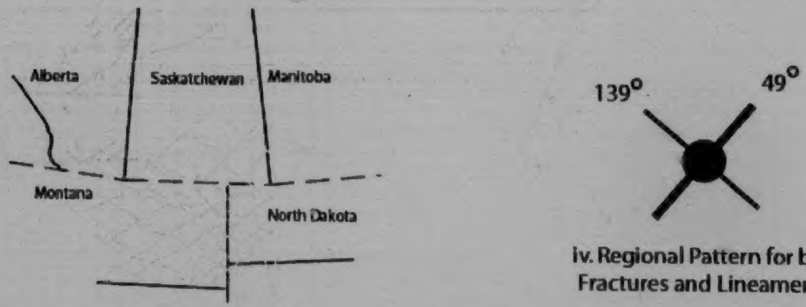

Alberta
Saskatchewan
Manitoba
Montana
North Dakota
139°
49°

iii. Modern Lineaments

iv. Regional Pattern for both Fractures and Lineaments

Figure 7-9. Fractures in Late Cretaceous to Late Pleistocene sediments in the Williston Basin, modified after Stauffer and Gendzwill [207]

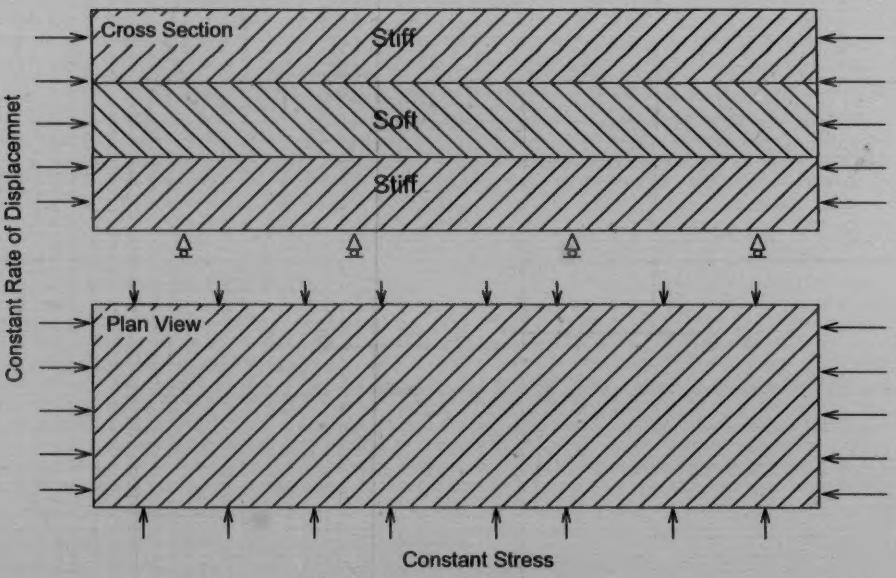
Cross Section
Stiff
Soft
Stiff
Plan View
Constant Rate of Displacemnet
Constant Stress

Figure 7-10. Model used to analyze the change in stresses in formations with different stiffnes due to shortening in one direction

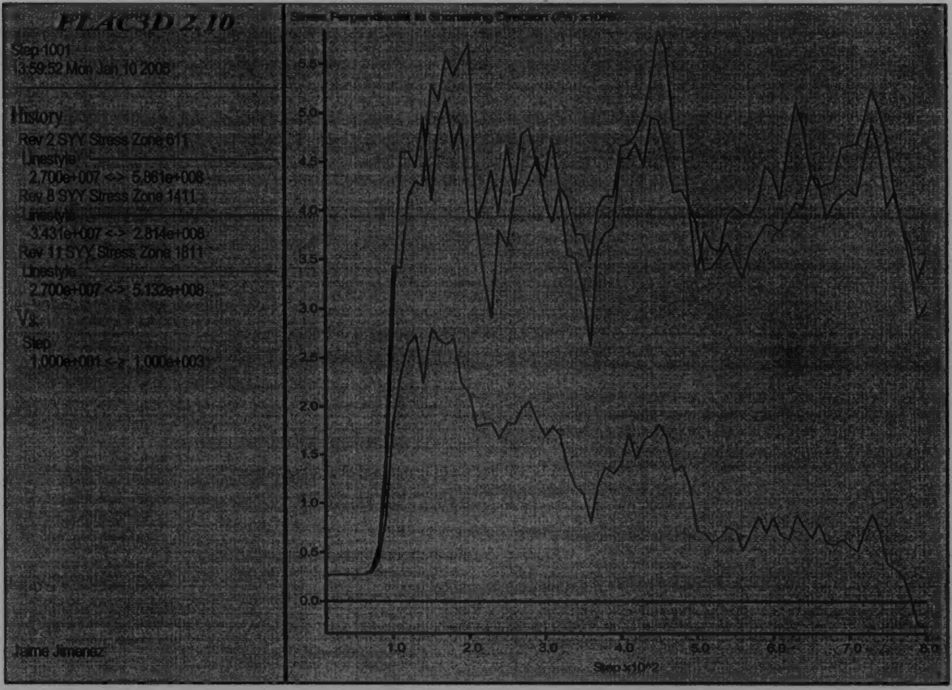

Figure 7-11. Change in stresses perpendicular to shortening direction. The two top lines are the stiff Midale and Frobisher Evaporite, and the lower line is the Midale Beds. Notice how the stresses in the softer bed tend towards tensional values

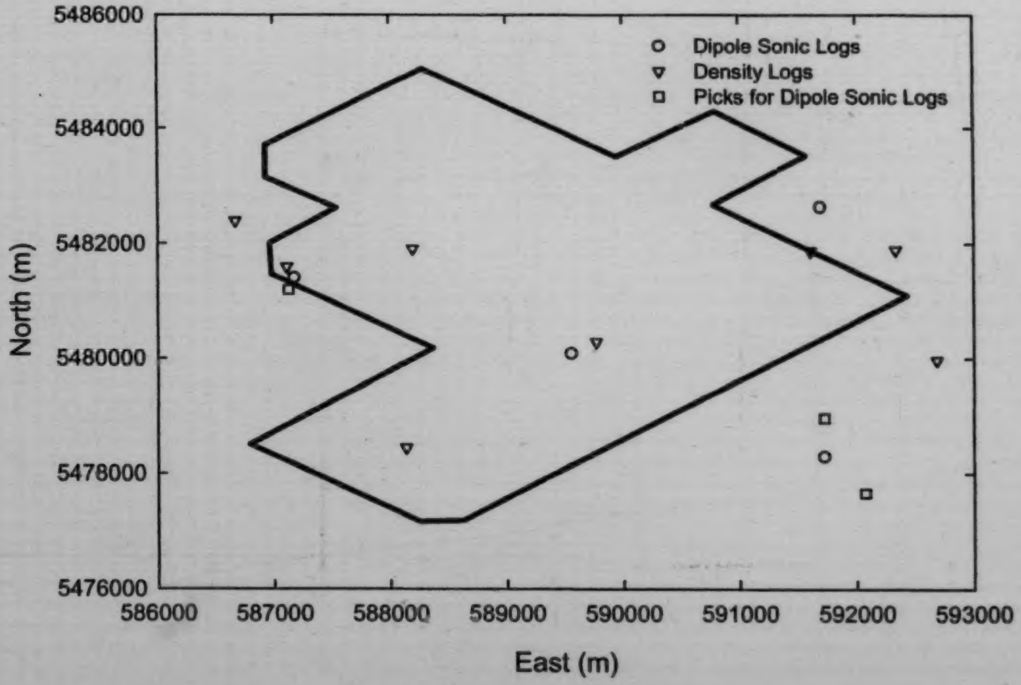

Figure 7-12. Location of dipole sonic logs, density logs, and geophysical picks used for geological information to correlate with dynamic elastic properties of the caprock system

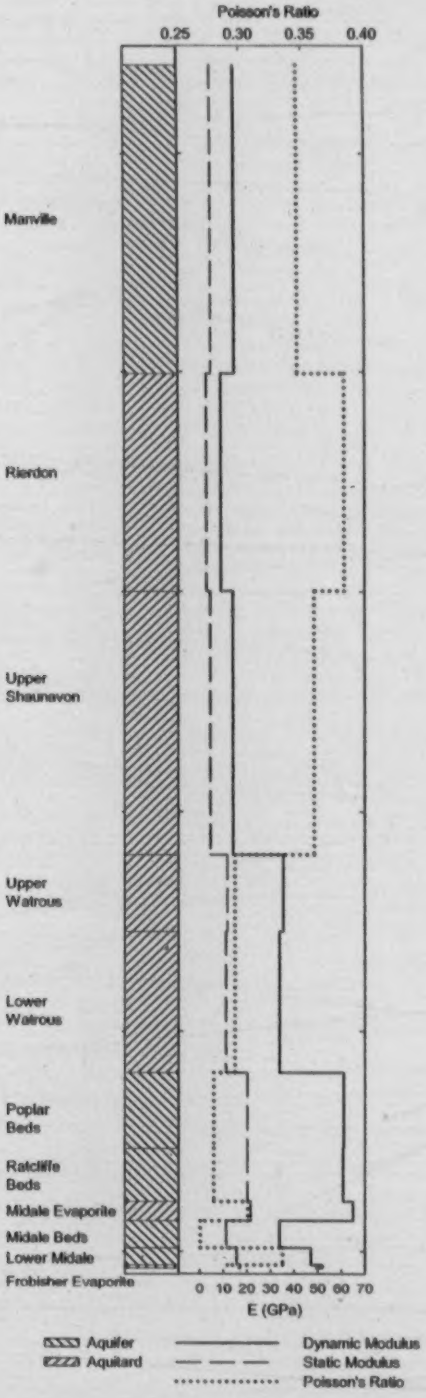

Figure 7-13. Elastic properties of the stratigraphic column at Weyburn

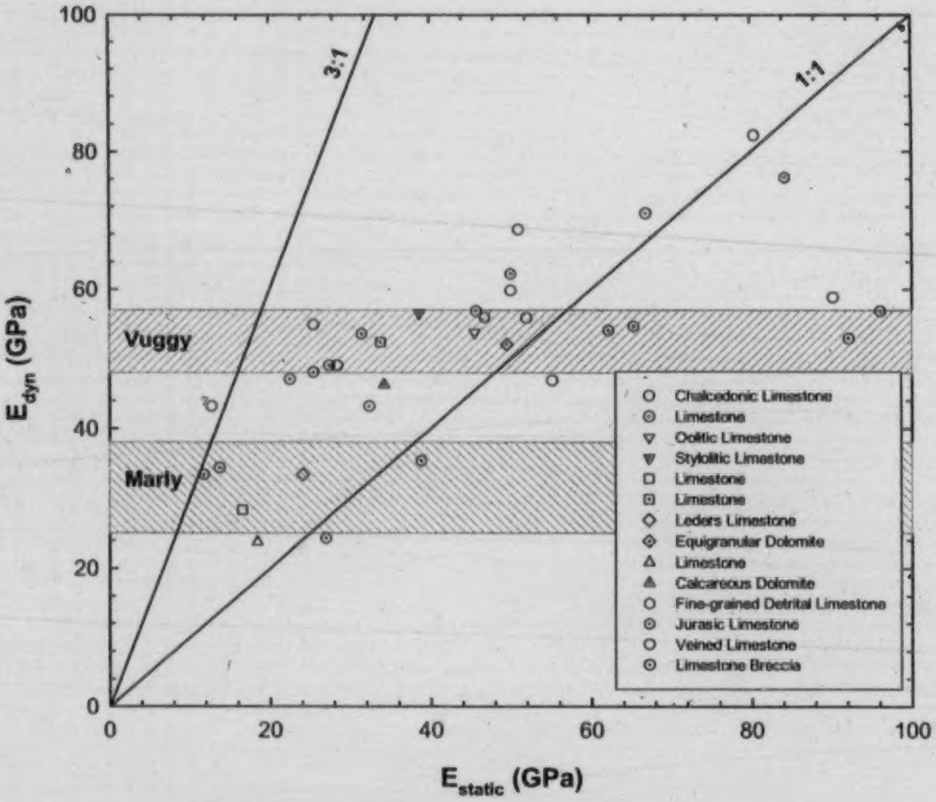

Figure 7-14. Relation between dynamic and static Young's modulus for various sedimentary rocks, data from different authors [224-226]

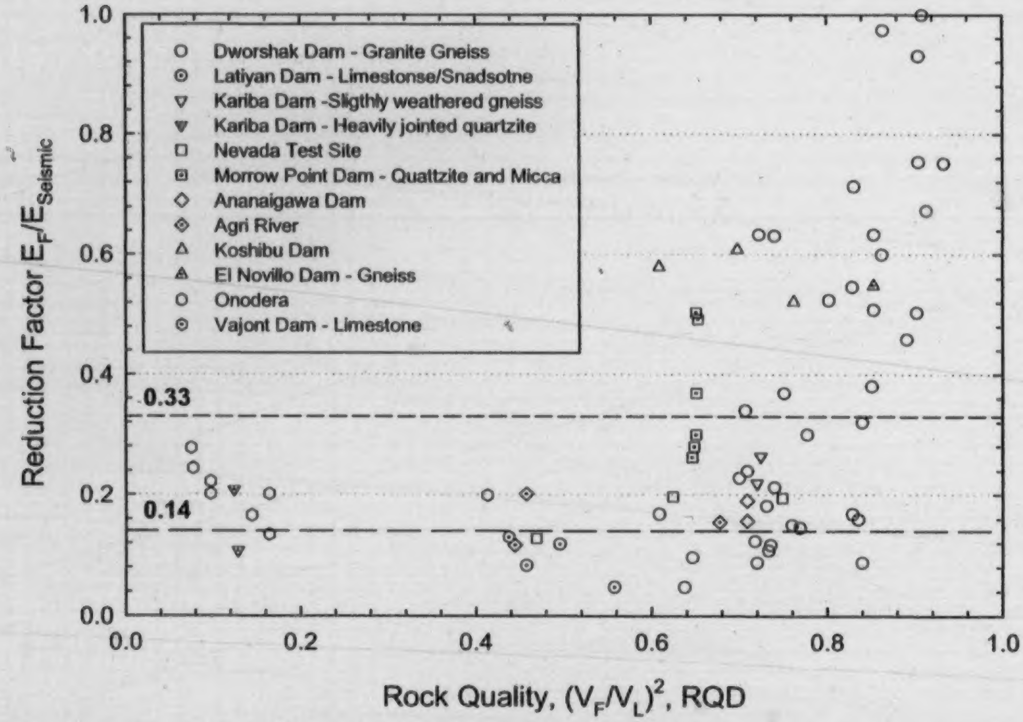

Figure 7-15. Variation of field over dynamic moduls against rock quality for dams built in different lithologies, modified after Deere [175]

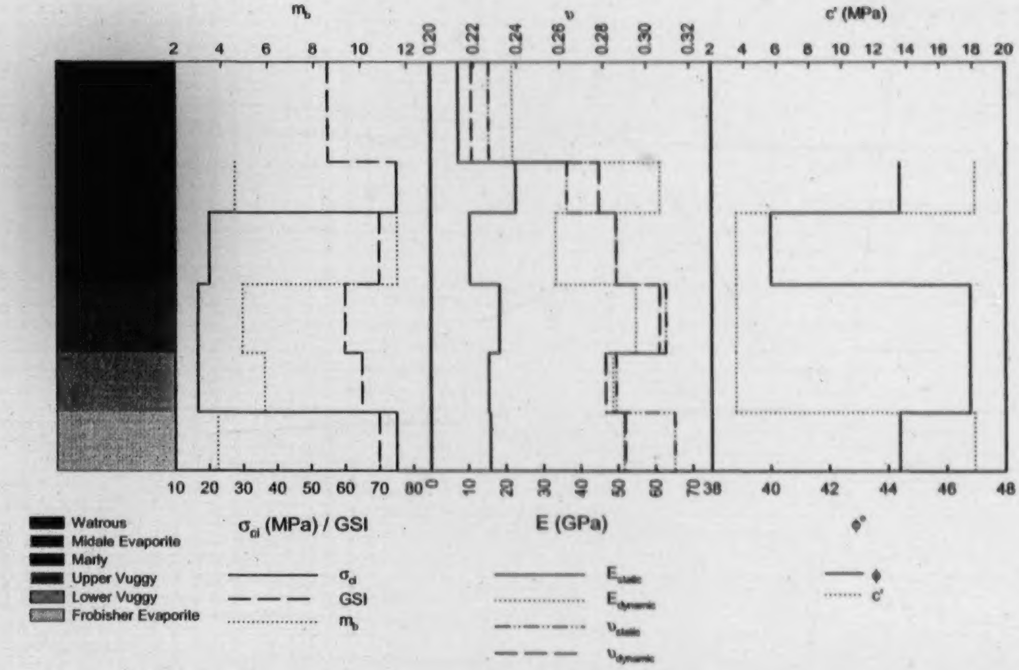

Figure 7-16. Elastic and mechanical properties of the caprock system at Weyburn, Phase 1A

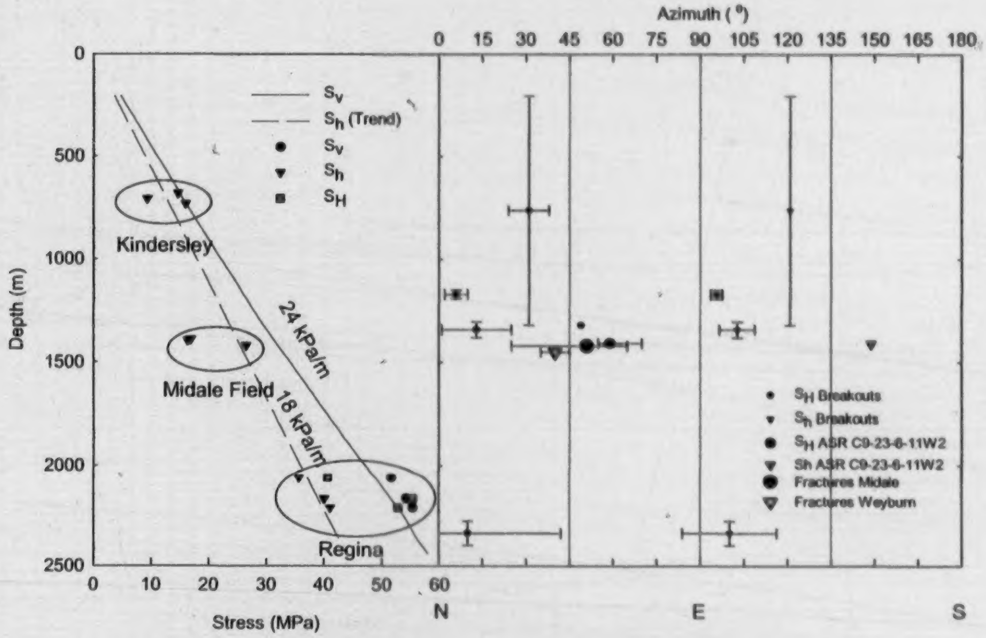

Figure 7-17. Estimated in-situ stress regime at Weyburn

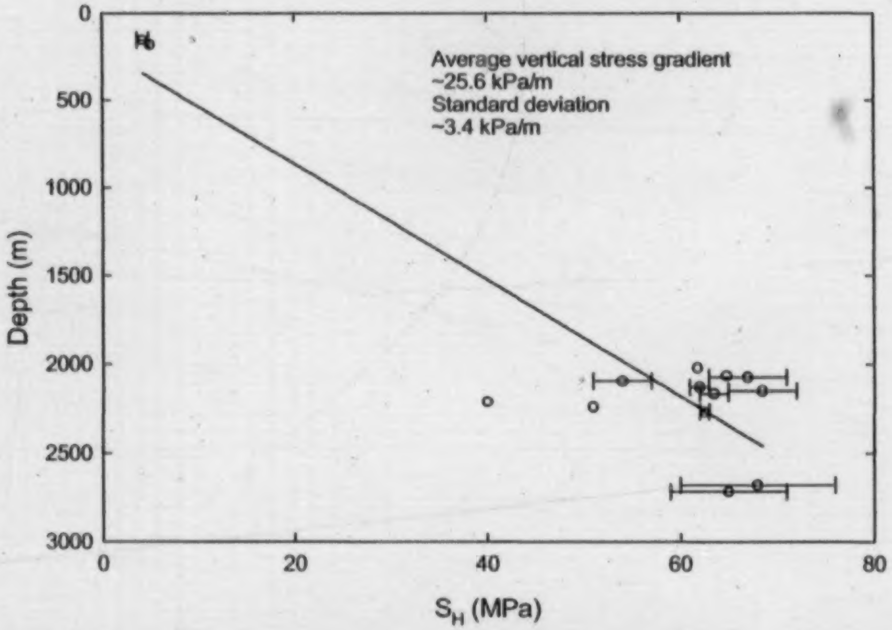

Figure 7-18. Maximum horizontal stress at the Western Canadian Sedimentary Basin. Data from Bell, Price and McLellan [194]

8 Geomechanical Performance of the Weyburn Field

8.1 Introduction

Chapter 4 reviewed the likely geomechanical processes that can affect the hydraulic integrity of a CO_2-EOR storage project from the moment the field produces oil up to the end of CO_2 injection. Chapter 7 developed a MEM of the Weyburn Field, and multiple scenarios that include the most relevant features of the system to consider during the geomechanical performance assessment. This chapter will carry out the geomechanical simulations based on the scenario analysis to track the performance of Weyburn's caprock system from the late 1950's until today, and then explore its performance when the focus of the project shifts towards CO_2 storage.

8.2 Geomechanical Model

8.2.1 Hydromechanical Coupling

The fundamentals of fluid flow and solid mechanics interaction are based on the concept of effective stress formulated by Terzaghi [113]. Based on this concept and Terzaghi's one-dimensional theory of consolidation, Biot [227] investigated the coupling between stress and pore pressure in a porous medium and developed a generalized three-dimensional theory of consolidation. This theory since then has been reformulated in more convenient ways, and with the development of computers its application has become common. Likewise, reservoir simulation is well-developed for a variety of problems, but the use of conventional reservoir simulators cannot explain some phenomena that occur during production such as subsidence, compaction, casing damage, wellbore stability among others [228]. Therefore, geomechanical effects have slowly been incorporated into reservoir simulation to address these issues, an area where substantial development has been achieved during the last 20 years.

A typical porous flow simulator expresses the pore volume V_P for a grid block as

$$V_p = V_p^0\left[1 + c_r(p - p_0)\right]$$

where V_p is the pore volume, p is the fluid pressure, c_r is the compressibility-like term which is an user defined variable, and the sub- or superscript *0* implies the earlier time step, [228]. For poroelastic calculations the pore volume for infinitesimal displacements may be expressed as

$$V_p = V_p^0\left[\phi_0 + \alpha\varepsilon_{kk} + \frac{1}{M}(p - p_0)\right]$$

where ϕ_0 is the initial porosity, ε_{kk} is the bulk strain, and α and $1/M$ are Biot's parameters. The fluid pressure enters the deformation calculations through the linear poroelastic constitutive equation

$$\sigma_{ij} = \sigma_{ij}^0 + \lambda \varepsilon_{kk} \delta_{ij} + 2G\varepsilon_{ij} - \alpha(p - p_0)\delta_{ij}$$

where σ_{ij} is the stress tensor, and λ and G are elastic constants.

Despite recent advances, the interaction between reservoir fluid flow and solid deformations still presents many challenges such as accuracy, convergence, and computing efficiency [228]. There are essentially four different methods for coupling fluid flow and solid deformation:

- Fully coupled approach where porous flow and displacements calculations are carried out together through a system of equations with pressure, temperature and displacements as unknowns [228, 229]. This approach is the most stable and reliable, but it is not an easy matter to couple a reservoir simulator and a geomechanical simulator. This usually requires code development and can be slower than any of the other approaches. It is sometimes called implicit coupling [228].

- Iterative coupled approach where the fluid flow equations and geomechanics deformations are solved separately and sequentially by a reservoir and a geomechanics simulator respectively, and the coupling terms are iterated on at each time step [228, 229]. It is an attractive option as it is very straightforward, but may require a larger number of iterations for difficult problems due to convergence issues [228].

- Explicitly coupled approach where a reservoir simulator solves the fluid flow equations for each time step, and geomechanical simulations are carried out during selected time steps. The frequency of geomechanical calculations is driven by the magnitude of pore volume changes during the time steps [228]. It is also called one way coupling as changes in the pore pressure field induce changes in stresses and strains, but changes in the stress and strain field do not affect pore pressures or pore volumes [229]. Its advantages are that it is very straightforward and less time consuming as the calculation of displacement takes most of the time in the previous approaches [228]. However, it cannot always capture the true physics of the problem in situations such as when either diferential deformations or fluid gradients are large, transport properties are very susceptible to stress changes, or there are faults or weak planes present.

- Pseudo coupling approach where a conventional reservoir simulator can compute some geomechanics response such as compaction and horizontal stress change through simple relations between porosity and vertical stress, and porosity and stress, respectively [229].

The geomechanical simulations for this work were explicitly coupled, where the history matching of the field was carried out in ECLIPSE [230] by EnCana, and its results at certain time steps were imported into FLAC 3D [231], a geomechanical simulator. This approach was chosen because of the geomechanical and geometric features of the Weyburn Field. Yale et al. [232] show that the effects of coupling are larger when the width/thickness relationship is in the order of 50 but for the Weyburn model the width/thickness ratio is around 150. Likewise, the effects of coupling are strongly dependant in the stiffness contrasts between overburden and the reservoir. Fully coupled approaches yield more accurate results when the overburden is significantly stiffer than the reservoir [228, 232], but at Weyburn the contrast is between 1.5 and 3.0 for the multiple scenarios so the explicit coupling is expected to yield accurate results suitable for performance assessment purposes.

Moreover an iterative approach would have required a new history match as the flow grid has aspects ratios in the order of 60:1, which are not acceptable in FLAC 3D (10:1 is the limit for accurate results) [231]. Also Weyburn is a mature, heavily exploited field but there is no evidence of subsidence/heave or movement in weak planes, and there are a large number of wells present and this translates into relatively small fluid pressure gradients. These aspects also suggest that the explicit approach will yield reliable results.

8.2.2 Boundary Conditions

Figure 8-1 shows a nine-pattern area from Phase 1A that was used for the simulations. This area is embedded in the middle of the Weyburn Field. To minimize the influence of the boundary conditions the model was extended in every direction around the area of interest and the material properties of each layer were applied to this 'buffer zone' around the field. A set of simulations with different size of buffer zones lead to a 6 km extension of the model in every direction to minimize the influence of the boundary conditions. Figure 8-2 shows displacements in the horizontal direction for different size of buffer zones and clearly the change between 3 and 6 km is small. Consequently it was decided that 6 km was an appropriate size for a 'buffer zone' around the simulated area.

Figure 8-3 explores the differences between a constant stress boundary and a fixed boundary. Clearly there is no significant difference in the results within the reservoir. Nonetheless, none of these boundary conditions reflects the reality of the field as it is very likely that the most appropiate boundary condition is a step-wise constant stress, where the horizontal stresses are changing as a function of the pore pressure change (see Section 8.4.2). Unfortunately, no information on pore pressures around the field, the lack of actual measurements of in-situ stresses and their variation during the history of the field does not permit the application of this type of boundary condition.

8.2.3 Grid and Pressures

Flow simulators work well with grid blocks with very large aspect ratios as in Weyburn where the aspect ratios were in the order of 60:1. However, geomechanical simulators are very limited in this aspect in order to permit reasonable solution for deformations. The limit for FLAC 3D is in the order of 10:1 [231]. Therefore, it was necessary to generate a new grid for FLAC 3D and map the pressures from the flow simulation grid into the FLAC 3D grid. Considering the diffusive character of pressure and the lack of flow barriers inside the reservoir, simple arithmetic averaging was used to calculate the pressures for the FLAC 3D grid. Figure 8-4 shows the grid used for the simulations, which respects the geological structure of the field.

8.3 Reservoir History

As mentioned in Chapter 2, the field has gone through a variety of exploitation and EOR techniques and this history of the reservoir is reflected in its pressure history. Figure 8-5 shows the pressure history of the field through maximum, minimum and average pressures in the area for modeling. The most relevant events in exploitation and stimulation are also shown. From 1957 to 1964 primary production which was pressure driven was favoured but a substantial decline in pressure in the field lead to a substantial decrease in production rates. Therefore, the field was waterflooded to both increase the pressure and sweep efficiency. A very significant pressure increase in a short period of time occurred throughout the field and average pressures have been above in-situ pressure since then. By 1986 and 1991 vertical and horizontal infilling were carried out respectively. This means that the density of vertical wellbores was increased and horizontal drilling was introduced to aim at areas with poor recovery such as the Marly. In the fall of 2000 CO_2 injection began as an EOR activity, where the goal was to inject CO_2 into the Marly. Water is intermittently injected as well as means of conformance control as the CO_2 tends to flow towards the Vuggy because of its larger permeability.

Clearly the reservoir has gone through significant pressure changes in its almost 50 years of production. However, Figure 8-5 must be interpreted carefully as maximum and minimum pressures are tied partially to wellhead measurements of injection and production pressures, and wellhead readings are not always representative of bottomhole pressures [233]. Moreover, it would seem that the pressure gradients in the field are large, but histogram plots of pressure at four different years indicate that most of the pressures are near the average value, Figure 8-6. This is likely due to the large density of wellbores and the large permeability in the direction of the natural fractures that do not permit the development of large gradients inside the field.

8.4 Geomechanical Modeling and Performance

As mentioned above, an explicitly coupled approach was employed to carry out geomechanical simulations. Simulations were carried out for both the history of the reservoir up to 2001 using the pressure data record and the CO_2 injection. To model the pressures post 2001 CO_2 injection, the final pressure distribution was "artificially" elevated to explore the integrity during high injection pressures and significant overpressuring of the reservoir. Thus, simulations were carried out for the following dates: January 1961, July 1964, July 1966, July 1968, January 1971, January 1976, January 1979, January 1983, July 1987, July 1993, January 2000, January 2001, and May 2001. The pressures then were increased by 16%, 32%, 48% and 64%, the latter being sufficient to induce hydraulic fracturing conditions. The following sections will address the geomechanical mechanisms that were identified in Chapter 4 as likely to cause loss of hydraulic integrity in the field based on the simulations for the multiple scenarios developed in Chapter 7.

8.4.1 Capillary Leakage

While the geomechanical simulations do not specifically address this point, the pressure history of the reservoir shows maximum pressures post-CO_2 injection 10 MPa above in-situ pressure. This pressure difference is similar to the breakthrough pressures for CO_2 that Dong et al. [70] measured for Weyburn's caprock, Figure 6-34b. Nonetheless, permeability is fairly low, so the rate of movement of CO_2 through the caprock is potentially very slow, and the volumes that could leak are very small. However, more fundamental research is needed in this area, but early evidence from experimental work indicates that for actual injection pressures in the field CO_2 would enter into the caprock, but migration would be very small due to the low permeability of the Midale Evaporite. This situation was not predicted initially as it is generally accepted that the capillary entry pressure of anhydrites is very large.

8.4.2 Hydraulic Fracturing

The geomechanical simulations lead to the conclusion that the reservoir will hydraulically fail once pressures reach the minimum horizontal stress, and shear failure will not occur. However, as was briefly mentioned in the boundary condition section, the minimum in-situ horizontal stress changes as pressure changes but these changes cannot be predicted precisely analytically, and it can only be determined by in-situ stress measurements. Therefore, the uncertainty as to the actual stress field in a CO_2-EOR storage project is increased by exploitation and production. Moreover, it has not yet been proven whether pressures return to original in-situ pressures and the horizontal stresses return to their original value. Actually, evidence exists that is not generally the case. However, this evidence comes from chalk reservoirs in the North Sea where waterflooding has been used to counteract massive subsidence unsuccessfully, but the material had already collapsed during depletion [81], and the waterflooding apparently induced very large thermal stresses [234].

Poroelastic theory predicts that for an isotropic, porous and elastic reservoir that is laterally extensive with respect to its thickness, the changes in stress with depletion can be predicted as:

$$\left(\frac{\Delta\sigma_h}{\Delta P_p}\right) = \alpha\frac{1-2\nu}{1-\nu} = A$$

$$\alpha = 1 - \frac{K_b}{K_g}$$

where α is Biot's parameter, υ is Poisson's ratio, K_b is the bulk modulus of the rock mass, and K_g is the bulk modulus of the mineral grains [235]. Assuming α as 1 and υ betweem 0.25 and 0.35 the relation between stress change and pore pressure change is between 0.46 and 0.67. However, in-situ stress measurements in a variety of fields has found this value between 0.47 and 0.87, Figure 8-7, and often in disagreement with elastic properties measured in cores [81, 236, 237]. Nonetheless this difference is strongly marked in chalk reservoirs, while in sandstone reservoirs the values of A fall into the range expected from elastic properties, considering that the truly elastic properties of the rock mass must be slightly different from the core values. Likewise, the rate of change between horizontal and vertical effective stress has a large variation range with values between 0.15 and 0.30 for chalk reservoirs, and 0.5 to 1.00 for sandstone reservoirs, Figure 8-8.

Figure 8-9 and Figure 8-10 show the change in horizontal stress with pore pressures at Weyburn, and the change in horizontal and vertical effective stress respectively as predicted by the geomechanical simulations. The value of A from the simulations is 0.53 for the Marly, 0.43 for the Upper Vuggy and 0.51 for the lower Vuggy, which for α of 1.0 leads to a Poisson's ratios of 0.32, 0.36 and 0.33 respectively. These values are slightly larger than the values used in the simulations, Table 7-5. The difference is expected as the reservoir response is a rock mass response, therefore the overlying and underlying formations where the pore pressures do not change influence the response of the rock mass. The change in vertical effective stress with respect to horizontal effective stress is 0.53, similar to the McAllen Ranch field. The response of the field is similar to the two sandstone reservoirs where in-situ stress measurements are available, and which did not present subsidence. Thus, clearly there is a contrast in the response among reservoirs where subsidence is meaningful and where it is not, as can be seen in Figure 8-11. This contrast in the response is important because deformations in the chalk reservoirs were plastic, while deformations in the sandstone reservoirs where subsidence was not observed must be elastic. If the deformations are elastic it would be expected that the change in horizontal stress with pressure is reversible, as it has been observed in overpressured basins where large overpressuring leads to large horizontal stresses, with an average value of A of 0.7 [238] (overpressuring is a slow process), or the Wilmington Field in California where maximum subsidence was in the order of 8.8 m and covered an area of 75 km^2, but after water injection there was a rebound of as much as 33 cm over a period of eight years and subsidence was limited to an area of 8 km^2 [239].

Therefore, from a performance assessment point of view the question is whether after depletion the change in horizontal stress is reversible, meaning the reservoir behaves elastically. Works by Martin [176], Diederichs [213], and Kaiser et al. [214] have addressed the issue of damage initiation in hard rocks, which follows this criterion:

$$\sigma_{1,Initiation} = A_D * UCS + B\sigma_3$$

where A_D is around 0.3 and B is 1.3-1.5 for granite, and 2 for sandstone [176, 213]. The elastic properties remain constant before damage initiation [213], therefore the response of the rock must be elastic if the stress path does not reach the damage threshold. If the response of a reservoir is elastic and subsidence has not been observed, it is fair to assume that the vertical and horizontal stresses are the principal stress. Figure 8-12 shows in Hoek-Brown space the principal stresses after depletion in the Rulinson Field, and before and after depletion in the McAllen Field. The elastic properties of both materials were reported by Lin [240] and Salz [241], and damage initiation lines for A_D of 0.3 and B of 1.5-2.0 were plotted. In both cases stresses after depletion are below the damage initiation threshold, so an elastic response is expected in these two fields as well as minimum amounts of subsidence. Similarly, at Weyburn the stresses before CO_2-injection did not induce damage in the Midale Beds, so an elastic response of the rock is expected and the change in the minimum horizontal stress must be reversible, Figure 8-13. Once EOR stops and CO_2 is injected the damage criteria may be crossed, which will lead to heave and a change in the elastic properties of the Midale Beds, but because the caprock is such a strong material, the concerns about damage in the caprock are minimum. Moreover, the mechanical properties used for the Midale Beds come from tests by McLellan [216], but the quality of the samples was doubtful (core plugs), underestimating the strength of these formations. Note that the damage threshold is also associated with change (increase) in permeability, as it has been observed in salt rock [78].

8.4.3 Shear Failure

Due to the coupling between fluid flow and deformations, the stress field will change during production in oil fields as the pressure changes in both the payzone and its overburden. These stress changes are a function of the pore pressures, the elastic properties of the system, and the original in-situ stresses. Figure 8-14 shows the results in terms of stress paths for the scenarios developed in Chapter 7. The left side has the results for the history of the reservoir, and the right side once pressure is increased artificially. The bottom figure in each column shows the pressure changes, and the hydraulic fracture thresholds for different minimum in-situ stress gradients. Appendix B has stress and pressure contours for the base case scenario.

From the left side of Figure 8-14 it is clear that the history of exploitation and production is predicted to not lead to shear failure of Weyburn's caprock or any of the formations of the caprock system. It is postulated that if the caprock were a shale it would be very likely that shear failure would have been induced as shales are substantially weaker than anhydrites. Once pressures are maximized, shear failure can occur in the Midale Beds for pressures that are 32% more than the actual pressures, but not failure in the Midale Evaporite would occur. However, at pressures around 32% of in-situ pressures the minimum in-situ stress would be overcome and hydraulic fracture would be the failure mechanism, and these hydrofractures would allow important volumes of leakage and a quick depressurization of the reservoir.

The stress path for the different scenarios is a function of the initial in-situ stresses, the change in pore pressures, and the value of *A*. In the isotropic case a change in slope can be seen as there is a shift in principal stresses from the in-situ pressure. When pressure is below the in-situ pressure, the vertical stress is the major principal stress, and when pressure is above original in-situ pressure, horizontal stress is the major principal stress. A similar phenomenon is observed for the normal faulting regime (NF). There is no shift in principal stress directions for the other scenarios, but this is specific to Weyburn, and not general to every CO_2 storage facility. Therefore, in case of shear failure the direction of the shear planes cannot be determined only by the original in-situ stresses, but it will be necessary to understand how the horizontal stresses evolve with pressure. Massive amounts of leakage require a fracture that crosses the caprock, and the acting stresses at failure can lead to vertical fractures (hydraulic fractures or strike-slip regime), steep dipping fractures (normal stresses), or gently dipping fractures (reverse stresses). The likelihood of massive leakage increases as a function of the acting stresses in the failure plane, the roughness and strength of the fracture walls, the amount of displacement, the presence of gouge and the fluid pressure [166, 242]. Therefore, the transport properties of induced fractures can change significantly from depletion to storage because the effective stresses increase during depletion and decrease during storage. Consequently fractures can develop during depletion but leakage will be minimum, but once storage increases the fluid pressures that fracture may become conductive. This is why it is so important to include the exploitation and production history of the reservoir into the geomechanical performance assessment.

Finally, the production and injection of fluids in the reservoir causes deformations in the caprock system. These deformations can lead to failure of wellbores, and the potential release of CO_2. At Weyburn deformations were uniform through the stratigraphic column as a consequence of the fairly uniform change in pore pressures of the system. Contours of displacements for the base case scenario are presented in Appendix B and a detailed analysis of deformation between formations for three wellbores is presented in Figure 8-15, Figure 8-16 and Figure 8-17. Clearly the deformations in the horizontal direction were practically identical for every formation, and vertical deformation is larger in the top formations and decreases gradually to the lower formations. The magnitude and direction of deformations is a function of the pore pressures and their location in the reservoir, so when pore pressures are above in-situ pressure the reservoir swells, the maximum swelling in the outer parts of the field, and vice versa for pressures below in-situ. The influence of location, Figure 8-1, is clear from the three wells in Figure 8-15, Figure 8-16 and Figure 8-17 because the reservoir act as a 'sponge', so the well in Figure 8-15 has mainly deformations in the West-east direction, the well in Figure 8-17 has mainly deformation in the North-South direction, and the well in Figure 8-16 has much smaller deformations, similar in both directions as it is close to the center of the field.

The stiffness of the system controls the amount of deformation, and the stiffness of the system is controlled by the stiffest formations. Figure 8-18 shows the deformations for the base case scenario in well 101-14-14-006-14W200 for different elastic properties. The displacements for the soft system are substantially larger than for the stiff system as the contrast between properties is about three. The differences between the stiff system and the system with stiff overlying and underlying formations and soft payzone is small. Clearly the elastic properties of the anhydrites (the stiffer rocks of the whole system) control the displacements. This is in contrast with shales where their stiffness can vary orders of magnitude, and the presence of weak planes can potentially control the deformations of the caprock system [243]. Initial in-situ stresses have little relevance in the displacements of the system as its behavior is elastic, Figure 8-19. Its influence would be more marked if shear failure were present. Figure 8-20 shows a summary of the displacements in all the boreholes monitored, Figure 8-1, at the Midale Evaporite level for the base case scenario. Clearly pressure and location control the displacements throughout the reservoir as mentioned previously.

8.4.4 Fault-Related Flow

Faults can act as either flow barriers or flow conducts depending on the acting in-situ stresses, the amount of displacement, the mineralogy of the fault gouge, and the presence of cements in the fault plane. Likewise, fault reactivation and the possibility of dilation can enhance the transport properties of faults, allowing significant amounts of fluid to flow. Therefore, it is necessary to evaluate the risk of fault reactivation during both depletion and CO_2 storage in a CO_2-EOR storage project.

The Mohr-Coulomb criterion represents very well the frictional strength of planar surfaces such as faults. The criteria can be expressed in terms of pressure to induce fault reactivation as:

$$\tau_f = c' + \tan\phi \cdot (\sigma_n - P_f)$$

$$P_f = \sigma_n - \frac{\tau_f - c'}{\tan\phi}$$

where ϕ is the friction angle of the fault, c its cohesion, τ_n and σ_n the shear and normal stress acting on the plane at failure respectively, and P_f the pressure at failure. Assuming that the plane of failure contains σ_2, the shear and normal stress can be written in terms of principal stress as:

$$\tau_f = \frac{\sigma_1 - \sigma_3}{2}\sin 2\theta$$
$$\sigma_n = \frac{\sigma_1 + \sigma_3}{2} - \frac{\sigma_1 - \sigma_3}{2}\cos 2\theta$$

where θ is the angle of the fault respect to the major principal stress. Thus in the case of a normal stress regime P_f can be written as:

$$P_f = \frac{\sigma_V + \sigma_h}{2} - \frac{\sigma_V - \sigma_h}{2}\cos 2\theta - \frac{\sigma_V - \sigma_h}{2\tan\phi}\sin 2\theta$$

where

$$\sigma_h = \sigma_{h0} + A\Delta P$$
$$\Delta P = P_f - P_0$$
$$2P_f = \sigma_V + \sigma_{h0} + A\Delta P - (\sigma_V - \sigma_{h0} - A\Delta P)\cos 2\theta - (\sigma_V - \sigma_{h0} - A\Delta P)\frac{\sin 2\theta}{\tan\phi}$$
$$2P_f = \sigma_V\chi + \sigma_{h0}\psi + A\Delta P\psi$$

where

$$\chi = 1 - \cos 2\theta - \frac{\sin 2\theta}{\tan\phi}$$
$$\psi = 1 + \cos 2\theta + \frac{\sin 2\theta}{\tan\phi}$$

and

$$P_f = \frac{\sigma_V \dfrac{\chi}{\psi} + \sigma_{h0} - AP_0}{\dfrac{2}{\psi} - A}$$

where P_0 is the original in-situ pressure. Proceding in a similar way equations for pressure to active the faults in reverse and strike-slip stress regimes can be obtained. Thus for a reverse stress regime:

$$P_f = \frac{\sigma_{H0}\chi + \sigma_V\psi - A\chi P_0}{2 - A\chi}$$

and for a strike-slip regime:

$$P_f = \frac{\sigma_{H0}\chi + \sigma_{h0}\psi - 2AP_0}{2 - 2A}$$

These equations are only valid if the change in pressure does not cause as stress rotation. Thus, it is possible that while a stress regime is strike-slip under in-situ conditions, it may become normal during depletion as the horizontal stresses decrease and the vertical stress remain constant. Similar methodologies to evaluate the fault stability have been developed by Streit and Hill [244, 245] and Hawkes et al. [246].

Figure 8-21 shows the pressures necessary to reactivate faults in a strike-slip regime at Weyburn (base case scenario) for different friction angles in the fault. Faults in strike-slip regimes can be activated only through pressure increase, and for a friction angle and a fault orientation of 30° the pressure would be in the order of 25 MPa, approximately the current injection pressure. Therefore, the potential to reactivate a strike-slip fault during CO_2 injection in a CO_2-EOR storage project is significant. However, as was mentioned in Chapter 7, there are no faults in the area of Phase 1A but there are faults in the risk assessment area[15].

In the case of a reverse stress regime (reverse fault scenario), faults can only be reactivated by increasing the pressure as well, but the pressures are slightly larger than the pressures in the strike-slip regime, Figure 8-22. Consequently, the potential to reactivate these faults during CO_2 injection is medium, emphasizing again the need of a good geological model, and the need to know the stress regime of a potential CO_2 storage reservoir.

Finally in the case of normal faulting (normal fault scenario), faults can be reactivated by depletion when pressure decreases, Figure 8-23. However, in the case of Weyburn if the stress regime were normal, the likelihood of reactivating a normal fault will be low as the friction angle of the fault would have to be less than 17.7°, Figure 8-24. However, in faults where large displacements have occurred, and shales are a significant part of the geology, friction angles can be very low depending on the amount and type of clay present in these faults. Normal fault reactivation is believed to have occurred in the Ekofisk field [236, 245]. The limit angle assuming poroelastic behavior can be evaluated as:

$$\sin\phi_m = \frac{\sigma_v - \sigma_h + AP_0}{\sigma_v + \sigma_h - AP_0}$$

---

[15] The risk assessment area is a geological model that extends 10 kM beyond the limits of the CO_2 injection area, which was used for the long-term simulations to quantify the volumes of CO_2 that were stored and that migrate out of the reservoir.

The methodology presented here can be misleading as faults can cause stress reorientations as shown by Martin and Chandler [247]. Therefore, techniques to evaluate fault stability that incorporate the three principal stresses such as the one developed by Pascal [248] are more realistic as long as there are reliable in-situ stress measurements.

8.4.5 Pre-Existing Fissures

The lack of pre-existing fissures in the caprock, and the fact that the damage threshold is not crossed due to the stress changes means that there won't be any leakage through fissures in the caprock. However, leakage in pre-existing fissures is enhanced by both shear stresses and high pore pressures, both existing at Weyburn. Consequently, in a typical CO_2-EOR storage project a fissured caprock may eventually leak at a significant rate, which will be a function of the fissure density, fluid pressure and in-situ stresses. Thus, numerical experiments have shown that the permeability of fractured rocks decreases with increase in stress magnitude when the stress ratio is not large enough to cause shear dilation of fractures, whereas permeability increases with increased stress when the stress ratios are large enough [249]. Therefore the state of stress, dilation and connectivity between fractures are the factors that will control the leakage in fissured caprocks.

8.5 Summary

The geomechanical modeling for the multiple scenarios developed for Weyburn was presented. The results clearly indicate that the reservoir and its caprock are a safe and sound sink for geological storage as long as pressures are kept below hydraulic fracturing pressure. The production from 1950 until now has likely not affected the hydraulic integrity of the caprock as the predicted stress changes remain below the established damage threshold. Also, an elastic response is expected for the same reason, which implies that horizontal stresses may recover once pressure was increased during the waterflood. However, this last postulate remains unproven due to a lack of in-situ stress measurements. In general, the knowledge and understanding available regarding stress evolution in oil reservoirs is poor. Therefore CO_2-EOR storage projects may require mandatory stress measurements before injection and close to the end of injection to validate the modeling results. A methodology to evaluate the potential of fault reactivation for any stress regime was developed, which can be used for screening of faults in potential storage reservoirs.

8.6 Figures

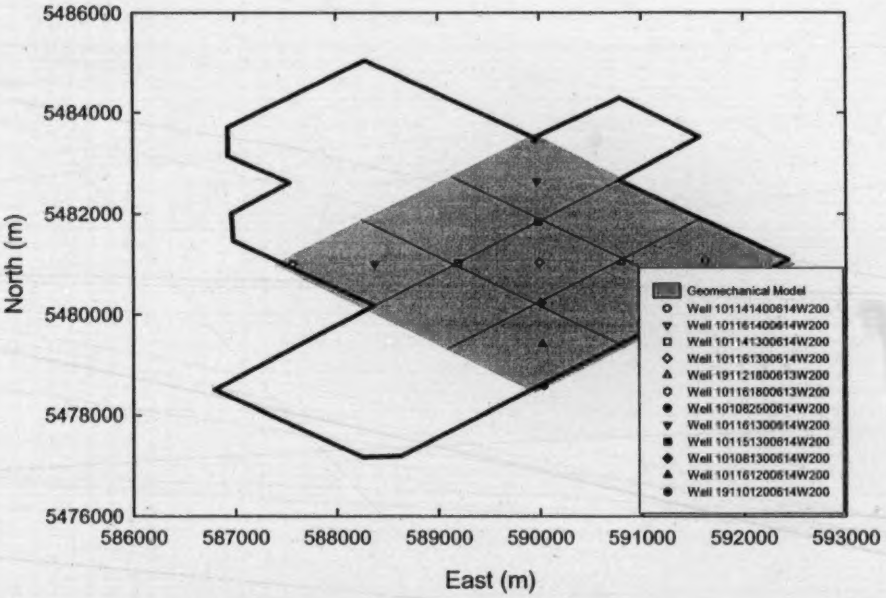
5486000
5484000
5482000
5480000
5478000
5476000
North (m)
586000
587000
588000
589000
590000
591000
592000
593000
East (m)
▨ Geomechanical Model
○ Well 101141400614W200
▼ Well 101161400614W200
□ Well 101141300614W200
◇ Well 101161300614W200
△ Well 191121800613W200
○ Well 101161800613W200
● Well 101082500614W200
▼ Well 101161300614W200
■ Well 101151300614W200
◆ Well 101081300614W200
▲ Well 101161200614W200
● Well 191101200614W200

Figure 8-1. Nine-pattern spot at Phase 1A used for geomechanical modeling with the location of the wells used to track displacements

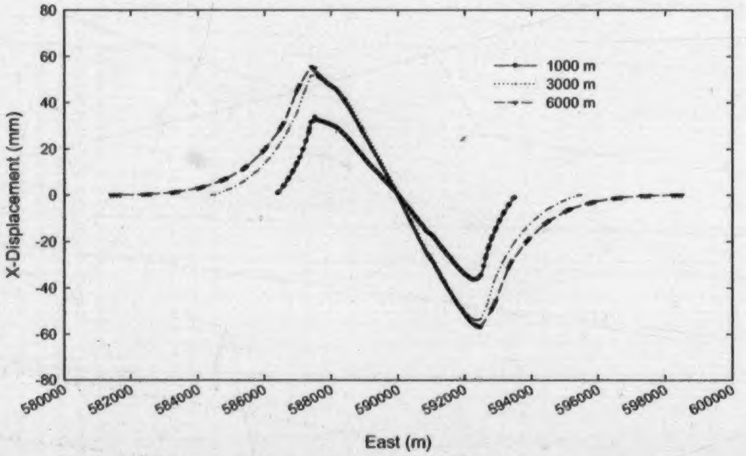

Figure 8-2. Displacements in the west-east direction for different "buffer zone" sizes. A buffer zone of 6 km was used for the geomechanical modeling as displacements were becoming insensitive to the size of the buffer

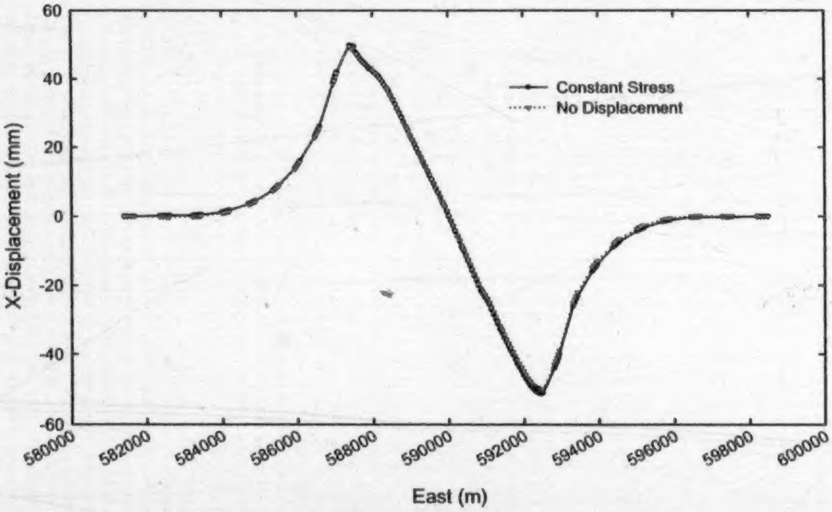

Figure 8-3. Displacements in the west-east direction for both constant stress and fixed boundary conditions

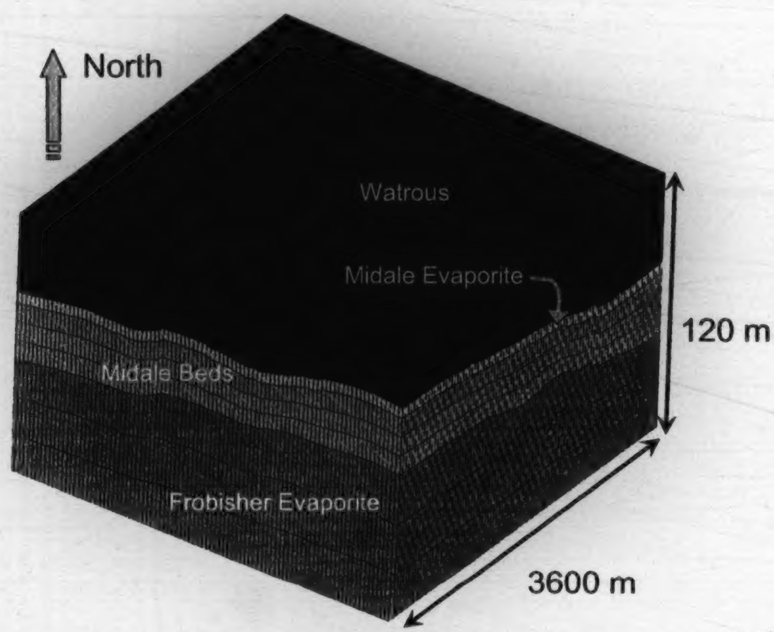
North
Watrous
Midale Evaporite
Midale Beds
Frobisher Evaporite
120 m
3600 m

Figure 8-4. FLAC 3D grid used for the geomechanical modeling. The grid honors the geological structure as much as possible

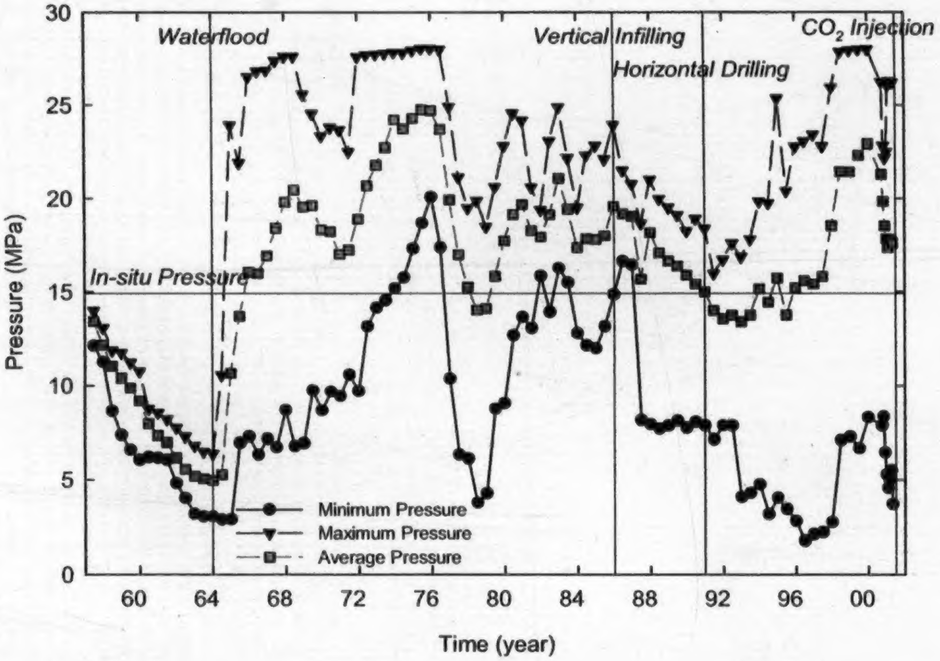

Figure 8-5. Reservoir pressure history at Phase 1A depicted through maximum, minimum and average pressure. Notice how the reservoir pressure has been maintained in average above the in-situ pressure since the waterflood

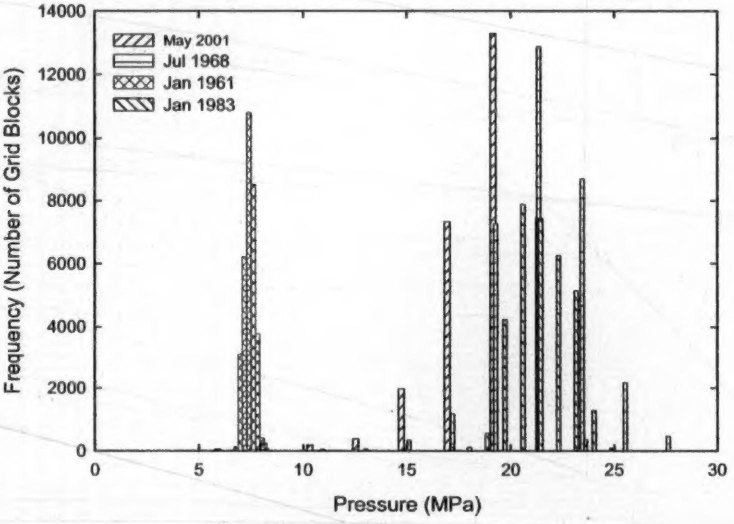

Figure 8-6. Histograms of pressure at four different points in the reservoir's history

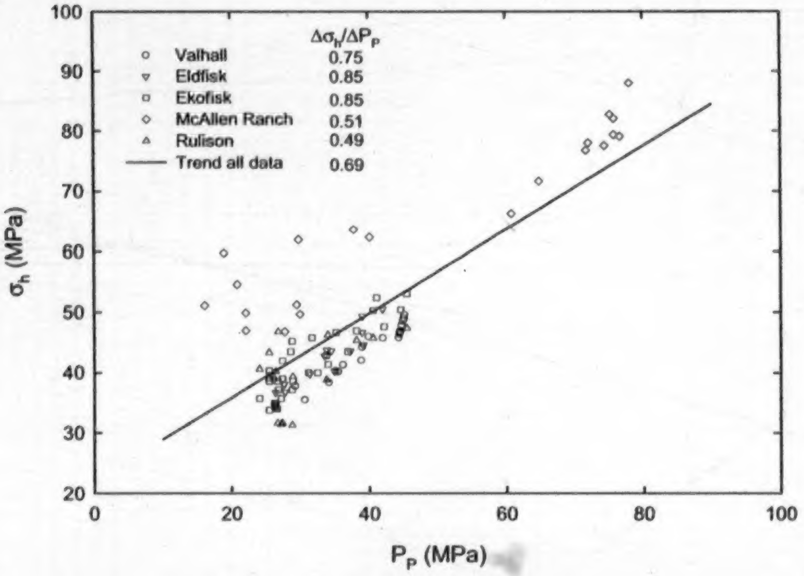

Figure 8-7. Change of horizontal stress with pressure during depletion for multiple oilfields worldwide, data from Teufel [237]

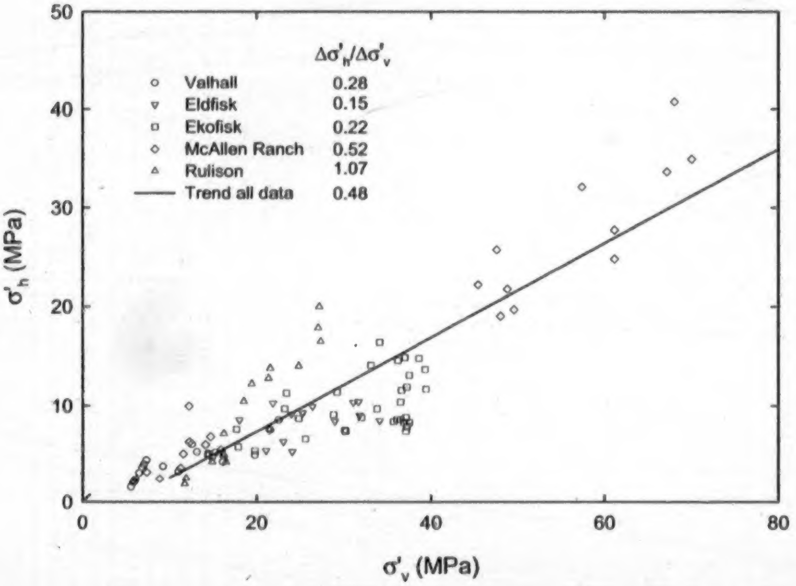

Figure 8-8. Change of both horizontal and vertical effective stress during depletion for multiple oilfields worldwide, data from Teufel [237]

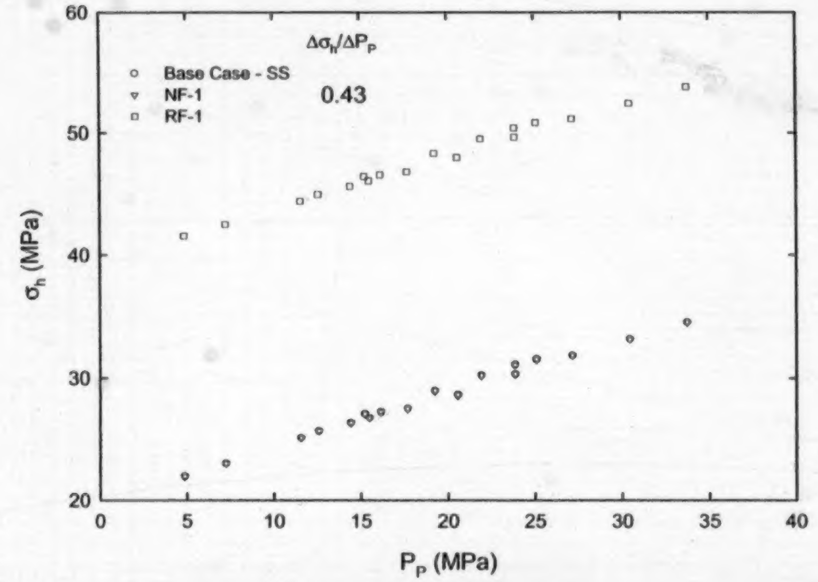

Figure 8-9. Change in horizontal stress due to depletion in the Upper Vuggy at Weyburn from the geomechanical simulations

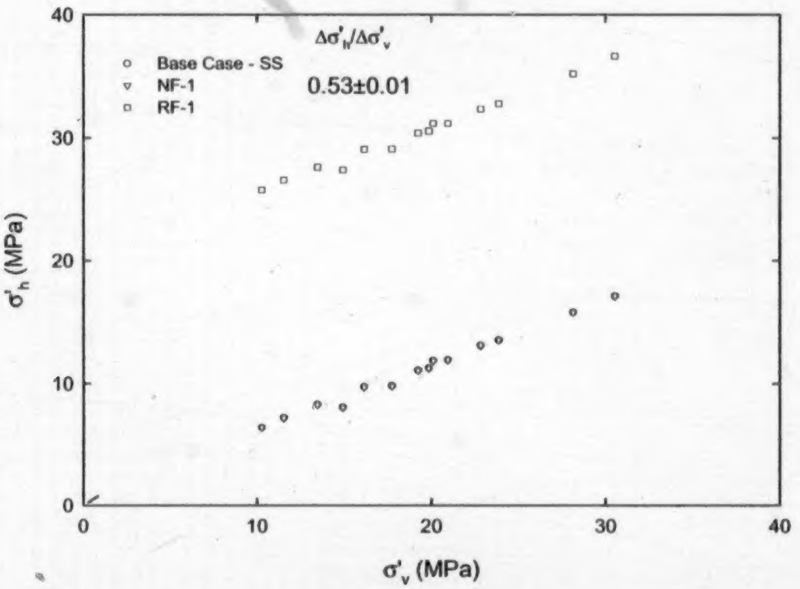

Figure 8-10. Change of horizontal and vertical effective stresses at Weyburn from the geomechanical simulations

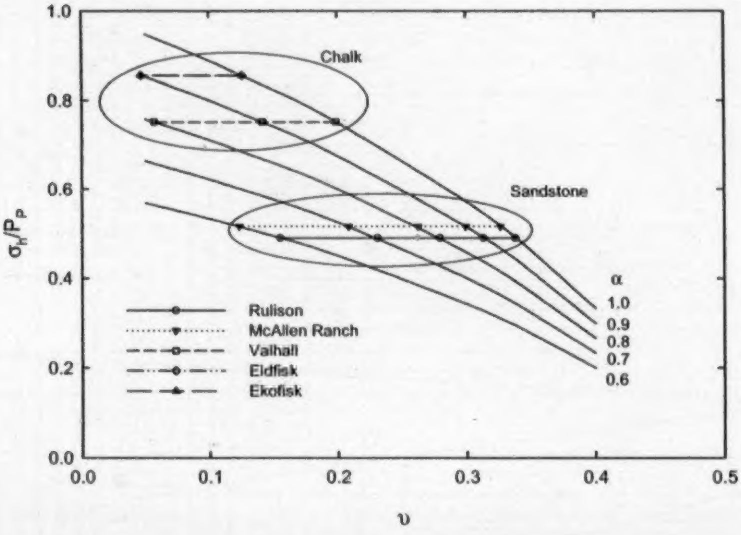

Figure 8-11. Theoretical relation between horizontal stress and pore pressure as a function of Poisson's ration and Biot's coefficient. Notice that the chalk reservoirs presented large subsidence while the sandstone reservoirs did not

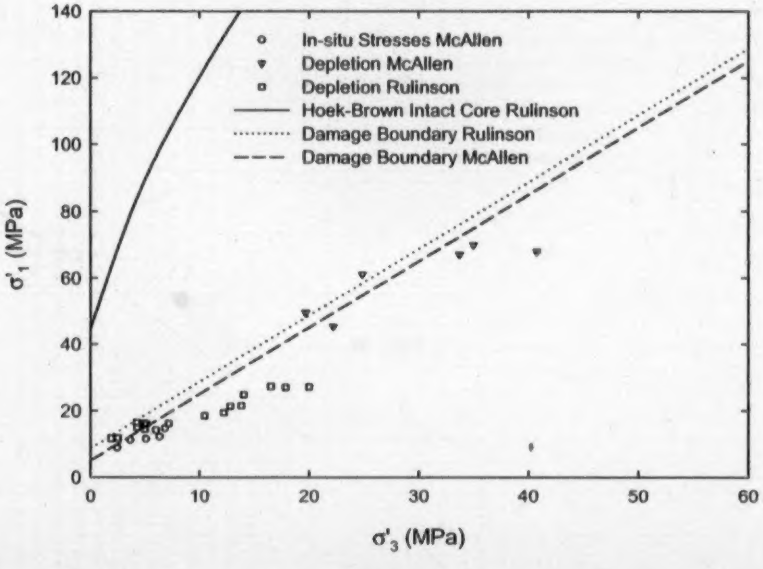

Figure 8-12. Principal stresses for the Rulison (before and after depletion), and the McAllen field (after depletion). Notice that in both cases the final state of stresses is below the damage line. Strength data from Lin [240] and Salz [241]

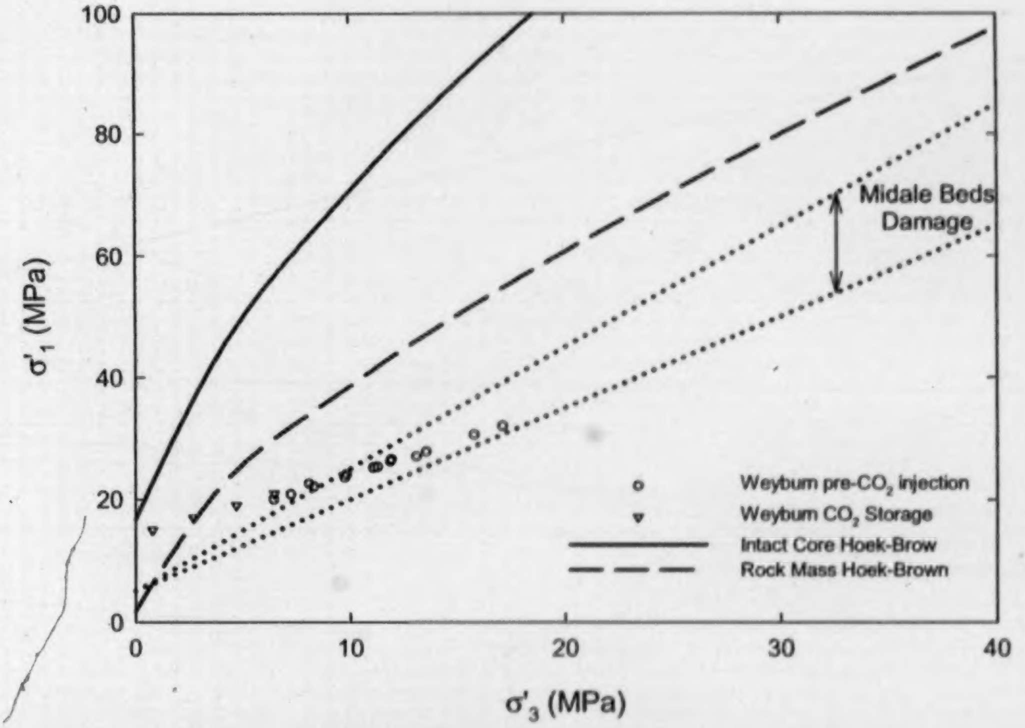

Figure 8-13. Principal stresses for the Weyburn field (before and after CO$_2$ injection) for the base case scenario. Notice that the final state of stresses is below the damage line during the history of the reservoir. However, once injection pressures are increased around 16% from actual pressures the boundary is crossed

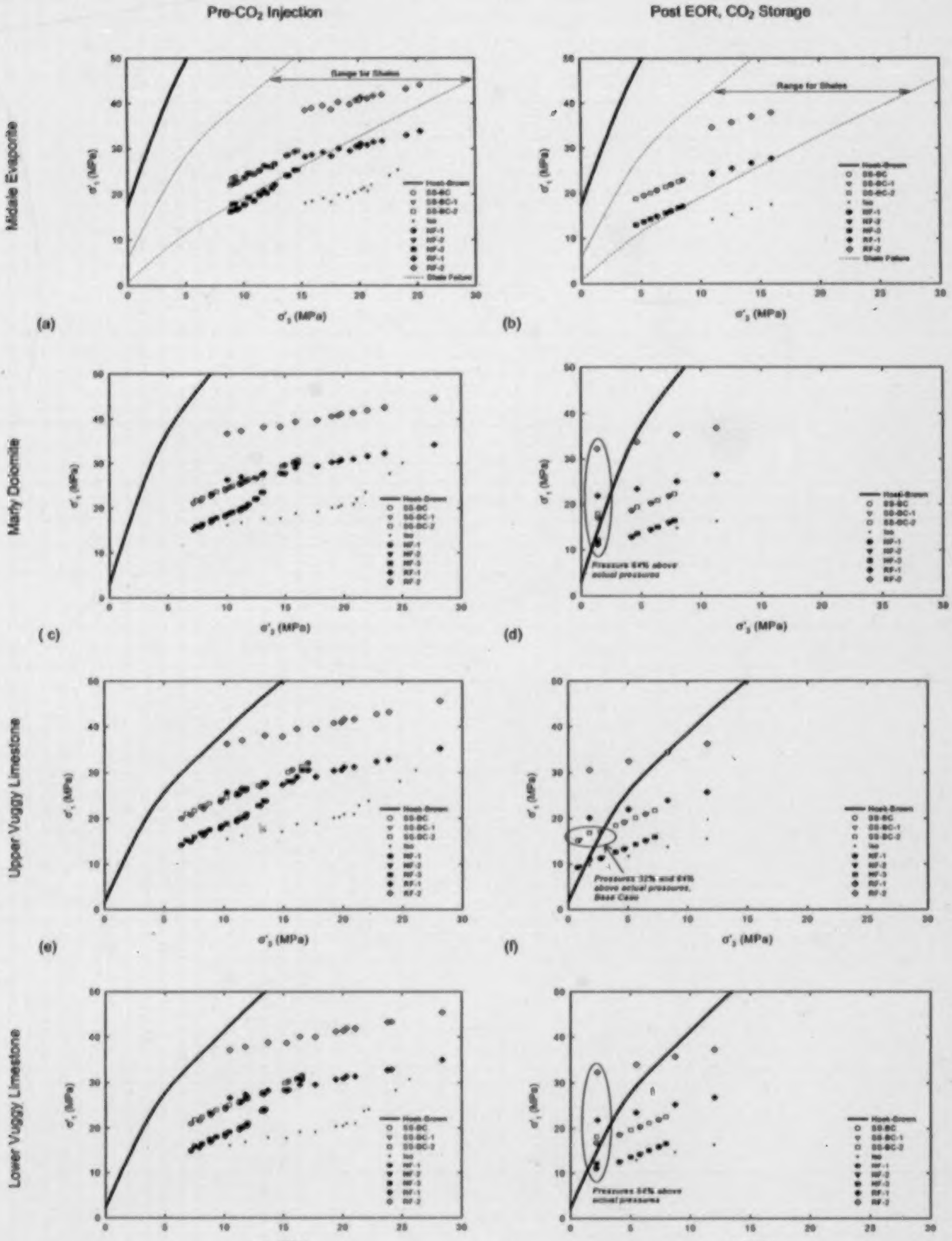

Pre-CO₂ Injection
Post EOR, CO₂ Storage
Midale Evaporite
Marly Dolomite
Upper Vuggy Limestone
Lower Vuggy Limestone
Range for Shales
σ'₁ (MPa)
σ'₃ (MPa)
Hoek-Brown
SS-BC
SS-BC-1
SS-BC-2
Iso
RF-1
RF-2
RF-3
RF-1
RF-2
Shale Failure
Pressures 64% above actual pressures
Pressures 32% and 64% above actual pressures, Base Case
Pressures 64% above actual pressures
(a)
(b)
(c)
(d)
(e)
(f)
(g)
(h)

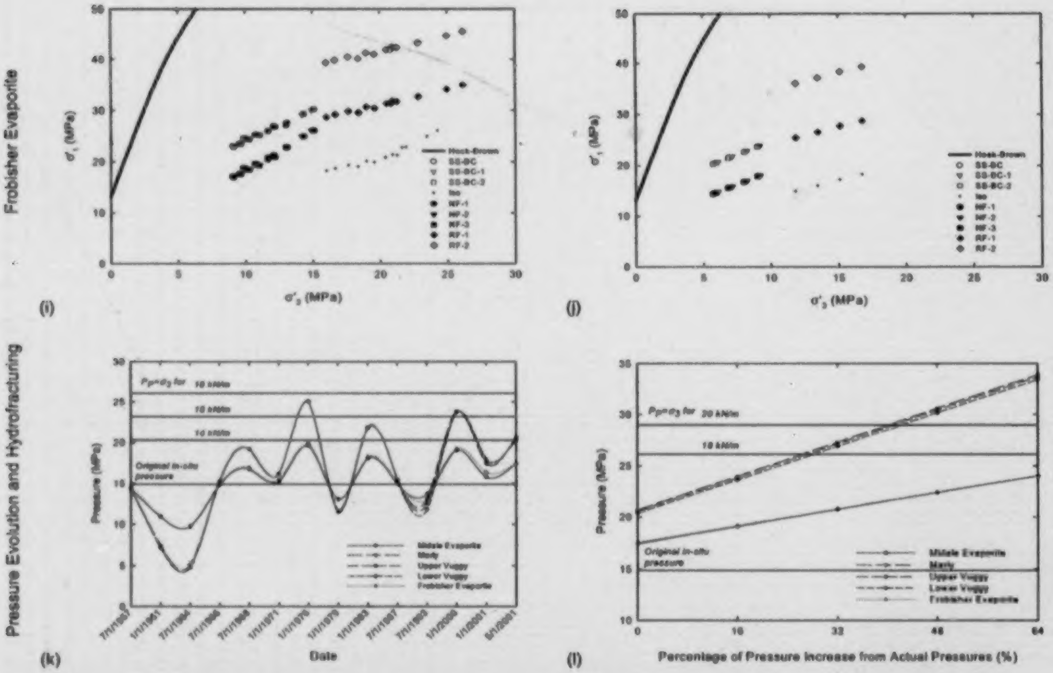

Figure 8-14. Stress results from the geomechanical models and pressure evolution. Plots (a), (c), (e), (g), (i), (k) illustrate pre-CO_2 injection results and plots (b), (d), (f), (h), (l) illustrate post-EOR CO_2 storage results where injection pressures have been elevated above operating pressures to test performance limits of caprock.

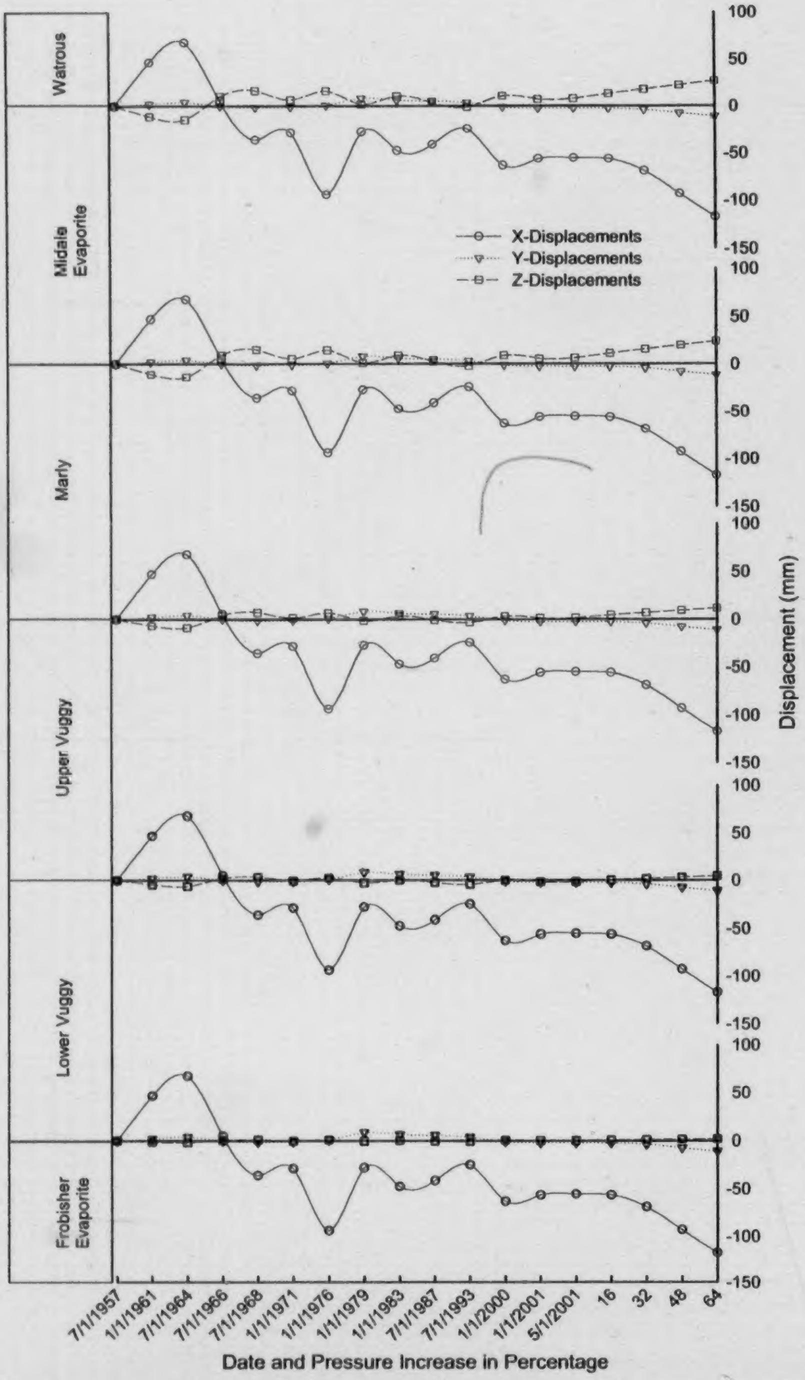

Figure 8-15. Displacements at every formation in the Well 101-14-14-006-14W200 (location shown in Figure 8-1) for the base case cenario.

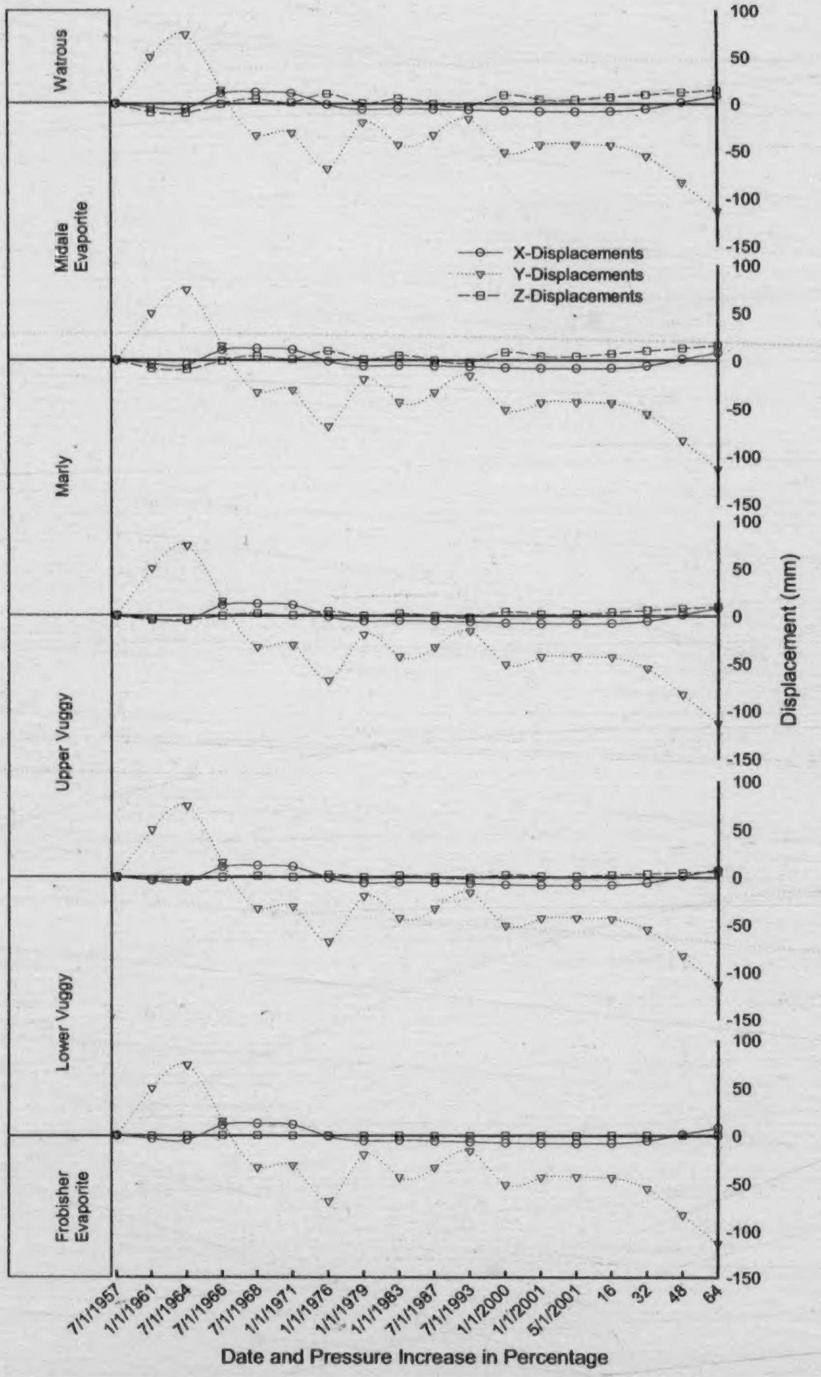

Figure 8-16. Displacements at every formation in the Well 191-10-12-006-14W200 (location shown in Figure 8-1) for the base case scenario

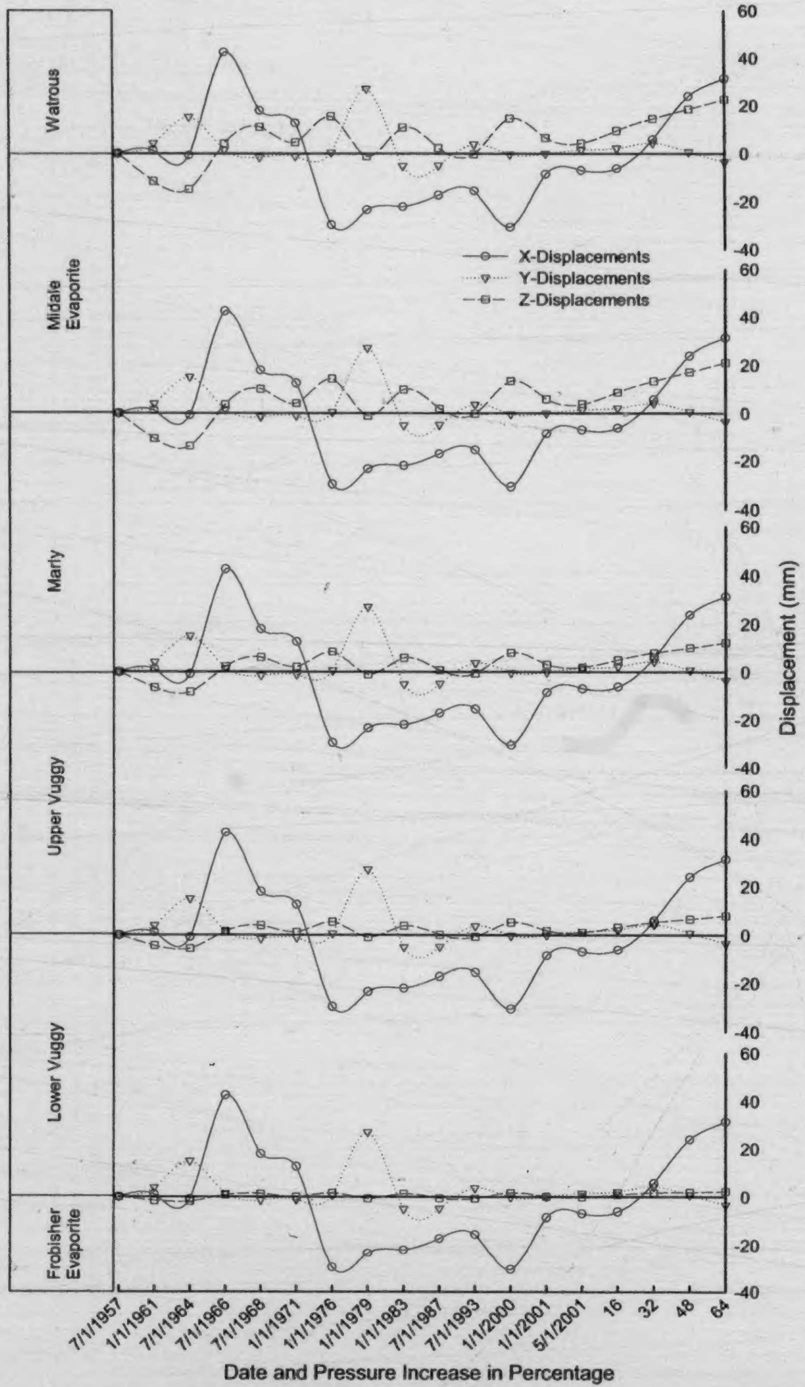

Figure 8-17. Displacements at every formation in the Well 101-16-13-006-14W200 (location shown in Figure 8-1) for the base case scenario

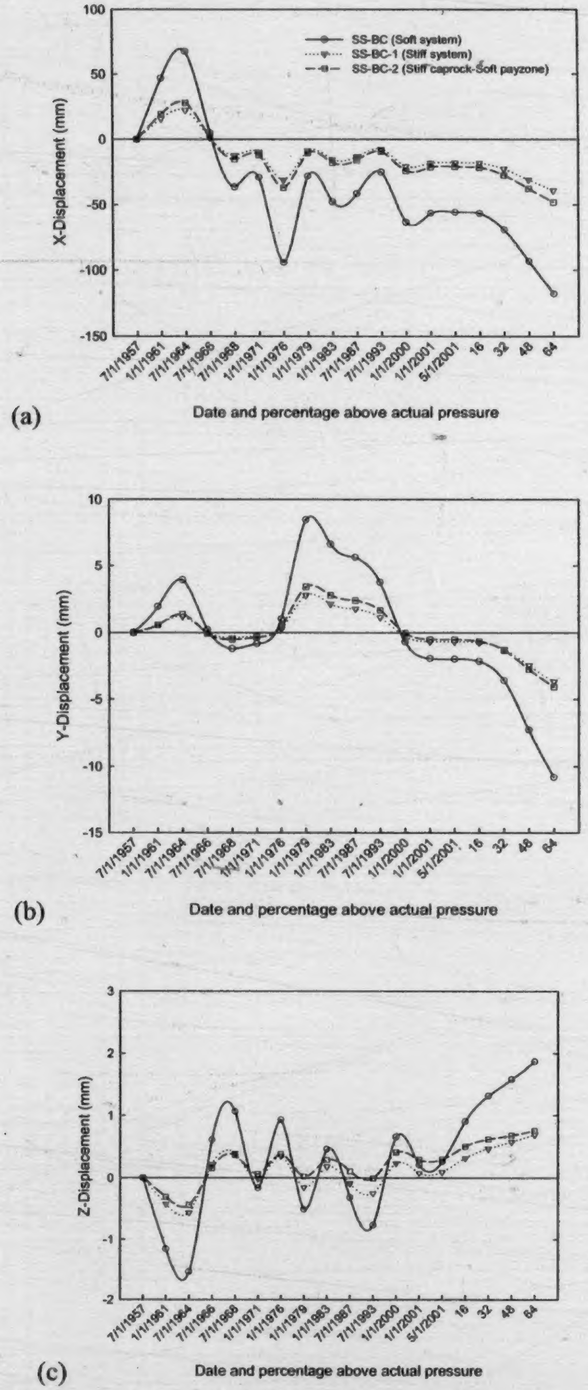

Figure 8-18. Influence of stiffness in deformations, Well 101-14-14-006-14W200 (location shown in Figure 8-1)

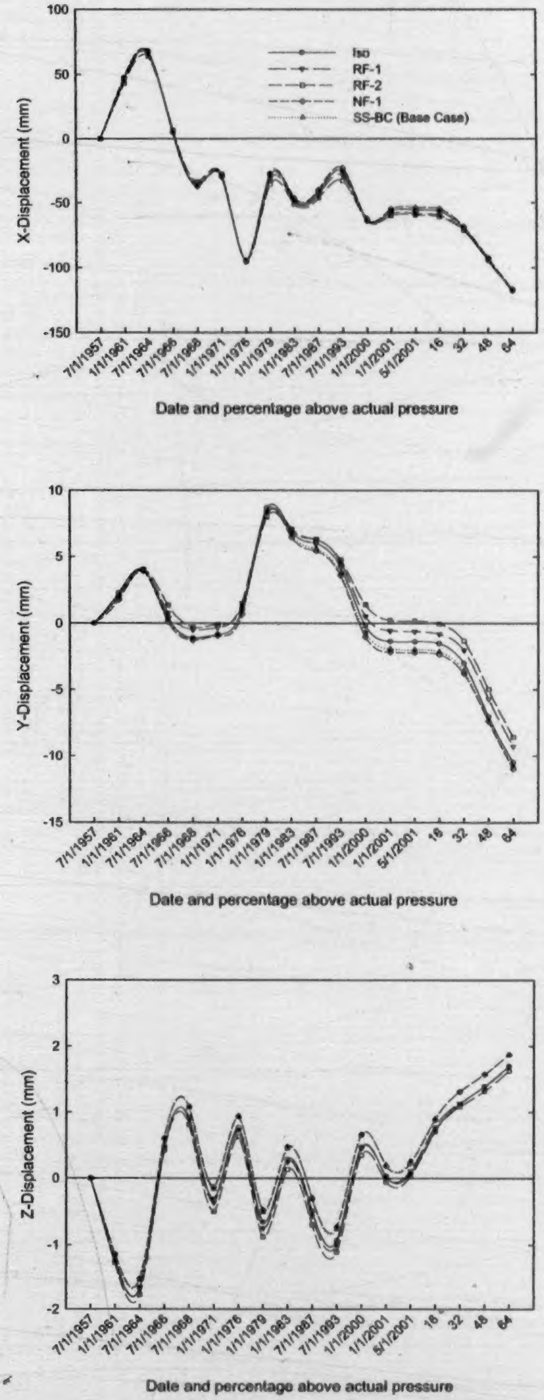

Figure 8-19. Influence of initial state of stress in deformations, Well 101-14-14-006-14W200 (location shown in Figure 8-1)

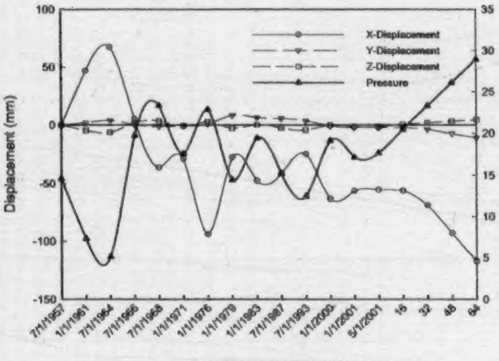

Well 101141400614W200

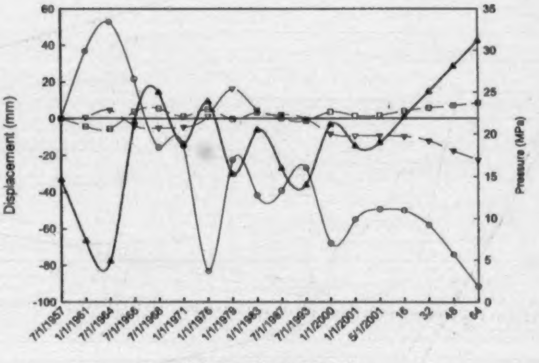

Well 101161400614W200

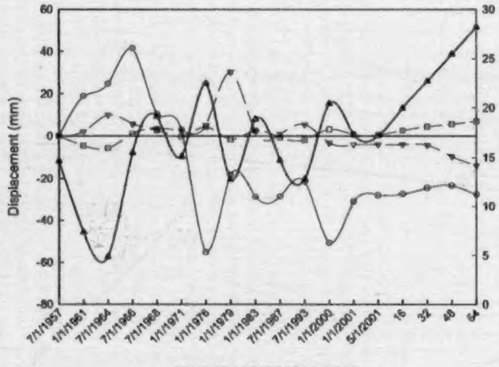

Well 101141300614W200

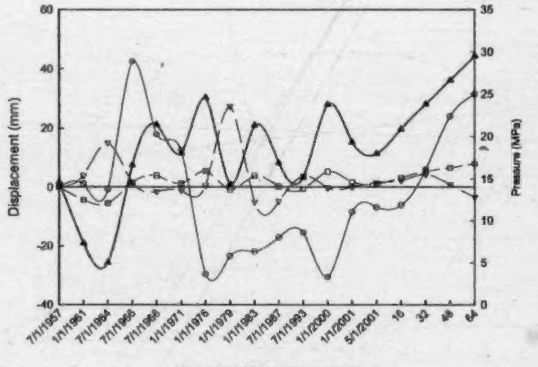

Well 101161300614W200

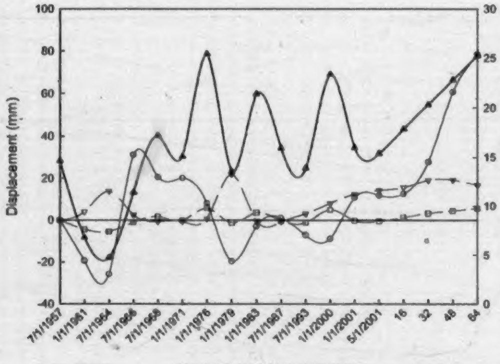

Well 191121800613W200

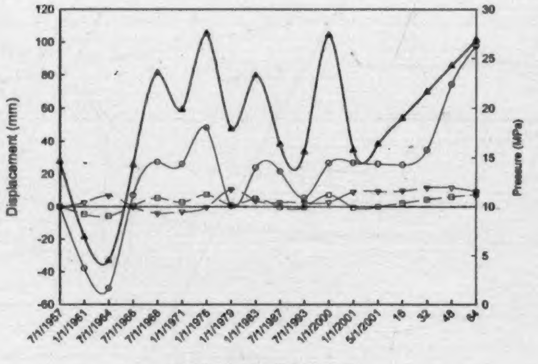

Well 101161800613W200

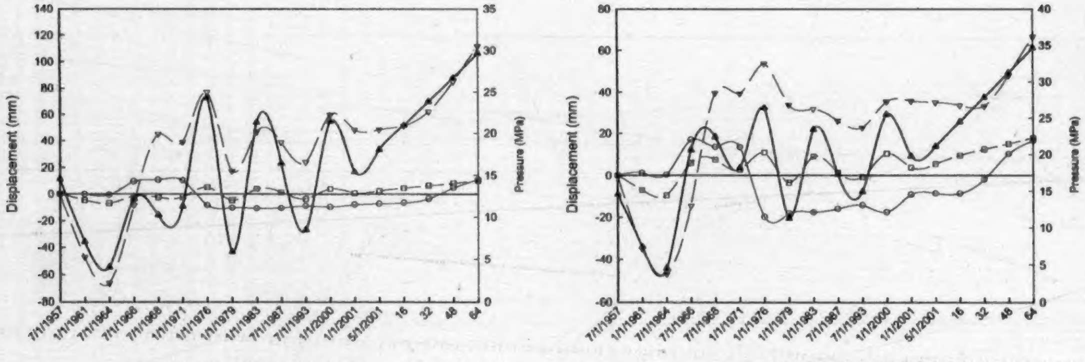

Well 101082500614W200 Well 101161300614W200

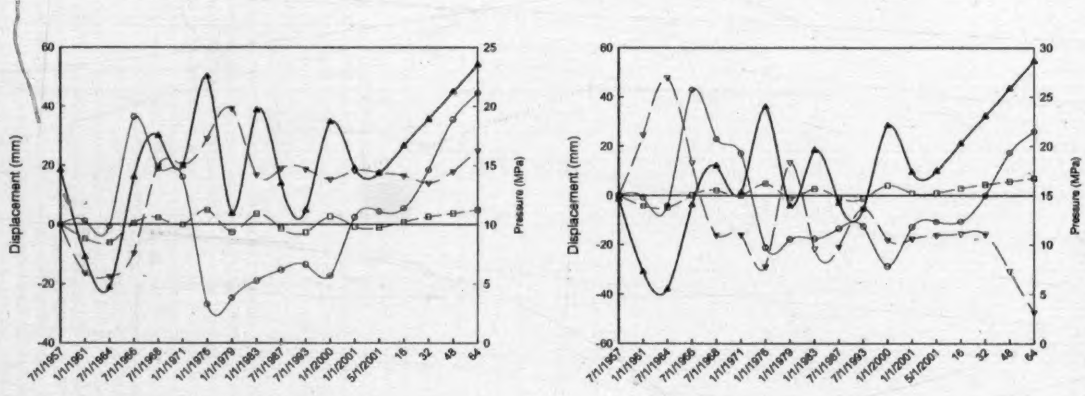

Well 101151300614W200 Well 101081300614W200

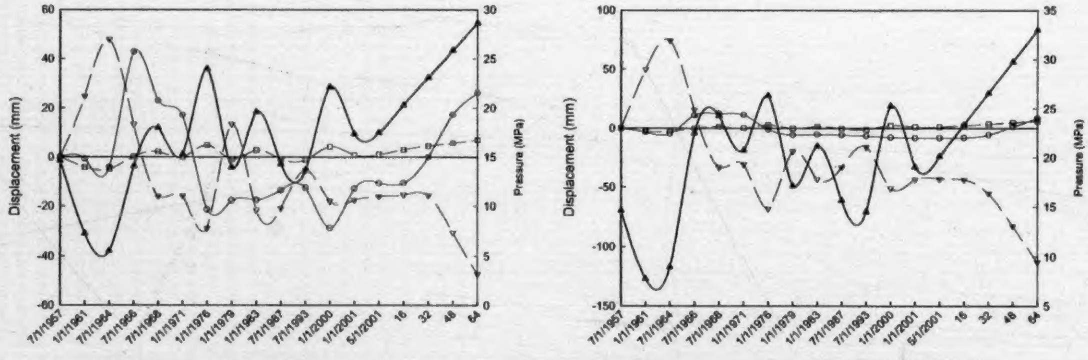

Well 101081300614W200 Well 191101200614W200

Figure 8-20. Displacement at each well location showed in Figure 8-1 at the Midale Evaporite for the base case scenario

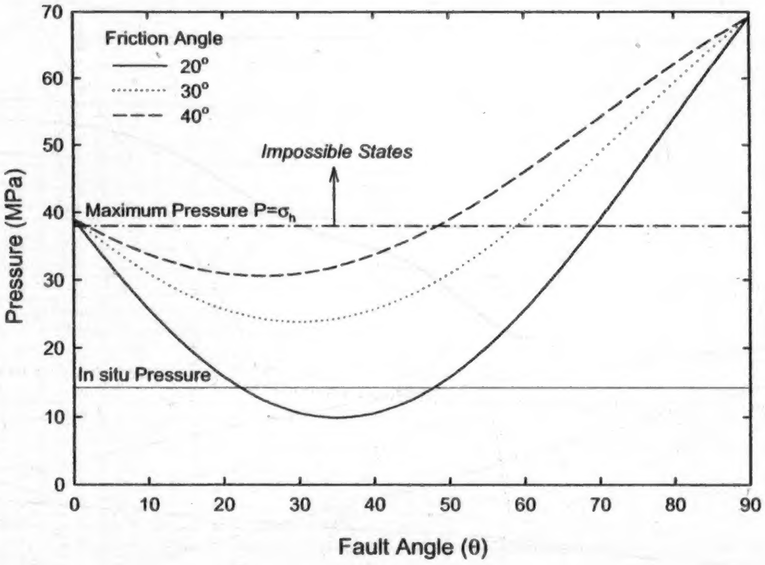

Figure 8-21. Pressure to induce fault reactivation for the base case scenario in a strike slip regime

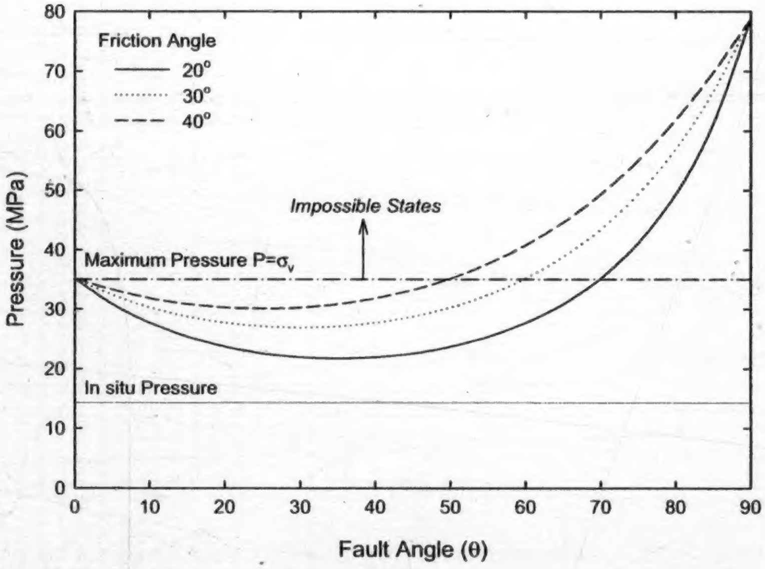

Figure 8-22. Pressure to induce fault reactivation in a reverse fault setting

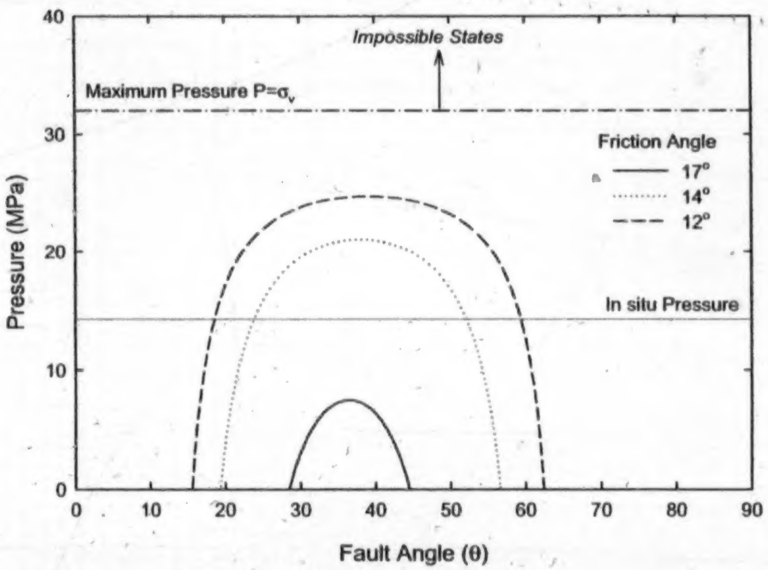

Figure 8-23. Pressure to induce fault reactivation in a normal fault setting

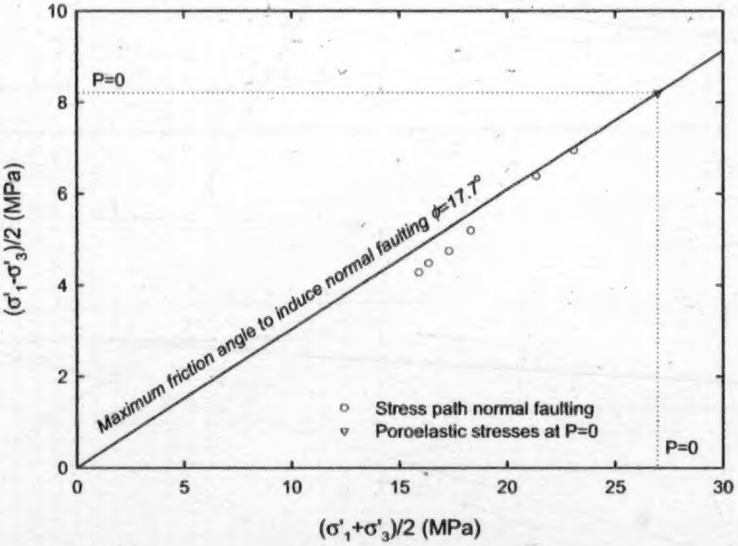

Figure 8-24. Maximum friction angle at which it is possible to induce normal fault reactivation at Weyburn

9 Impact of Salt Dissolution on Weyburn's Performance

9.1 Introduction

Conceptually, salt dissolution is a well-understood phenomenon having been observed throughout the world. However, its consequences in the mechanical and hydraulic integrity of overlying formations are not clear. The presence of extensive dissolution features in the Prairie Evaporite (PE) is an element included in the long-term risk assessment for the Weyburn Field, and it is considered one of the alternative scenarios for such risk assessment [35] The Weyburn Field is located around 800 m above the PE, a formation that has undergone substantial dissolution throughout its geological history. To understand the causes and consequences of dissolution a review of the dissolution phenomenon and what is known about dissolution in the PE was undertaken. Likewise, the MEM of Weyburn is used to build a geomechanical model, which is employed to predict if such existing features and their reactivation might have an effect on the hydraulic integrity of the reservoir.

9.2 Mechanisms of Salt Dissolution

Salt removal by solution is a chemical process by which the salt mineral passes into solution. Such a process leads to the development of "voids" or "caverns" that may significantly impact the tectonic history of a basin where evaporites are an important component, such as the Forth Approaches Basin [250], the Devonian Carbonates of Western Canada [251-253] and others around the world. The mechanisms that cause salt dissolution are not well understood as it is difficult to establish clearly which mechanisms acted on a salt formation in a specific basin and the development time [254]. The reasons for these difficulties come from complete dissolution of the formation (no geological record), cessation of the dissolution process a long time ago, or simply a lack of information about the geology and geological history in a region.

9.2.1 Classification of Salt Dissolution Mechanisms

All models of salt dissolution require that unsaturated fluids come into contact with the salt body and the dissolved salt is carried away from the solution site through regional- or local-scale fluid movements. The amount of dissolution and its geological "signature" are a consequence of how this water accesses the salt formation, and how dissolution propagates in the formation. Cartwright et al. [250] classified dissolution events depending on how dissolution propagates, and such classification is useful to look at the consequences of dissolution, which is the main goal of this chapter, Figure 9-1:

- superjacent dissolution: dissolution caused by undersaturated fluids migrating over the main salt body. However it can be the result of local or intermediate flow regimes;
- subjacent dissolution: dissolution caused by undersaturated fluids migrating along the base of the body. Subjacent dissolution is associated with centrifugal and centripetal flow regimes, flow through faults or fractures, and flow induced by glacial loading and/or unloading; and
- lateral dissolution: dissolution caused by undersaturated fluids migrating along the edges of the salt body.

9.2.2 Salt Dissolution Consequences

One of the most obvious consequences of the salt dissolution process is subsidence of overlying strata and anomalous thickening of sediments in areas where deposition is contemporaneous with or immediately following periods of salt dissolution. Such subsidence can be either continuous or discontinuous:

- Continuous or trough subsidence: continuous subsidence involves the formation of a smooth surface subsidence profile that is free of steep changes. Subsidence like that has been observed in seismic sections in the Williston Basin where massive dissolution of the Prairie evaporate has occurred, and an anticline has formed trapping hydrocarbons [251-253]. Nonetheless, continuous dissolution does not preclude the formation of breccia as described by Stanton Jr. [255] in his paper on the brecciation process. Thus intermediate steps associated with dissolution lead to gradual subsidence, brecciation, small-scale solution precipitation, and evaporate flowage occurring simultaneously with solution.
- Discontinuous subsidence: discontinuous subsidence is characterized by large surface displacements over limited surface areas and the formation of discontinuities in the surface profile, and collapse chimneys. Such dissolution and subsequent brine flow and chamber collapse is likely responsible for the formation of breccia chimneys [256]. An example of collapse chimney is present in the Delaware Basin, where undersaturated water flow from the upper part of the Captain Aquifer flows under artesian pressure through fractures to contact salt creating a dissolution wedge.

9.3 Dissolution of the Prairie Evaporite

9.3.1 Prairie Evaporite

The Prairie Evaporite is a thick interbedded sequence of halite, sylvite, bedded anhydrite, and minor dolostones that grade westward into shales [257]. Its thickness is more than 200 m in some parts, and around 150 m in the Weyburn area. The Prairie Evaporite is divided into the lower Whitkow and upper Leofnard salt members and the intervening anhydritic Shell Lake Member [257-259].

The Witkow Member is a sequence of salts and anhydrites that overlies the Winnipegosis Formation and underlies the Shell Lake Member. The anhydrite is present only adjacent to the mounds and the halite occupies the interval away from the mounds [258]. The Shell Lake Member is a massive anhydrite, and it forms the base of the Prairie Evaporite Formation where the Whitkow member is absent. Its thickness ranges from 0 to 35 m [257, 258]. The upper Prairie Evaporite known as the Leofnard Member is as much as 100 m thick and consists of halite in its lower portion and up to three potash members in its upper portion [258].

9.3.2 Dissolution and Timing

In an area west of the Weyburn Field the PE has been completely removed (Prairie salt-free area) from a large area by the process of salt dissolution, Figure 7-4. In other areas, only partial dissolution has taken place. The origin of salt dissolution features are likely the result of a combination of different processes acting simultaneously or at different times. Work on salt dissolution in the Lloydminster area of west-central Saskatchewan by Anderson et al. [251] suggests several potential large scale mechanisms resulting in salt dissolution, including near surface exposure, centripetal flow of unsaturated waters, regional faulting/fracturing, glacial loading and/or unloading, dissolution of underlying salt beds and salt creep. The removal of salt in the Prairie salt-free area appears to have started soon after deposition of the Prairie Formation and continues to the present day [260, 261]. Two types of salt collapse have been recognized in the literature in this area, one that is spatially related to underlying porous and permeable Winnipegosis mounds [258, 262] and the other from dissolution related to periodic movement along faults rooted in the Precambrian basement [253, 260, 261, 263]. Both mechanisms are subjacent dissolution.

Timing of the dissolution is rather difficult to establish, however a rough estimate can be established from isopach maps, structural anomalies and compensational deposition in the overlying layers. The work of Hajnal et al. [264] was useful in delineating the structural framework for the salt dissolution areas. The work by Hamid et al. [263] found that the spatial interpolation of well picks used in subsurface mapping results in uncertainties of the positions of salt edges of approximately 1.5 km, which is quite good, and it is being improved by the inclusion of seismic studies. Holter [261] reviewed the literature available up to 1969 and concluded that late Devonian dissolution was restricted to localized channels and lows mainly in southwestern Saskatchewan and in the Hummingbird area and other local areas in southeastern Saskatchewan, Figure 7-4. Most of the salt dissolution during the Mississipian-Jurassic occurred at scattered localities over much of southern Saskatchewan, except within and immediately north of the Hummingbird area [265]. Within the map area shown, post-Jurassic dissolution was concentrated to a great extent north of the Roncott- Hummingbird area. Similarly, De Mille [253] found that salt removal may have begun as early as late Devonian time, and recurred repeatedly, with maximum leaching occurring during the post-Mississippian erosional interval and during the post-Second White Specks time.

9.3.3 Dissolution near the Weyburn Field

Near the reservoir there are two significant dissolution features. The first one is the edge of the massive feature west of the field where more than 150 m of salt have been dissolved, Figure 7-4. This feature is present around 80 km from the reservoir, occupying a large area in southern Saskatchewan. The second feature is a small dissolution area south-east of Phase 1A, which apparently has a circular shape, approximately 8 km in diameter approximately, and a dissolved thickness of 30 to 50 m, Figure 9-2a. Such a feature is about 7 km away from Phase 1A. Dissolution in this feature beneath Phase 1B occurred before deposition of the Midale Beds [189]. This feature has also been seen in seismic surveys, Figure 9-2B, and it is associated with a strike-slip fault that seems related to the Winnipegosis mound [202], Figure 9-2c. However, until now there is no clear connection between the presence of this fault, and salt dissolution at this location.

9.4 Geomechanical Modeling

9.4.1 Model

A geomechanical model was built using average properties of the MEM for the formations above the Frobisher. The properties of the underlying formations were taken from data available in the literature [266]. The Devonian was split into the formations above the PE, and the PE. Beneath the PE a stiff Precambrian material was used. Table 9-1 shows the properties of the different formations.

Table 9-1. Elastic properties used for the geomechanical model

Formation	*Bulk Modulus K (GPa)*	*Shear Modulus G (GPa)*
Cenozoic	4	2
Cretaceous	5	2
Jurassic-Triassic	9	4.5
Mississippian	16	7
Upper Devonian	34	17
Prairie Evaporite	25	11
Precambrian	35	20
Breccia	9	4.5

Multiple models in both FLAC 4.0 [267] (finite difference method) and Phase2 [268] (finite element method) were built, which were run elastically and plastically. A dissolution front was advanced from a distance of 4 km to the reservoir until it was lying below the reservoir. Salt dissolution was modeled by removing large volumes of the PE –in increments of 1000 m in the elastic model, and 500 m in the plastic model--, allowing equilibration of the model, and then replacing these zones with a softer material to simulate the breccia, Figure 9-3. These large dissolution steps make arching less relevant, and subsequently the impact on overlying formations is larger. However, the plastic model frequently lead to confusing, physically impossible and/or unreliable results, and the input parameters were critical to achieve a stable, converging solution. Therefore, most of the results reported here are from the elastic analyses, and only one set of plastic results are presented. It is important to bear in mind that the end goal of this modeling exercise was to analyze the influence of future salt dissolution on the hydraulic integrity of the Weyburn Field, and obtain a clear phenomenological picture of the important mechanisms. Problems with stress-strain analyses have been long recognized for large excavations in the mining industry, where subsidence is mainly predicted by empirical methods based on field measurements [269]. Moreover, analyses for performance assessment can be both quantitative and qualitative, and for the current study an improved understanding and insight into the problem is more relevant than the precise analysis results. The simulations do not include provisions for salt creep, as the mechanics of dissolution are not well understood and the idea of making the model more complicated without an acceptable understanding of the phenomenological processes is not warranted.

9.4.2 Results and Discussion

9.4.2.1 Elastic Analysis

Figure 9-4 summarizes the results for the elastic simulations. The left column of the figure shows the results along the reservoir, Figure 9-3, and the right column shows the results with depth at the edge of the reservoir, Figure 9-3. The reservoir only begins to 'feel' the dissolution front at a distance of 2 km. Consequently, any dissolution feature that is present currently, independent of when it occurred, likely has no effect on the integrity of the Phase1A reservoir region. Likewise, the change in K_0 is rather small as it is only slightly altered in the shallower depths of the vertical profile, Figure 9-4b.

Once the front begins to approach the reservoir, the principal stresses increase indicating that deformations associated with the stress increase may influence the integrity of the reservoir. Thus at 1.0 km, the closest part of the reservoir sees a significant change in principal stresses, especially for an extensional setting (K_0<1.0), Figure 9-4c. Cleary the horizontal stress is relaxing as the dissolution causes mainly horizontal displacements beyond the area of dissolution. Thus, in a compressional setting (K_0>1.0) the relation between principal stresses tends to 1.0, Figure 9-4c. Moreover, the principal stresses are rotating as the values of K_0 are different from the principal stress relationship. The K_0 vertical profile is altered substantially through the stratigraphic column, at shallower depths the horizontal decreases while at depths similar to the PE K_0 is increasing as the vertical stress decreases due to relaxation of the underlying formation because of the nearby 'void' as the floor of the excavation heaves. The gaps in the profile are due to changes in elastic properties between formations. Still, dissolution effects appear insufficient to cause failure in the reservoir and/or a loss of hydraulic integrity

Once the dissolution front reaches the edge of the reservoir, the elastic analysis predicts a likely failure of the caprock system for extensional settings (K_0<1.0), Figure 9-4e. However, the plastic analysis indicates that the elastic analysis becomes non-conservative when the dissolution front is this close, and failure is likely to occur with any of the states of stress analyzed in this work, as it will be seen below. Yet, the trend in stress changes is similar for both analyses, therefore the elastic analysis provides insight into the problem. There is a very significant decrease in horizontal stresses below and above the PE, Figure 9-4f, which is likely to accelerate the dissolution process initially as the permeability of both overlying the underlying formations is likely enhanced. If the undersaturated water comes through faults, they will likely open as the acting normal stress in the faults is lower. If the water is flowing through bounding formations, these formations will intensely fracture and ease the flow of undersaturated waters. A third potential mechanism of flow enhancement is hydraulic failure (tensional failure) of underlying aquitards as the minimum horizontal stress is lower, and they may be in contact with overpressured aquifers, as it has been seen in Potash mines in Saskatchewan [266]. After large pressures in the source aquifers are dissipated, salt dissolution rates decrease and may even stop as the fluid flow regime moves toward a hydrostatic regime.

Finally the dissolution front moves below the reservoir, and the analysis indicates a stress redistribution that will lead to failure and loss of hydraulic integrity of the reservoir for any stress state, Figure 9-4g. Observations in coal mining have shown that collapsed material above mining galleries increases its volume by a 100% [269], so disintegration of the material won't be seen all the way up to the ground but it will be a gradual process where further up the effects of having an underlying caved zone are less noticeable. Still, significant fracturing can be expected in the Weyburn Field as all of the formations up to the sub-Mesozoic unconformity are quite stiff, and prone to fracturing. The process will ease into the Watrous as this is a more ductile and thick formation, but its hydraulic integrity may be affected as well.

The influence of the amount of dissolution was studied by carrying out a set of simulations with an isotropic state of stress and 150 m of dissolution instead of 50 m. The results did not show a significant difference in terms of stress change, especially when the front of dissolution was still 1 km away from the reservoir, Figure 9-4. The most likely influence of the thickness of dissolution will be the distance that collapse propagates upwards, as a larger volume will be needed to fill up the empty volume. Therefore, from a performance assessment point of view, dissolution thickness becomes quite relevant as dissolution gets closer to the field, because it will determine how far up in the stratigraphic column that formations are significantly disturbed.

The results presented above are qualitative in nature, as the geomechanical modeling of dissolution is approximate; elastic analyses do not allow for stress redistribution due to yielding, and there is no clear understanding of the mechanisms and timing of the dissolution. Nonetheless, these results show that dissolution will only have a serious impact on the integrity of the reservoir when it occurs very close (less than one km) or below the reservoir itself.

9.4.2.2 Plastic Analysis

Multiple trials of plastic analyses were attempted, but the fact that the dissolution process produces large caverns that must be replaced by collapsed material makes continuum mechanics unable to reproduce the physics of the dissolution process. However, a few models that were successful had mechanical properties assigned to the formations in the upper limit for each formation. Phase2 [268] was employed for this axisymmetric analysis, but because of the impossibility of capturing the physics, it is likely that the stress calculations above the dissolution area are not very accurate, but stresses around this area are a good indicator of how arching affects the stress redistribution. Figure 9-5 shows the result for both elastic and plastic analyses for 50 m of dissolution in an isotropic state of stress. Principal stress relationships along the reservoir for a moving dissolution front are presented. The first thing worth noting is that the stress distribution for a plastic analysis of a dissolution front at 500 m is in between the elastic analysis for a front dissolution that is between a 1000 m and the edge of the reservoir. Clearly, the plastic analysis is providing similar results in the elastic range, which firstly validates the plastic analysis, and secondly and most importantly, indicates it is unlikely that a dissolution front 1 km away from the field will have any significant effect on the hydraulic integrity of the caprock system.

Once the dissolution front is at the edge of the reservoir, the difference between the elastic and plastic analysis is enormous as the maximum value for the principal stress relationship is around three times more in the plastic than in the elastic analysis. This suggests that the elastic analysis is unconservative, and loss of hydraulic integrity in the caprock system is likely. Stress distributions for dissolution below the reservoir are similar in both analyses, but as mentioned above, the plastic analysis results above the dissolution front are not very reliable. However, it is clear that between 1000 to 2000 m along the reservoir both plastic and elastic stress distributions are similar, validating the idea that dissolution 1000 m from the reservoir will have a very small impact in the safety of the project.

Subsidence studies where supercritical extraction occurs (the relation between the width of extraction, and depth of extraction are larger than 1.4) have shown an angle of draw or limit angle (the angle subtended between the horizontal and a line joining the extraction edge with the limit of subsidence) of 15 to 35° [269, 270], Figure 9-6. This angle limits the zone of large deformations, and for a distance of 800 m between the field and the PE, a horizontal distance of maximum 600 m will see major displacements. Therefore, field measurements from mining seem to validate the results presented here where a 1 km distance from the field to the dissolution front is considered safe. Nonetheless, subsidence at surface will occur up to 1500 m from the edge of dissolution, and this is one of the reasons shallower formations show a more pronounce change in K_0 than deeper formations when the dissolution front has not reached the reservoir, Figure 9-4.

9.5 Summary

Salt dissolution is included as an alternative scenario for consideration in the long-term performance assessment of the Weyburn project. Geomechanical modeling of the dissolution processes shows how the existing dissolution features near the reservoir do not compromise the integrity of the reservoir. In addition, dissolution will likely only affect the hydraulic integrity of the reservoir if it occurs very close to the reservoir (less than 1 km) or below the reservoir itself. As dissolution has not occurred beneath the reservoir and the risk assessment area in recent geological times, dissolution is unlikely to disrupt the safety and robustness of the Weyburn field as a storage site for CO_2.

9.6 Figures

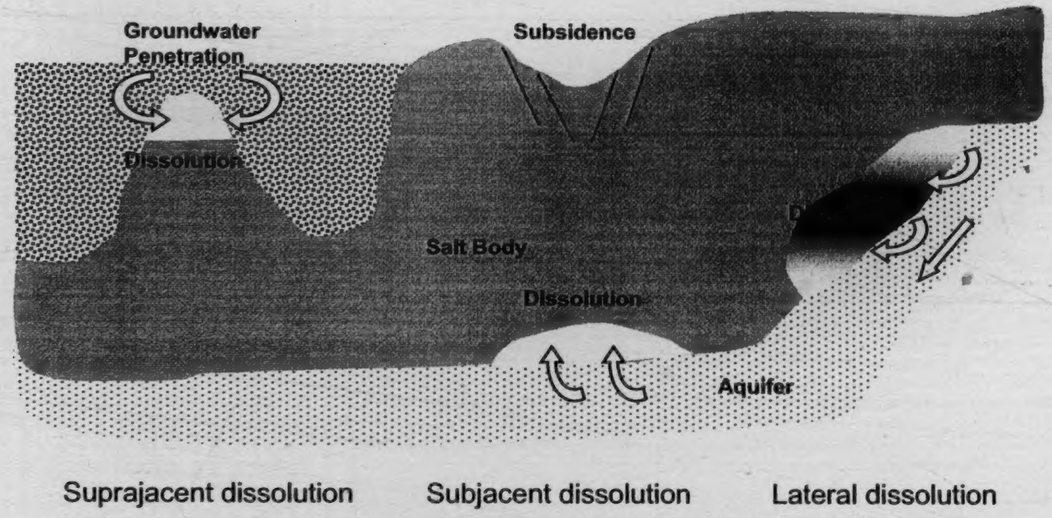
Groundwater Penetration
Subsidence
Dissolution
Salt Body
Dissolution
Aquifer
Suprajacent dissolution
Subjacent dissolution
Lateral dissolution

Figure 9-1. Modes of salt dissolution [250]: suprajacent dissolution resulting from groundwater penetration; subjacent dissolution resulting from groundwater flow along sub-salt aquifer units; and, lateral dissolution resulting from circulation along the lateral margins of the salt body

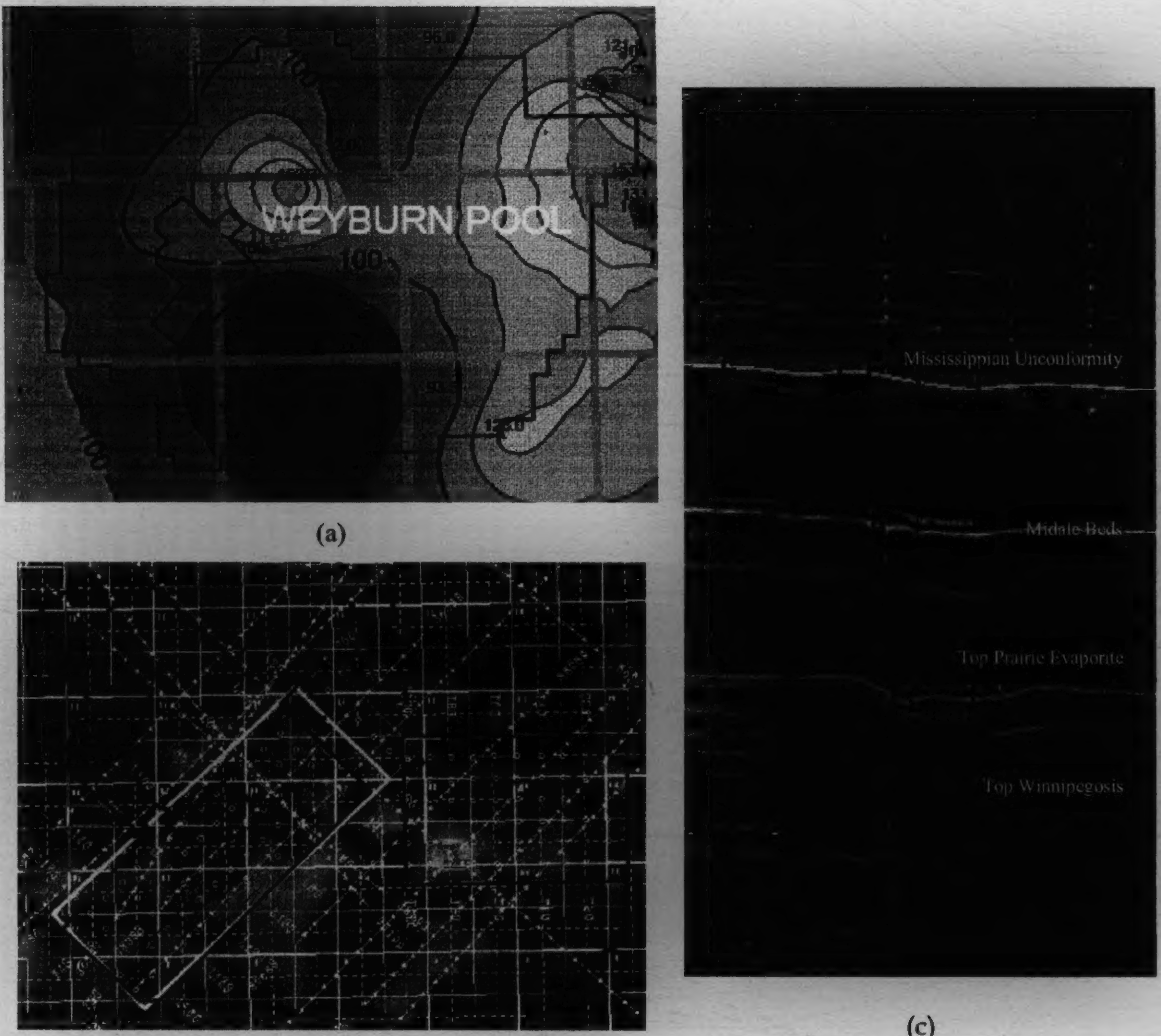
WEYBURN POOL
100
100
100
96.0
Mississippian Unconformity
Midale Beds
Top Prairie Evaporite
Top Winnipegosis

(a)

(b)

(c)

Figure 9-2. (a) Minor salt dissolution feature east of Phase 1A, below Phase 1B. This feature has been observed in (b) seismic, and (c) there is a fault that pass by the dissolution zone, after Kreis [223], and Bunge [202]

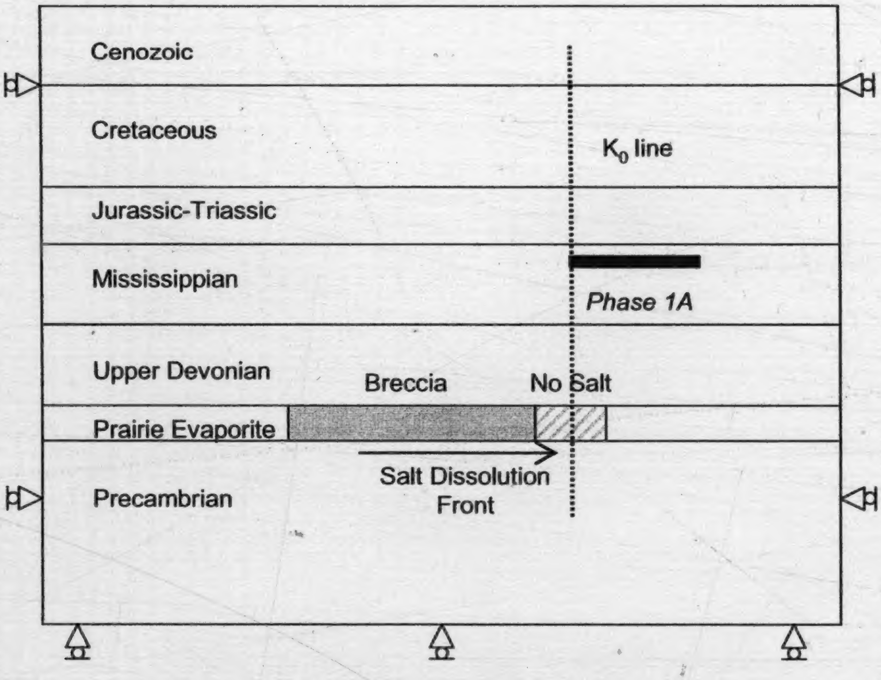
Cenozoic
Cretaceous
K0 line
Jurassic-Triassic
Mississippian
Phase 1A
Upper Devonian
Breccia
No Salt
Prairie Evaporite
Salt Dissolution Front
Precambrian

Figure 9-3. Schematic of the geomechanical model

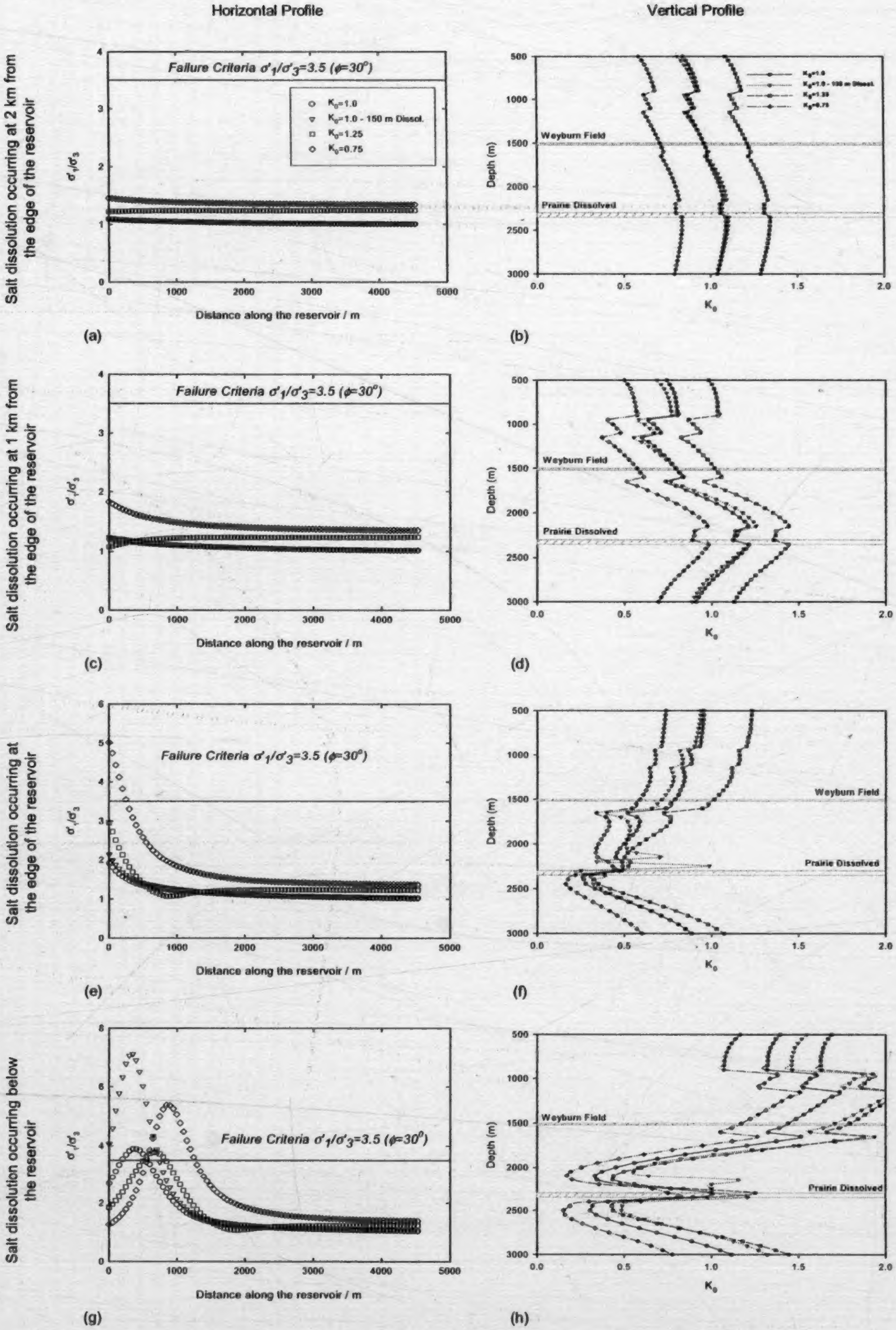

Figure 9-4. Results from elastic analysis for salt dissolution

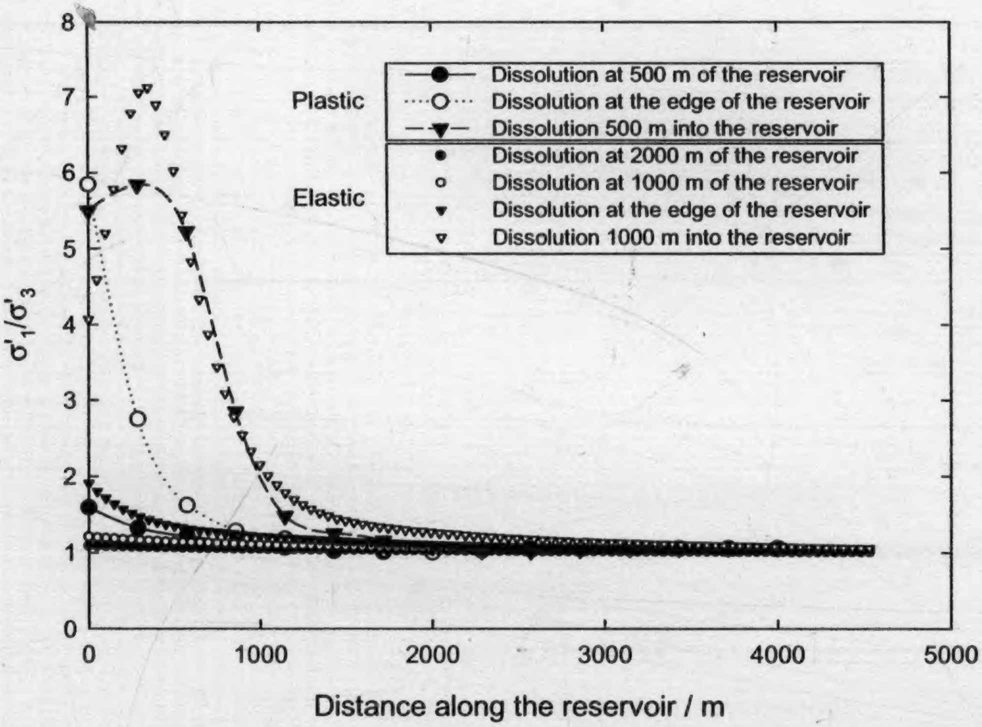

Figure 9-5. Elastic and plastic analysis for 50 m of salt dissolution, K_0=1.0

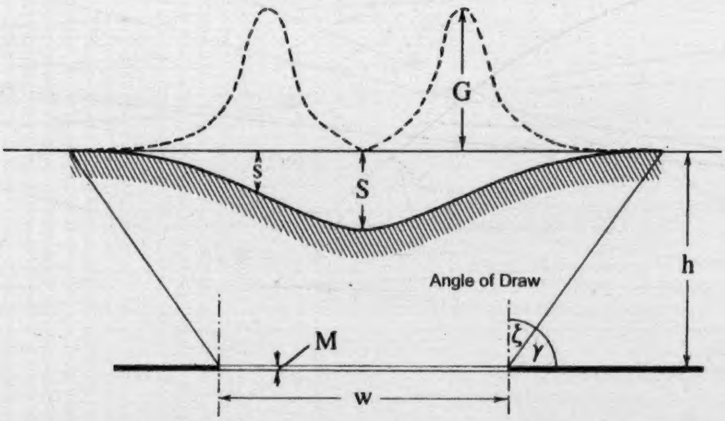
G
s
S
h
Angle of Draw
M
ζ
γ
w

Figure 9-6. Subsidence profile and terminology, modified after Whittaker and Reddish [269]

10 Thermal Effects Associated with CO_2 Injection in the Integrity of Bounding Seals[16]

10.1 Introduction

The injection of CO_2 gives rise to a variety of coupled physical chemical processes that may affect the hydraulic integrity of bounding seals and the injectivity of CO_2. Bounding seals are composed of overburden immediately above the injection horizon (typically termed caprocks) and underburden, and the wellbore systems used to access the injection horizon. A comprehensive review of hydro-mechanical mechanisms that may lead to the underperformance of bounding seals was discussed in Chapter 4, but the impact of temperature was not considered. Operational considerations require a dense stream of CO_2 at the wellhead, which is easily achieved by cooling off the CO_2. Consequently, the injected stream of CO_2 downhole could potentially be considerably cooler than the in-situ temperature of the injection horizon.

The thermomechanical behavior of a saturated porous medium has become a relevant issue with the advent of technologies such as geothermal energy, thermal stimulation of hydrocarbon reservoirs, nuclear waste disposal or issues with borehole stability in the oil industry. The study of coupled thermo-hydro-mechanical (T-H-M) effects has shown the strong coupling between heat flow, fluid flow, and solid matrix deformation. In light of this established coupling response associated with the injection of a cooler stream of CO_2, the integrity of the caprock system becomes an important consideration. This chapter analyzes such influence from a simplistic approach, but still the insight gained and results are clear in showing the large role that T-H-M effects can have under certain circumstances in the soundness and robustness of CO_2 geological storage as a safe and environmentally acceptable technology to control emissions of CO_2 into the atmosphere.

10.2 Theoretical Background

Governing equations for a fluid-saturated thermoporoelastic porous media have been developed by different authors [271-276]. A change in either solid body strain, pressure or temperature results in the corresponding unequilibrium of momentum, mass and energy systems [276]. A fully coupled thermoporoelastic formulation can be described as:

---

[16] The TOUGH2 modeling in this chapter was carried out by Dr. Stephen Talman

$$Gu_{i,jj} + (\lambda + G)u_{k,ki} = \alpha p_{,i} + \beta T_{,i}$$

$$\frac{k}{\mu} p_{,kk} = \alpha \dot{\varepsilon}_{kk} - \alpha_h \dot{T} + \alpha^* \dot{p} + Q_f$$

$$K^* T_{,kk} = q_f s T_{,k} + \beta T_0 \dot{\varepsilon}_{kk} + s^* \dot{T} + Q_h$$

Index notation is used; a comma stands for differentiation with respect to spatial co-ordinates and a superscripted dot means derivate with time. T is the temperature, u is the displacement, p is the pressure, ε_{kk} is the total body strain, λ and G are elastic constants, α is Biot's parameter, β is the thermal expansion factor, k is the fluid permeability, μ is the fluid viscosity, α^* is the lumped compressibility, α_h is the thermal expansion coefficient, K^* is the thermal conductivity, q_f is Darcy's velocity of fluid flow, s is the intrinsic heat capacity for fluid, s^* is the lumped intrinsic heat capacity, T_0 is the reference temperature, Q_f and Q_h are the fluid and heat sources [276].

The first two-terms of the right-hand side of each equation are the coupling terms. In the first equation these terms adjust the effective stress due to changes in fluid pressure and the total strains due to thermal expansion respectively [276]. In the second equation the terms adjust the mass rate changes due to solid volumetric strain, and the rate variation due to thermal expansion (or contraction) of fluid and solid respectively [276]. Finally in the last equation the first term accounts for unequilibrium of energy transport due to forced thermal convection in fluid flow, and the second one for energy lost as a result of solid deformation in the form of thermal expansion or contraction [276].

10.3 Conceptual Models

CO_2 injection is a rather complex problem where a stream of CO_2 flows into a saturated reservoir. Typically the reservoir will be either water or oil/hydrocarbon saturated. The injected fluid will most likely be at a different temperature than the in-situ one particularly if the injection period is great compared to the time required to remove significant quantities of heat from the vicinity of the wellbore. Consequently the injection will cause deformation of the porous media and a change in its stress state [277]. CO_2 injection is essentially a complex multiphase-thermomechanical problem, and in the long-term there will also be an important chemical component. Because of the complexity of the problem the model has been simplified, and it has the following features:

- It assumes that the reservoir in its natural condition is CO_2 saturated. Therefore there is flow of only one component, and uncertainties about relative permeability and capillary pressures are eliminated.

- The flow of heat and mass is modeled using TOUGH2 [278] modified to incorporate the CO_2 equation of state (EOS) proposed by Span and Wagner [277]. The simulation treats the injection of pure CO_2 with an enthalpy content of -300 kJ/kg into a reservoir filled with CO_2. The enthalpy content corresponds to injection of a fluid at about 280 K and 20 MPa.

- The in-situ stress field assumes that both vertical and horizontal stresses are similar (K_0=1.0), which implies that the stress field is irrotational, and the pore pressure field may be decoupled from the governing equations and determined independently [279].

- The equations for heat flow and fluid flow are solved coupled using TOUGH2, and the temperature and pressure field are taken to FLAC 4.0 [267] at the desired times to solve the mechanical equations. As mentioned above, the pressure field can be decoupled because of the irrotational stress field. Likewise, the temperature field can be calculated without calculating simultaneously the strains because of their weak coupling [275]. Note however that the converse is not true.

In order to simulate the most likely scenarios for CO_2 injection --enhanced oil recovery (EOR) and deep saline aquifers--, two different models are considered. The first model is a thin carbonate reservoir capped by a thin anhydrite, which is capped by a thick shale, Figure 10-1. Such geometry is not uncommon for existing hydrocarbon reservoirs, and consequently is a potential site for EOR activities. The reservoir is at a depth of 1500 meters, an in-situ temperature of 313 K (40° C), and CO_2 is injected through a horizontal well in the middle point of the reservoir at a rate of 0.05 kg/s per meter into the page and a temperature of 280 K (7° C). The second model is a typical deep saline aquifer, composed of a 100 m thick sandstone capped by thick shales, an in-situ temperature of 320 K (47° C), and CO_2 is injected at a similar rate as in the first case. Table 10-1 and

Table 10-2 show the T-H-M properties of the materials used in both models.

The flow boundary condition for the models was constant pressure at the outer vertical boundary with no flow conditions imposed at the horizontal and inner vertical boundaries. Heat transfer was allowed at the horizontal boundaries using the semi-analytical heat transfer option available in TOUGH2. The mechanical boundaries assumed symmetry at the centre line, and non-displacement boundaries at the base and outer boundary. The top boundary was assumed as constant stress. It will be demonstrated that the impact of such boundaries is rather small compared to the consequences of injecting cool CO_2.

Table 10-1. Thermal and hydraulic properties for the formations used in the models

	Porosity ϕ	Density ρ (kg/m^3)	Permeability k (m^2)	Specific Heat c_p (J/kg-K)	Conductivity k_T (W/m-K)
Shale	0.21	2650	3E-18	977	1.5
Anhydrite	0.001	2980	1E-20	744	5.0
Sandstone	0.20	2260	3E-14	852	3.0
Limestone	0.20	2800	2E-14	852	3.0

Table 10-2. Mechanical properties for the formations used in the models

	Bulk modulus K (GPa)	Shear modulus G (GPa)	Cohesion c (MPa)	Tensional strength T (MPa)	Friction angle ϕ	Linear coefficient of thermal expansion α (1/K)
Shale	13	8	10	1	30	1.5E-5
Anhydrite	74	25	60	6	40	1.5E-5
Sandstone	37	18	30	3	35	3.0E-5
Limestone	37	18	30	3	35	3.0E-5

10.4 Results

10.4.1 Carbonate Reservoir

The injection of CO_2 at 280 K into a 313 K reservoir causes a rapid cooling of the nearby wellbore region, and a rapid increase of pressure, which reaches its maximum at the injection point around two months later. Subsequently, the cooling front keeps traversing the reservoir but the pressure inside the reservoir remains constant, Figure 10-2. The pressure development demonstrates the influence of the fixed pressure imposed at the outer boundary condition and the large permeability of the reservoir. Notice how after less than 20 days the cooling front has advanced around 15 m into the reservoir, and in two months more than 30 m.

The alternative of treating the outer boundary with a no flow condition will lead to higher pore pressures, and slightly higher reservoir temperatures. However, the enthalpy of CO_2 at reservoir conditions is reasonably pressure independent, Figure 10-3, so that any cooling of the reservoir will not be greatly impacted by the choice of boundary conditions.

The impact of cooling on the stress state inside the reservoir is significant. The cooling causes a decrease in the stresses, while the pressures are increasing due to the CO_2 injection, which eventually leads to tensional failure of the reservoir. Figure 10-4 shows the horizontal stresses along the centerline of the reservoir for isothermal and non-isothermal cases after 208 days of CO_2 injection. The non-isothermal case is analyzed elastically and plastically. From the elastic analysis it is clear that the total horizontal stress decreases significantly towards the cooling front, becoming negative well into the reservoir, and the effective stress is negative over an even greater distance. However, such a state of stress is impossible because the tensional strength of the material will be insufficient to prevent failure; therefore a plastic analysis was carried out. The plastic analysis shows that eventually the total horizontal stress becomes identical to the pressure inside the reservoir, and the effective stress is zero. A zone of zero effective stress in the plastic analysis implies that the tensional strength has actually been overcome, causing hydraulic fracturing, and the material has lost its tensional strength. Notice the difference in size of the zones affected by tensional failure between an elastic analysis and a plastic analysis. The elastic analysis predicts a much larger zone of failure because there is not a redistribution of stresses once the tensional strength is overcome. Figure 10-5 shows the horizontal stresses in a top to bottom cross-section near the injector. These results clearly show how the tensional strength is overcome from top to bottom into the reservoir, and starts to propagate inside the caprock.

10.4.2 Deep Saline Aquifer

A typical saline aquifer for CO_2 injection will be a long thick sandstone capped by shales. The response of this thicker formation is similar to the thin injection horizon in the preceding case, but the fracturing occurs essentially only in the injection horizon. Consequently, the injection of a cooler CO_2 stream into a thick formation may be positive because it will stimulate the permeability nearby the wellbore, creating a "sweet" spot for injection that will help to maximize the volume of CO_2 storage without affecting the integrity of the bounding seals. However, uncertainty on how fracturing propagates inside the reservoir and localization of temperature effects around hydraulic fractures will lead to a different flow regime, and it may make this apparently beneficial effect misleading because the integrity of the bounding seals may be affected. Figure 10-6 shows the temperature and pressure profiles along the centerline of the reservoir after 20 years of CO_2 injection. Notice how far into the formation the cooling front has propagated, but the pressure has not increased dramatically. Figure 10-7 shows the zone of tensional failure, which is restricted to the injection horizon in contrast with the thin reservoir.

10.5 Discussion

It is clear that the injection of CO_2 at cooler temperatures than in-situ has a large impact on the integrity of both the injection horizon and its bounding seals. A cooler stream of CO_2 causes an important decrease in total stresses that may eventually lead to tensional failure of the injection horizon, Figure 10-4. This failure might propagate to the overburden and underburden, affecting the hydraulic integrity of the bounding seals. The initial effect of hydraulic fracturing around the injector may be positive, especially for thick formations where CO_2 will flow easily, pressure will be kept low, and a larger volume of CO_2 can be injected. Similar calculations by Noorishad and Tsang [280] have shown that the difference in temperature between the reservoir and injected waters lowers the injection pressure required for hydrofracturing by as much as 10 MPa. However, in the long-term and in realistic conditions CO_2 will concentrate below the caprock, which may lead to an important change of stresses and pressures in the caprock, potentially affecting its integrity. Consequently there is the need to carry out the modeling with a more realistic approach where all the multiphase flow effects are considered as well as flow through fractures that are either induced or natural. On the other hand, in the case of a thin reservoir for CO_2-EOR storage it is clear even from a simple model like the one used here that the hydraulic integrity of the caprock will be affected, and other parameters such as the thickness of the sealing rocks, and the potential for leaking into an aquifer become more relevant. Moreover, the fracturing and loss of CO_2 will be a detriment to EOR activities where the sweep efficiency will decrease, and significant amounts of CO_2 which otherwise could be reutilized will be lost.

Hitherto it has been assumed that the situation can be modeled as a continuum, but it is important to bear in mind that once tensional failure is induced , the continuum approximation and hence the mechanical model is no longer valid. Moreover, the presence of fractures will change the flow field, and the problem becomes three-dimensional. Nonetheless, the results shown above are still valuable because a more realistic model will show a more dramatic picture near the injector. The zone of hydraulic fracturing will be smaller, but the fluid will concentrate in the fractures, with local fluctuations of pressure that will make the fractures grow, and the temperature field will change locally slightly. The fracture will propagate in its own plane at different rates in different directions depending on the near field stress and mechanical properties of the formation. Consequently, the caprock will be affected substantially more than the model shows because the fracture will propagate into the reservoir, and upwards and downwards. This underscores the important role that the in-situ state of stress plays in geomechanical modeling, and even more in a case where hydraulic fracturing is expected to occur, because hydraulic fractures propagate perpendicular to the direction of the minimum in-situ stress. Therefore, more accurate modeling of the situation will require a better knowledge of the in-situ stresses, and a mechanical model that can handle continuous and discontinuous media such as discrete element modeling (DEM). However, fracture initiation is a rather complex phenomenon that cannot be modeled realistically and efficiently in a complex situation like CO_2 injection at the moment.

Fracture propagation will need to be considered as well. Initial fracture shapes in a multi-layered medium are fairly well understood from reservoir stimulation technologies and numerical modeling. Hydrofracturing for reservoir stimulation is a controlled process where fluid and proppant volumes are known before hand, and there is a reasonably accurate idea of the final shape of the fracture. On the other hand there is little experience for fracture propagation when the injected volumes will be many orders of magnitude larger than in reservoir stimulation and will go on for a very long period of time. Therefore there is the need to understand how the fracture will evolve with time, when it will stop, whether a new set of fractures coming off the main fracture will form or the fracture will become a conduit for CO_2 to flow into the matrix. These are just some of the questions that will need to be addressed because of the massive scale of CO_2 storage operations.

The treatment of the reservoir as being CO_2 saturated will also impact the results. In the treatment presented here CO_2 will tend to flow throughout the entire thickness of the reservoir, rather than concentrated just under the caprock. This leads to a more uniform heating front, rather than developing a larger zone of cooling at the top of the reservoir. Despite this discrepancy, the net heat transferred into the reservoir will be realistic. Furthermore, heat effects associated with dissolution of CO_2 into reservoir fluids are ignored. There will be a heat associated with the dissolution of CO_2 into the existing reservoir fluids. Heat will be generated by CO_2 dissolution into aqueous fluids, whereas it will be removed by CO_2 dissolution into hydrocarbons. Consequently, the cooling effects will be overestimated in the aquifer case and underestimated in the EOR case. The magnitude of the error will be time dependent; initially the capacity to hold CO_2 may lead to warming around the injector, however, the capacity to absorb CO_2 will be quickly exhausted and so cooling will develop. Modeling by Pruess et al. [281] suggests that less than 10% of the injected CO_2 can be incorporated into the aqueous phase. In the long term the heat contribution associated with the CO_2 injection will overwhelm those associated with solution into the reservoir fluid. Whether or not there are associated heat effects associated with CO_2/reservoir fluid interactions may effect the time required to achieve a given temperature within the reservoir, however, it will not, in the long-term affect the conclusions regarding the eventual cooling.

Another phenomenon that needs to be understood better is how pore pressures change inside a low permeability material when it cools off substantially. It is clear that when low permeability materials warm the pore pressure increases and that the process is linear, with a change of about 1 MPa per 1 ºC [279]. However, there is little public experimental evidence of which the authors are aware that the same happens when a material is cooled off. Additionally, the existing models assume that there is a continuous fluid phase which is true for shales, but uncertain for anhydrites. Therefore, it is the author's point of view that more research is needed in the response of low permeability materials to cooling, especially in anhydrites.

10.6 Summary

A simplified approach to show the significant effects of CO_2 injection at cooler temperatures than in-situ reservoir has been presented. The results clearly indicate the potential that cooling off the reservoir while injecting CO_2 might have in the integrity of bounding seals, through stress re-distribution, pore pressure increase and eventually tensional failure of the caprock. Therefore, when CO_2 is injected into a reservoir a close look must be given to the thermal effects that may jeopardize the hydraulic integrity of the caprock, and the successful storage of CO_2. A good knowledge of the in-situ state of stress is fundamental to understand the possible influence of thermal effects in the bounding seals. Moreover, there is the need to develop and implement more realistic, complex models that can handle different phenomena such as multiphase flow, flow in a discontinuous medium, and fracture initiation and propagation.

10.7 Figures

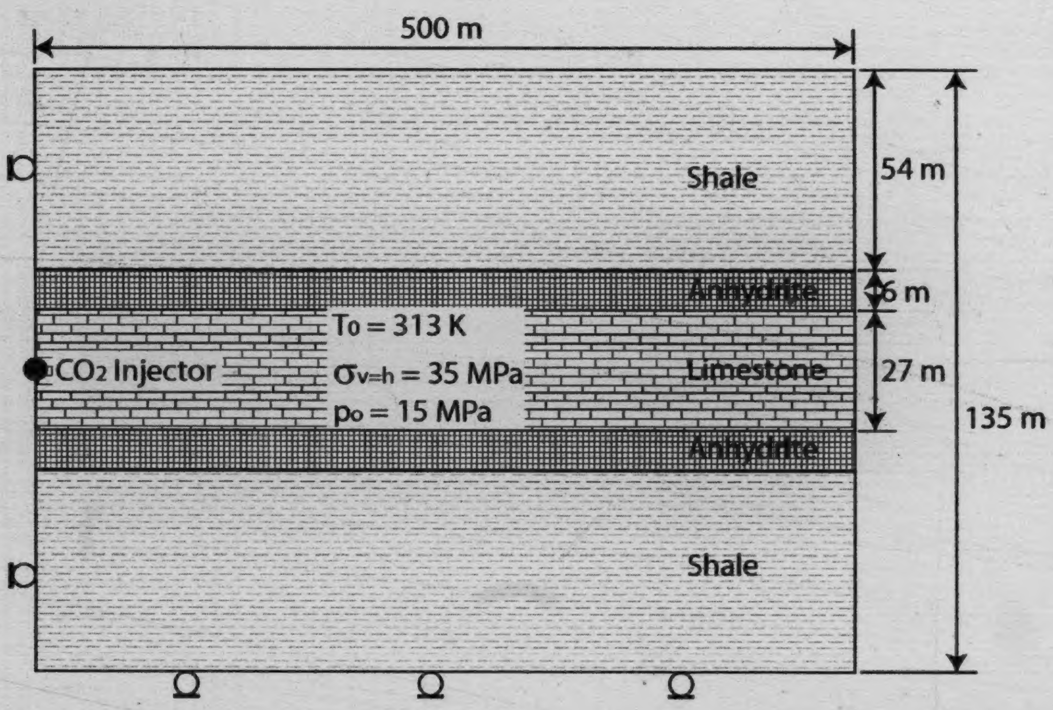
500 m
Shale
54 m
Anhydrite
6 m
To = 313 K
CO2 Injector
σv=h = 35 MPa
Limestone
27 m
po = 15 MPa
135 m
Anhydrite
Shale

Figure 10-1. Model of carbonate reservoir used as a potential CO_2-EOR storage sink

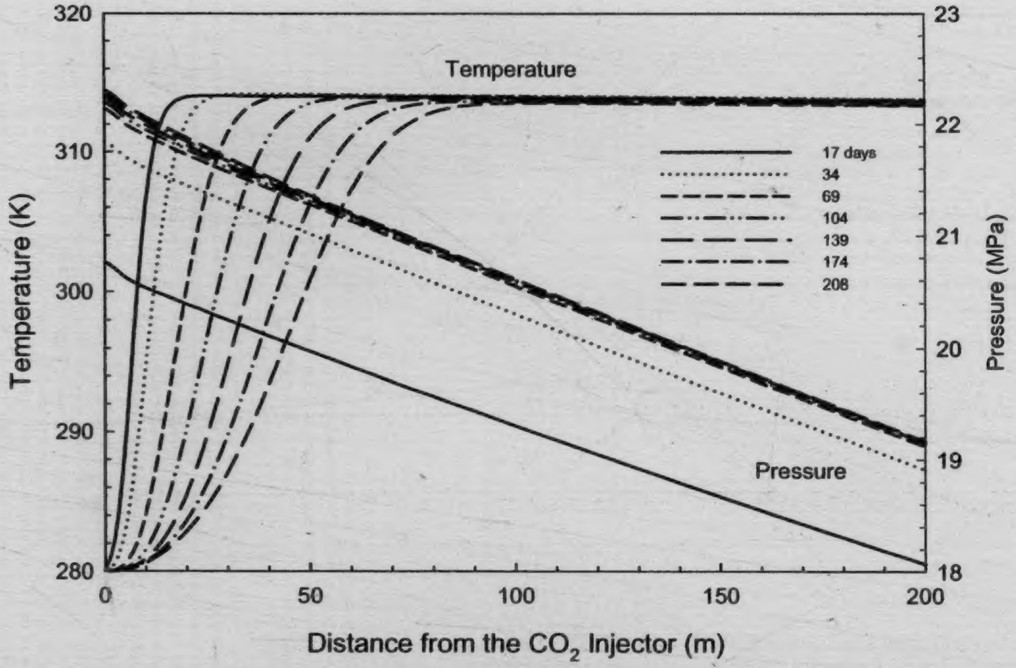

Figure 10-2. Temperature and pressure profiles along the centerline of the carbonate reservoir from 17 days to 208 days of injection

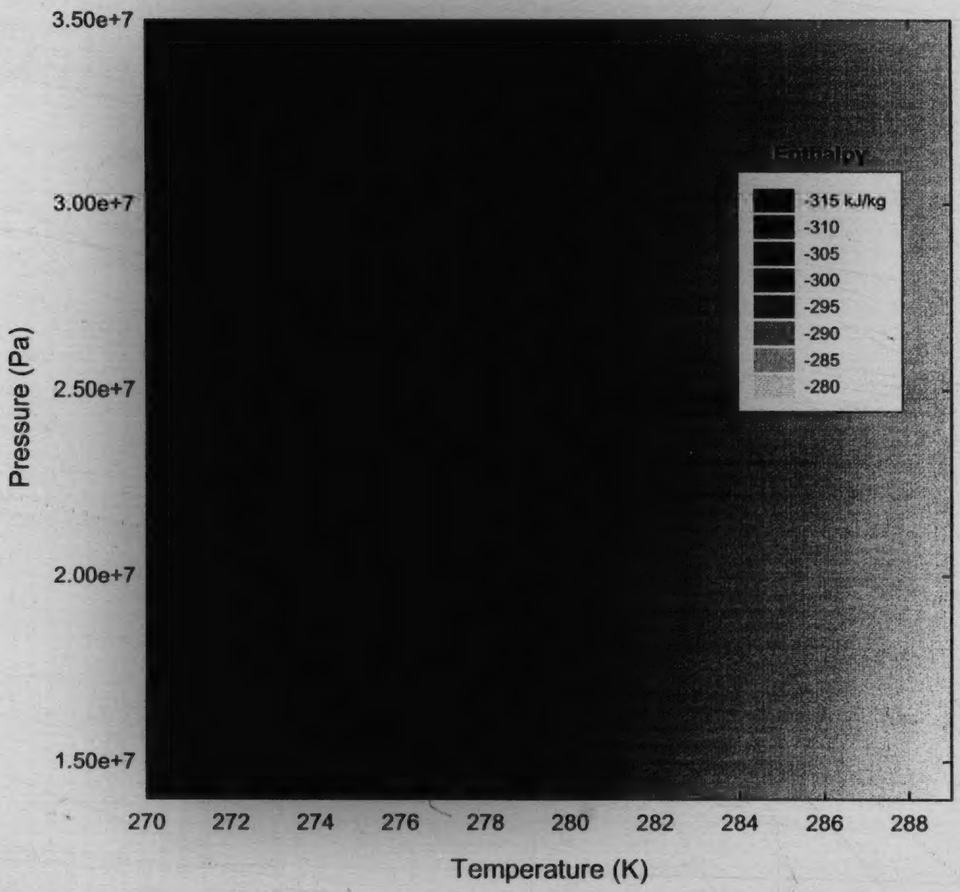

Figure 10-3. CO_2 enthalpy at different pressures and temperatures

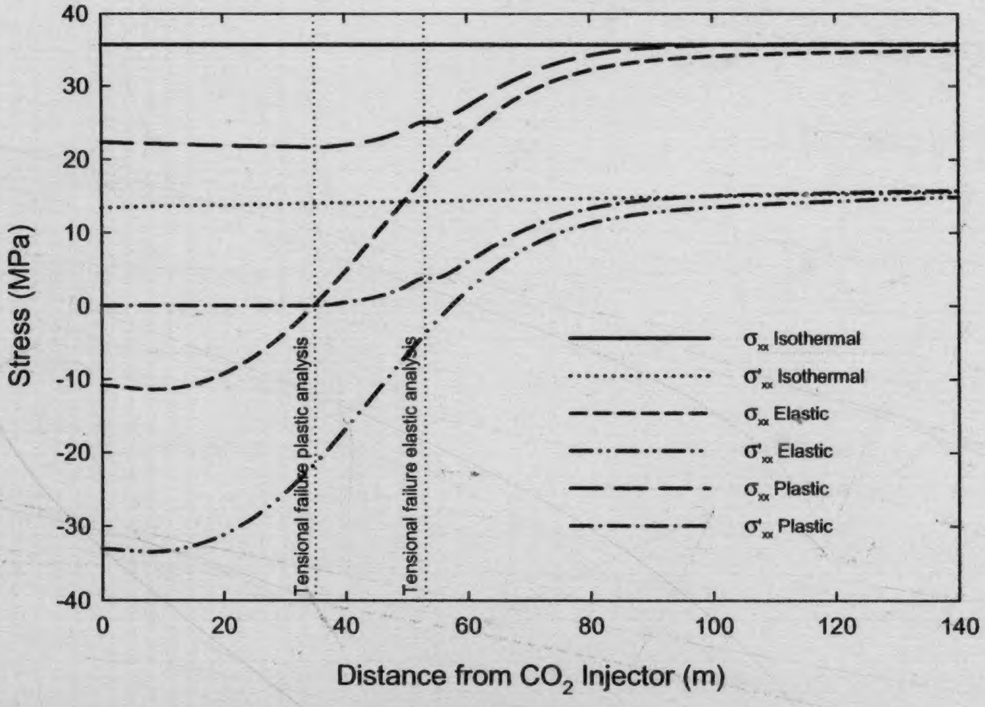

Figure 10-4. Horizontal stresses along the centerline of the reservoir for isothermal and non-isothermal cases, after 208 days of CO_2 injection

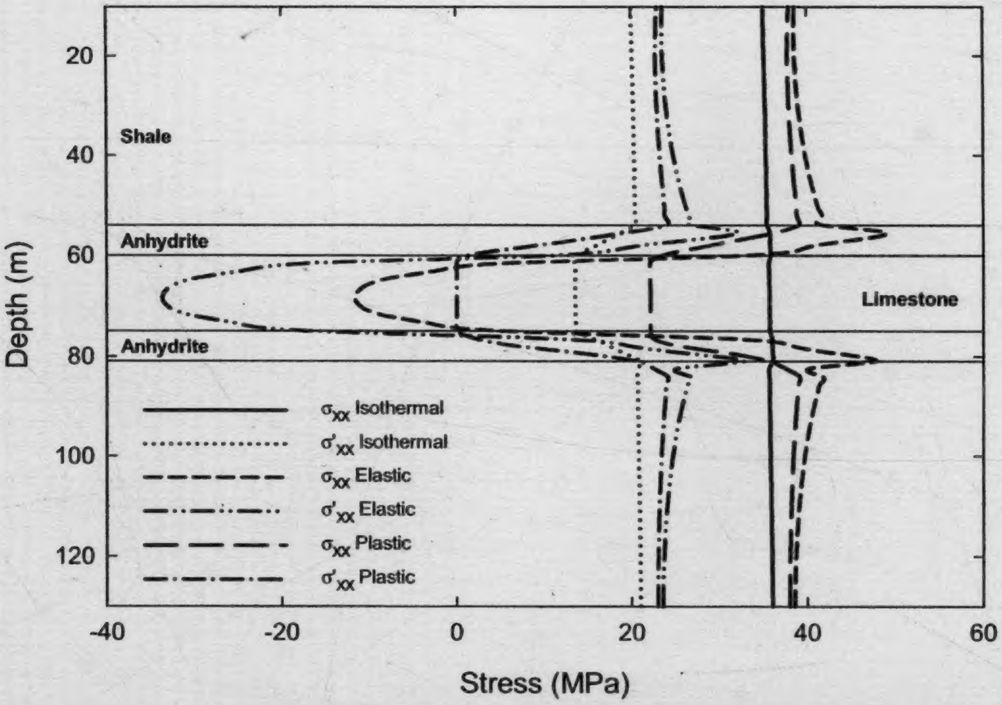

Figure 10-5. Horizontal stresses from top to bottom of the model at a distance of 7.5 m from the injector, after 208 days of CO_2 injection

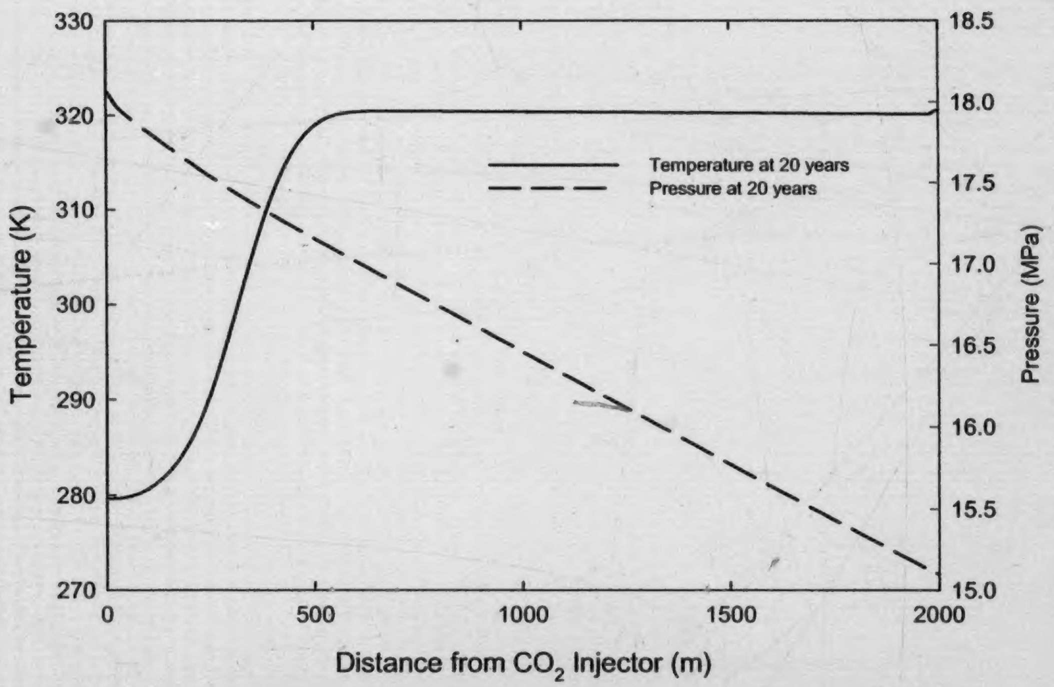

Figure 10-6. Temperature and pressure profile along the centerline of the formation after 20years of CO_2 injection, deep saline aquifer

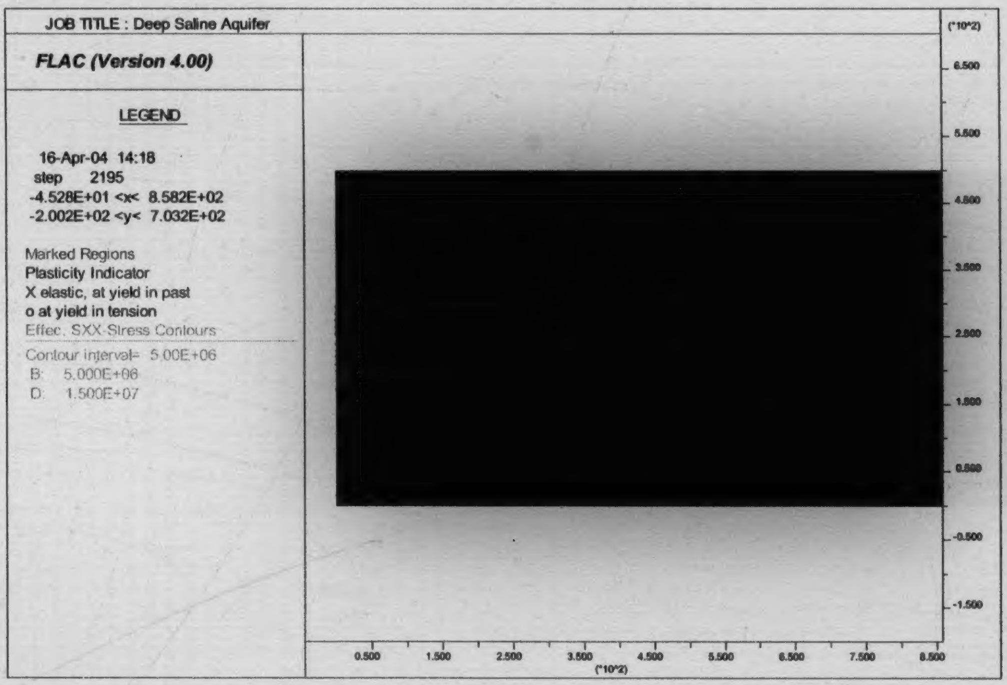

Figure 10-7. Horizontal effective stress and zone that has failed in tension due to CO_2 injection after 20 years, deep saline aquifer

11 Geomechanical Performance Assessment of Caprock Systems in CO_2-EOR Storage Projects

11.1 Introduction

A CO_2 geological storage system has four components: a reservoir with its caprock (caprock system), the overburden between the containment zone and exposure zone, the CO_2 exposure zone comprising the shallow saturated and undersaturated zone, and preferential CO_2 migration paths like wells or faults. A safety assessment is required to quantitatively and qualitatively analyze the overall performance of this system, and compare its performance against regulatory limits and targets. However, most systems are complex and require assumptions and simplifications that would render the system treatable and the analysis results reliable and verifiable. On the other hand, a performance assessment of some subset of processes or components of the system would allow more comprehensive and complex analyses to be undertaken and would provide valuable input towards the safety assessment. Thus, performance assessments of multiple processes and/or components of the CO_2 geological storage system are logical steps towards a final safety assessment, and as such, the geomechanical performance assessment of the caprock system is a basic component of both safety and risk assessment for geological storage of CO_2.

11.2 Performance Assessment: Transparency and Elements

Chapter 3 addressed the concept of performance assessment, its general methodology and main components. Reviews of performance assessment methodologies in nuclear waste disposal (NWD) have established some guidelines to promote transparency [282]:

- Present the method to carry out the performance assessment.
- Present the assumptions made and their basis.
- Present the modeling accurately. An accurate description of exactly what conceptual features and processes are represented in the models, and by what algorithms.
- Present the data used and their sources.
- Present intermediate results.
- Analyze the results to identify key assumptions, models, data and uncertainties.
- Explain the results.

- Identify points of weakness.

Moreover, performance assessment is a combination of qualitative and quantitative elements that should be assembled logically and congruently. Ideally, a performance assessment includes the following elements [282]:

- A context or perspective.
- Criteria should be set by a regulatory body or by design targets.
- Objectives and scope of the assessment.
- A description of the system both at a conceptual level and a detailed one.
- Approach to performance assessment.
- Interpretation and elicitation of the databases.
- Scenario analysis. The description of the system combined with the identification of FEPs makes up the scenario analysis.
- Description of models. The conceptual basis and mathematical expression of models should be described.
- Results and interpretation.
- Confidence in key arguments.
- Compliance with the criteria.
- Conclusions

The geomechanical performance assessment of Weyburn has been carried out trying to incorporate these elements while addressing transparency issues. Exceptions are a clear approach, which was outlined in Chapter 3, but is to be developed further in this chapter, and the description and validation of analytical models for both fluid flow and solid mechanics as these models are well developed. The use of commercially validated software makes this step unnecessary. Therefore, there is a framework in place to develop a comprehensive methodology to evaluate the geomechanical performance assessment of caprock systems for CO_2-EOR storage projects.

11.3 Methodology

One of the goals of this thesis was to develop a methodology to evaluate the geomechanical performance of caprocks in CO_2-EOR storage projects. Such a methodology is described below and summarized in Figure 11-1.

11.3.1 Objective

In geological storage a seal or caprock is a geological formation with appropriate hydraulic properties to effectively contain injected CO_2 for a sufficient period of time to ensure maximum impact on emission reductions and to satisfy health, safety and environmental concerns. Granted the present understanding of transport properties for shales and anhydrites in the presence of CO_2 is not good, the geomechanical performance assessment is generally concerned with the presence of conducting features. Conducting features are zones of relatively high hydraulic conductivity which are interconnected, and occupy a small portion of the domain, although their scale can vary from micro- to megascale [60]. These conducting features which may disrupt the hydraulic integrity of an otherwise suitable caprock and can be either storage-activated or storage-induced (see Chapter 4).

11.3.2 Time Frame

A timeframe for geological storage projects is not in place yet, but it will range from a few hundred years to a few thousand. However, geomechanical effects due to CO_2 injection will only play a role until injection stops and pressure decays to its equilibrium state defined as the in-situ pressure in open systems. Therefore, the geomechanical performance assessment only considers the time until the pressure decays. Nonetheless, there can be geomechanical effects due to geological events such as tectonic failure or salt dissolution, which play an important role on in the long-term performance assessment. These geomechanical effects are considered for the long-term assessment as alternative scenarios and are analyzed individually.

The geomechanical performance assessment should be carried out in three phases for CO_2-EOR storage projects. The first two phases are interrelated. The first phase is a ***pre-CO_2 injection performance assessment*** that goes from the moment exploitation and production began up to the moment CO_2 injection starts. The second phase is the ***short-term performance assessment*** that goes from the initial injection of CO_2 up until pressure decay. A peculiarity of the first step is that scenario analyses, which try to establish the existing conditions of the caprock system before exploitation, gathers a substantial part of its information during exploitation and production, so a large amount of engineering judgment goes into developing this start-up scenario with information gathered at later times than the time the scenario is representing. Likewise, the base case and alternative scenarios used for the short-term performance assessment use not only the results from the pre-CO_2 injection performance assessment, but the same information that was used to build the cases for the pre-CO_2 injection performance assessment. Therefore the process becomes iterative and there is a constant synergy between both assessments through an iterative process. The final phase is the ***long-term performance assessment*** that, as was mentioned previously, addressed specific scenarios such as tectonic activity, mining, or salt dissolution. The timeframe for this phase is determined by either the timeframe of the project or by the possibility of one of these phenomena or activities occurring. For example, it is known that salt dissolution has occurred in the Williston Basin and it has been active for thousands of years, therefore it is a scenario that needs to be considered without a specific timeframe.

11.3.3 Uncertainty

Uncertainty is inherent to any geological system, and its sources are well understood as seen in Chapter 3. There are essentially two broad methods for quantitatively handling uncertainty in the assessments: deterministic and probabilistic approaches. The main difference between deterministic and probabilistic methods is that the latter explicitly tries to quantify probabilities and to combine these into risk estimates, whereas deterministic methods do not take this quantitative step. The approach to uncertainty in this work is deterministic for two reasons; one conceptual and one practical. Conceptually the link between performance assessment and safety assessment is stated by Dewiere et al. [283] as "… the role of safety assessment is to determine the area of acceptability, while performance assessment is to determine the limits of possibilities and ranges of uncertainties in predictions…". Thus, a deterministic approach relies on the possibility of making bounding analyses. These analyses have as a goal to either support the conservatism of the 'reference assumption' or to illustrate the impact of conditions deviating from reference conditions [282]. Some assessments may implicitly assume that the variants represent less plausible situations, and in others an effort is made to show qualitatively that the likelihood of detrimental cases is low [282].

The practical reason to justify a deterministic approach is that while probabilistic methods have come a long way into geotechnical analysis, although not in daily practice, a probabilistic approach for reservoir geomechanical simulations is not sufficiently meaningful given the present state-of-the-art. The three basic inputs to these models are in-situ stresses, type of boundary conditions, and geomechanical properties. Uncertainty associated with in-situ stresses is better addressed by in-situ stress measurements, but they are expensive, and usually from an oil production perspective they lack relevance, which makes them uncommon and not easily included into the budget of a typical project. However, if these measurements are not available, a good understanding of the depositional and geological history of the basin combined with soft data, such as geophysical logs, evidence of drilling and borehole stability issues, and good judgment, can provide reasonable estimates of the in-situ state of stress without resorting to a probabilistic approach. Uncertainty associated with the type of boundary condition for reservoirs such as Weyburn is epistemic. Our understanding of stress changes during oil depletion is poor, our geomechanical models cannot handle the scale of the Weyburn pool, therefore simulations are made in small portions such as the nine-pattern area in Phase 1A where the boundaries of the model are embedded into the field and perhaps stresses at the boundaries evolve with pressure. Finally, uncertainty about geomechanical properties in theory could be handled probabilistically but this approach is beyond present computational capabilities, as each simulation can take long periods of time --each simulation at Weyburn took approximately 3 days of CPU time--.

11.3.4 Pre-CO2 Injection Performance Assessment

11.3.4.1 Scenario Analysis

Scenario analysis for geomechanical performance assessment has two goals: the identification of the possible geomechanical mechanisms that may affect the hydraulic integrity of the caprock system, and the construction of a realistic 3D geomechanical model with its appropriate boundary conditions and properties. The first step includes the identification of all possible geomechanical mechanisms that may affect hydraulic integrity. These mechanisms and their potential consequences are well known in geotechnical engineering and lately they have become more relevant in the oil industry. Unfortunately, these were often overlooked in the early stages of geological storage. Ranking of the processes is a common practice in scenario analysis, but the geomechanical mechanisms that may affect hydraulic integrity of bounding seals are explicitly included in reservoir and geomechanics simulators. Therefore all of these can be addressed precluding the need for such a ranking. Instead, the results of the modeling will provide a rank of these mechanisms to determine which ones are relevant in specific cases. These must be included in the safety and risk assessments. These mechanisms were presented and organized in an effective manner in Chapter 4.

The construction of the 3D geomechanical model is an iterative process because the characteristics of the caprock system at the time exploitation begins are poorly known. However, the characterization of the reservoir improves dramatically with development of the field because additional knowledge is gathered when more wells are drilled, and stimulation activities are undertaken to improve primary production. Initially a start-up model can be developed with the existing geological and hydrogeological models at both regional and reservoir scales, which is further populated with geomechanical properties gathered from both laboratory and field experiments, and soft data such as geophysical logs and literature reviews. This initial model will allow identifying gaps and formulating questions regarding the validity of model assumptions. Thus, Weyburn is a naturally fractured reservoir and questions such as "can fractures be present in the caprock and if so, are they conductive?" need to be addressed.

This leads to the need to integrate logically the relevant information available into the mechanical earth model (MEM). This model is not simply the amalgamization of existing information, but it has to 'put the pieces of the puzzle together', i.e. the widespread evidence of similar fractures in the Williston Basin indicates a similar mechanism of fracturing. On the other hand, the regional hydrogeological studies show no evidence of cross flow through major aquitards and, while at first glimpse these two observations appear to be contradictory, geomechanical considerations such as the mechanism of formation of the fractures can explain why fracturing is observed presently in certain formations, or how geochemical processes may have self-healed some of these formations. Moreover, uncertainty needs to be addressed because in projects of this type and magnitude it is not uncommon to find large sources of uncertainty. One of those uncertainties at Weyburn is the in-situ stress state. There are no field measurements available, but a global understanding of the stress field is gathered from its geological and tectonic history, and that combined with data from nearby reservoirs and soft data such as the presence of strike-slip faults can be used to bound the state of stresses. Nonetheless, alternative scenarios with different in-situ stresses or geomechanical properties are built for further analysis to bound the analysis deterministically and carry out a sensitivity analysis.

11.3.4.2 Model Development

Once the base case and alternative scenarios are developed, model development is the next step for performance assessment. The generic methodology includes conceptual model development, validation of the models, and the actual numerical modeling. However, as was mentioned previously, the use of commercial validated software shifts the focus of this step towards numerical modeling. EOR-CO_2 projects have a long history and it is expected that the boundaries of the field are well-defined. Its geometry is known and whether there is any evidence of geomechanical activity in the way of subsidence/heave, wells sheared after completion and even in some cases seismicity. Consequently, it will be fairly easy to identify which approach modeling shall take; i.e., Weyburn is a very large field surficially, but thin, where neither subsidence/heave or borehole stability issues have been observed. Therefore an explicit approach would be able to provide useful results and take advantage of the existing history match. On the other hand fields where geomechanical activity has been observed would require an iterative or implicit approach depending on the tools available and the magnitude and frequency of the geomechanical events.

An issue with these simulations in 'geomechanically inactive' fields such as Weyburn, is their calibration and validation. Monitoring instrumentation for deformation or seismic activity is installed as a response to problems encountered during production in oil fields, and otherwise it would never be in place. Therefore, at least in the early stages of geological storage, the installation of monitoring wellbores with tiltmeters and geophones, and in-situ stress measurements at different reservoir pressures are necessary to build confidence in our performance predictions.

11.3.4.3 Evaluation Against Performance Criteria-Scenario Adjusment

Finally, the results of scenario development and numerical modeling lead to the scenarios that will be used to carry out the short-term performance assessment. These analyses of Weyburn lead to the conclusion that the hydraulic integrity of the reservoir has been preserved during exploitation and production of the field pre-CO_2 injection. Therefore, it was not necessary to adjust the existing scenarios and it was possible to proceed with the short-term performance assessment. However, in other cases it is possible that the hydraulic integrity of the reservoir may have been affected, and the scenarios need it to be adjusted either by changing the mechanical or hydraulic properties or developing new scenarios; i.e., if the caprock was significantly affected, the scenario of a reservoir with a leaky caprock would have to be considered for the safety and risk assessment of the Weyburn Project, and the geomechanical properties of the caprock system would need adjustment for the remainder of the geomechanical performance assessment. While this has to be an alternative scenario considering the 'belts and suspenders' approach, it may have become the base case scenario and it might even threaten the viability of the project.

11.3.5 Short-Term Performance Assessment

11.3.5.1 Scenario Analysis

The short-term performance assessment takes the final results from the pre-CO_2 injection performance assessment as scenarios, with the adjustments that were considered necessary. There is no scenario analysis per se for this step in the performance assessment but involves either an adjustment of the existing scenarios or change in their ranking. However monitoring and verification may provide new insights into the features of the system and the scenarios may need to be adjusted to reflect this new reality.

11.3.5.2 Model Development

Here both reservoir simulation and geomechanical simulations have to move together because more than performance assessment is driving these simulations, but also optimization of both the EOR process and the volume of CO_2 stored. At Weyburn the modeling work lead to the conclusion that hydraulic fracturing is going to be the controlling mechanism once EOR stops in order to store the maximum possible volume of CO_2. Therefore, a combined effort between geomechanics and reservoir simulation may lead to an adjustment of the field operations to raise the pressures uniformly throughout the field. However, such integration was not achieved in this thesis because the reservoir simulations were still ongoing when the geomechanical simulations were nearing completion. The issue of calibration and validation is as relevant here as it is in the pre-CO2 injection performance assessment, and it can be considered the 'weakest link' of geomechanical performance assessment because usually there are not enough measurements to validate geomechanical simulations.

11.3.5.3 Evaluation Against Performance Criteria

The final results of this analysis will be used as input for both the performance assessment of the overburden and the safety assessment. Thus, the results in Weyburn showed that shear failure would not occur during CO_2 injection. Consequently, in the safety assessment the caprock must be considered as a competent seal for the stored CO_2, and the likelihood of having a leaky caprock is low. These two conclusions are very important for the risk assessment, which eventually will be presented in terms of volumes of CO_2 reaching the biosphere and its consequences.

11.3.5.4 Monitoring and Verification

Due to the multiple uncertainties and novelty of geological storage projects, the short-term performance assessment must be complemented by monitoring in an iterative process combined to either verify or adjust the performance predictions. This will be the focus of the second phase of the Weyburn project that will begin in late 2005. The information that will be gathered will be used to adjust and calibrate the flow and geological models available, especially at the reservoir scale, and this may lead to adjustment of the short-term geomechanical performance assessment of the caprock system. Moreover, if new evidence that contradicts the existing MEM is produced, it is likely that the whole process may need to be repeated using the new information available.

Nonetheless, the results from seismic and geochemical monitoring indicate so far that CO_2 is effectively being contained by the caprock system, and that it is not unrealistic to think of CO_2 as permanently stored (early estimates of leakage indicate that less than 3% of the CO_2 injected will leak out in the next 5000 years) [25].

11.3.6 Long-Term Performance Assessment

The last step in the geomechanical performance assessment is its long-term stability against specific phenomena or events, which can be affected by geomechanical phenomena such as tectonic activity, mining induced effects or salt dissolution. Usually this analysis is more of qualitative in nature as uncertainties are large. If numerical modeling is carried out, the models used are simple representations of the scenarios used for more complex performance assessments. Thus, at Weyburn salt dissolution is an existing possibility that was addressed through geomechanical modeling in Chapter 9. A simplified version of the MEM developed in Chapter 7 was used for the analysis. The results from the modeling were more of a qualitative nature, a defined set of conditions in which salt dissolution can affect the hydraulic integrity of the caprock system was established. This analysis needs to be complemented by a better understanding of the geological conditions that trigger dissolution at Weyburn, and the likelihood that dissolution will occur in the future.

11.4 Geomechanical Performance Assessment of Weyburn

11.4.1 Scenario Analysis

Scenario analysis starts with a FEP analysis, where FEPs are identified, classified, ranked and screened to build the scenarios, and it is followed by the development of a 3D geomechanical model. At Weyburn this was accomplished by:

- Processes or mechanisms that may affect the hydraulic integrity of the caprock system were identified in Chapter 4. These mechanisms are generic to any geological storage project, and can be addressed by fluid flow and deformation models.
- The features of the caprock system were evaluated from the geological and hydrogeological models that were developed as part of the project. Mechanical testing on Weyburn's caprock, soft data such as geophysical logs, basin scale information, and literature reviews complemented this information. This information was assembled together in a MEM which lead to a base case scenario and alternative scenarios.
- Events such as salt dissolution were recognized early on in the project, and were addressed through the use of simplified scenarios.

11.4.2 Uncertainty

Uncertainty was handled deterministically as explained previously. Therefore, a set of scenarios with different features such as different stress states and geomechanical properties were developed to find bounding limits in the performance of the caprock system that would help to build confidence in the results. Conservative values were used for both elastic and mechanical properties. Mechanical properties, as long as the values are realistic, can be adjusted by tweaking the values of the Geological Strength Index (GSI) in the Hoek-Brown failure criterion. On the other hand, the project would have benefited immensely if in-situ stress measurements were available. However, its relevance to examining the soundness of performance assessment was not well recognized in the first phase of the Weyburn Project but there is potential to measure in-situ stresses in the final phase of the project.

11.4.3 Model Development

The model development focused on modeling of the multiple scenarios developed and interpretation of results. An explicit approach was considered as the most beneficial for the project because the resources to carry it out were available, it was technically sound (see Chapter 8), it was the quickest approach and it did not require any model or software validation. The results prove that hydraulic fracturing is the primary potential mechanism of failure within the caprock at Weyburn, that almost 50 years of reservoir exploitation and production did not affect the hydraulic integrity of the caprock and salt dissolution is highly unlikely to affect the performance of the system. Deformations of the caprock system have been uniform throughout the reservoir, so their effect in wellbore integrity is expected to be minimal.

11.4.4 Compliance with Performance Criteria

A working criterion for geomechanical performance assessment of caprocks was developed in Chapter 3. Such criteria were met during the three stages of geomechanical performance assessment. Therefore, the Weyburn reservoir is considered as a safe sink for geological storage of CO_2 from a geomechanical perspective.

11.4.5 Implications for Weyburn's Risk Assessment

The caprock system is a safe and sound sink for CO_2 storage as long as injection pressures remain below minimum in-situ stress. However the in-situ stresses have not been measured so the risk assessment credibility would benefit from in-situ stress measurements that would provide operational limits as to the injection pressures. The likelihood of having an ineffective caprock is minimal as no evidence of conducting features was found before exploitation, and conducting features have likely not been induced during production as the geomechanical modeling showed. Therefore, while it is worth considering an ineffective caprock as a bounding case, the safety assessment simulations must have as an important component a low permeability continuous Midale Evaporite overlying the injection formations.

During the geological characterization carried out for this project only a strike-slip fault was found in the risk assessment area, but no faults where found in the Phase 1A area. The analysis for faults in a strike-slip regime in Chapter 8 showed that a fault would have to have a friction angle between 25 and 30° with no cohesion to reactivate at the actual pressures in the field. These values are around the lower limit of frictional strength for faults that have not gone through large displacement, and there is no evidence of large displacements in the fault present in the risk assessment area [189]. This fault is fairly distant from the injection area and the pressure changes must be substantially smaller near the fault. Consequently the likelihood of fault-reactivation-induced leakage is minimal at Weyburn.

Deformations in the caprock system are uniform through the payzone and caprock and consequently mechanically induced deformations at the caprock system do not affect wellbore integrity. Therefore, geomechanical wellbore integrity issues are limited to drilling and completion related effects that are beyond the scope of this thesis.

Salt dissolution, one of the alternative scenarios considered for risk assessment, was analyzed from a geomechanical perspective, and it was found that dissolution would have to occur within a kilometer of the reservoir to affect its hydraulic integrity. Therefore, with a proper understanding of how the CO_2 plume will migrate during the timeframe of the project (5000 years in Weyburn), it will be necessary to identify whether the geological conditions that may lead to salt dissolution are present in the area coved by the plume.

Finally thermal effects due to the injection of a cooler stream of CO_2 into the reservoir were considered. The geomechanical implications are the development of tensional stresses in both the reservoir and the caprock in thin reservoirs such as Weyburn. Therefore, Weyburn's caprock may underperform as a consequence of thermal induced fracturing. However, this scenario can only be validated by direct monitoring of temperatures inside the reservoir during CO_2 injection.

11.5 Summary

A methodology to carry out geomechanical performance assessments of caprock systems has been presented. This methodology is based on the experience gathered from the IEA Weyburn CO_2 Monitoring and Storage Project. The methodology is as general as possible in order to avoid the particularities of Weyburn affecing its application elsewhere. The methodology addresses the different phases a geomechanical performance assessment for CO_2-EOR projects must go through, how to carry out the scenario analysis and model development in each phase and how to manage uncertainty. A brief summary of the main findings in each phase at Weyburn is presented and its implications for risk assessment.

11.6 Figures

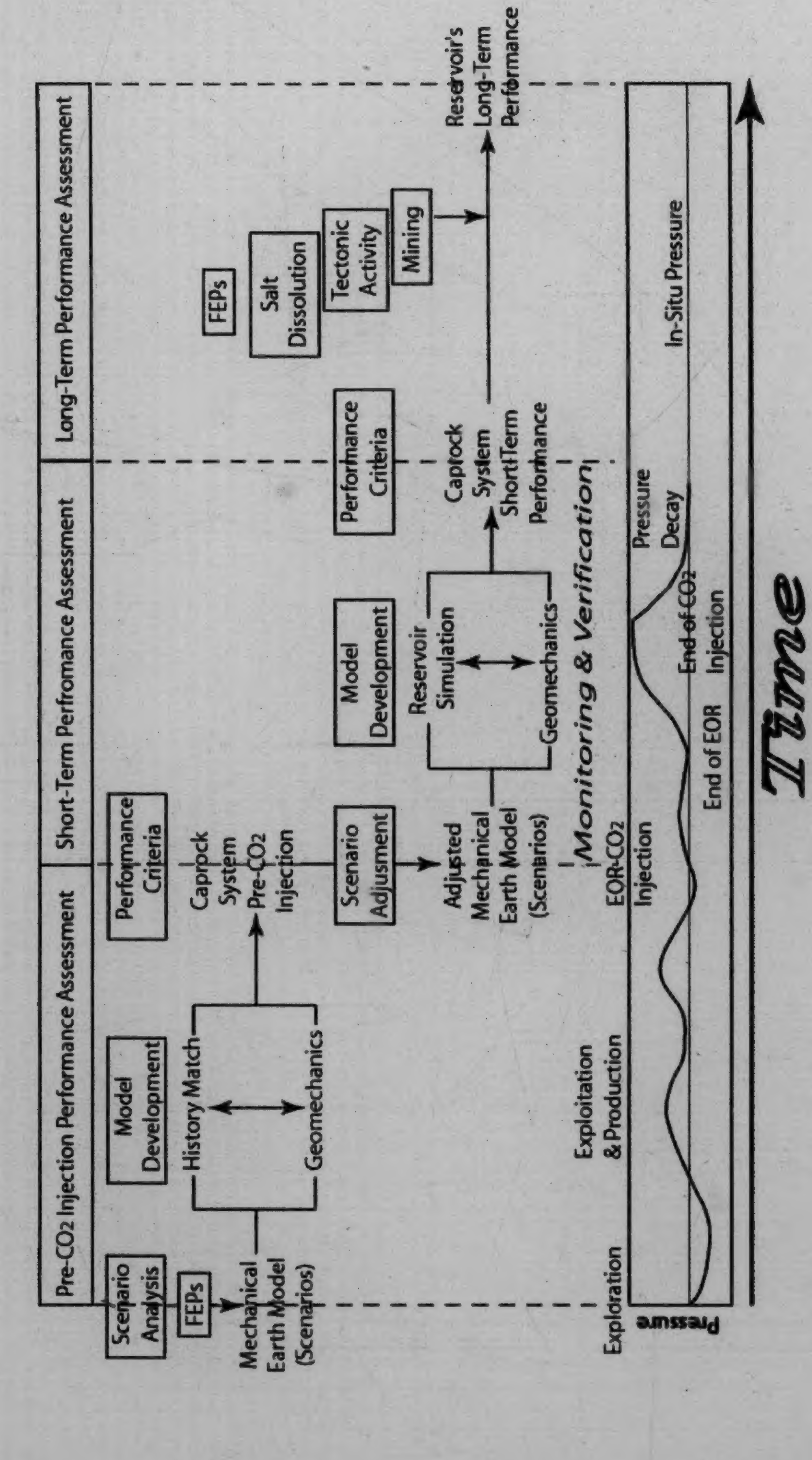
Pre-CO2 Injection Performance Assessment
Short-Term Perfromance Assessment
Long-Term Performance Assessment
Scenario Analysis
FEPs
Mechanical Earth Model (Scenarios)
Model Development
History Match
Geomechanics
Performance Criteria
Caprock System Pre-CO2 Injection
Scenario Adjusment
Adjusted Mechanical Earth Model (Scenarios)
Model Development
Reservoir Simulation
Geomechanics
Performance Criteria
Caprock System Short-Term Performance
FEPs
Salt Dissolution
Tectonic Activity
Mining
Reservoir's Long-Term Performance
Monitoring & Verification
Exploration
Exploitation & Production
EOR-CO2 Injection
End of EOR
End of CO2 Injection
Pressure Decay
In-Situ Pressure
Pressure
Time

Figure 11-1. Methodology to assess the geomechanical performance of caprock system in CO_2-EOR storage projects

12 Conclusions and Recommendations

12.1 Summary

The natural greenhouse effect is a well-understood phenomenon where gases such as methane, ozone, carbon dioxide, and water vapor contribute to the warming of the earth's atmosphere by absorbing and re-emitting the infrared or heat radiation. Among the different greenhouse gases CO_2 accounts for around 56% of the anthropogenic emissions, and although hotly debated, there is growing acceptance that increasing CO_2 emissions are contributing to the rise of global temperature. The possible consequences of such climate change are causing international concern.

Geological storage can serve a powerful role as an emissions reduction technology but the acceptance of this new "paradigm" will require a view of geological storage as safe and environmentally sound. Bounding seals and reservoir integrity as well as an adequate understanding of the possible leakage mechanisms through the caprock is one of the technical development issues of critical importance to the safe and effective implementation of geological storage. The IEA Weyburn CO_2 Monitoring and Storage Project presents an excellent opportunity to conduct a performance assessment of a caprock system overlying a large scale CO_2-EOR storage project.

In the short-term or injection stages the main trapping element is a competent caprock. The caprock will see large injected volumes of CO_2 that will dramatically increase near wellbore pressures, change the flow regime, the temperature, and the chemical environment in the sink. One primary concern in the short-term is the stability of the caprock seals, the integrity of the reservoir, and the sink reaction to a rapidly changing environment, which in turn affects their geomechanical, geochemical, and hydrogeological properties. Therefore, in the short-term the caprock and its performance assessment become critical to the successful implementation of geological storage of CO_2.

A performance assessment is analyses to predict the performance of a system or subsystem, followed by comparison of the results of such analyses with appropriate standards and criteria. A performance assessment of CO_2 sequestration consists of three major steps: scenario analysis, model development, and compliance with a working criteria.

From a performance assessment perspective there is a widespread view that depleted oil and gas reservoirs can be considered as safe sinks for geological storage of CO_2 because hydrocarbon reservoirs have existed within structural and stratigraphic traps over geological time and that this uniquely demonstrates their suitability for CO_2 storage. However, oil and gas reservoirs have usually undergone a variety of processes during primary recovery and may have been subjected to secondary and tertiary recovery processes. These reservoir production processes imply that the reservoir and the bounding sealing horizons (caprock) have undergone physical and/or chemical changes such as changes in in-situ effective stresses, consolidation, depressurization, repressurization and temperature. There are a number of distinctive geomechanical mechanisms that can affect the hydraulic integrity of caprocks, leading to leakage and/or failure of the seal. Effects of the initial massive injection can be classified as those that are storage-induced, and those that are storage-activated. Capillary leakage, hydraulic fracturing and shear deformation/fracturing of caprocks are considered as storage-induced; flow through faults, fractures and fissures are considered storage-activated. It is important to recognize in the case of disused oil and gas reservoir how the history of exploitation and production may trigger and/or affect these mechanisms, and lead to the loss of hydraulic integrity in bounding seals.

The hydro-mechanical coupling in both shales and anhydrites is strong; therefore new experimental facilities were developed for the hydro-mechanical testing of geomaterials at high pressures and temperatures. The system has proven capabilities of measuring a large range of permeabilities which can be as low as 10^{-21} m^2, and with future improvements in temperature control even lower permeabilities could be measured. The system can measure local strains with great accuracy and stability and it has the potential to measure seismic velocities axially and radially while shearing. Tests were carried out in the Midale Evaporite of the Weyburn field with mixed results as the new system produced results of excellent quality, but problems with infrastructure did not allow for a comprehensive testing program on this material.

A mechanical earth model (MEM) was developed for Weyburn Phase 1A. Generation of such a model reviewed and analyzed the geological, hydrogeological, geophysical and geomechanical information and models available. All this information was used to build a Base Case scenario and a set of Alternative scenarios to evaluate the geomechanical performance assessment of the caprock system for this CO_2-EOR storage project. Likewise the issue of fractures in the caprock was addressed, and it was proven that the presence of fractures in the Midale Evaporite was minimal to absent before exploitation and production of the field began.

The geomechanical modeling for the multiple scenarios developed for Weyburn indicate that the reservoir and its caprock are a safe and sound sink for geological storage as long as pressures are kept below hydraulic fracturing pressure, and no tensional stresses are induced due to the injection of CO_2 cooler than the reservoir temperature. The production from 1950's until now did not affect the hydraulic integrity of the caprock as the stresses remain below the damage threshold for hard rocks. Likewise, a methodology to evaluate the potential of fault reactivation for any stress regime was developed, which can be used for screening of faults in potential storage reservoirs.

The possibility of salt dissolution was addressed from a geomechanical perspective, and it was found that as long as dissolution does not occur within a kilometer of the reservoir its hydraulic integrity will not be affected.

Finally a methodology to carry out geomechanical performance assessments of caprock systems was presented. Such methodology was based on the experience gathered from the IEA Weyburn CO_2 Monitoring and Storage Project. The methodology addresses the different phases of a geomechanical performance assessment for CO_2-EOR projects must go through, how to carry out the scenario analysis and model development in each phase, and how to manage uncertainty.

12.2 Conclusions

Geological storage of CO_2 in disused oil and gas reservoirs is perhaps the most promising technique to reduce CO_2 emissions into the atmosphere because of the economic benefits that incremental oil recovery brings in a tight energy market. Besides, the possibility of a future trading carbon market is drawing the attention of industry and governments that are viewing CO_2 as a potential source of economic development. However, CO_2 storage as an option to manage CO_2 emissions and an economical commodity requires a scientific and technical framework to make it viable. Moreover, catastrophic releases of CO_2 can harm both humans and the ecosystem. Therefore, it is necessary to make CO_2 storage predictable to avoid any negative impacts on life or society and move ahead with a carbon market. Considering the risks to health, safety, the environment and economy, risk assessment and risk management programs are being implemented, and performance assessment is a vital component of these. In order to carry out risk assessment efficiently a CO_2 storage project has been divided in four basic components [40]:

- CO_2 containment zone consisting of the CO_2 reservoir and the overlying seal (caprock system).
- Overburden in between the containment zone and exposure zone.
- CO_2 exposure zone comprising the shallow saturated and undersaturated zone, fresh or marine surface water, and atmosphere.
- Preferential CO_2 migration paths like well zones or fault zones.

The performance assessment of the caprock system is critical as the public may oppose options where CO_2 remains underground but it migrates out of its primary sink, and any credits for CO_2 storage may be limited to CO_2 remaining in the injection horizon.

Leakage during the operational phase of a CO_2 storage facility may occur mainly through conducting features in its caprock, which will be storage-activated or storage-induced. Therefore, the hydromechanical behavior of the caprock system has to be included in the performance assessment of any geological storage project. In CO_2-EOR storage projects, oil and gas reservoirs have usually undergone a variety of processes during primary recovery and may have been subjected to secondary and tertiary recovery processes. These reservoir production processes imply that the reservoir and the bounding sealing horizons (caprock) have undergone physical and/or chemical changes such as in in-situ effective stresses, consolidation, depressurization, repressurization and temperature, which may affect its hydraulic integrity.

The IEA Weyburn CO_2 Monitoring and Storage Project is the first CO_2-EOR storage project in the world. It has offered a unique opportunity to address the geomechanical issues that these projects have. The results of the performance assessment carried out in this thesis can be used as a base for future CO_2-EOR storage projects. The most relevant findings of this geomechanical performance assessment were:

- Scenario analysis provides a valuable insight into the characteristics of the system, and is perhaps the most important step in performance assessment. The logical and congruent organization of the geoscience and engineering information, from a geomechanical perspective, collected during the lifetime of an oil or gas field can be achieved through a mechanical earth model, MEM. Such a model must include both regional and local data, a comprehensive understanding of the geology, structure and hydrogeology of the field, and a recognition of their impact in the hydraulic and mechanical properties of the caprock system. The development of a MEM helps to identify uncertainties and form hypotheses on the likely response of the system.
- Shales and anhydrites are the two most common caprocks in oil and gas fields worldwide. The coupling between hydraulic and mechanical response in both materials is strong but different. The mechanical properties of shales cover a large range, and their hydraulic properties are controlled by the presence of conductive discontinuities. These conductive discontinuities are usually of tectonic origin and their transport properties are a function of the acting effective stress and presence of cements. Moreover, when shales deform in a brittle manner, a distinctive shear plane develops where its particles are aligned in the

direction of displacement and permeability is enhanced by this new particle orientation and dilation. However, permeability is only enhanced by the full development of these shear planes. On the other hand, when shales deform in a ductile manner, there is no substantial change in their fabric and structure and permeability is not enhanced. The limit between brittle and ductile deformation is not clear and site specific hydro-mechanical testing is the best way to address this issue. Therefore, reservoirs capped by shales will require hydro-mechanical testing of caprock samples, and back calculation of caprock transport properties by hydrogeological modeling (which may identify the presence of conductive features).

- Anhydrites are medium to hard rocks, and shear failure is unlikely to occur during a geological storage project. However, permeability in hard rocks is enhanced through microfracturing as the rock is stressed beyond its damage threshold, which is different from the ultimate strength, and this threshold could be overcome during a typical geological storage project. Such thresholds can be found generically by unconfined compression tests, and there is no need to characterize the material fully as shales. However, more fundamental research in anhydrites is needed to establish the damage threshold and change in permeability before using a generic approach.

- The Weyburn Field is a sound and safe sink for geological storage of CO_2, whose hydraulic integrity was not affected by 50 years of oil production and stimulation. Hydraulic fracturing will control the volume of CO_2 that could potentially be stored in the field. Thus, it is likely that reservoirs that have gone through an aggressive production history such as Weyburn and have not experienced any geomechanical activity are limited in their capacity to store CO_2 by hydraulic fracture as long as large thermal stresses are not induced. However, geomechanical modeling must be carried out in any geological storage project as the results are influenced by the properties of the system, its geometry, production and injection schemes, gradients and in-situ stresses.

- In-situ stress measurements are perhaps the single most relevant parameter in a geomechanical performance assessment. In-situ stresses are not stationary as they change with pressure in oil and gas reservoirs and the state-of-the-art cannot predict accurately those changes. Moreover, it is clear that pressure depletion leads to a decrease in horizontal stresses, but it is not known whether these stresses fully recover after pressures come back to in-situ, and if these stresses keep increasing once pressures are above in-situ values. This question is very important from a performance assessment perspective because most CO_2-EOR storage projects have already gone through large pressure changes, and while it is common to find in the literature that the 'safe' thing to do is inject CO_2 up to the point where pressure is back to original in-situ values, the reality is that a large percentage of these fields have been or are at pressures larger than in-situ. Weyburn has been 'overpressured' for around 40 years and when CO_2 injection started, the average pressure in the field was 6 MPa above original in-situ pressure. This overpressuring was due to an aggressive waterflood, the most common enhanced recovery technique in oil fields. Therefore in-situ stress measurements should be mandatory as part of the approval process by the regulatory entity for any CO_2-EOR storage project.

- Salt dissolution is an alternative scenario for consideration in the long-term performance assessment of the Weyburn project. Geomechanical modeling of the dissolution processes showed how the existing dissolution features near the reservoir did not compromise the integrity of the reservoir. In addition, dissolution will likely only affect the hydraulic integrity of the reservoir if it occurs very close to the reservoir (within a kilometer) or below the reservoir itself. Therefore, dissolution is unlikely to disrupt the safety and robustness of the Weyburn field as storage site for CO_2, as dissolution has not occurred beneath the reservoir and the risk assessment area in recent geological times.
- The approach to modeling must be given by the experience with the field pre-CO_2 injection. Thus, if seismic activity, subsidence or wellbore shearing has been observed during the history of the field the modeling must be done by either iterative or fully coupled approaches. On the other hand, if the field has not shown any geomechanical activity (as in Weyburn), the modeling can be done using an explicit approach. However, there are still serious limitations as to the size of the model that can be handled efficiently with the present state-of-the-art.
- Fault reactivation can be easily screened initially using a poroelastic approach like the one presented in Chapter 8. However, this approach is a function of the stress regime, and the horizontal stresses change as pressure changes, so it requires in-situ stress measurements to be used with confidence. Moreover, stress reorientation due to faulting is common, so if CO_2 injection is occurring near the fault, or the change in pressure expected near the fault is large, in-situ stress measurements and numerical modeling must be done to address the issue of fault stability.

- Operational considerations at surface require a dense stream of CO_2, which is easily achieved by cooling off the CO_2. Upon injection it is unlikely that the CO_2 will reach the reservoir temperature and consequently thermal stresses will develop in the caprock system as it cools. The cooling of the reservoir lowers the total stresses in the reservoir and its bounding seals while the injection increases the pressure. Therefore, hydraulic fracturing migth occur in the reservoir, and in thin reservoirs such fracturing may propagate into the caprock affecting the hydraulic integrity of the caprock system. Hence, close monitoring of downhole injection temperatures and pressures is required to avoid the loss of hydraulic integrity during the injection of CO_2 at cooler temperatures than the in-situ temperature.

12.3 Recommendations and Future Work

This research has produced a series of questions that need to be addressed to further enhance geomechanical performance assessments and aid in developing safe and economic carbon capture and storage projects. Among the most relevant are:

- Groundbreaking work in the behavior of hard rocks has made it possible to identify the damage threshold of these materials, and permeability measurements in hard rocks have found that permeability is enhanced after damage. However, the amount of experimental results is not enough to quantify a relation between damage and permeability and how much the permeability increases, especially for anhydrites where the geomechanical information available altogether is scarce. Therefore more research in this area must be conducted as the damage threshold can easily be crossed during the lifetime of an oilfield and the permeability of the caprock may need to be adjusted for the safety assessment. Moreover, the criteria developed in Chapter 3 may require adjustment depending on the type and properties of the caprock.

- Laboratory testing in caprocks should include acoustic measurements as an indicator of damage that can be correlated with permeability measurements. Such measurements can be very useful if instrumented wells with geophones are installed in geological storage projects as part of monitoring and verification programs. This helps to build confidence in our predictions of caprock response during CO_2 injection. Moreover, the thermomechanical response and properties of anhydrites should be studied experimentally as there is no information available in the literature.

- Fundamental research as to how horizontal stresses change with pressure is needed, especially in reservoirs that have not undergone significant subsidence, as most of the existing evidence comes from chalk reservoirs that are not representative of most geomaterials. Moreover, the effects of depletion on vertical stresses, especially in anticlinal or domed reservoirs, are poorly understood and need to be considered for further research. This would not only benefit the area of geological storage but also the area of borehole stability in exploited fields, which has been very costly to the oil and gas industry.

- Phase II of the Weyburn project should have in-situ stress measurements as this is the only option to improve the geomechanical simulations, address with more confidence the issue of natural fractures in the reservoir, and build confidence in the risk assessment of the system.

- The fact that there were limitations with the maximum loads that could be applied with the equipment developed in this thesis leave room for a new set of experiments at higher pressures and stresses. Moreover, there is no experience with geomaterials and the effect of long-term CO_2 exposure on hydromechanical materials. Therefore hydromechanical testing using CO_2 at reservoirs conditions (pressure and temperature) as a fluid must be carried out.

- The performance criteria developed in this thesis needs to be refined through both modeling, and a more in depth review of the learning gathered in challenging hydrocarbon reservoirs from a geomechanical perspective. The modeling exercise can provide a valuable insight as to how reservoirs will responde to CO_2 injection under different conditions (stress field, material properties, temperature and pressure). In this case the use of 2D modeling is advised because it is more robust and efficient.

- More research and development is needed to be able to carry out geomechanical modeling in oil fields with the geometry of Weyburn, i.e. thin and long reservoirs. Presently the limitations in computational capabilities and more efficient solutions to geomechanical models is a limit as to how realistic a model can be built. Bearing that in mind, our present models provide a fair insight to the problems that are commonly faced in hydrocarbon geomechanics.

- There is the need to develop an implement more realistic, complex models that can handle different phenomena such as non-isothermal multiphase flow, flow in a discontinuous medium, and fracture initiation and propagation in a coupled approach.
- The cycle of pressurization and depressuriation of reservoirs causes consolidation and expansion of reservoirs over large periods of time. Therefore creep effects can play an important role in the evolution of the hydromechanical properties of caprocks. Consequently more fundamental research is needed to address this topic.

13 References

1. Hitchon, B., 1996. Aquifer Disposal of Carbon Dioxide : Hydrodynamic and Mineral Ttrapping - Proof of Concept. Geoscience Publishing Ltd., Sherwood Park, AB, 165 p.
2. Houghton, J.T., 1994. Global Warming: The Complete Briefing. Lion Publishing Inc., Oxford, England, 251 p.
3. Rochelle, C.A., Pearce, J.M., and Holloway, S., 1999. The underground sequestration of carbon dioxide: containment by chemical reaction in the deep geosphere. In: *Chemical containment of waste in the geosphere*. Ed: Metcalfe, R., Rochelle, C.A., and Geological Society of London. Geological Society special publication No. 157, London, p. 117-129.
4. Galley, J.E., 1968. Economic and industrial potential of geologic basins and reservoir strata. In: *Subsurface Disposal in Geologic Basins; a Study of Reservoir Strata*. Ed: Galley, J.E. AAPG Memoir 6, Tulsa, Okla., p. 1-10.
5. Galley, J.E., 1968. Subsurface Disposal in Geologic Basins; A Study of Reservoir Strata. AAPG Memoir 6, Tulsa, Okla., 253 p.
6. Warner, D.L., 1968. Subsurface disposal of liquid industrial wastes by deep-well injection. In: *Subsurface Disposal in Geological Basins; A Study of Reservoir Strata*. Ed: Galley, J.E. AAPG Memoir 6, Tulsa, Okla., p. 11-20.
7. Koide, H., Tazaki, Y., Noguchi, Y., Nakayama, S., Iijima, M., Ito, K., and Shindo, Y., 1992. Subterranean containment and long-term storage of carbon dioxide in unused aquifers and in depleted natural gas reservoirs. *Energy Conversion & Management*, **36**: 619-626.
8. Hangerbrauck, R.P., 1993. Technological considerations for planning the global carbon future. *Energy Conversion & Management*, **34**: 737-744.
9. Bachu, S., Gunter, W.D., and Perkins, E.H., 1996. Carbon dioxide disposal. In: *Aquifer Disposal of Carbon Dioxide : Hydrodynamic and Mineral Ttrapping - Proof of Concept*. Ed: Hitchon, B. Geoscience Publishing Ltd., Sherwood, AB, p. 11-22.
10. United States Department of Energy, 1999. Carbon Sequestration Research and Development. U.S. Government Printing Office, Washington, DC, 250 p.
11. Bachu, S., Gunter, W.D., and Perkins, E.H., 1994. Aquifer disposal of CO_2: hydrodynamic and mineral trapping. *Energy Conversion & Management*, **35**: 269-279.
12. Benson, S., Gasperikova, E., and Hoversten, M., 2004. Overview of Monitoring Techniques and Protocols for Geological Storage Projects. Lawrence Berkeley National Laboratory, Berkeley, 89 p.
13. Gunter, W.D., Wiwchar, B., and Perkins, E.H., 1997. Aquifer disposal of CO2 rich greenhouse gases: extension of the time scale of experiment for CO2 sequestration reactions by geochemical modelling. *Mineralogy and Petrology*, **59**: 121-140.
14. Jimenez, J.A. and Chalaturnyk, R.J., 2002. Integrity of bounding seals for geological storage of greenhouse gases. In: *SPE/ISRM Rock Mechanics Conference*. Irving, Texas, SPE 78196.
15. Jimenez, J.A. and Chalaturnyk, R.J. 2003. Are disused hydrocarbon reservoirs safe for geological storage of CO_2? In: *Greenhouse Gas Control Technologies*. Ed. Gale, J. and Kaya, J. Elsevier Science Ltd., Kyoto, Japan, p. 471-476.

16. Bachu, S., 2000. Sequestration of CO_2 in geological media: criteria and approach for site selection in response to climate change. *Energy Conversion & Management*, **41**: 953-970.

17. Fisher, Q., Harris, S.D., McAllister, E., Knipe, R.J., and Bolton, A., 2001. Hydrocarbon flow across faults by capillary leakage revisited. *Marine and Petroleum Geology*, **18**: 251-257.

18. Herzog, H.J., 2001. What future for Carbon capture and sequestration? *Environmental Science & Technology*, **7**: 148-153.

19. Holloway, S., 1997. Safety of the underground disposal of carbon dioxide. *Energy Conversion & Management*, **38**: S241-S245.

20. Gunter, W.D., Bachu, S., Law, D.H.-S., Marwaha, V., Drysdale, D.L., MacDonald, D.E., and McCann, T.J., 1996. Technical and economic feasibility of CO_2 disposal in aquifers within the Alberta sedimentary basin, Canada. *Energy Conversion & Management*, **37**: 1135-1142.

21. Holloway, S., Heederik, J.P., Van de Meer, L.G., Crenichowski-Lauriol, I., Harrison, R., Linderberg, E., Summerfield, I.R., Rochelle, C.A., Schwarzkopf, T., Kaarstad, O., and Berger, B., 1996. The Underground Disposal of Carbon Dioxide Summary Report, Joule II. British Geological Survey, Keyworth, Nottingham, 24 p.

22. Adam, D., 2001. The North Sea bubble. *Nature*, **411**: 519.

23. Korbol, R. and Kaddour, A., 1995. Sleipner Vest CO_2 disposal injection of removed CO_2 into the Utsira formation. *Energy Conversion & Management*, **36**: 509-512.

24. Bachu, S., Brulotte, M., Grobe, M., and Stewart, S., 2000. Earth Sciences Report 2000-11: Suitability of the Alberta Subsurface for Carbon Dioxide Sequestration in Geological Media. Alberta Energy and Utilities Board, Alberta Geological Survey, Edmonton, 86 p.

25. Chalaturnyk, R.J., Zhou, W., Stenhouse, M., Sheppard, M., and Walton, F., 2004. Theme 4: Long-Term Risk Assessment of the Storage Site. In: *IEA GHG Weyburn CO_2 Monitoring & Storage Project Summary Report 2000-2004*. Ed: Monea, M. 211-245.

26. White, D.J., Hirsche, K., Davis, T., Hutcheon, I., Adair, R., Burrowses, G., Graham, S., Bencini, R., Majer, E., and Maxwell, S.C., 2004. Theme 2: Prediction and Monitoring of CO_2 Movements. In: *IEA GHG Weyburn CO_2 Monitoring & Storage Project Summary Report 2000-2004*. Ed: Wilson, M.A. and Monea, M. PTRC, Regina, p. 73-148.

27. Law, D.H.-S., Huang, S., Freitag, N., Perkins, E.H., Wassmuth, F., Dunbar, B., and Asghari, K., 2004. Theme 3: CO_2 Storage Capacity and Distribution Predictions and the Application of Economic Limits. In: *IEA GHG Weyburn CO_2 Monitoring & Storage Project Summary Report 2000-2004*. Ed: Wilson, M.A. and Monea, M. PTRC, Regina, p. 149-209.

28. Burrowes, G., 2001. Investigating CO_2 storage potential of carbonate rocks during tertiary recovery from a billion barrel oil field, Weyburn, Saskatchewan: Part 2 - reservoir geology (IEA Weyburn CO_2 Monitoring and Storage Project). In: *Summary of Investigations 2001*. Ed: Saskatchewan Geological Survey. Saskatchewan Energy Mines, Saskatchewan, p. 64-71.

29. Whittaker, S.G. and Rostron, B. 2003. Geologic storage of CO_2 in a carbonate reservoir whitin the Williston Basin, Canada: An update. In: *Greenhouse Gas Control Technologies*. Ed. Kaya, J. Elsevier Science Ltd., Kyoto, Japan, p. 385-390.

30. Morgenstern, N.R., 2000. Performance in geotechnical practice. Hong Kong Institution of Engineers, Hong Kong, 15 p.

31. NEA/OECD, 1991. Review of Safety Assessment Methods. OECD, Paris, 75 p.

32. NEA/OECD, 1992. Systematic Approaches to Scenario Development. OECD, Paris, 73 p.

33. NEA/OECD, 1996. Radioactive Waste Management in Perspective. OECD, Paris, 142 p.

34. Ewing, R.C., Tierney, M.S., Konikov, L.F., and Rechard, R.P., 1999. Performance Assessments of Nuclear Waste Repositories: A Dialogue on Their Value and Limitations. *Risk Analysis*, **19**: 933-958.

35. Chalaturnyk, R.J., 2004. Performance assessment of geological storage projects. 23 p.

36. Helton, J.C., Anderson, D.R., Basabilvazo, G., Jow, H.-N., and Marietta, M.G., 2000. Summary discussion of the 1996 performance assessment for the Waste Isolation Pilot Plant. *Reliability Engineering and System Safety*, **69**: 437-451.

37. Standards Australia, 2004. HB 436:2004 Risk Management Guidelines: A Companion to AS/NZS 4360:2004. Australia, 116 p.

38. Wildenborg, T., Leijnse, T., Kreft, E., Nepveu, M., and Obdam, A. 2004. Long-term safety assessment of CO_2 storage: The scenario approach. In: *Seventh International Conference of Greenhouse Gas technologies*. Ed. Wilson, M.A., Gale, J., Rubin, E.S., Keith, D.W., Gilboy, C.F., Morris, T., and Thambimuthu, T. Elsevier Science Ltd, Vancouver, B.C., p. 1263-1267.

39. Kreft, E., Egberts, P., Wildenborg, T., and van Bergen, F., 2004. Risk assessment using FEPs. In: *TNO-NITG Information*, Number of 12-14 p.

40. Leijnse, T., Wildenborg, T., Nepveu, M., and Obdam, A., 2004. Safety assessment methodology for underground CO_2 sorage emerging. In: *TNO-NITG Information*, Number of 1-4 p.

41. Morgenstern, N.R. 1994. The observational method in environmental geotechnics. In: *1st International Conference on Environmental Geotechnics*. Ed. Carrier, W.D. Edmonton, Alberta, p. 963-976.

42. Peck, R.B., 1969. Advantages and limitations of the observational method in applied soil mechanics. *Geotechnique*, **19**: 171-187.

43. Vick, S.G., 2002. Degrees of Belief: Subjective Probability and Engineering Judgment. ASCE Press, Reston, Virginia, 455 p.

44. National Research Council, 1990. Rethinking High-Level Radioactive Waste Disposal. National Academy Press, Washington, 46 p.

45. Jarrell, P.M., Fox, C.E., Stein, M.H., and Webb, S.L., 2002. Practical Aspects of CO_2 Flooding. SPE, Richardson, Texas, 220 p.

46. Pruess, K. and Garcia, J., 2002. Multiphase flow dynamics during CO_2 disposal into saline aquifers. *Environmental Geology*, **42**: 282-295.

47. Darby, D., Haszeldine, R.S., and Couples, G.D., 1996. Pressure cells and pressure seals in the UK Central Graben. *Marine and Petroleum Geology*, **13**: 865-878.

48. Bredehoeft, J.D., Wesley, J.B., and Fouch, T.D., 1994. Simulations of the the origin of fluid pressure, fracture generation, and the movement of fluids in the Uinta Basin, Utah. *AAPG*, **78**: 1729-1747.

49. McPherson, B.J.O.L. and Bredehoeft, J.D., 2001. Overpressures in the Uinta basin, Utah: Analysis using three-dimensional basin evolution model. *Water Resources Research*, **37**: 857-871.

50. Caillet, G., 1993. The caprock of the Snorre Field, Norway: A possible leakage by hydraulic fracturing. *Marine and Petroleum Geology*, **10**: 42-50.

51. Leith, T.L., Kaarstad, I., Connan, J., Pierron, J., and Caillet, G., 1993. Recognition of caprcok leakage in the Snorre Field, Norwegian North Sea. *Marine and Petroleum Geology*, **10**: 29-41.

52. Capuano, R.M., 1993. Evidence of fluid flow in microfractures in geopressured shales. *AAPG*, **77**: 1303-1314.

53. Wensaas, L., Shaw, H.F., Gibbons, K., Aagaard, P., and Dypvik, H., 1994. Nature and causes of overpressuring in mudrocks of the Gullfaks area, North Sea. *Clay Minerals*, **29**: 439-449.

54. Grauls, D.J. and Baleix, J.M., 1994. Role of overpressures and in-situ stresses in fault-controlled hydrocarbon migration: A case study. *Marine and Petroleum Geology*, **11**: 734-742.

55. Finkbeiner, T., Zoback, M., Flemings, P., and Stump, B., 2001. Stress pore pressure, and dynamically constrained hydrocarbon columns in the South Eugene Island 330 field, northern Gulf of Mexico. *AAPG*, **85**: 1007-1031.

56. Araktingi, R.E., Benefield, M.E., Bessenyei, Z., Coats, K.H., and Tek, M.R., 1984. Leroy Storage Facility, Uitna County, Wyoming: A case of attempted gas-migration control. *Journal of Petroleum Technology*, **46**: 132-140.

57. Eresman, R.K., Grant, R.A., and Mungan, N., 1990. Suffield Upper Mannville I Gas Storage Project. In: *65th Annual Technical Conference and Exhibition of the SPE*. New Orleans, SPE 20767.

58. Knepper, G.A., 1997. Underground storage operations. *Journal of Petroleum Technology*, **49**: 1112-1114.

59. Benson, S., Hepple, R., Apps, J., Tsang, C.F., and Lippmann, M., 2002. Comparative Evaluation of Risk assessment, Management and Mitigation Approaches for deep Geologic Storage of CO_2. E.O. Lawrence Berkeley National Laboratory, 133 p.

60. NEA/OECD, 1998. Water-Conducting Features in Radionuclide Migration. OECD, Barcelona, 376 p.

61. Howard, B.A., Crawford, M.B., Galson, D.A., and Marietta, M.G., 2000. Regulatory basis for the Waste Isolation Pilot Plant performance assessment. *Reliability Engineering and System Safety*, **69**: 109-127.

62. Peck, R.B., 1980. "Where has all the judgment gone?" *Canadian Geotechnical Journal*, **17**: 584-590.

63. Whitman, R.V., 1984. Evaluating calculated risk in geotechnical engineering. *Journal of the Geotechnical Engineering Division, ASCE*, **110**: 145-188.

64. IEA, 2000. Barriers to Overcome in Implementation of CO_2 Capture and Storage in Disused Oil and Gas Fields. IEA, 116 p

65. Jimenez, J.A. and Chalaturnyk, R.J. 2001. Geomechanical Behaviour of Stiff Clays and Mudstones as Caprocks for Geological Sequestration of CO_2. In: *2001 an Earth Odyssey: 54th Canadian Geotechnical Conference*. Ed. CGS. Calgary, AB, p. 7.

66. Rostron, B.J., 1993. Numerical simulations of how cap-rock properties can control differential entrapment of oil. In: *68th Annual Technical Conference and Exhibition of the Society of Petroleum Engineering*. Houston, Texas, SPE 26442.

67. Corcoran, D.V. and Doré, A.G., 2002. Top seal assessment in exhumed basin settings - some insights from Atlantic Margin and borderland basins. In: *Hydrocarbon Seal Quantification*. Ed: Norwegian Petroleum Society Special Publication No. 11. Norwegian Petroleum Society, Oslo, p. 89-107.

68. Watts, N.L., 1987. Theoretical aspects of cap-rock fault seals for single- and two-phase hydrocarbon columns. *Marine and Petroleum Geology*, **4**: 274-307.

69. Hildenbrand, A. and Kroos, B.M., 2003. CO_2 migration processes in argillaceous rocks: pressure-driven volume flow and diffusion. *Journal of Geochemical Exploration*, **79**: 169-172.

70. Dong, M., Nickel, E.H., Zhang, P., and Huang, S., 2004. Influence of CO_2/Brine Interfacial Properties on the Long-Term fate of CO_2 Injected into Weyburn Reservoir. IEA Weyburn CO_2 Monitoring and Storage Project, 12 p.

71. Neuzil, C.E. and Belitz, K. 1996. Fracture control of the hydrology of the North American Midcontinental Cretaceous Shales. In: *Fluid Flow Through Faults and Fractures in Argillaceous Formations*. Ed. NEA/EC. Berne, Switzerland, p. 157-162.

72. Boisson, J.-Y., Bertrand, L., Heitz, J.-F., and Moreau-Le Golvan, Y., 2001. In situ and laboratory investigations of fluid flow through an argillaceous formation at different scales of space and time, Tournemire tunnel, southern France. *Hydrogeology Journal*, **9**: 108-123.

73. Bossart, P., Meier, P.M., Moeri, A., Trick, T., and Mayor, J.C., 2002. Geological and hydraulic characterisation of the excavation disturbed zone in the Opalinus Clay of the Mont Terri Rock Laboratory. *Engineering Geology*, **66**: 19-38.

74. Gautschi, A. 2001. Self-sealing faults in the Opalinus clay – Evidence from field observations, hydraulic testing and porewater chemistry. In: *Self-Healing Topical Session*. Ed. NEA/RWM, Nancy-France, p. 27-30.

75. Gautschi, A., 2001. Hydrogeology of a fractured shale (Opalinus Clay): Implications for deep geological disposal of radioactive wastes. *Hydrogeology Journal*, **9**: 97-107.

76. Bolton, A. and Maltman, A., 1998. The importance of overpressure timing and permeability evolution in fine-grained sediments undergoing shear. *Journal of Structural Geology*, **20**: 1013-1022.

77. Gutierrez, M., Oino, L.E., and Nygard, R., 2000. Stress-dependent permeability of a de-mineralised fracture in shale. *Marine and Petroleum Geology*, **17**: 895-907.

78. Schulze, O., Popp, T., and Kern, H., 2001. Development of damage and permeability in deforming rock salt. *Engineering Geology*, **61**: 163-180.

79. Cosgrove, J.W., 2001. Hydraulic fracturing during the formation and deformation of a basin: A factor in the dewatering of low permeability sediments. *AAPG*, **85**: 737-748.

80. Ruistuen, H., Teufel, L.W., and Rhett, D.W., 1999. Influence of reservoir stress path on deformation and permeability of weakly cemented sandstone reservoirs. *SPE Reservoir Evaluation & Engineering*, **2**: 266-272.

81. Teufel, L.W., Rhett, D.W., and Farrell, H.E. 1991. Effect of reservoir depletion and pore pressure drawdown on in situ stress and deformation in the Ekofisk Field, North Sea. In: *Rock Mechanics as a Multidisciplinary Science*. Ed. Roegiers, J.-C. Balkema, Norman, Okla., p. 63-72.

82. Hamilton, J.M., Maller, A.V., and Prins, M.D. 1992. Subsidence-induced shear failures above oil and gas reservoirs. In: *Rock Mechanics Contributions and Challenges*. Ed. Hustrulin, W.A. and Johnson, C.A. A.A. Balkema, Golden, Colorado, p. 273-282.

83. Sperrevik, S., Gillespie, P.A., Fisher, Q.J., Halvorsen, T., and Knipe, R.J., 2002. Empirical estimation of fault rock properties. Hydrocarbon Seal Quantification. In: *Hydrocarbon Seal Quantification*. Ed: Norwegian Petroleum Society Special Publication No. 11. Norwegian Petroleum Society, Oslo, p. 109-125.

84. Sibson, R.H., 1990. Conditions for fault-valve behavior. In: *Deformation Mechanisms, Rheology and Tectonic*. Ed: Knipe, R.J. and Rutter, E.H. Geological Society, London, p. 15-28.

85. Grunau, H.R., 1987. A worldwide look at the caprock problem. *Journal of Petroleum Technology*, **10**: 245-266.

86. Dusseault, M.B., Bruno, M.S., and Barrera, J., 1998. Casing shear: causes, cases, cures. In: *SPE International Oil and Gas Conference and Exhibition*. Beijing, SPE 72060.

87. Bruno, M.S., 2001. Geomechanical analysis and decision analysis for mitigating compaction related casing damage. In: *SPE Annual Technical Conference and Exhibition*. New Orleans, Louisiana, SPE 71696.

88. Hart, D.J. and Wang, H.F., 2001. A single test method for determination of poroelastic constants and flow parameters in rocks with low hydraulic conductivities. *International Journal of Rock Mechanics & Mining Sciences*, **38**: 577-583.

89. Mitchell, J.K., 1993. Fundamentals of Soil Behavior. J. Wiley & Sons, 437 p.

90. Olsen, H.W., Morin, R.H., and Nichols, R.W. 1988. Flow pump applications in triaxial testing. In: *Advanced Triaxial Testing of Soil and Rock*. Ed. Donaghe, R.T., Chaney, R.C., and Marshall, L. ASTM, Philadelphia, p. 68-81.

91. Morin, R.H. and Olsen, H.W., 1987. Theoretical analysis of the transient pressure response from a constant rate hydraulic conductivity test. *Water Resources Research*, **23**: 1461-1470.

92. Esaki, T., Zhang, M., Takeshita, A., and Mitani, Y., 1996. Rigorous theoretical analysis of a flow pump permeability test. *Geotechnical Testing Journal*, **19**: 241-246.

93. Zhang, M., Esaki, T., Olsen, H.W., and Yasuhiro, M., 1997. Integrated shear and flow parameter measurement. *Geotechnical Testing Journal*, **20**: 296-303.

94. Brace, W.F., Walsh, J.B., and Frangos, W.T., 1968. Permeability of granite under high pressure. *Journal of Geophysical Research*, **73**: 2225-2236.

95. Lin, W., 1982. Parametric analysis of the transient method of measuring permeability. *Journal of Geophysical Research*, **87**: 1055-1060.

96. Trimmer, D.A., Bonner, B., Heard, H.C., and Duba, A., 1980. Effect of pressure and stress on water transport in intact and fractured gabbro and granite. *Journal of Geophysical Research*, **85**: 7059-7071.

97. Hsieh, P.A., Tracy, J.V., Neuzil, C.E., Bredehoeft, J.D., and Silliman, S.E., 1981. A transient laboratory method for determining the hydraulic properties of 'tigth' rocks - I. Theory. *International Journal of Rock Mechanics & Mining Sciences*, **18**: 245-252.

98. Neuzil, C.E., Cooley, C., Silliman, S.E., Bredehoeft, J.D., and Hsieh, P.A., 1981. A transient laboratory method for determining the hydraulic properties of 'tigth' rocks - II. Application. *International Journal of Rock Mechanics & Mining Sciences*, **18**: 253-258.

99. Kranz, R.L., Saltzman, J.S., and Blacic, J.D., 1990. Hydraulic diffusivity measurements on laboratory rock samples using an oscillating pore pressure method. *International Journal of Rock Mechanics & Mining Sciences*, **27**: 345-352.

100. Fischer, G.J. and Paterson, M.S., 1992. Measurement of permeability and storage capacity in rocks during deformation at high temperature and pressure. In: *Fault Mechanics and Transport Properties of Rocks*. Ed: Evans, B. and Wong, T.-f. Academic Press, San Diego, p. 213-252.

101. Fischer, G.J., 1992. The determination of permeability and storage capacity: Pore pressure oscillation method. In: *Fault Mechanics and Transport Properties of Rocks*. Ed: Evans, B. and Wong, T.-f. Academic Press, San Diego, p. 187-211.

102. Zhang, M., Takahashi, M., Morin, R.H., and Esaki, T., 2000. Evaluation and application of the transient-pulse technique for determining the hydraulic properties of low-permeability rocks—part 1: theoretical evaluation. *Geotechnical Testing Journal*, **23**: 83-90.

103. Zhang, M., Takahashi, M., Morin, R.H., and Esaki, T., 2000. Evaluation and application of the transient-pulse technique for determining the hydraulic properties of low-permeability rocks—part 2: experimental application. *Geotechnical Testing Journal*, **23**: 91-99.

104. Brace, W.F., 1980. Permeability of crystalline and argillaceous rocks. *International Journal of Rock Mechanics & Mining Sciences*, **17**: 241-251.

105. Trimmer, D.A., 1981. Design criteria for laboratory measurements of low permeability rocks. *Geophysical Research Letters*, **8**: 973-975.

106. Walder, J. and Nur, A., 1986. Permeability measurement by the pulse-decay method: effects of poroelastic phenomena and non-linear pore pressure difusion. *International Journal of Rock Mechanics & Mining Sciences*, **23**: 225-232.

107. Johnston, I.W. and Novello, E.A. 1993. Soft rocks in the geotechnical spectrum. In: *Geotechnical Engineering of Hard Soils - Soft Rocks*. Ed. Anagnostopoulos, A., Schlosser, F., Kaltteziotis, N., and Frank, R. A.A. Balkema, Athens, Greece, p. 177-182.

108. Novello, E.A. and Johnston, I.W., 1995. Geotechnical Materials and the critical state. *Geotechnique*, **45**: 223-235.

109. Morgenstern, N.R. and Eigenbrod, K.D., 1974. Classification of Argillaceous Soils and Rocks. *Journal of the Geotechnical Engineering Division, ASCE*, **100**: 1137-1156.

110. Grainger, P., 1984. The classification of mudrocks for engineering purposes. *Q. J. Eng. Geol. London*, **17**: 381-387.

111. Mesri, G. and Cepeda-Diaz, A.F., 1986. Residual shear strength of clays and shales. *Geotechnique*, **36**: 269-274.

112. Lambe, T.W. and Whitman, R.V., 1969. Soil Mechanics. J. Wiley & Sons, 553 p.

113. Terzaghi, K., Peck, R.B., and Mesri, G., 1996. Soil Mechanics in Engineering Practice. J. Wiley & Sons, 549 p.

114. Hvorslev, M.J. 1960. Physical components of the shear strength of natural clays. In: *Research Conference on Shear Strength of Cohesive Soils*. Ed. ASCE. Boulder, Colorado, p. 169-273.

115. Chandler, R.J., 2000. Clay sediments in depositional basins: the geotechnical cycle. *Quarterly Journal of Engineering Geology and Hydrogeology*, **33**: 7-39.

116. Burland, J.B., 1990. On the compressibility and shear strength of natural clays. *Geotechnique*, **40**: 329-378.

117. Sridharan, A. and Prakash, K., 1999. Influence of clay mineralogy and pore-medium chemistry on clay sediment formation. *Canadian Geotechnical Journal*, **36**: 961-966.

118. Skempton, A.W., 1970. The consolidation of clays by gravitational compaction. *Q. J. Geol. Soc. London*, **125**: 373-411.

119. Kavvadas, M.J. and Anagnostopoulos, A. 1998. A framework for the mechanical behaviour of structured soils. In: *The Geotechnics of Hard Soils - Soft Rocks*. Ed. Evangelista, A. and Picarelli, L. A.A. Balkema, Athens, Greece, p. 591-601.

120. Clayton, C.R.I. and Serratrice, J.F. 1997. General report session 2: The mechanical properties and behavior of hard soils and soft rocks. In: *Geotechnical Engineering of Hard Soils - Soft Rocks*. Ed. Anagnostopoulos, A., Schlosser, F., Kaltteziotis, N., and Frank, R. A.A. Balkema, Athens, Greece, p. 1839-1875.

121. Petley, D., Jones, M., Fan, C., Stafford, C., Leddra, M., and Kageson-loe, N. 1993. Deformation and fabric changes in weak fine-grained rocks during high pressure consolidation and shear. In: *Geotechnical Engineering of Hard Soils - Soft Rocks*. Ed. Frank, R., p. 737-743.

122. Cotecchia, F. and Chandler, R.J. 1998. One-dimensional compression of a natural clay: structural changes and mechanical effects. In: *The Geotechnics of Hard Soils - Soft Rocks*. Ed. Evangelista, A. and Picarelli, L. A.A. Balkema, Athens, Greece, p. 103-113.

123. Horseman, S.T., Winter, M.G., and Entwisle, D.C. 1993. Triaxial experiments on Boom Clay. In: *The Engineering Geology of Weak Rock*. Ed. Cripps, J.C., Coulthard, J.M., Culshaw, M.G., Forster, A., Hencher, S.R., and Moon, C.F. A.A. Balkema, Leeds, UK, p. 35-43.

124. Amorosi, A. and Rampello, S. 1998. The influence of natural soil structure on the mechanical behavior of a stiff clay. In: *The Geotechnics of Hard Soils - Soft Rocks*. Ed. Evangelista, A. and Picarelli, L. A.A. Balkema, Athens, Greece, p. 395-402.

125. Calabresi, G. 1980. The effect of sample size on strength parameters for intact and fissured stiff clays. In: *Proc. Euromech. Coll. No. 134*. Ed. Denmark, T.U.o., p.

126. Skempton, A.W., 1985. Residual strength of clay in landslides, folded strata and the laboratory. *Geotechnique*, **35**: 3-18.

127. Petley, D.N., 1999. Failure envelops of mudrocks at high confining pressures. In: *Muds and Mudstones: Physical and Fluid-FLow Properties*. Ed: Aplin, A.C., Fleet, A.J., and Macquaker, H.S. Geological Society Special Publication No. 158, London, p. 61-71.

128. Malandraki, V. and Toll, D.G., 1996. The definition of yield for bonded materials. *Geotechnical and Geological Engineering*, **14**: 67-82.

129. Burland, J.B., Rampello, S., Georgiannou, V.N., and Calabresi, G., 1996. A laboratory study of the strength of four stiff clays. *Geotechnique*, **46**: 491-514.

130. Lupini, J.F., Skinner, A.E., and Vaughan, P.R., 1981. The drained residual strength of cohesive soils. *Geotechnique*, **31**: 181-213.

131. Picarelli, L., Leroueil, S., Delisle, M.C., Urciuoli, G., and Guerriero, G. 1998. Ocurrence and features of shear zones in clay. In: *Localization and Bifurcation Theory for Soils and Rocks*. Ed. Adachi, T., Oka, F., and Yashima, A. A.A. Balkema, Gifu, Japan, p. 259-268.

132. Skempton, A.W. and Petley, D. 1967. The strength along structural discontinuities in stiff clays. In: *Proceedings of the Geotechnical Conference Oslo 1967*. Ed. NGI. Oslo, Norway, p. 3-20.

133. Archambault, G., Daigneault, R., Rouleau, A., and Tavchandjian, O. 1990. Mechanics of shear zones and fault belts development by anastomosing patterns of fractures at all scales. In: *Mechanics of Jointed and Faulted Rock*. Ed. Rossmanith, H.-P. A.A. Balkema, Vienna, Austria, p. 197-204.

134. Morgenstern, N.R. and Tchlaneko, J.S. 1967. Microstructural observations on shear zones from slips in natural clays. In: *Proceedings of the Geotechnical Conference Oslo 1967*. Ed. NGI. Oslo, Norway, p. 147-152.

135. Morgenstern, N.R. and Tchlaneko, J.S., 1967. Microscopic structures in kaolin subjected to direct shear. *Geotechnique*, **17**: 309-328.

136. Roscoe, K.H., 1970. The influence of strains in soil mechanics. *Geotechnique*, **20**: 129-170.

137. Turner, F.J. and Weiss, L.E., 1963. Structural Analysis of Metamorphic Tectonites. McGraw-Hill, 545 p.

138. Botts, M.E. 1998. Effects of slaking on the strength of clays shales: a critical state approach. In: *The Geotechnics of Hard Soils - Soft Rocks*. Ed. Evangelista, A. and Picarelli, L. A.A. Balkema, Athens, Greece, p. 447-458.

139. Morgenstern, N.R. 1990. Instability mechanisms in stiff soils and weak rocks. In: *10th SEAGC Conference*. Ed. SAGS. Taipei, Taiwan, p. 12.

140. Barton, M.E. and Cooper, M.R., 1998. Major joint trends in the Gault Clay at Selborne. *Geotechnique*, **48**: 123-128.

141. Marsland, A., 1971. The shear strength of stiff fisured clay. In: *Stress-Strain Behaviour of Soils*. Ed: Parry, R.H.G. G.T. Foulis & Co. Ltd., Cambridge, p. 59-68.

142. Vallejo, L.E., Alaasmi, A., and Yoo, H. 1993. Behavior under compression of stiff clays with multiple cracks. In: *Geotechnical Engineering of Hard Soils - Soft Rocks*. Ed. Anagnostopoulos, A., Schlosser, F., Kaltteziotis, N., and Frank, R. A.A. Balkema, Athens, Greece, p. 825-831.

143. White, W.A., 1961. Colloid phenomena in sedimentation of argillaceous rocks. *Journal of Sedimentary Petrology*, **31**: 560-570.

144. Fookes, P.G., 1965. Orientation of fissures in stiff overconsolidated clay of the Siwalik system. *Geotechnique*, **15**: 195-206.

145. D'Elia, B., Federico, G., Grisolia, M., Rossi, M., and Tancredi, G. 1977. Mechanical behaviour of a highly tectonized Miocenic "mudstone". In: *Proceedings of International Symposium on the Geotechnics of Structurally Complex Formations*. Ed. AGI. AGI, Milano, p. 183-198.

146. Cruden, D.M., Thomson, S., and Tsui, P., 1989. The geotechnical characteristics of an ice-thrust mudstone, Wabamun Lake area, Alberta. *Canadian Geotechnical Journal*, **26**: 277-234.

147. Cruden, D.M., Morgenstern, N.R., Thomson, S., and Tsui, P., 1991. Some influences of ice thrusting in geotechnical engineering. In: *Quaternary Engineering Geology*. Ed: Moon, C.F. Geological Society, 127-134.

148. Tsui, P., Cruden, D.M., and Thomson, S., 1989. Ice-thrust terrains and glaciotectonic setting in central Alberta. *Canadian Journal of Earth Sciences*, **26**: 1308-1318.

149. Fookes, P.G. and Denness, B., 1969. Observational studies on fissure patterns in Cretaceous sediments of South-East England. *Geotechnique*, **19**: 453-477.

150. McGown, A., Saldivar-Sali, A., and Radwan, A.M., 1974. Fissure patterns and slope failures in till at Hulford, Ayrshire. *Quarterly Journal of Engineering Geology and Hydrogeology*, **7**: 1-26.

151. McGown, A. and Radwan, A.M., 1975. The presence and influence of fissures in the boulder clays of West Central Scotland. *Canadian Geotechnical Journal*, **12**: 84-97.

152. Matheson, D.S. and Thomson, S., 1973. Geologic implications of valley rebound. *Canadian Journal of Earth Sciences*, **10**: 961-978.

153. Ferguson, H.F. and Hamel, J.V. 1981. Valley stress relief in flat-lying sedimentary rocks. In: *Weak Rock Soft, Fractured and Weathered Rock*. Ed. Akai, K., Hayashi, M., and Nishimatsu, Y. A.A. Balkema, Tokyo, p. 1235-1240.

154. Barton, M.E. 1984. The preferred path of landslide shear surfaces in over-consolidated clays and soft rocks. In: *IV International Symposium on Landslides*. Ed. ISSMFE. NRC Research Press, Toronto, p. 75-79.

155. Neuzil, C.E., 1986. Groundwater flow in low-permeability environments. *Water Resources Research*, **22**: 1163-1195.

156. Neuzil, C.E., 1994. How permeable are clays and shales? *Water Resources Research*, **30**: 145-150.

157. Bredehoeft, J.D., Neuzil, C.E., and Milly, P.C.D., 1983. Regional flow in the dakota Aquifer: A study of the role of confining layers. USGS, 45 p.

158. Sanderson, D.J. and Zhang, X., 1999. Critical stress localization of flow associated with deformation of well-fractured rock masses, with implications for mineral deposits. In: *Fractures, Fluid Flow and Mineralization*. Ed: McCaffrey, K., Lonergan, L., and Wilkinson, J. Geological Society Special Publication No. 155, London, p. 69-81.

159. Kroos, B.M., Schloemer, S., and Ehrlich, R., 1998. Experimental investigation of molecular transport and fluid flow in unfaulted and faulted pelitic rocks. In: *Faulting, Fault Sealing and Fluid Flow in Hydrocarbon Reservoirs*. Ed: Jones, G., Fischer, Q.J., and Knipe, R.J. Geological Society Special Publications No. 147, Bath, p. 135-146.

160. Faulkner, D.R. and Rutter, E.H., 1998. The gas permeability of clay-bearing fault gouge at 20°C. In: *Faulting, Fault Sealing and Fluid Flow in Hydrocarbon Reservoirs*. Ed: Jones, G., Fischer, Q.J., and Knipe, R.J. Geological society, 147-156.

161. Zhang, S. and Cox, S.F., 2000. Enhancement of fluid permeability during shear deformation of a synthetic mud. *Journal of Structural Geology*, **22**: 1385-1393.

162. Faulkner, D.R. and Rutter, E.H., 2000. Comparisons of water and argon permeability in natural clay-bearing fault gouge under high pressure at 20°C. *Journal of Geophysical Research*, **105**: 16415-16426.

163. Bolton, A. and Maltman, A.J., 1998. Fluid-flow pathways in actively deforming sediments: the role of pore fluid pressures and volume change. *Marine and Petroleum Geology*, **15**: 281-297.

164. Renner, J., Hettkamp, T., and Rummel, F., 2000. Rock mechanical characterization of an argillaceous host rock of a potential radioactive waste repository. *Rock Mechanics and Rock Engineering*, **33**: 3.

165. Bolton, A., 2000. Some measurements of permeability and effective stress on a heterogeneous soil mixture: implications for recovery of inelastic strains. *Engineering Geology*, **57**: 95-104.

166. Barton, N.R., Bandis, S., and Bakhtar, K., 1985. Strength, deformation and conductivity coupling of rock joints. *International Journal of Rock Mechanics & Mining Sciences*, **22**: 121-140.

167. Makurat, A. and Gutierrez, M., 1996. Fracture flow and fracture cross flow experiments. In: *SPE Annual Technical Conference and Exhibition*. Denver, Colorado, SPE 36732.

168. Jenyon, M.K., 1986. Salt Tectonics. Elsevier Applied Science Publishers, New York, NY, 191 p.

169. Kinsman, D.J.J. 1974. Calcium sulphate minerals of evaporite deposits: their primary mineralogy. In: *4th Symposium on Salt*. Ed. Coogan, A.H. A.A. Balkema, Cleveland, Ohio, p. 343-348.

170. Murray, R.C., 1964. Origin and diagenesis of gypsum and anhydrite. *Journal of Sedimentary Petrology*, **34**: 512-523.

171. Pfeifle, T.W. and Hansen, F.D., 1998. Database of Mechanical and Hydrological Properties of WIPP Anhydrite Derived from Laboratory-Scale Experiments. Sandia National Laboratories, 74 p.

172. Handin, J. and Hager Jr., R.V., 1957. Experimental deformation of sedimentary rocks under confining pressure: Tests at room temperature on dry samples. *Bulletin of the American Association of Petroleum Geologists*, **41**: 1-50.

173. Bilgin, N., 1982. The cuttability of evaporites. *Bulletin on the International Association of Engineering Geology*, **25**: 85-90.

174. Fabre, D. and Dayre, M., 1982. Propietes geotechniques de gypses et anhydrites du trias des Alps de Savoie (France). *Bulletin on the International Association of Engineering Geology*, **25**: 91-98.

175. Deere, D.U., 1968. Geological considerations. In: *Rock Mechanics in Engineering Practice*. Ed: Stagg, K.G. and Zienkiewicz, O.C. John Wiley & Sons, New York, NY, p. 1-20.

176. Martin, C.D., 1997. Seventeenth Canadian Geotechnical Colloquium: The effect of cohesion loss and stress path on brittle rock strength. *Canadian Geotechnical Journal*, **34**: 698-725.

177. Martin, C.D., Kaiser, P., and McCreath, D.R., 1999. Hoek–Brown parameters for predicting the depth of brittle failure around tunnels. *Canadian Geotechnical Journal*, **36**: 136-151.

178. Hoek, E. and Brown, E.T., 1997. Practical estimates of rock mass strength. *International Journal of Rock Mechanics & Mining Sciences*, **34**: 1165-1186.

179. Marinos, P.G. and Hoek, E. 2000. GSI: A geological friendly tool for rock mass strength estimation. In: *Proceedings of the International Conference on Geotechnical and Geological Engineering (GeoEng 2000)*. Ed. The Australian Geomechanics Society. CRC, Melbourne, Australia, p. 1422-1440.

180. Howarth, S.M. and Christian-Frear, T., 1997. Porosity, Single-Phase Permeability, and Capillary Pressure Data from Preliminary Laboratory Experiemnts on Selected Samples from Marker Bed 139 at the Waste Isolation Pilot Plant. Sandia National Laboratories, 94 p.

181. Beauheim, R.L. and Roberts, R.M., 2002. Hydrology and hydraulic properties of a bedded evaporite formation. *Journal of Hydrology*, **259**: 66-88.

182. Beauheim, R.L., Wawersik, W.R., and Roberts, R.M., 1993. Coupled Permeability and Hydrofracture Tests to Assess the Waste-Containment Properties of Fractured Anhydrite. *International Journal of Rock Mechanics & Mining Sciences*, **30**: 1159-1163.

183. Press, W.H., Flannery, B.P., Teukolsky, S.A., and Vetterling, W.T., 1992. Numerical Recipes : The Art of Scientific Computing. Cambridge University Press, 963 p.

184. Neuzil, C.E., 1995. Abnormal pressures as hydrodynamic phenomena. *American Journal of science*, **295**: 742-786.

185. Bolton, A., Clennell, M.B., and Maltman, A., 1999. Nonlinear stress dependence of permeability: A mechanism for episodic fluid flow in accretionary wedges. *Geology*, **27**: 239-242.

186. Martin, C.D., Kaiser, P.K., and Christiansson, R., 2003. Stress, instability and design of underground excavations. *International Journal of Rock Mechanics & Mining Sciences*, **40**: 1027-1047.

187. Ali, A.H.A., Brown, T., Delgado, R., Lee, D., Plumb, D., Smirnov, N., Marsden, R., Prado-Valverde, E., Ramsey, L., Spooner, D., Stone, T.W., and Stouffer, T., 2003. Watching rocks change - mechanical earth modeling. *Oilfield Review*, **15**: 22-39.

188. Gerhard, L.C., Anderson, S.B., and Fischer, D.W. 1991. Petroleum geology of the Williston Basin. In: *Interior Cratonic Basins*. Ed. Leighton, M.W., Kolata, D.R., Oltz, D.F., and Eidel, J.J. AAPG Memoir No. 51, Tulsa, Okla., p. 507-560.

189. Whittaker, S.G., Rostron, B.J., Khan, D., Hajnal, Z., Qing, H., Penner, L., Maathuis, H., and Goussev, S., 2004. Theme 1: Geological characterization. In: *IEA GHG Weyburn* CO_2 *Monitoring & Storage Project Summary Report 2000-2004*. Ed: Wilson, M.A. and Monea, M. PTRC, Regina, p. 15-69.

190. Churcher, P.L. and Edmunds, A.C., 1994. Reservoir Characterization and Geological Study of the Weyburn Unit, Shoutheastern Saskatchewan: Report Number 1. Proposed

Miscible Flood, Horizontal Well, and Waterflood Optimization Areas. PanCanadian, 28 p.

191. Wegelin, A. 1984. Geology and reservoir properties of the Weyburn Field, Southeastern Saskatchewan. In: *Oil and Gas in Saskatchewan*. Ed. Lorsong, J.A. and Wilson, M.A. Saskatchewan Geological Society, Regina, p. 71-82.

192. Khan, D.K. and Rostron, B.J. 2004. Regional Hydrogeological investigation around the IEA Weyburn CO_2 Monitoring and Storage Project site. In: *Seventh Greenhouse Gas Control Technologies*. Ed. Wilson, M.A., Gale, J., Rubin, E.S., Keith, D.W., Gilboy, C.F., Morris, T., and Thambimuthu, T. Elsevier Science Ltd, Vancouver, BC, p. 741-750.

193. Redly, P., 1998. Tectonostratigraphic Evolution of the Williston Basin. University of Saskatoon, 360 p.

194. Bell, J.S., Price, P.R., and McLellan, P.J., 1994. In-situ Stress in the Western Canada Sedimentary Basin. In: *Geological Atlas of the Western Canada Sedimentary Basin*. Ed: Mossop, G.D. and Shetsen, I. Canadian Society of Petroleum Geologists and Alberta Research Council, Calgary, Alberta, p.

195. Wegelin, A., 1985. Reservoir characteristics of the Weyburn field, Southeastern Saskatchewan. In: *First Annual Technical Meeting of the South Saskatchewan Section, CIM*. Regina, CIM 17.

196. Kent, D.M., 2004. Characterization of lithologies and fractures in the Frobisher Beds and the Midale and Frobisher evaporites underlying the Weyburn Oil Pool. IEA GHG Weyburn CO_2 Monitoring and Storage Project, 15 p.

197. Nickel, E.H., 2003. Investigation of the Fracturing and Sealing Potential of the midale Evaporite and Diagenetically Altered Midale Carbonates. IEA GHG Weyburn CO_2 Monitoring and Storage Project, 37 p.

198. Core Laboratories Ltd., 1986. Fracture Study for PanCanadian Petroleum, Weyburn, Sakatchewan. PanCanadian Petroleum, 28 p.

199. Fischer, B.F., 1994. Fracture Analysis: Midale Field, SE Saskatchewan. Shell Canada Limited, 48 p.

200. Beliveau, D.A. and Payne, D.A., 1991. Analysis of a tertiary CO_2 flood pilot in a naturally fractured reservoir. In: *66th Annual Technical Conference and Exhibition of the Society of Petroleum Engineers*. Dallas, SPE 22947.

201. Beliveau, D.A., Payne, D.A., and Mundry, M., 1993. Waterflood and CO_2 flood of the fractured Midale Field. *Journal of Petroleum Technology*.

202. Bunge, R.J., 2000. Midale Reservoir Fracture Characterization Using Integrated Well and Seismic Data, Weyburn Field, Saskatchewan. Colorado School of Mines, 146 p.

203. Beliveau, D.A., 1986. Interwell pressure transient testing in Midale: A naturally fractured reservoir. In: *61st Annual Technical Conference and Exhibition of the Society of Petroleum Engineers*. LA, SPE 15635.

204. Elsayed, S.A., Baker, R., Churcher, P.L., and Edmunds, A.C., 1993. A multidisciplinary reservoir characterization and simulator study of the Weyburn Unit, Saskatchewan, Canada. In: *SPE Rocky Mountain Regional/Low Permeability Reservoirs Symposium*. Denver, SPE 25852.

205. Ko, S.C.M., Balkes, P.A., Kehrig, R., and Chodzicki, J., 1993. Simulation of horizontal well performance while waterflooding the Weyburn Midale beds pool of Southeastern Saskatchewan. *Journal of Canadian Petroleum Technology*, **32**: 28-36.

206. Narr, W. and Burruss, R.C., 1984. Origin of reservoir fractures in Little Knife Field, North Dakota. *AAPG*, **68**: 1087-1100.

207. Stauffer, M.R. and Gendzwill, D.J., 1987. Fractures in the northern plains, stream patterns, and the midcontinent stress field. *Canadian Journal of Earth Sciences*, **24**: 1086-1097.

208. Zoback, M.L. and Zaman, M., 1980. State of stress in the conterminous United States. *Journal of Geophysical Research*, **85**: 6113-6156.

209. Rives, T., Rawnsley, K.D., and Petit, J.-P., 1994. Analogue simulation of natural orthogonal joint set formation in brittle varnish. *Journal of Structural Geology*, **16**: 419-429.

210. van der Pluijm, B.A., Craddock, J.P., Graham, B.R., and Harris, J.H., 1997. Paleostress in cratonic North America: implications for deformation of continental interiors. *Science*, **277**: 794-796.

211. Pollard, D.D. and Segall, P. 1987. Theoretical displacements and stresses near fractures in rocks with applications to faults, joints, veins, dikes and solution surfaces. In: *Fracture Mechanics of Rock*. Ed. Atkinson, B.K. Academic Press, London, p. 277-349.

212. Bourne, S.J., 2003. Contrast of elastic properties between rock layers as a mechanism for the initiation and orientation of tensile failure under uniform remote compression. *Journal of Geophysical Research*, **108**: 14-1-14-12.

213. Diederichs, M.S., 2003. Rock fracture and collapse under low confinement conditions. *Rock Mechanics and Rock Engineering*, **36**: 339-381.

214. Kaiser, P.K., Diederichs, M.S., Martin, C.D., Sharp, J., and Steiner, W., 2002. Underground Works in Hard Rock Tunnelling and Mining. 87 p.

215. Core Laboratories Ltd., 1998. Advanced Rock Properties Study for PanCanadian Resources. PanCanadian, 22 p.

216. McLellan, P.J., 1996. Assessing the risk of wellbore instability in horizontal and inclined wells. *Journal of Canadian Petroleum Technology*, **35**: 21-32.

217. Hoek, E. and Brown, E.T., 1980. Underground Excavations in RockLondon, 527 p.

218. Hoek, E., Carranza-Torres, C., and Corkum, B., 2002. Hoek-Brown Failure Criterion - 2002 Update. Rocscience, 7 p.

219. McLellan, P.J., Lawrence, K.H., and Cormier, K.W., 1992. A multiple-zone acid stimulation treatment of a horizontal well, Midale, Saskatchewan. *Journal of Canadian Petroleum Technology*, **31**: 71-82.

220. McLennan, J.D., Hasegawa, H.S., Roegiers, J.-C., and Jessop, A.M., 1986. Hydraulic fracturing experiment at the University of Regina Campus. *Canadian Geotechnical Journal*, **23**: 548-555.

221. Townend, J. and Zoback, M.D., 2000. How faulting keeps the crust strong. *Geology*, **28**: 399-402.

222. Zoback, M.D., Barton, C.A., Brudy, M., Castillo, D.A., Finkbeiner, T., Grollimund, B.R., Moos, D.B., Peska, P., Ward, C.D., and Wiprut, D.J., 2003. Determination of stress

orientation and magnitude in deep wells. *International Journal of Rock Mechanics & Mining Sciences*, **40**: 1049-1076.

223. Kreis, L.K., Thomas, P.L., Burke, R.B., and Whittaker, S.G., 2003. Devonian Isopach and Structure Maps, IEA Weyburn CO_2 Monitoring and Storage Project Area. Produced by Saskatchewan Industry and Resources & North Dakota Geological Survey

224. Al-Shayea, N.A., 2004. Effects of testing methods and conditions on the elastic properties of limestone rock. *Engineering Geology*, **74**: 139-156.

225. Rzhevsky, V.V. and Novik, G., 1971. The Physics of Rock. MIR Publishers, Moscow, 320 p.

226. US Bureau of Reclamation, 1953. Physical properties of some typical foundation rocks. Concrete Laboratory Report No. SP-39, 50 p.

227. Biot, M.A., 1941. General theory of three-dimensional consolidation. *Journal of Applied Physics*, **12**: 155-164.

228. Dean, R.H., Gai, X., Stone, C.M., and Minkoff, S.E., 2003. A comparison of techniques for coupling porous flow and geomechanics. In: *SPE Reservoir Simulation Symposium*. Houston, Texas, SPE/ISRM 79709.

229. Tran, D., Settari, A., and Nghiem, L., 2002. New iterative coupling between a reservoir simulator and a geomechanics module. In: *SPE/ISRM Rock Mechanics Conference*. Irving, Texas, SPE/ISRM 78192.

230. Schlumberger, 2003. ECLIPSE User's Guide. Schlumberger, 796 p.

231. Itasca, 2002. FLAC 3D User's Guide. Itasca Consulting Group Inc., Minneapolis, 176 p.

232. Yale, D.P., Lyons, S.L., and Qin, G. 2000. Coupled geomechanics-fluid flow modeling in petroleum reservoirs: coupled versus uncoupled response. In: *Pacific Rocks 2000*. Ed. Girard, J., Liebman, M., Breeds, C., and Doe, T. A.A. Balkema, Seattle, Washington, p. 137-146.

233. Pruess, K. 2004. Behavior of CO_2 injection wells. In: *Proceedings of the 3rd International Conference on Carbon Sequestration*. Ed. US Department of Energy, National Energy Technology Laboratory, p. 1-5.

234. Heffer, K.J., Last, N.C., Koutsabeloulis, N.C., Chan, H.C.M., Gutierrez, M., and Makurat, A. 1994. The influence of natural fractures, faults and earth stresses on reservoir performance -geomechanical analysis by numerical modelling. In: *North Sea Oil and Gas Reservoirs - III*. Ed. Norwegian Institute of Technology. Norwegian Institute of Technology, Oslo, p. 201-211.

235. Segall, P. and Fitzgerald, S.D., 1998. A note on induced stress changes in hydrocarbon and geothermal reservoirs. *Tectonophysics*, **289**: 117-128.

236. Zoback, M.D., Chan, A.W., and Zinke, J.C. 2001. Production-induced normal faulting. In: *Rock Mechanics in the National Interest*. Ed. Elsworth, D., Tinucci, J.P., and Heasley, K.A. A.A. Balkema, Washington D.C., p. 157-163.

237. Teufel, L.W., 1996. Influence of Pore Pressure and Production-Induced Changes in Pore Pressure on In Situ Stress. Sandia National Laboratories, Alburquerque, New Mexico, 54 p.

238. Engelder, T. and Fischer, M.P., 1994. Influence of poroelastic behavior on the magnitude of minimum horizontal stress, S_h, in overpressured parts of sedimentary basins. *Geology*, **22**: 949-952.

239. Lewis, R.W., Makurat, A., and Pao, W.K.S., 2003. Fully coupled modeling of seabed subsidence and reservoir compaction of North Sea oil fields. *Hydrogeology Journal*, **11**: 142-161.

240. Lin, W., 1983. Mechanical Properties of Mesaverde sandstone and Shale at High Pressures. Lawrence Livermore National Laboratory, 37 p.

241. Salz, L.B., 1977. Relationship between fracture propagation pressure and pore pressure. In: *52nd Annual Fall Technical Conference and Exhibition of the SPE*. Denver, Colorado, SPE 6870.

242. Smart, B.G.D., Somerville, J.M., Edlman, K., and Jones, C., 2001. Stress sensitivity of fractured reservoirs. *Journal of Petroleum Science and Engineering*, **29**: 29-37.

243. Chalaturnyk, R.J., 1999. Geomechanical Impact of Gas Production. Gulf Canada Resources Limited, Unpublished, Edmonton, 123 p.

244. Streit, J.E. and Hillis, R. 2003. Building geomechanical models for the safe underground storage of carbon dioxide in porous rock. In: *Greenhouse Gas Control Technologies*. Ed. Gale, J. and Kaya, J. Elsevier Science Ltd., Kyoto, Japan, p. 495-500.

245. Streit, J.E. and Hillis, R., 2003. Estimating fluid pressures that can induce reservoir failure during hydrocarbon depletion. In: *Oil/Rock 2002*. Kyoto, Japan, SPE/ISRM 78226.

246. Hawkes, C.D., McLellan, P.J., Zimmer, U., and Bachu, S. 2004. Geomechanical factors affecting geological storage of CO_2 in depleted oil and gas reservoirs: risks and mechanisms. In: *Gulf Rocks 2004*. Ed. ARMA/NARMS. A.A. Balkema, Houston, Texas, p. 12.

247. Martin, C.D. and Chandler, N.A., 1993. Stress heterogeneity and geological structures. *International Journal of Rock Mechanics & Mining Sciences*, **30**: 993-999.

248. Pascal, C., 2002. Interaction of faults and perturbation of slip: influence of anisotropic stress states in the presence of fault friction and comparison betweenWallace–Bott and 3D Distinct Element models. *Tectonophysics*, **356**: 307-322.

249. Min, K.-B., Rutqvist, J., Tsang, C.-F., and Jing, L., 2004. Stress-dependent permeability of fractured rock masses: a numerical study. *International Journal of Rock Mechanics & Mining Sciences*, **41**: 1191-1210.

250. Cartwrigth, J.A., Stewart, S.A., and Clark, J.A., 2001. Salt dissolution and salt-related deformation of the Forth Approaches Basin, UK North Sea. *Marine and Petroleum Geology*, **18**: 757-778.

251. Anderson, N.L. and Knapp, R., 1993. An overview of some large scale mechanisms of salt dissolution in western Canada. *Geophysics*, **58**: 1357-1387.

252. Christiansen, E.A., 1967. Collapse structures near Saskatoon, Saskatchewan, Canada. *Canadian Journal of Earth Sciences*, **4**: 757-767.

253. De Mille, G., Shouldice, J.R., and Nelson, H.W., 1964. Collapse structures related to evaporites of the Prairie Formation, Saskatchewan. *Geological Society of America Bulletin*, **75**: 307-316.

254. Burke, R.B., 2001. Some aspects of salt dissolution in the Williston Basin of North Dakota. *NDGS Newsletter*, **28**: 1-5.

255. Stanton, R.J.J., 1966. The solution brecciation process. *Geological Society of America Bulletin*, **77**: 843-847.

256. Anderson, R.Y. and Kirkland, D.W., 1980. Dissolution of salt deposits by brine density flow. *Geology*, **8**: 66-69.

257. Anderson, N.L. and Cederwall, D.A., 1993. Westhazel General Petroleums Pool: Case history of a salt-dissolution trap in west-central Saskatchewan, Canada. *Geophysics*, **58**: 889-897.

258. Gendzwill, D.J. and Wilson, N.L. 1987. Form and distribution of Winnipegois Mounds in Saskatchewan. In: *Williston Basin: Anatomy of a Cratonic Oil Province*. Ed. Longman, M.W. The Rocky Mountain Association of Geologists, Denver, Colorado, p. 109-117.

259. Fuzesy, A., 1982. Potash in Saskatchewan. Saskatchewan Energy and Mines, 44 p.

260. McTavish, G.J. and Vigrass, L.W. 1987. Salt dissolution tectonics, south-central Saskatchewan. In: *5th International Williston Basin Symposium*. Ed. Saskatchewan Geological Society. Saskatchewan Geological Society, Regina, Saskatchewan, p. 157-168.

261. Holter, M.E., 1969. The Middle Devonian Prairie Evaporite of Saskatchewan. Saskatchewan Department of Mineral Resources, 134 p.

262. Gendzwill, D.J., 1978. Winnipegosis Mounds and Prairie Evaporite Formation of Saskatchewan--seismic study. *AAPG*, **62**: 73-86.

263. Hamid, H., Morozov, I.B., and Kreis, L.K. 2004. Progress in seismic delineation of the southern margin of the Midle Devonian Prairie Evaporite Formation in the Elk Point Basin, south-central Saskatchewan. In: *Summary of Investigations 2004*. Ed. Saskatchewan Geological Survey. Saskatchewan Industry and Resources, p. Paper A5.

264. Hajnal, Z., Pandit, B., Sule, S., and Closson, J. 2004. Subsurface seismic images of the structural framework encompassing the CO_2 depository Weyburn reservoir in Saskatchewan, Canada. In: *Seventh International Conference on Greenhouse Gas Control Technologies*. Ed. Vancouver, B.C., p. 2131-2134.

265. Christopher, J.E., 1978. Transitional Devonian-Mississippian Formations of Southern Saskatchewan. Saskatchewan Department of Mineral and Resources, 103 p.

266. Morgenstern, N.R. and Sepehr, K., 1991. Time-dependant hydraulic fracturing in potash mines. *International Journal of Rock Mechanics & Mining Sciences*, **28**: 187-197.

267. Itasca, 2000. FLAC 4.0 User's Guide. Itasca Consulting Group Inc., Minneapolis, 155 p.

268. Rocscience, 2000. Phase2. Rocscience Inc, Toronto, 181 p.

269. Whittaker, B.N. and Reddish, D.J., 1989. Subsidence Ocurrence, Prediction and Control. Elsevier, 528 p.

270. Institution of Civil Engineers, 1977. Ground Subsidence. Thomas Telford Ltd., 99 p.

271. Bai, M. and Roegiers, J.-C., 1994. Fluid flow and heat flow in deformable fractured porous media. *Int. J. Engng. Sci.*, **32**: 1615-1633.

272. Charlez, P.A., 1991. Rock Mechanics Theoretical Fundamentals. Editions Technip, Paris, 333 p.

273. Kurashige, M., 1989. A thermoelastic theory of fluid-filled porous materials. *Int. J. Solids Structures*, **25**: 1039-1052.

274. McTigue, D.F., 1986. Thermoelastic response of fluid-saturated porous rock. *Journal of Geophysical Research*, **91**: 9533-9542.

275. Zimmerman, R.Z., 2000. Coupling in poroelasticity and thermoelasticity. *International Journal of Rock Mechanics & Mining Sciences*, **37**: 79-87.

276. Bai, M., Abousleiman, Y., and Roegiers, J.-C. 1996. Some thougths on thermoporoelastic coupling. In: *Proceedings of the 11th Conference Engineering Mechanics*. Ed. Su, T.C. ASCE, p. 48-51.

277. Span, R. and Wagner, W., 1996. A new equation of state for carbon dioxide covering the fluid region from the triple-point temperature to 1100 K at pressures up to 800 MPa. *Journal of Physical and Chemical Reference Data*, **25**: 1509-1596.

278. Pruess, K., Oldenburg, C., and Moridis, G., 1999. TOUGH2 User's Guide, Version 2.0.p.

279. Wang, Y., 1994. Conductive heat flow and thermally induced fluid flow around a well bore in a poroelastic medium. *Water Resources Research*, **30**: 3375-3384.

280. Noorishad, J. and Tsang, C.F. 1987. Simulation of coupled thermal-hydraulic-mechanical interactions in fluid injection into fractured rocks. In: *Coupled Processes Associated with Nuclear Waste Repositories*. Ed. Tsang, C.-F. Academic Press, p. 673-678.

281. Pruess, K., Xu, T., Apps, J., and Garcia, J., 2001. Numerical modeling of aquifer disposal of CO_2. In: *SPE/EPA/DOE Exploration and Production Environmental Conference*. San Antonio, Texas, SPE 66537.

282. OECD/NEA, 1997. Lessons Learnt From Ten Performance Assessment Studies. OECD, Paris, 132 p.

283. Dewiere, L., Plas, F., and Tsang, C.F. 1997. Lessons learned from DECOVALEX I. In: *Mathematical and Experimental Studies of Coupled Thermo-hydro-Mechanical Processes of Fractured Media*. Ed. Stephansson, O., Jing, L., and Tsang, C.F. Elsevier, Amsterdam, p. 495-504.

A. Appendix A – Instruments Calibration

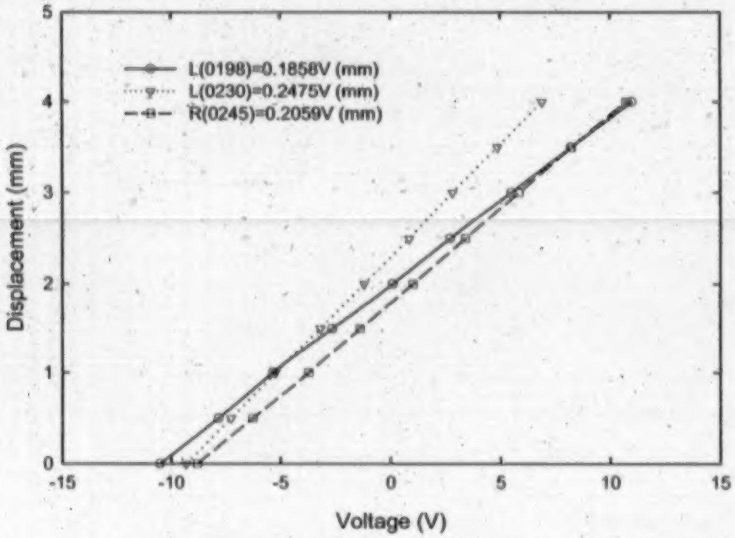

Figure A-1. Calibration of internal LVDTs, axial (L) and radial (R).

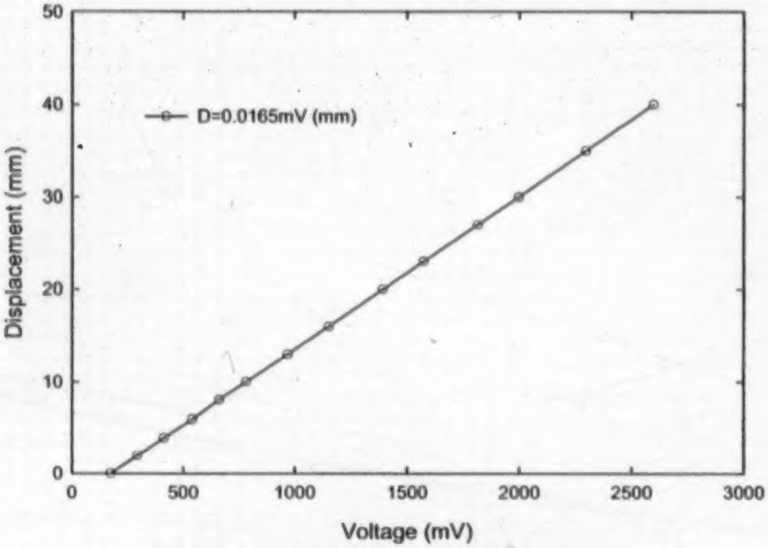

Figure A-2. Calibration of external LVDT.

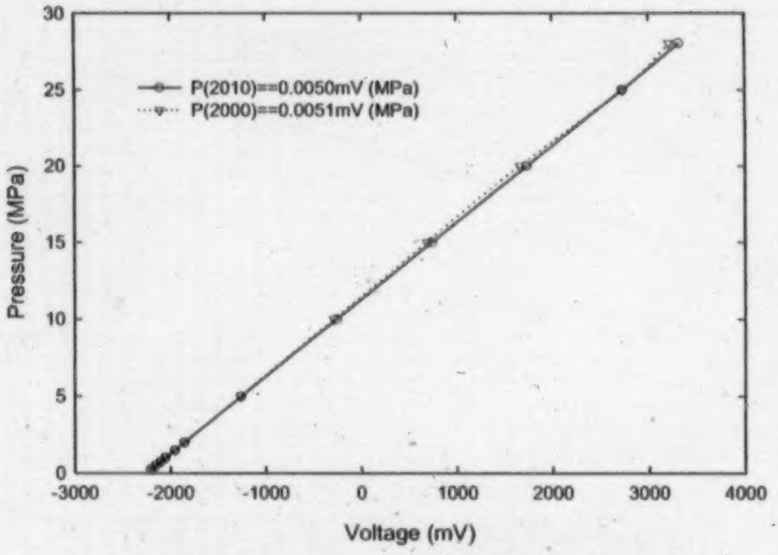

Figure A-3. Calibration of pore pressure gauges.

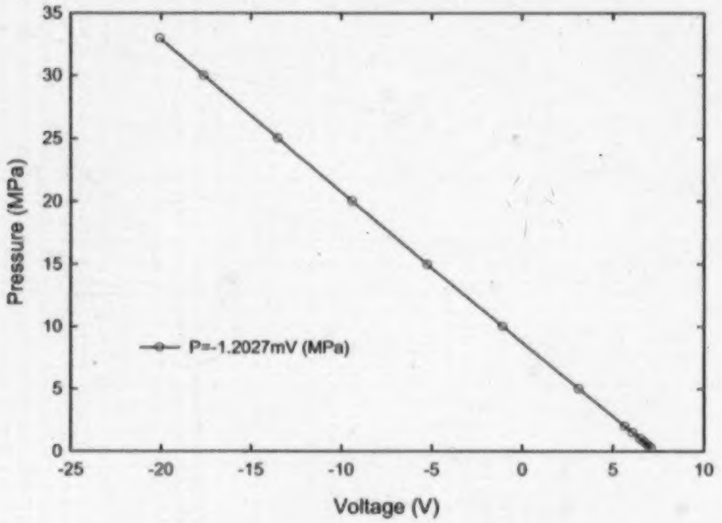

Figure A-4. Calibration of cell pressure gauge.

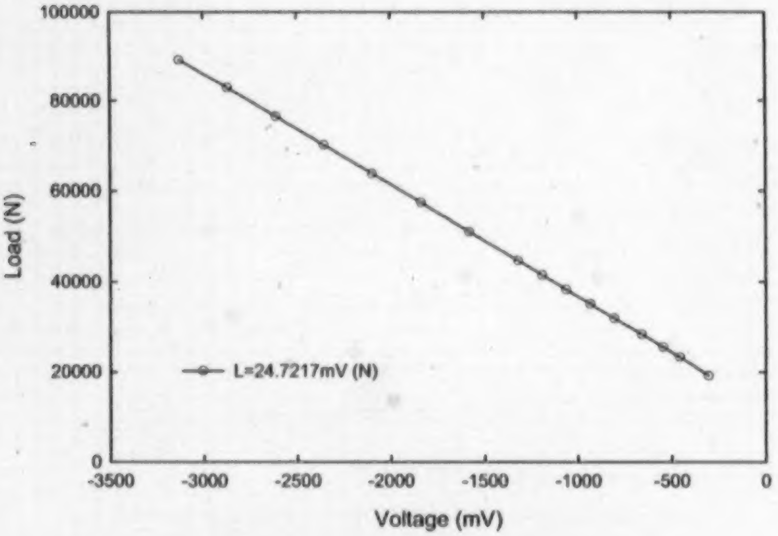

Figure A-5. Calibration of load cell.

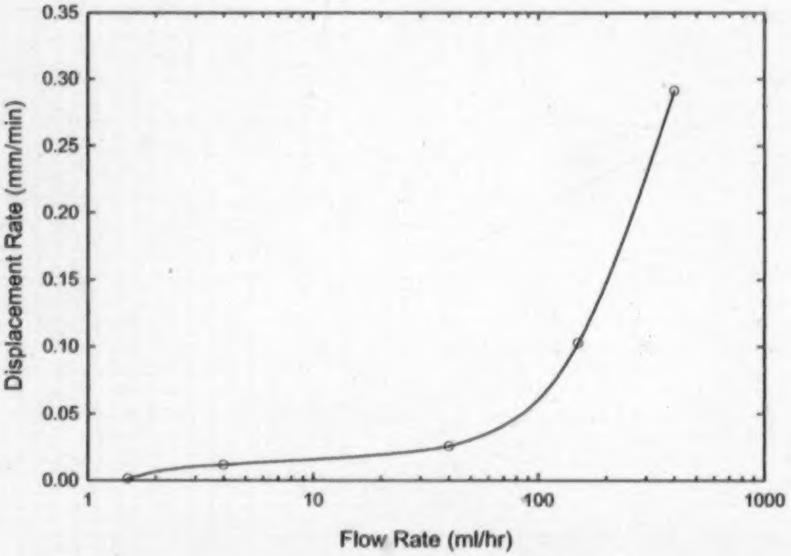

Figure A-6. Displacement rate vs. flow rate for loading system pump.

B. Appendix B – Stress and Displacement Contours for Base Case Scenario

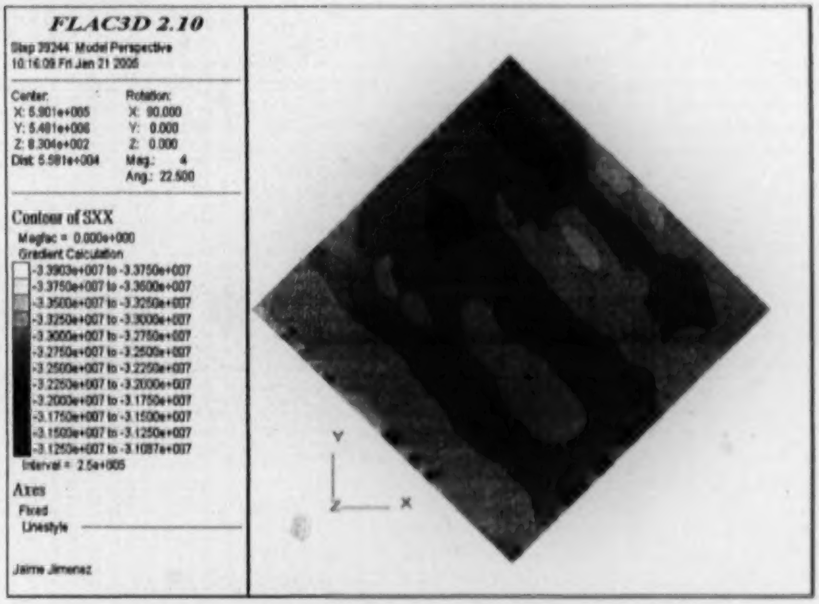

Figure B-1. West-East stresses in the Watrous Formation.

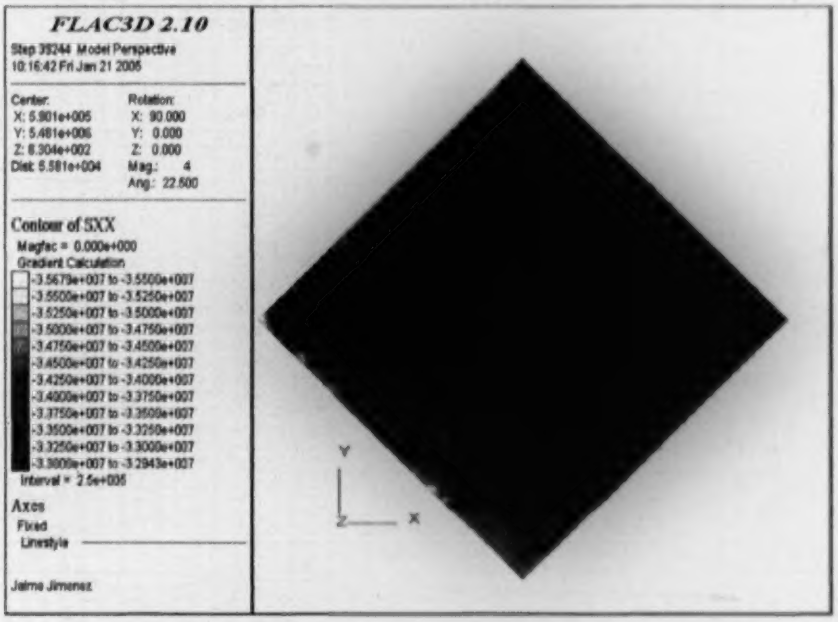

Figure B-2. West-East stresses in the Midale Evaporite Formation.

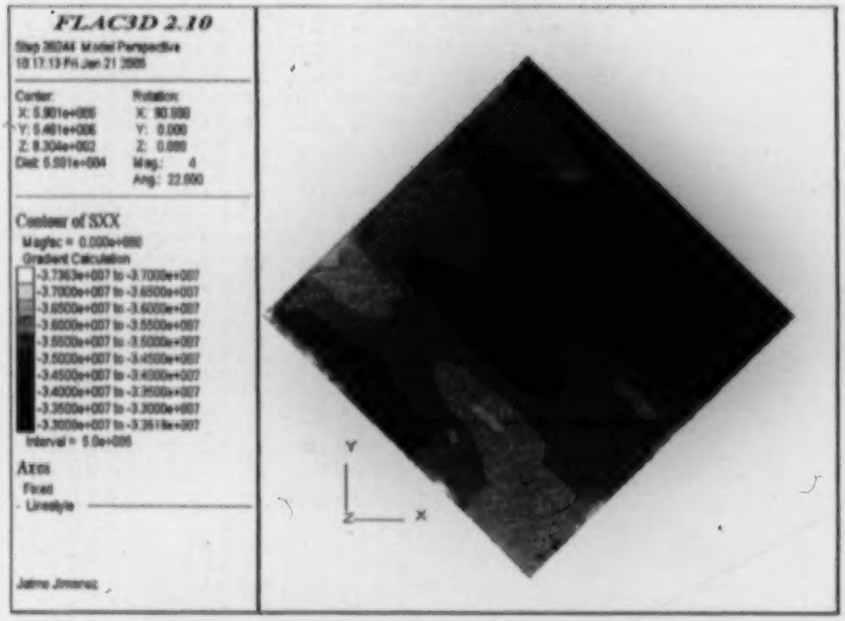

Figure B-3. West-East stresses in the Marly Formation.

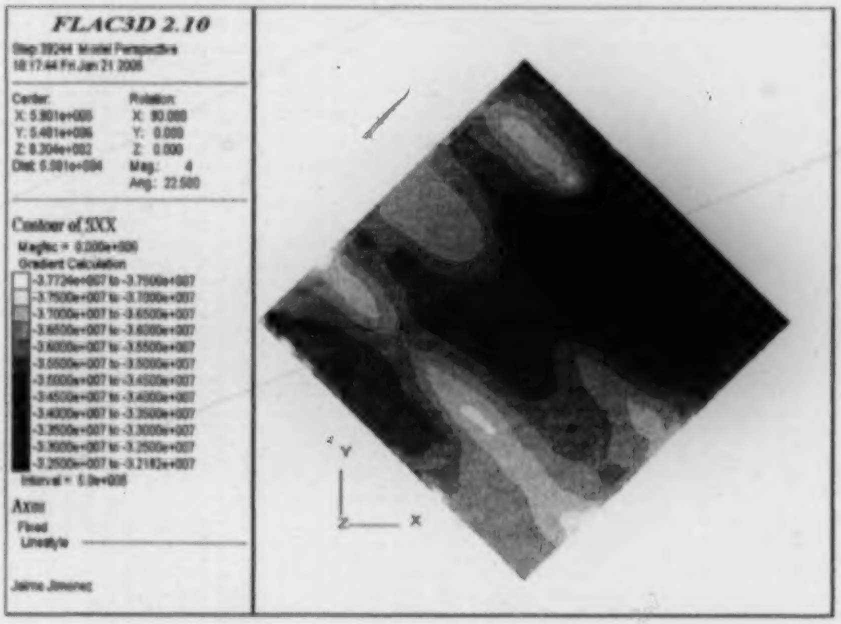

Figure B-4. West-East stresses in the Upper Vuggy Formation.

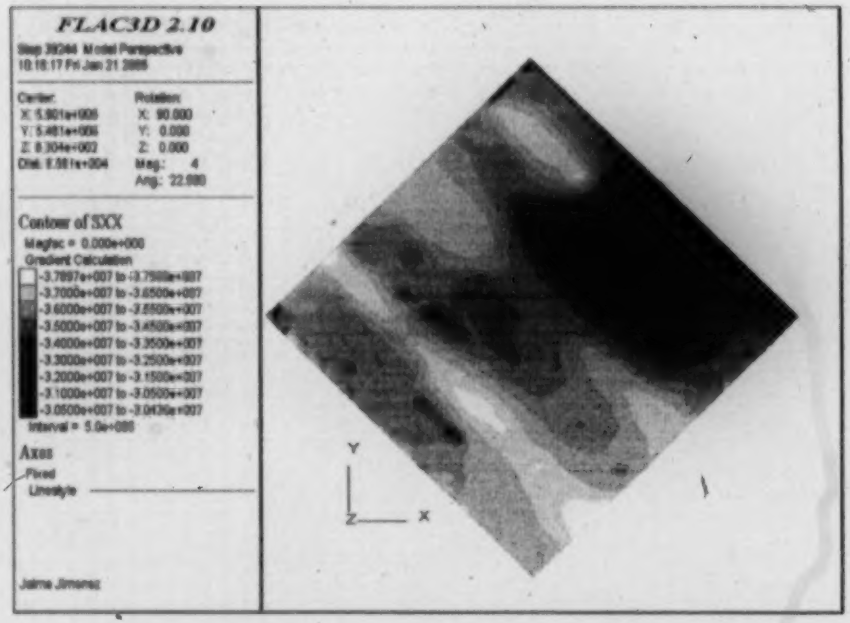

Figure B-5. West-East stresses in the Lower Vuggy Formation.

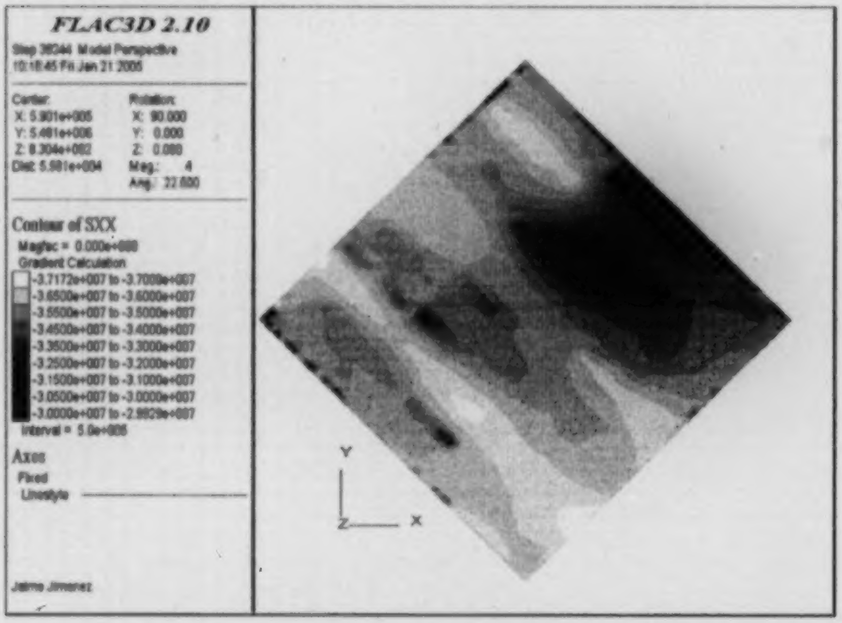

Figure B-6. West-East stresses in the Frobisher Evaporite Formation.

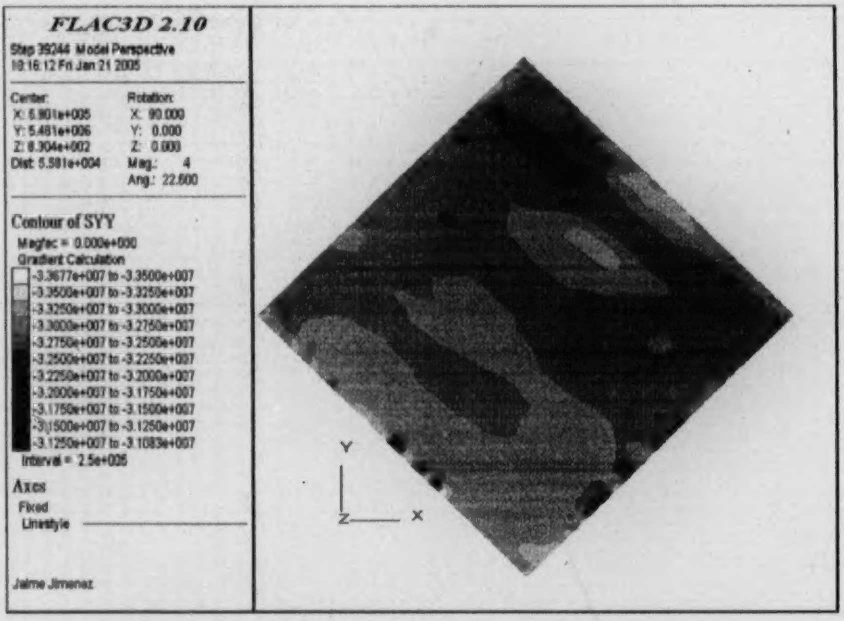

Figure B-7. North-South stresses in the Watrous Formation.

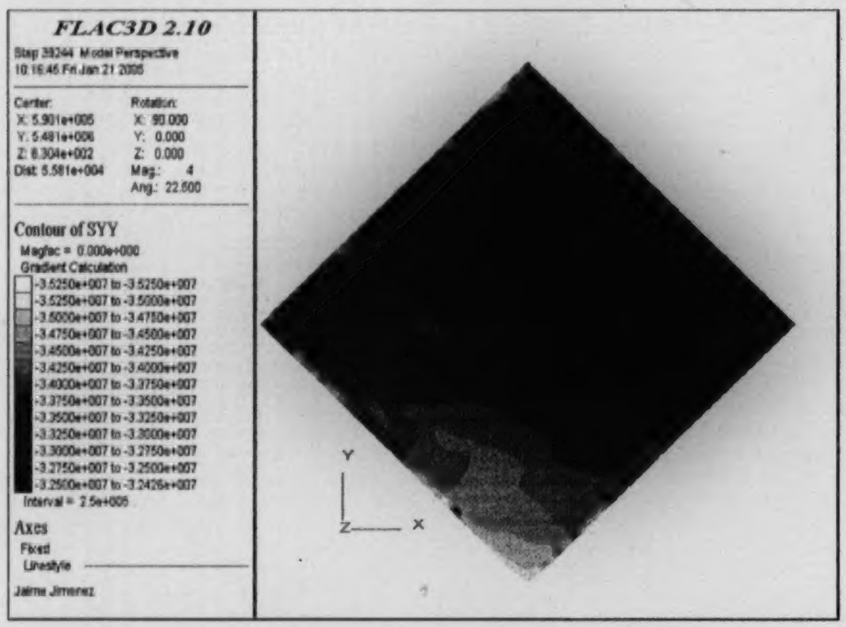

Figure B-8. North-south stresses in the Midale Evaporite Formation.

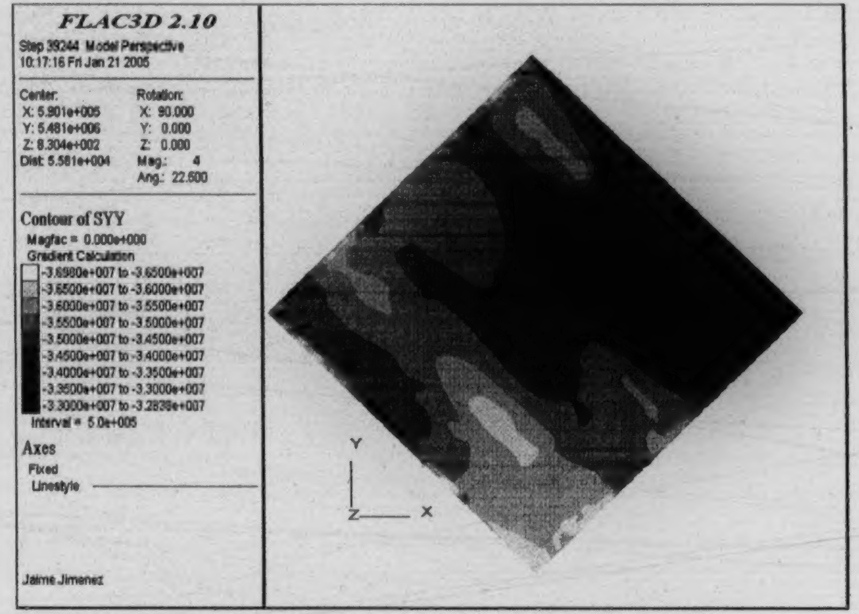

Figure B-9. North-South stresses in the Marly Formation.

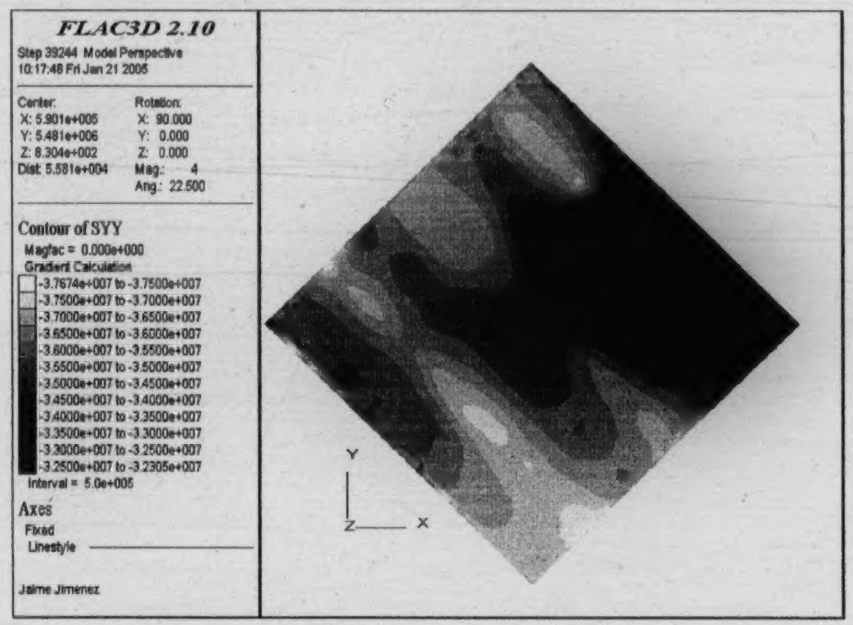

Figure B-10. North-South stresses in the Upper Vuggy Formation.

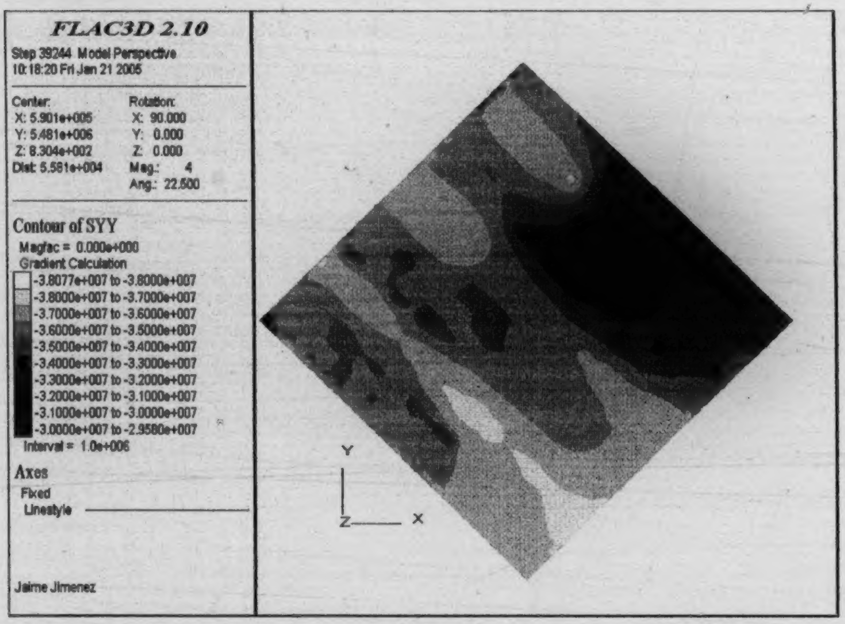

Figure B-11. North-South stresses in the Lower Vuggy Formation.

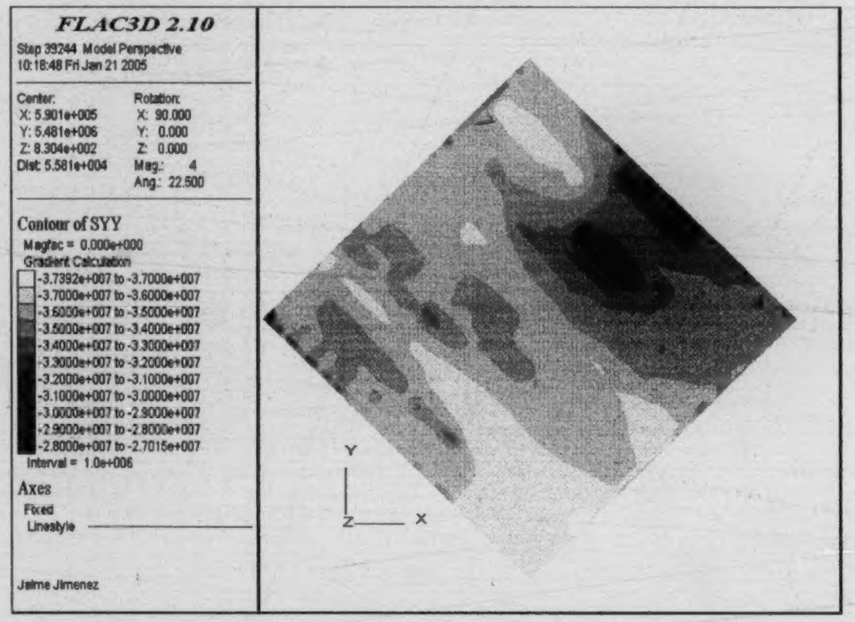

Figure B-12. North-South stresses in the Frobisher Evaporite Formation.

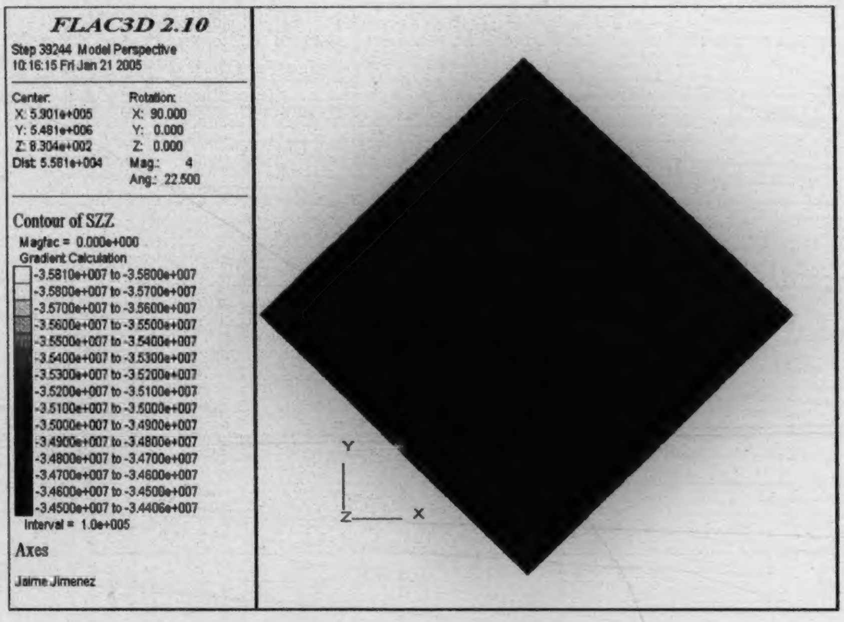

Figure B-13. Vertical stresses in the Watrous Formation.

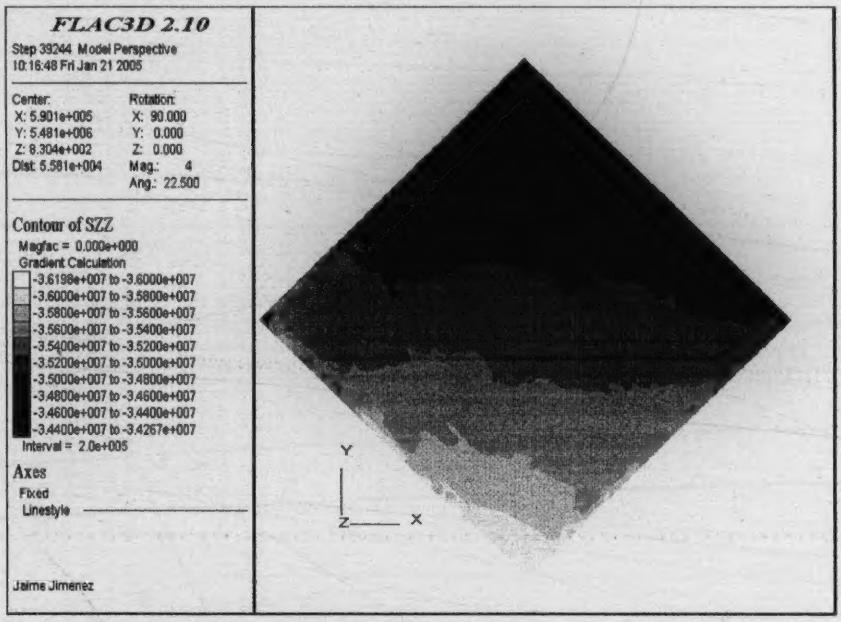

Figure B-14. Vertical stresses in the Midale Evaporite Formation.

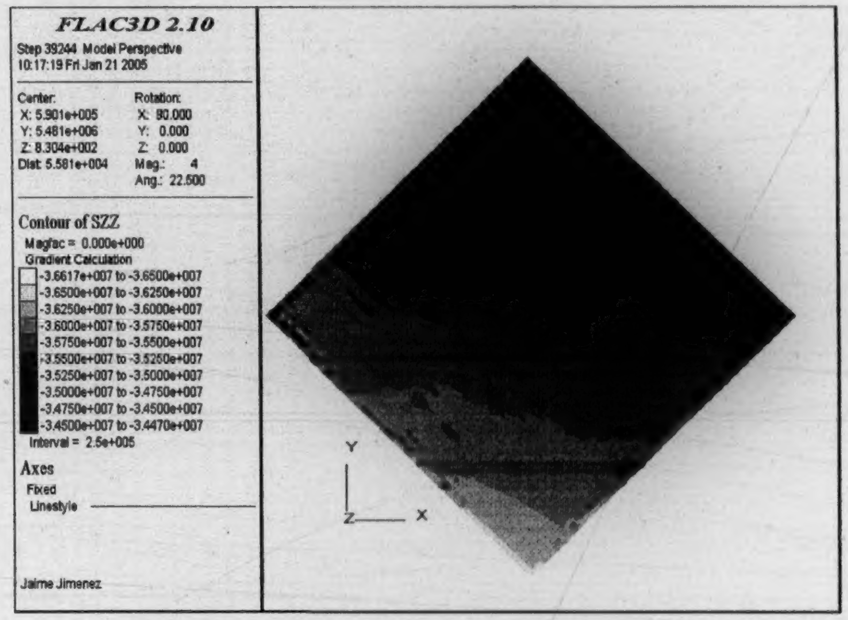

Figure B-15. Vertical stresses in the Marly Formation.

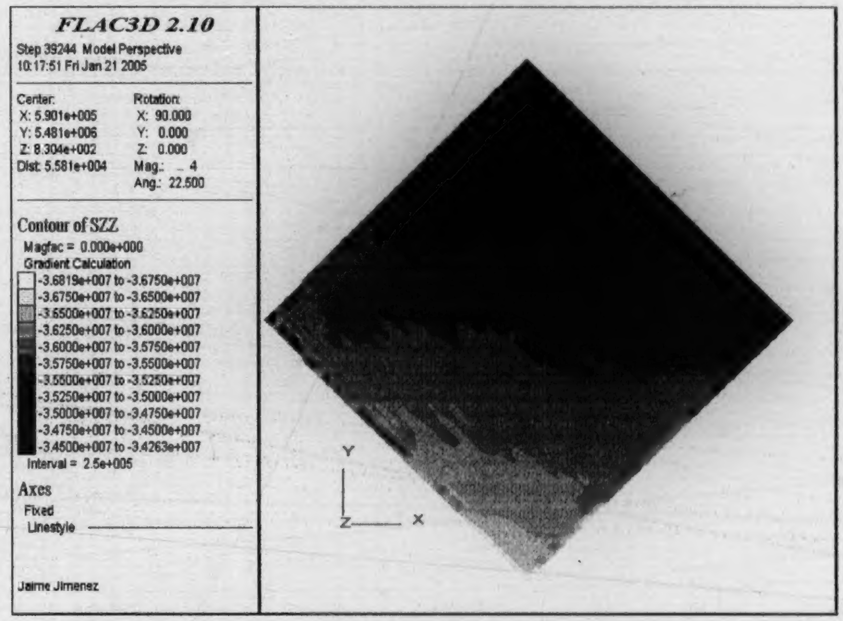

Figure B-16. Vertical stresses in the Upper Vuggy Formation.

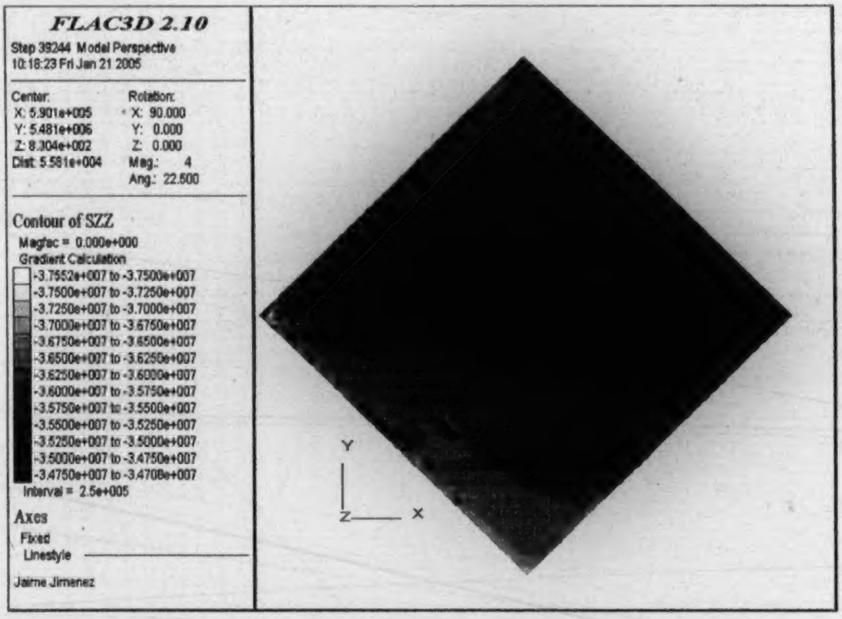

Figure B-17. Vertical stresses in the Lower Vuggy Formation.

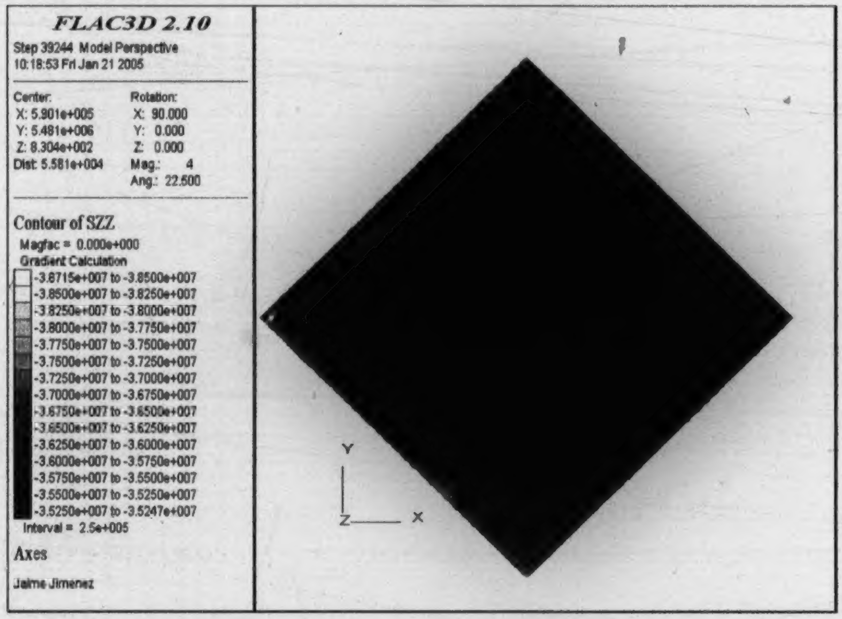

Figure B-18. Vertical stresses in the Frobisher Evaporite Formation.

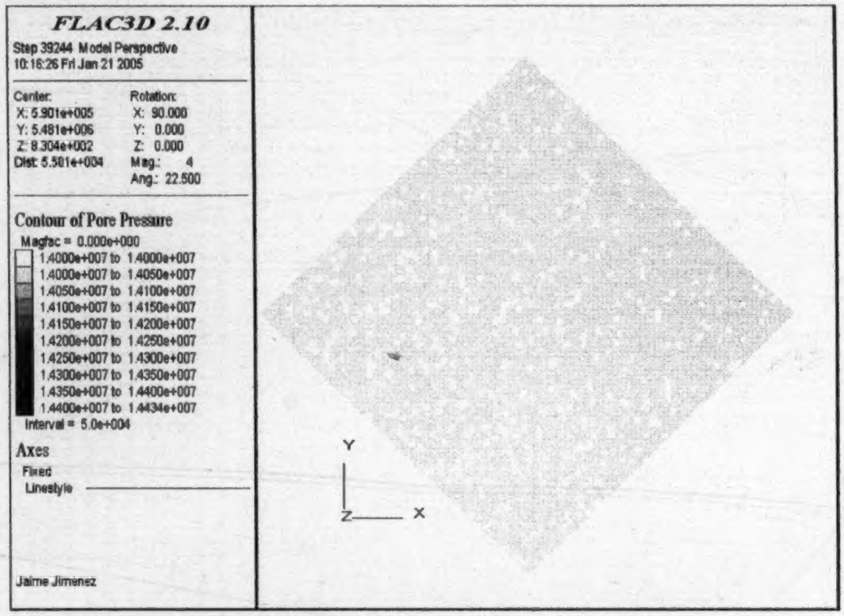

Figure B-19. Pore pressures in the Watrous Formation.

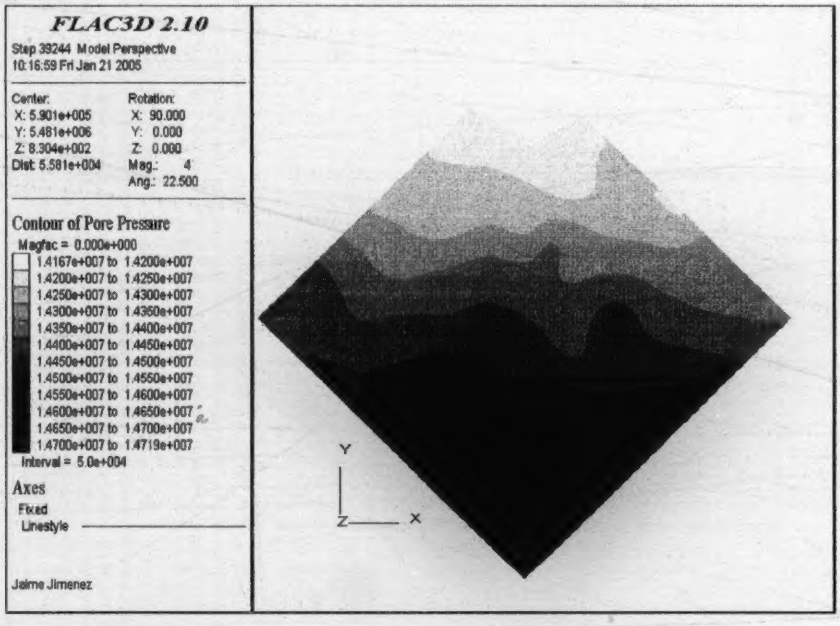

Figure B-20. Pore pressures in the Midale Evaporite Formation.

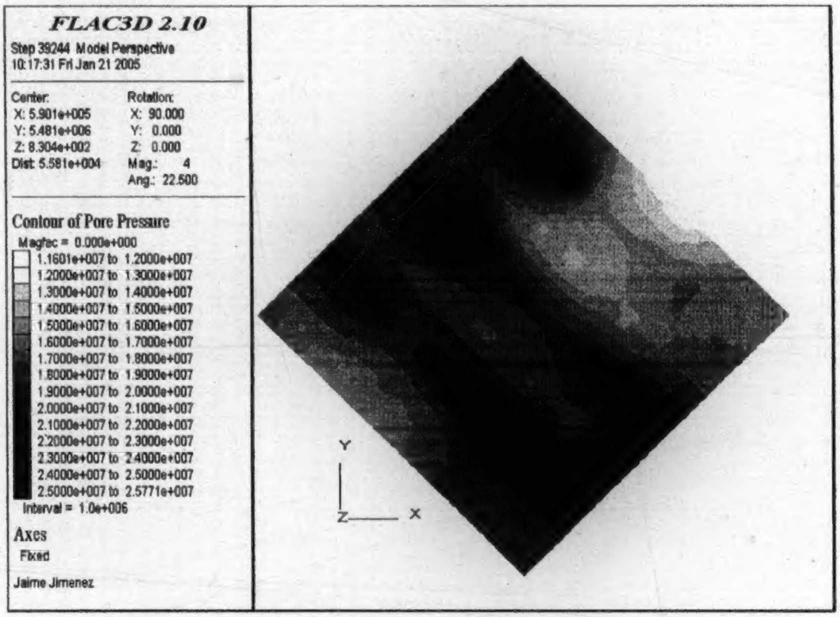

Figure B-21. Pore pressures in the Marly Formation.

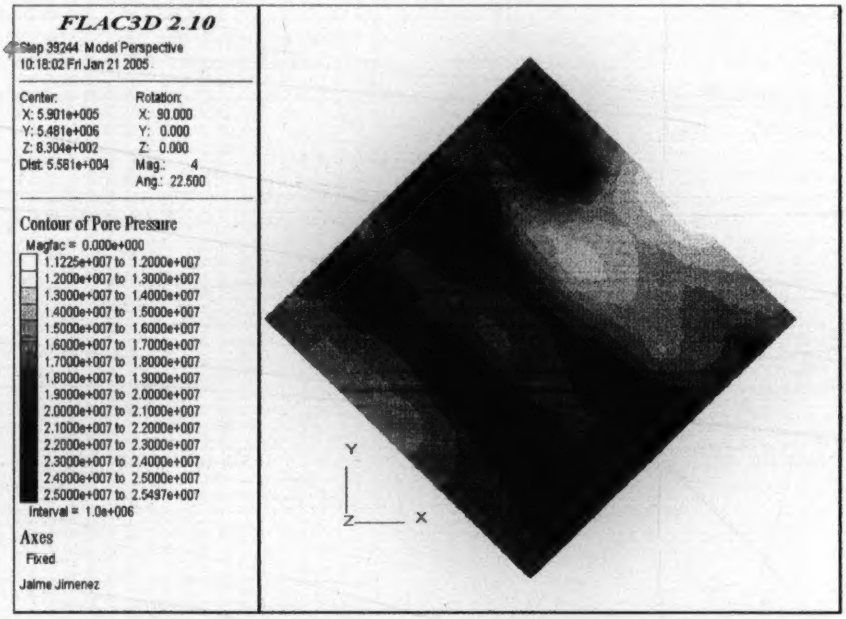

Figure B-22. Pore pressures in the Upper Vuggy Formation.

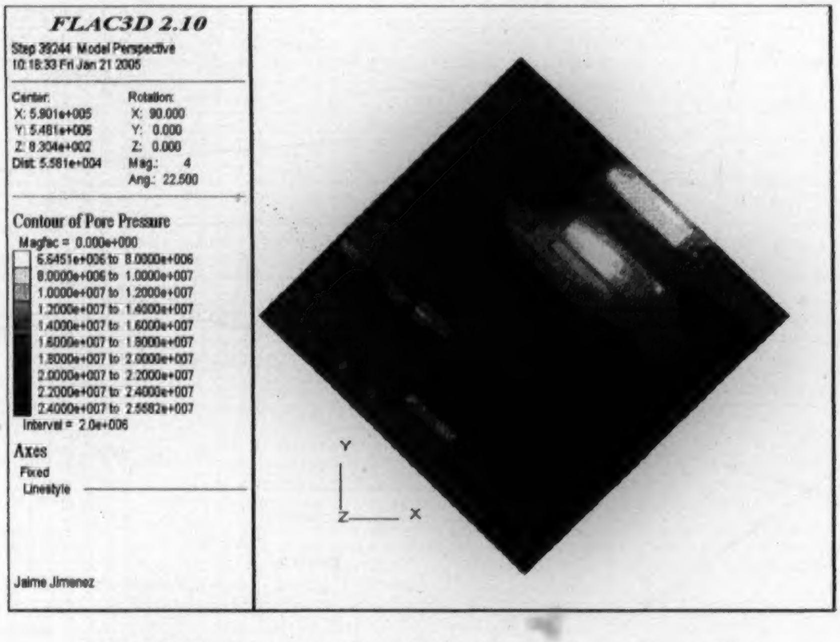

Figure B-23. Pore pressures in the Lower Vuggy Formation.

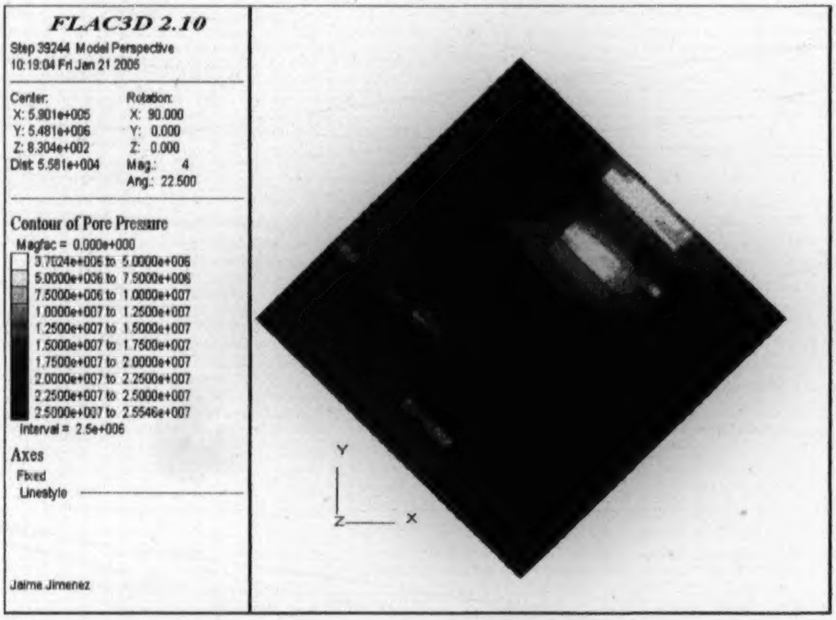

Figure B-24. Pore pressures in the Frobisher Evaporite Formation.

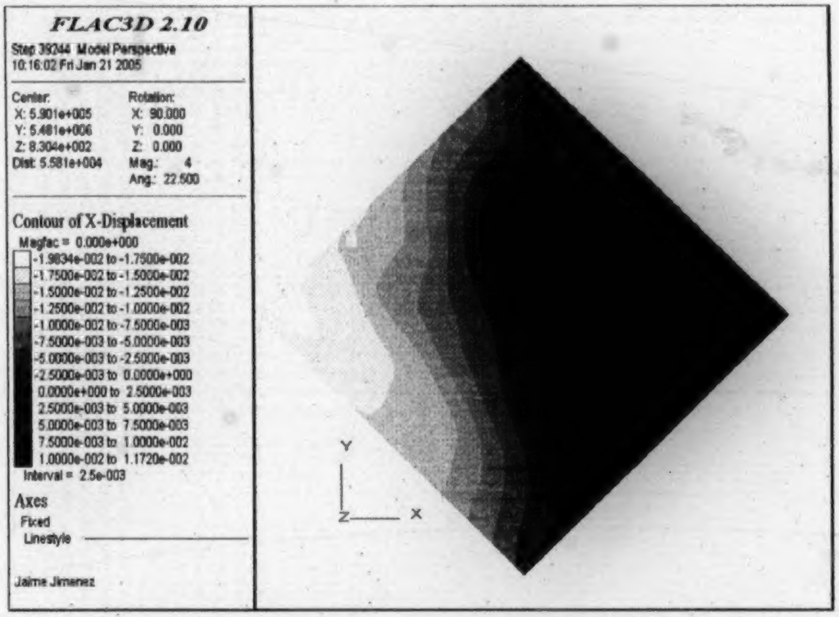

Figure B-25. West-East displacement in the Watrous Formation.

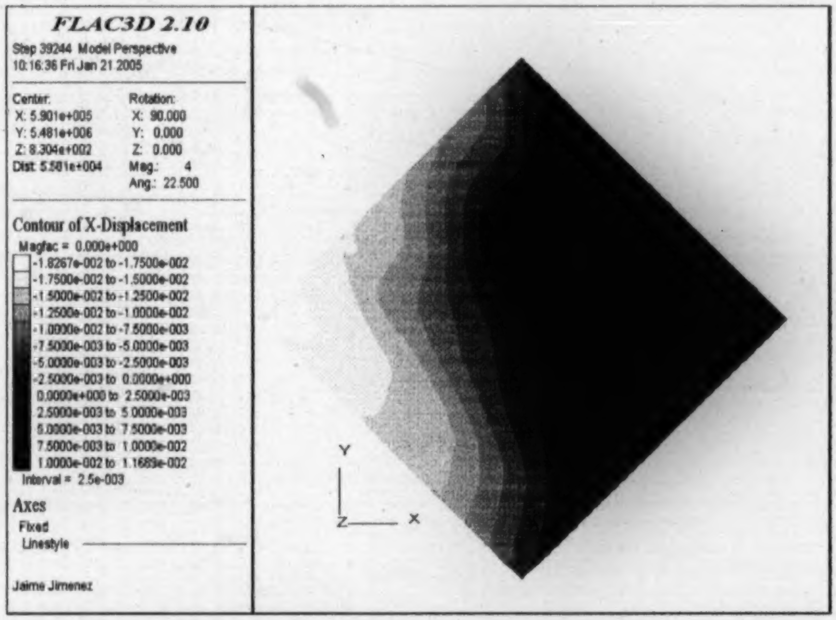

Figure B-26. West-East displacement in the Midale Evaporite Formation.

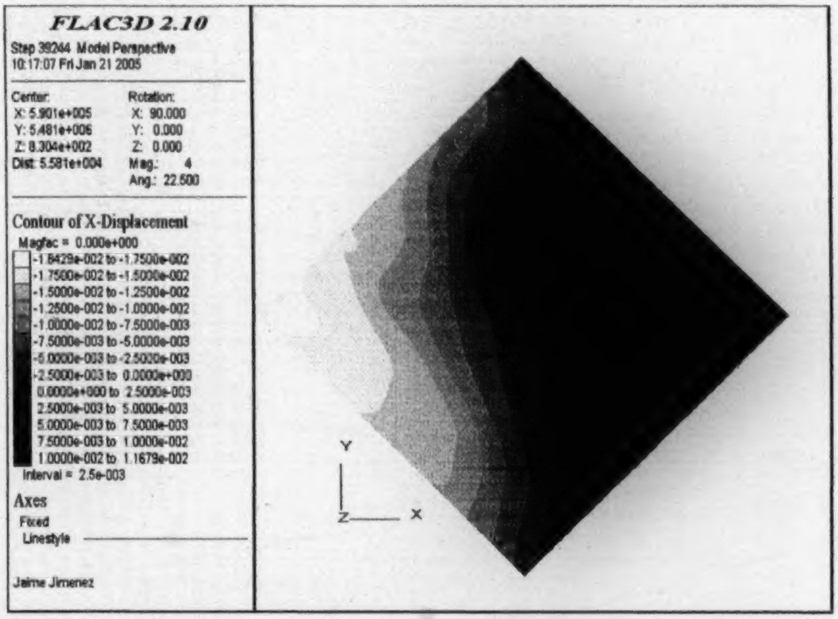

Figure B-27. West-East displacement in the Marly Formation.

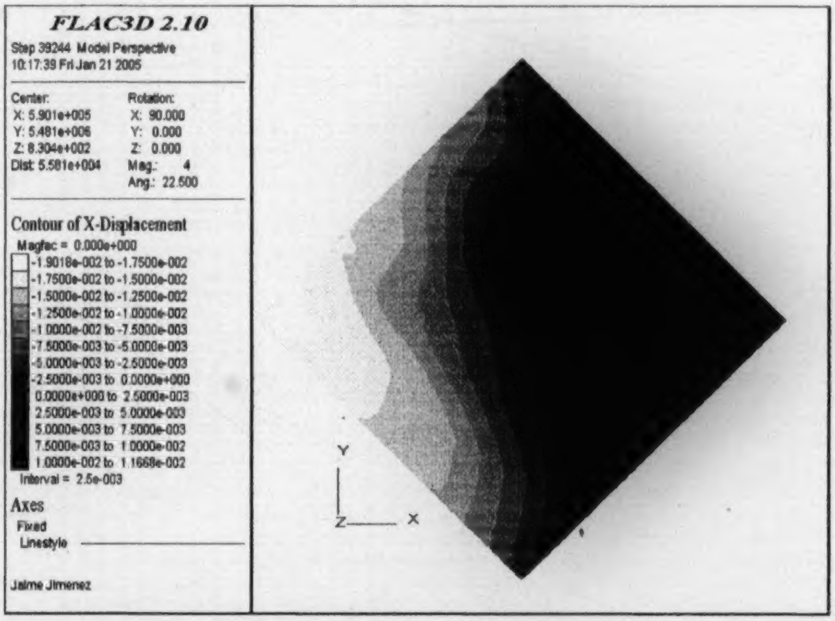

Figure B-28. West-East displacement in the Upper Vuggy Formation.

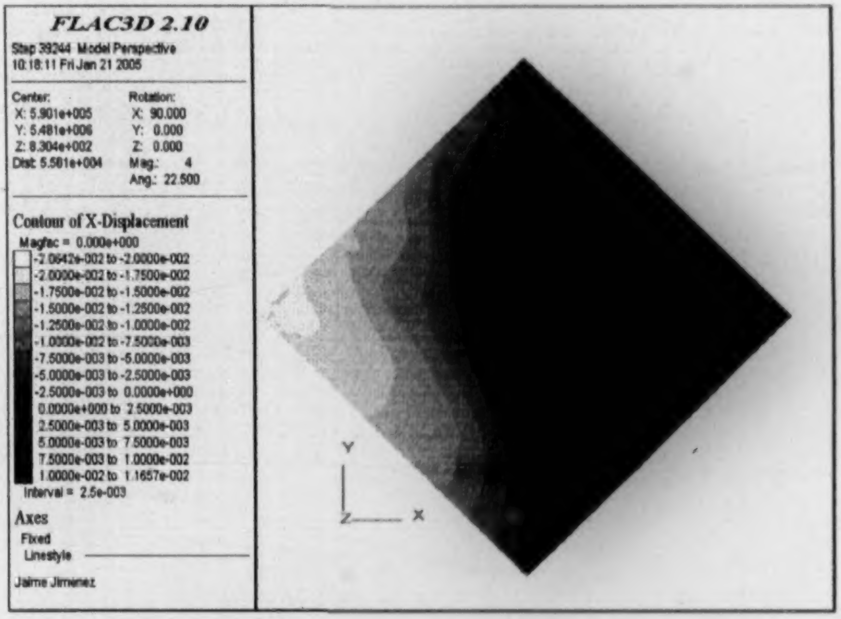

Figure B-29. West-East displacement in the Lower Vuggy Formation.

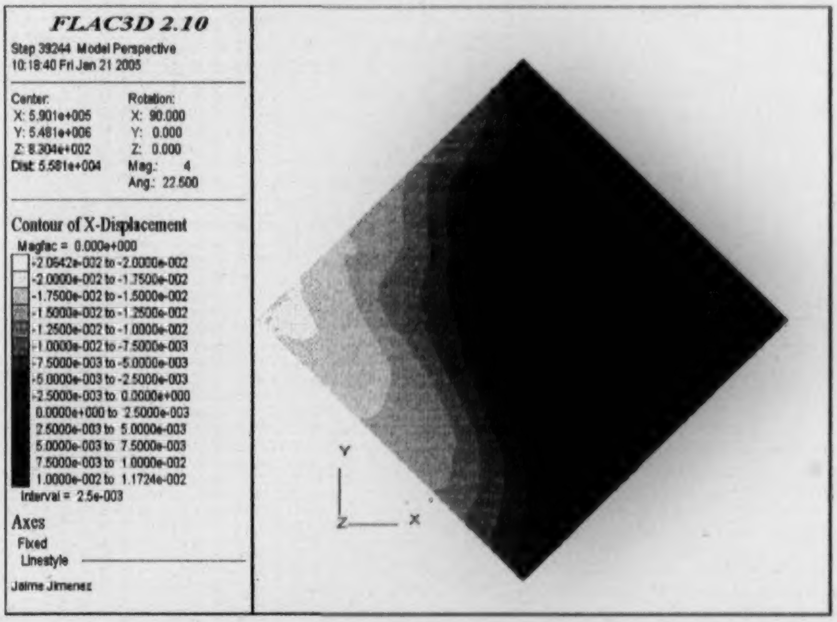

Figure B-30. West-East displacement in the Frobisher Evaporite Formation.

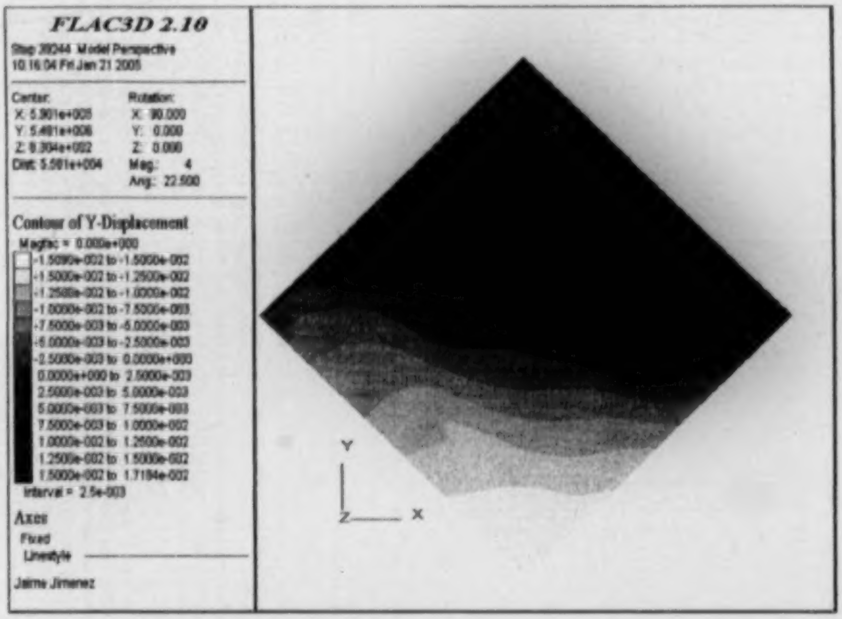

Figure B-31. North-South displacement in the Watrous Formation.

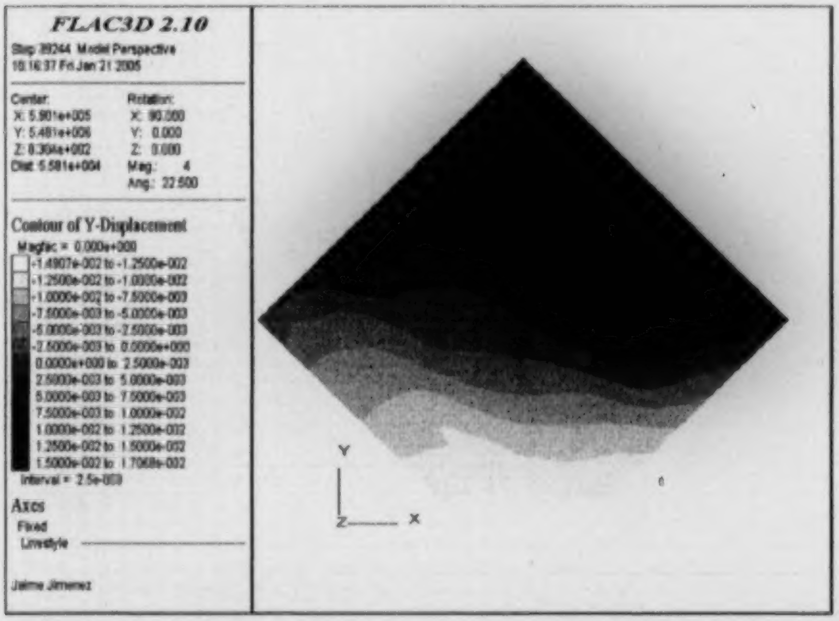

Figure B-32. North-South displacement in the Midale Evaporite Formation.

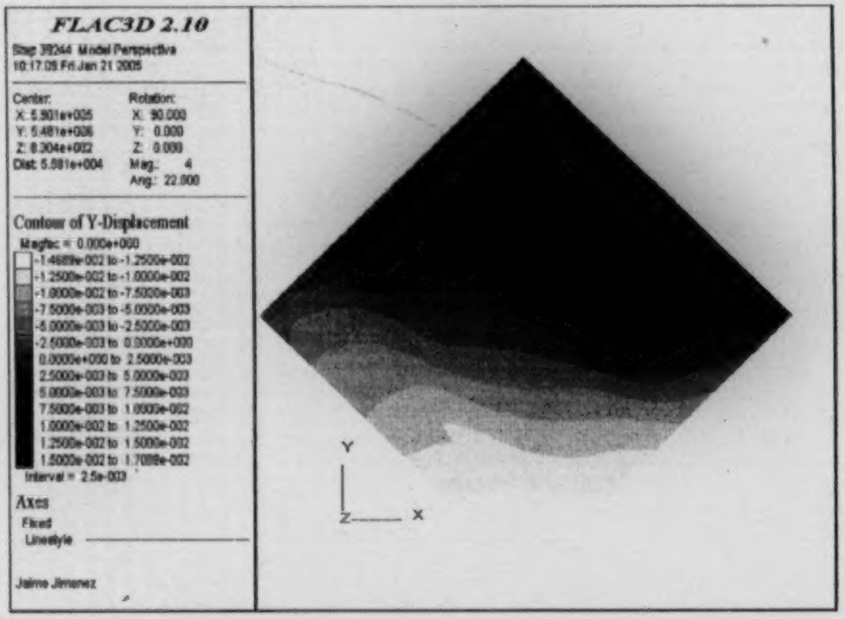

Figure B-33. North-South displacement in the Marly Formation.

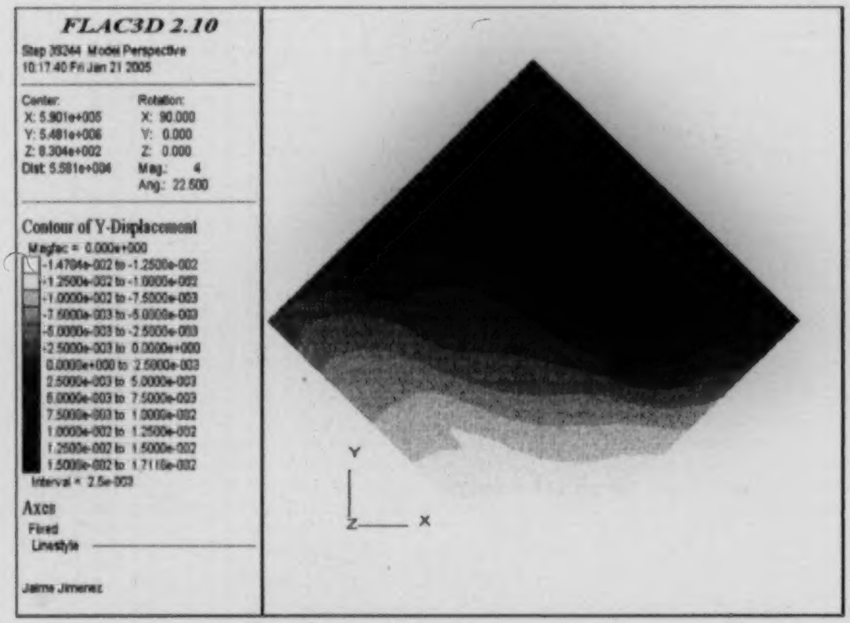

Figure B-34. North-South displacement in the Upper Vuggy Formation.

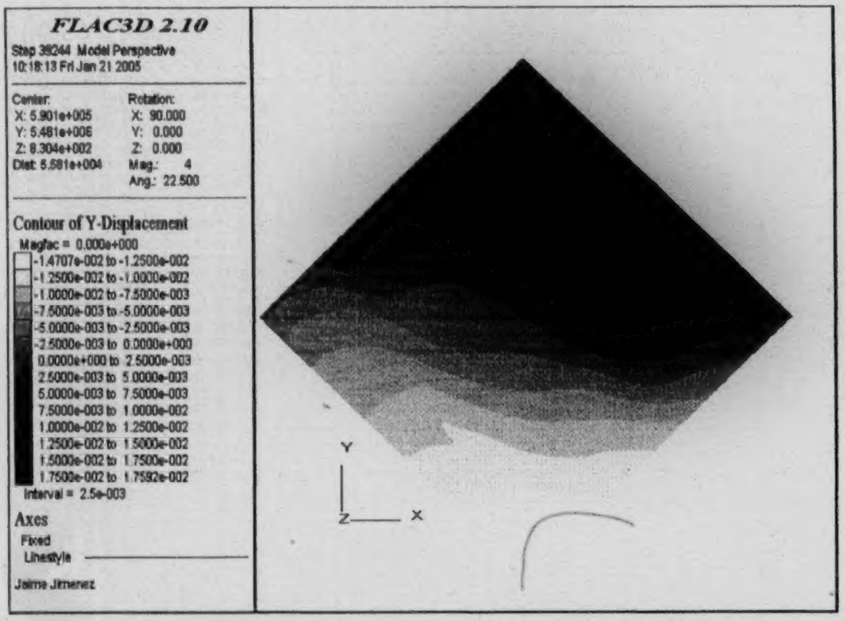

Figure B-35. North-South displacement in the Lower Vuggy Formation.

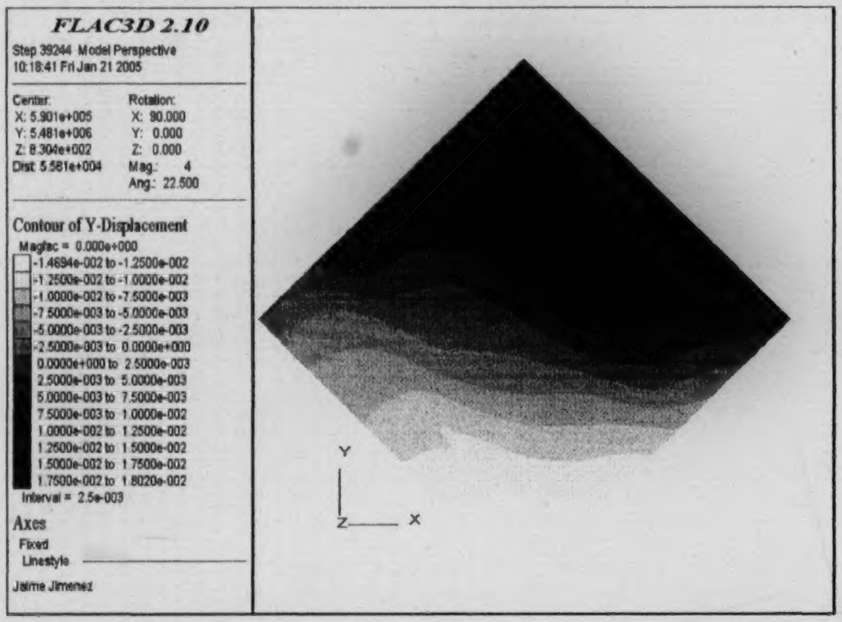

Figure B-36. North-South displacement in the Frobisher Evaporite Formation.

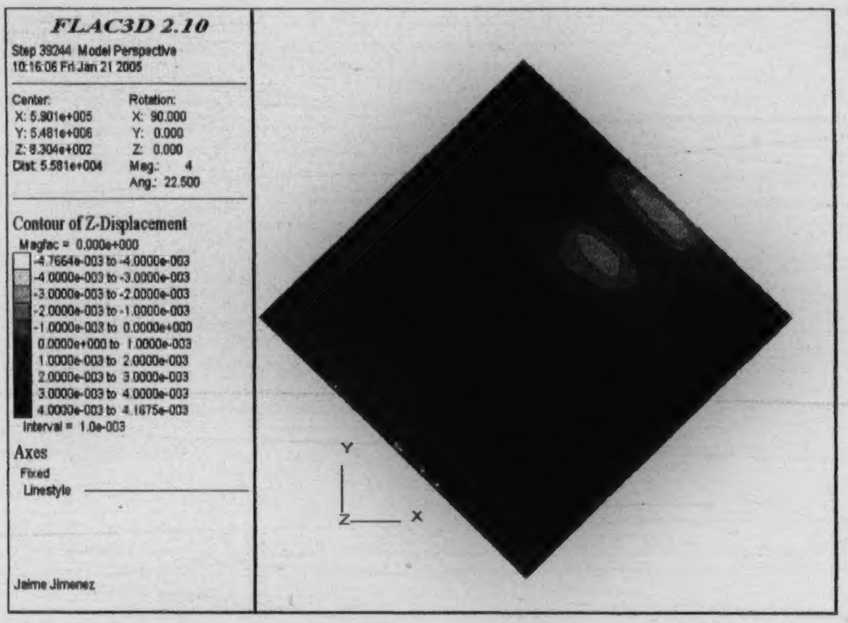

Figure B-37. Vertical displacement in the Watrous Formation.

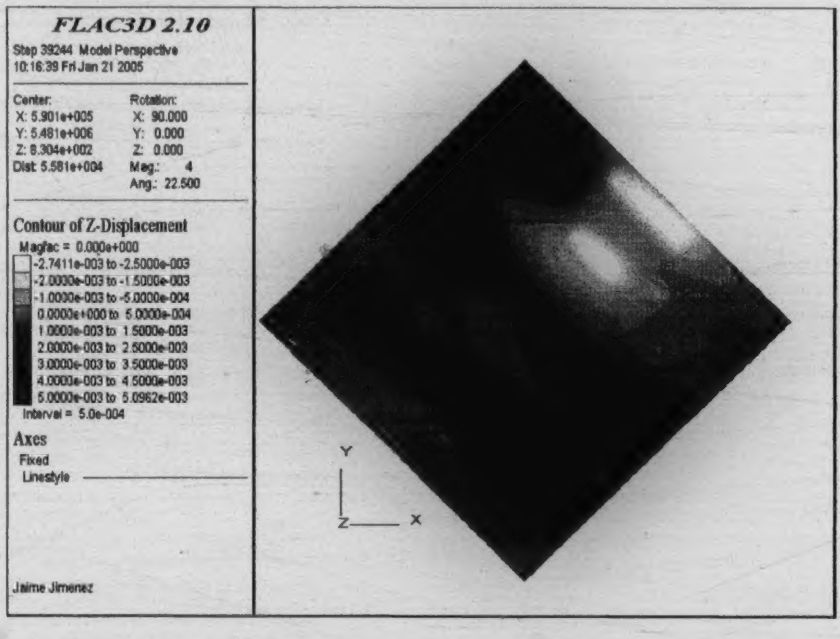

Figure B-38. Vertical displacement in the Midale Evaporite Formation.

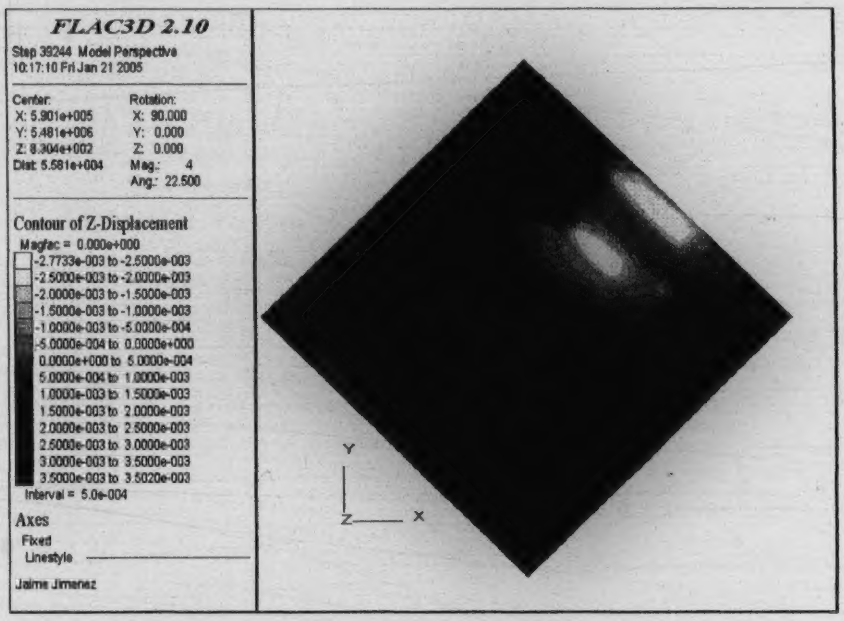

Figure B-39. Vertical displacement in the Marly Formation.

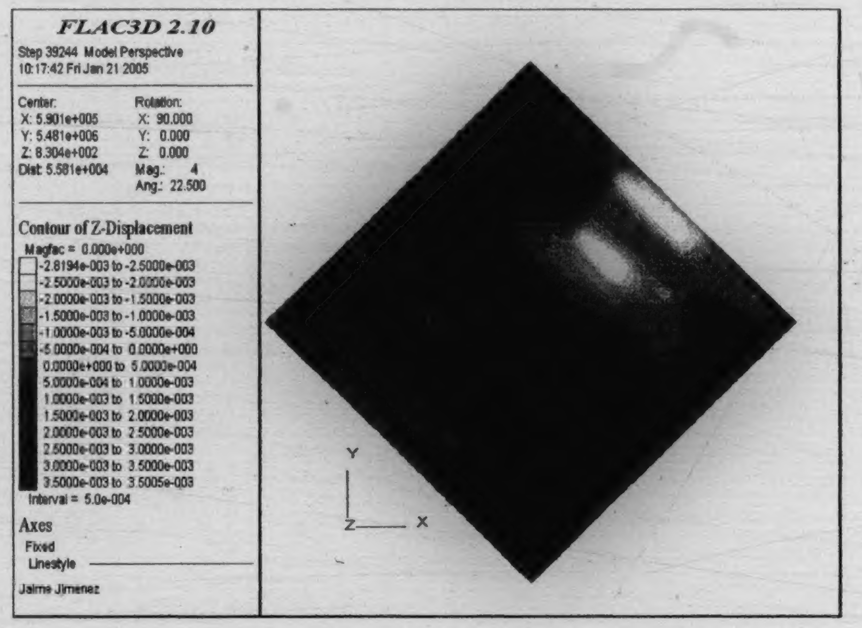

Figure B-40. Vertical displacement in the Upper Vuggy Formation.

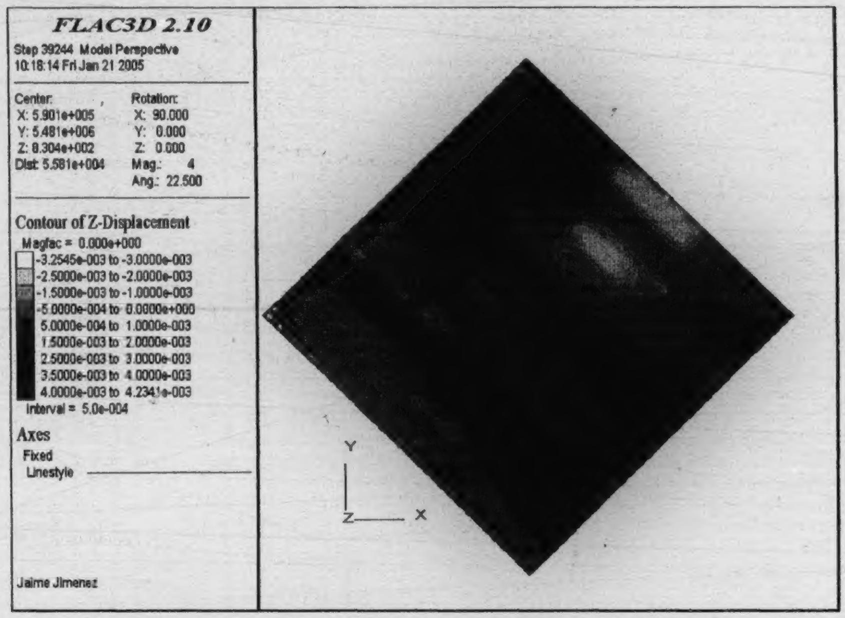

Figure B-41. Vertical displacement in the Lower Vuggy Formation.

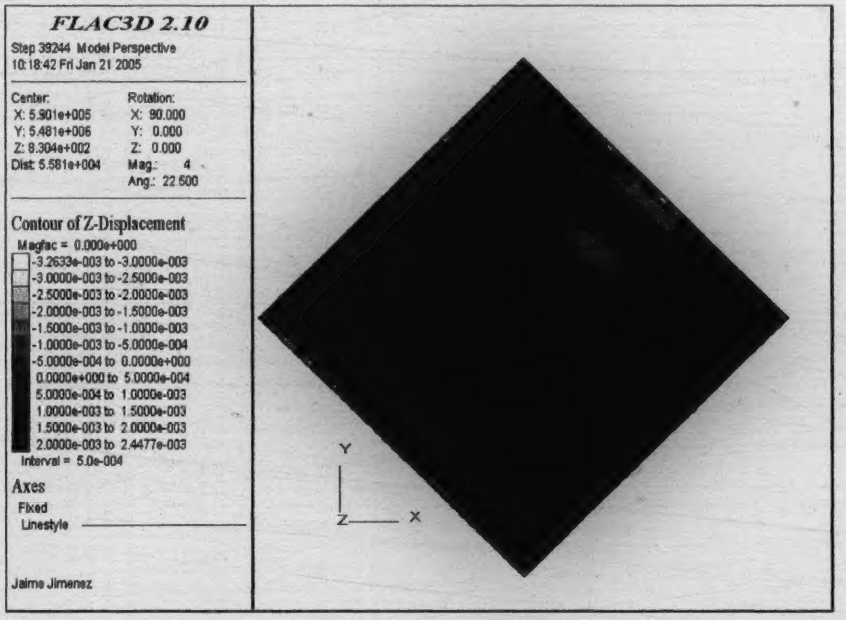

Figure B-42. Vertical displacement in the Frobisher Evaporite Formation.